THE DESIGN AND SYNTHESIS OF METAL-AMINE NETWORKS WITH APPLICATION TO SOLAR ENERGY CAPTURE

Katherine Szpakolski
Bachelor of Applied Science (Applied Chemistry)(Honours)
RMIT University 2007

A thesis presented in fulfilment of the award of
Doctor of Philosophy of Applied Science

School of Applied Sciences
RMIT University
2011

Statement of Authenticity

I declare that, except where due acknowledgement has been made, the work presented in this thesis is that of the author alone. This work has not been submitted previously, in whole or part, for any other academic award. The content of this thesis is the result of work carried out between March 2008 and September 2011 in the School of Applied Sciences, RMIT University, solely as a requirement for the award of a Doctor of Philosophy.

Katherine Szpakolski

September 2011

Acknowledgements

I would like to express my utmost gratitude to my two wonderful supervisors, Dr Kay Latham and Adjunct Professor Colin Rix, for their patience, motivation, enthusiasm, and immense knowledge, over the past four years. This thesis would not have been possible without them.

My sincere thanks also go to Associate Professor Jonathan White, School of Chemistry, Melbourne University, for giving me the opportunity to learn the art of crystallography.

I am also grateful to Dr Kourosh Kalantar Zadeh and Mr Hai Dong Zheng, School of Electrical and Computer Engineering, RMIT University, who welcomed me into their laboratory and assisted me in the assembly and testing of my solar cells.

Thanks to Professor Keith Murray and Dr Boujemaa Moubaraki, School of Chemistry, Monash University, for their assistance with magnetic measurements.

I would also like to acknowledge and express my gratitude to the following University staff that have helped in numerous ways, especially Mrs. Zara Homan, Mrs. Nadia Zakhartchouk, Ms Ruth Cepriano-Hall, Mrs Dianne Mileo, and Mr. Karl Lang.

Thanks also to all my fellow postgraduate students, Elsuida, Rhiannon, Hailey, Jarrod, Emma, Jos, Katie, Keith, and Steve, whose support and friendship made uni life more enjoyable.

To my brother, Michael, who always listened and gave me encouragement when I needed it most, thank you.

Finally, to my parents Jadwiga and Czeslaw, who always supported and believed in me. This thesis is dedicated to you.

Publications Arising from Work Presented in this Thesis

K. B. Szpakolski, K. Latham, C. J. Rix, J. M. White, B. Moubaraki, K. S. Murray, 'Synthetic and Structural Studies on Copper 1H-[1,10]-Phenanthrolin-2-one Coordination Complexes: Isolation of a Novel Intermediate During 1,10-Phenanthroline Hydroxylation', *Chemistry- A European Journal*, **2010**, *16*, 1691.

K. B. Szpakolski, K. Latham, C. J. Rix, J. M. White, 'Di-2-pyridyl ketone complexes of Cu(I) and Cu(II) containing iodide and thiocyanate ligands. An unusual case of a mixed-aldol condensation', *European Journal of Inorganic Chemistry*, **2010**, 5660.

K. B. Szpakolski, K. Latham, C. J. Rix, J. M. White, '2-picolinic acid and benzoic acid from di-2-pyridyl ketone and acetophenone: A case of two copper catalysed Baeyer-Villiger re-arrangements?', *Inorganica Chimica Acta*, **2011**, *376*, 628.

Abbreviations

bipy-sil	4,4'-dicarboxylic acid bis[(3-silatranylpropyl)amide]-2,2'-bipyridine
bipy-Br_2	4,4'-dibromo-2,2'-bipyridine
BV	Baeyer-Villiger
CB	Conjugate Base
CH	Covalent hydrate
dcbipy	4,4'-(dicarboxylic acid)-2,2'-bipyridine
DH	Direct Hydroxylation
depbipy	4,4'-(diethyl phosphonate)-2,2'-bipyridine
dpbipy	4,4'-(diphosphonic acid)-2,2'-bipyridine
dpk	Di-2-pyridyl ketone
DSSC	Dye-sensitized solar cell
EF	Edge-to-face
gem-diol	Geminal diol
HOphen	1H-[1,10]-phenanthrolin-2-one
HP	Hydroxy pyridine
IMS	Intramolecular Shift
LC	Ligand centred excitation
LMCT	Ligand-to-metal charge transfer
MC	Metal-centred
MLCT	Metal-to-ligand charge transfer
n/a	Not applicable
NMR	Nuclear Magnetic Resonance
OFF	Offset-face-to-face
phen	1,10-phenanthroline

pic	Picolinate = pyridine-2-carboxylate
UV-Vis	Ultra-Violet/Visible
XRD	X-ray Diffraction

List of Compounds prepared and/or described in this thesis

(1) $[Cu_2(Ophen)_2]$

(2) $[Cu(phen)_2(H_2O)].\ (NO_3)_2$

(3) $[Cu_2(Ophen)_2(phen)_2].\ (NO_3)_2\ .9H_2O$

(4) $[Cu(dpk)(NCS)]_n$

(5) $[Cu(dpk)(NCS)]_n$

(6) $[Cu_2(dpk.acetone)_2(NCS)_2]$

(7) $[Cu_2(dpk)_2I_2]$

(8) $[Cu(dpk)_2(NCS)_2]$

(9) $[Cu(dpk.H_2O)_2](NCS)_2$

(10) $[Cu(pic)_2]Na_2(NCS)_2.2H_2O$

(11) $Na_2[Cu(pic)_2(NCS)_2](H_2O)_2$

(12) $[Cu(pic)_2]\cdot Na_2\ [Cu(pic)_2(NCS)_2]$

(13) $[Ru(bipy)_2(dcbipy)](PF_6)_2$

(14) $[Ru(bipy)_2(dpbipy)](PF_6)_2$

(15) $[Ru(bipy)_2(bipy\text{-}sil)](PF_6)_2$

(16) $[Ru(dcbipy)_2Cl_2]$

(17) $[Ru(dcbipy)_2(NCS)_2]$

(18) $[Ru(bipy\text{-}sil)_2Cl_2]$

(19) $[Ru(bipy\text{-}sil)_2(NCS)_2]$

Abstract

The chemical and physical properties of coordination compounds can be tuned by altering the oxidation state of the metal ion(s), the ligands and the counter anion. This is of great importance as it enables the design of complexes for specific applications including solar cell technology, in particular dye-sensitized solar cells (DSSC) also known as Grätzel cells. To this end, the aim of the research presented in this thesis was to investigate and synthesize metal-amine complexes with light harvesting properties, known as "dyes" and, if possible, incorporate them in DSSC.

To date, the most common and extensively explored "dye" species have consisted primarily of ruthenium coordination complexes containing *N*-heterocyclic ligands, while other metal complexes with similar photochemical and photophysical properties to ruthenium, such as copper, have not been exploited to their full potential. Therefore, the overall aim of this work was to further extend the use of ruthenium and copper coordination compounds, by tuning their properties to improve their absorption of visible light, and adsorption onto semiconductor surfaces, so as to incorporate them into dye-sensitized solar cells.

The metal-amine complexes described in this thesis were characterised using a number of different techniques including: 1) elemental analysis, 2) Fourier transform infrared spectroscopy, 3) nuclear magnetic resonance spectroscopy, 4) ultraviolet-visible spectroscopy, 5) magnetic susceptibility, 6) fluorescence spectroscopy, and 7) single-crystal x-ray diffraction. Selected compounds were also evaluated for their efficiency in solar energy conversion in a DSSC.

To this end, several new ruthenium(II) complexes with bipyridine and bipyridine type coordination, including new ligands with alternative surface binding possibilities, were synthesized and characterised as possible dyes. Initially, ruthenium complexes containing either carboxylate or phosphonate linkages were used, but there are some limitations with this type of binding because it is not stable over the full pH range or to all solvents. Therefore, in this work an alternative linker has been investigated which is based on a silyl group. Two new complexes, $[Ru(\textit{bipy-sil})_2Cl_2]$ and $[Ru(\textit{bipy-sil})_2(NCS)_2]$, which contain this linker have been synthesised and characterised. Each of the ruthenium based dyes was incorporated into a DSSC, by adhering the dye onto a semiconducting surface of either TiO_2 or WO_3. The overall efficiency of the dye for solar energy capture was determined by measurement of the current and voltage.

A number of new copper(I) complexes which possess some of the favourable photochemical and photophysical properties required for "dye" species were synthesised, but were found to be unsuitable for use in a DSSC. Several copper(II) complexes were also isolated, and while copper(II) does not have the desired properties to be used as a dye, two of the dimeric species were examined for their magnetic properties, one of which exhibited ferromagnetic behaviour and the other anti-ferromagnetic behaviour, and thus may find application in data-storage systems, magnets, magnetic recording and sensing.

The ligand 1H-[1,10]-phenanthrolin-2-one (*HOphen*) was synthesised hydrothermally in the presence of Cu(II). During this study, a copper(I) complex containing the *HOphen* ligand, $[Cu_2(\textit{Ophen})_2]$ was isolated as a black compound, with favourable light absorption properties, but unfortunately it was too insoluble for use in a DSSC. However, a novel dinuclear heteroleptic copper(II) complex, $[Cu_2(\textit{Ophen})_2(\textit{phen})_2](NO_3)_2.9H_2O$, was isolated as a by-product, the formation of which allowed an alternative mechanism for the formation of 'covalent hydrates' to be proposed.

The final copper study investigated complexes which contained the ligand di-2-pyridyl ketone (*dpk*) with thiocyanate anions. Two, one-dimensional, isomeric, continuous polymeric chain complexes of copper(I) were synthesised,

$[Cu(dpk)(NCS)]_n$, which were found to be polymorphs of one another. The two complexes were isolated as black crystals and exhibited favourable light absorption properties for solar energy capture. However, when the polymers were allowed to stand in the supernatant a novel dinuclear copper(II) complex, $[Cu_2(dpk.acetone)_2(NCS)_2]$, was isolated. A mechanism is proposed for the formation of the aforementioned complex, whereby a transition-metal-promoted aldol condensation reaction has occurred. On the basis of the formation of the novel dinuclear copper(II) complex an investigation into alternative ketones led to the isolation of five further complexes, three of which contained the ligand, picolinic acid (*pic*) which is believed to have formed from *dpk* through a novel Baeyer-Villiger rearrangement.

Contents

List of Figures

List of Schemes

List of Tables

CHAPTER 1

Introduction

Metal Complexes and Solar Energy Capture

1.1. General Comments

The chemical and physical properties of coordination compounds can be manipulated by using different oxidation states of metal ion(s), altering the ligands and changing the counter anion. This is of great importance as it enables the design of complexes for specific applications including catalysis,[1] sensing,[1] solar cell technology,[1-24] optical[25-28] and magnetic properties.[29-32]

Bidentate *N*-heterocyclic ligands such as 2,2'-bipyridine, 1,10-phenanthroline, di-2-pyridyl ketone, and 2,9-dimethyl-1,10-phenanthroline (neocuproine) and their derivatives are important building blocks for the preparation of coordination compounds and metallo-supramolecular assemblies.[33]

1.2. Solar energy capture by complexes

World energy needs are constantly increasing and fossil fuels are rapidly declining, hence alternative renewable sources of energy need to be utilized. In particular, the capture and use of solar energy.

Photo-voltaic solar cells are able to convert light into electricity. First generation solar cells, also known as the silicon based solar cell, operate on the basis of a *p*-*n* junction type semi-conducting system. They usually consist of crystalline or amorphous silicon which are doped with inorganic solid-state materials. In conventional solar cells the semiconductor performs the task of light absorption and charge carrier.[34-35]

In 1991, O'Regan and Grätzel introduced a revolutionary solar cell, the so-called "Grätzel cell", now also known as dye-sensitized solar cells (DSSC) (Figure 1-1).[18] Such cells are attractive because of their relatively low cost and ease of production. Ruthenium coordination complexes which contain *N*-heterocyclic ligands have been explored extensively as dye species, and, to a lesser extent, compounds of copper have been considered.

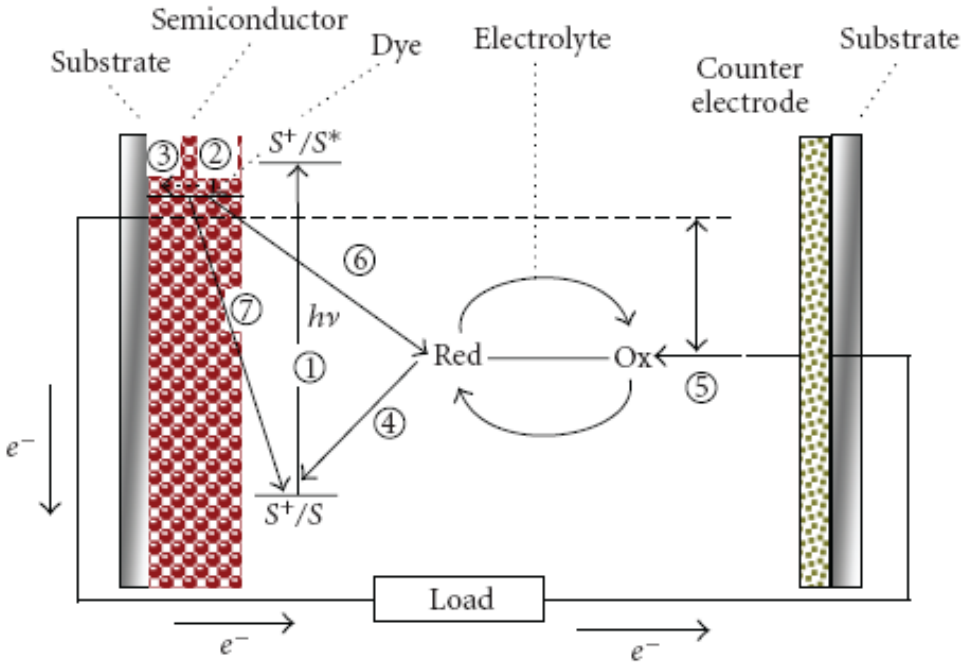

Figure 1-1 Schematic of a DSSC: (1) The dye molecule(s) becomes excited upon irradiation (S^*); (2) An electron from the photo-excited dye molecule is injected into the conduction band of the semiconductor to give S^+; (3), (4) and (6) the dye is then restored to its original form (S) regaining e^- through the electrolyte; (5) The electrolyte is regenerated at the counter electrode, with the circuit being completed through the external load; (7) The dye is reduced and a voltage generated. Overall -the generation of electrical power with no chemical consumption.[13]

The DSSC works on the principle of a dye molecule absorbing radiation and effectively "sensitizing" a semiconductor in a similar fashion to the accessory pigments in photosynthesis. In this case an electron from an electronically excited dye molecule is injected into the conduction band of a wide-band gap semiconductor,[36-37] as indicated in Equation 1-1:

Equation 1-1

$$Dye \xrightarrow{h\nu} Dye^{*} \longrightarrow Dye^{+} + e^{-}(to\ semiconductor)$$

The Dye^{+} cation is recycled via a redox reaction in the electrolyte, such as the one presented in Equation 1-2:

Equation 1-2

$$2\ Dye^{+} + 2\ I_3^{-} \longrightarrow 2\,Dye + 3\,I_2$$
$$2\ Dye^{+} + 3\ I^{-} \longrightarrow 2\,Dye + I_3^{-}$$

For a dye to be effective it must have a ground state which has a lower energy than the conduction band of the semiconductor and an excited state which is higher.[20] This arrangement allows for injection of electrons into the conduction band to occur through the dye rather than through the semiconductor.

In many cases, a ruthenium polypyridine complex has been used as the dye, which absorbs a photon and allows an electron to be injected into the conduction band of a semiconductor, such as TiO_2. The circuit is completed by the regeneration of the dye molecule by a redox reaction with an electrolyte such as iodide (Equation 1-2).[13-14, 18] See Table 1-1 for a summary of the overall process.

Table 1-1 Process steps and system requirements of a metal-ion based DSSC[38]

Process Steps	System Requirements
1) Absorption of solar energy by metal ion based redox system, e.g. Ru^{2+} and Cu^{+}	• Maximum absorption of incident solar energy (large ε for broad range of λ's) • highly soluble complex
2) Release of e^- to TiO_2 system bonded to FTO (FTO – Fluorine-doped Tin Oxide) e^- $(O + e^- \rightarrow O^- \rightarrow O^{2-})$	• Reversible and robust ($M^{(n+1)+/n+}$) photo-redox system • Appropriate redox potential of metal-ion system to allow donation of e^- to TiO_2 system • Rapid e^- transfer kinetics from reduced metal centre (e.g. Ru^{2+} or Cu^{+}) centre to electrode material (TiO_2)
3) Regeneration of metal-ion redox system by removal of e^- from I_3^-	• Rapid e^- transfer from I_3^- to oxidized metal centre (e.g. Ru^{3+} or Cu^{2+}) • Appropriate redox potential of metal-ion system for acceptance of e^- by oxidized form of metal (e.g. Ru^{3+} or Cu^{2+}) from I_3^- system

One of the major differences between the silicon photovoltaic cell and the DSSC is that in silicon cells the charge separation occurs by an electric field within a solid *p*- and *n*-doped semiconductor material, whereas in DSSC's the charge separation occurs by kinetic competition, similar to the electron transfer processes in photosynthesis.

DSSC's have numerous advantages over silicon cells which include:[13]

- Lower cost (lower energy payback time) and ease of production.
- Performance increase with temperature narrowing the efficiency gap.
- Bifacial configuration – advantage for diffuse light and albedo. The albedo refers to the extent to which an object can diffusely reflect light from the sun.
- Transparency for power.
- The range of wavelengths absorbed (colour) can be varied.
- They can outperform amorphous Si.

The major disadvantages of DSSC's relative to silicon cells are:

- They have a much lower incident monochromatic photon-to-current conversion efficiency (IPCE).
- Lower stability.
- Lower scalability.

The main components of the DSSC are the dye, the semiconductor and the electrolyte; changing one, two or all three, can potentially increase the efficiency. The total efficiency depends on the current, voltage and "fill factor", as shown in Equation 1-3.[2]

Equation 1-3 Power conversion efficiency[2]

$$\eta_{global} = \frac{i_{ph} V_{oc} ff}{I_s}$$

η_{global} = Overall conversion efficiency

i_{ph} = Photocurrent density

V_{oc} = Voltage measured at short circuit

ff = The "fill factor" is the ratio of the maximum power output of the cell to the potential power output of the cell.

I_s = Intensity of the incident light

The power output of the cell (p (J/s) =watt) is the product of the current and voltage $p\ (J/s) = i\ (coulomb/s) \times V\ (J/coulomb)$.

This equation will be utilized in Chapter 5.

1.2.1. Coordination Compounds "Dyes" in DSSCs

Coordination compounds that have the ability to absorb sunlight can initiate redox reactions from their excited states, and the electron transfer that ensues can subsequently generate electrical power, thus they are commonly used as "dyes".[15]

To date, d^6metals have been found to form the most efficient coordination compounds for solar energy harvesting. Ruthenium in the +2 oxidation state is a d^6 system[1] and is an excellent candidate due to its luminescent behaviour and appropriate $Ru^{3+/2+}$ redox potential when coordinated to polypyridyl ligands.

Ruthenium polypyridine complexes, in particular Ru(*bipy*)$_3^{2+}$ have been studied extensively over the past twenty years, mainly because of their ease of production, chemical stability, redox properties, excited state reactivity, luminescence (phosphorescence and fluorescence) and long excited state lifetime.[39-40] All of these factors are important when selecting a dye molecule.

Figure 1-2 is a schematic MO diagram for an octahedral transition metal coordination compound containing π-bonding (π-acceptor) ligands.[41]

The first step in the photochemical reaction is the absorption of a photon. Light absorption can promote electron transfer from the metal *d* orbitals (σ^b) to the ligand π^* orbitals, this process is known as metal-to-ligand charge transfer (MLCT).[38] The π^* acceptor and π donor orbitals are delocalised over the aromatic rings on the polypyridine ligand, whilst the σ donor orbitals are localised around the nitrogen atom.[1]

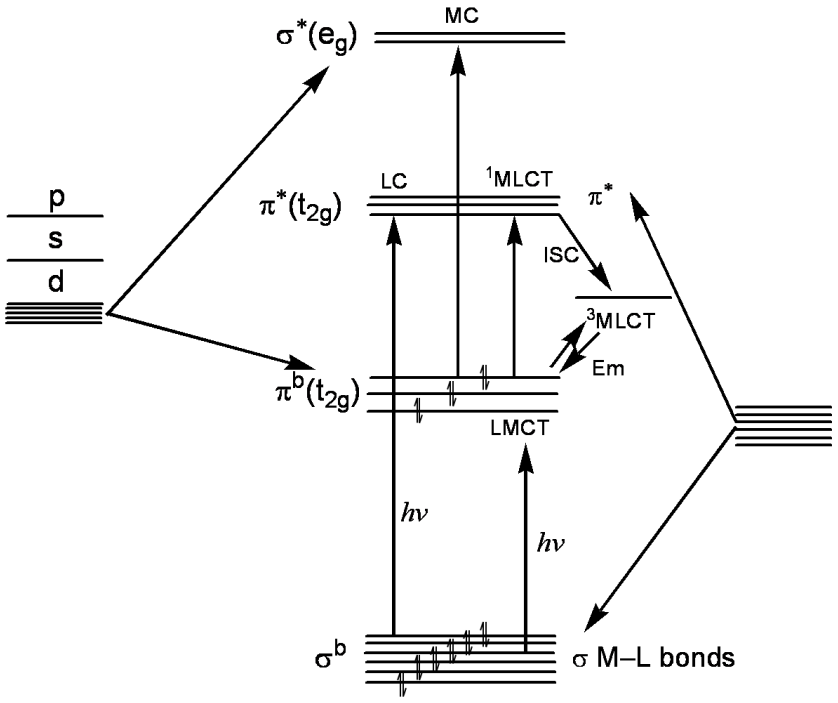

Figure 1-2 Molecular Orbital diagram of d^6 metal [2]

There are three possible ways in which the electrons of a ruthenium polypyridine complex can become excited (Figures 1-2 and 1-3), they include:

1) Metal Centred excitation (MC) is the promotion of an electron from the t_{2g} orbital to the e_g orbital, (π to σ^* orbitals)
2) Ligand Centred excitation (LC) which occurs when absorption across a C=C double bond is able to excite a π electron into an antibonding π^* orbital.
3) Metal-to-Ligand or Ligand-to-Metal Charge Transfer (MLCT or LMCT) which is the transfer of an electron from a metal *d* orbital to an empty ligand orbital, or electron transfer from a ligand orbital into a metal *d* orbital.

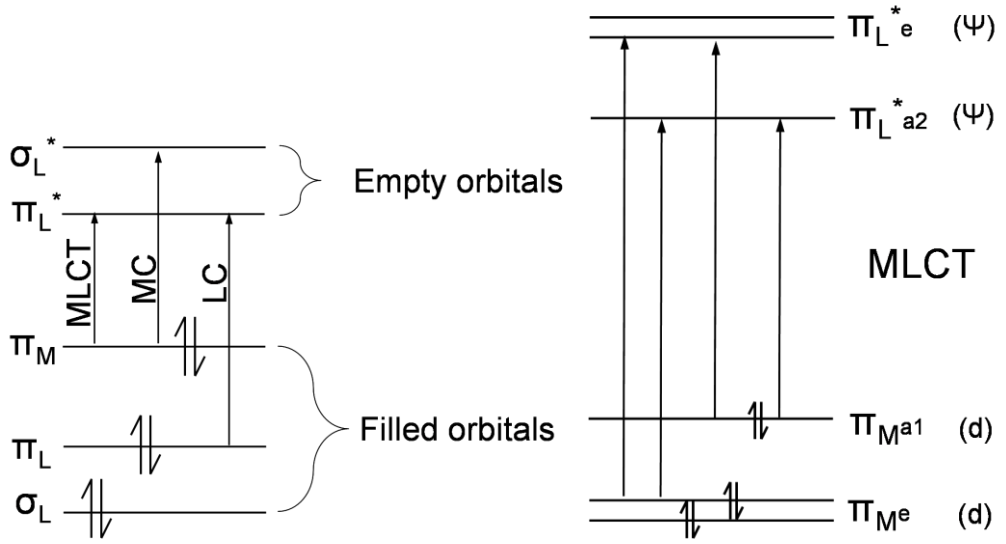

Figure 1-3 MO diagram for $Ru(L)_3$ complex (d^6) with octahedral symmetry and MLCT Transitions in D_3 symmetry[39, 42]

These processes give rise to an unstable excited state molecule which can deactivate via several modes. These include:

1) A photochemical reaction,
2) Luminescence,
3) Radiationless deactivation (when this occurs between the same spin states it is known as *internal conversion*, however when this occurs between different spin states, that is singlet to triplet, it is known as *intersystem crossing*),[39] and
4) A *quenching* process.

Electron excitation in the ground state can lead to electron transfer in the excited state as indicated schematically in Equation 1-4:

Equation 1-4[15, 39]

$$A + h\nu \rightarrow {}^*A \qquad \text{Photo-excitation}$$

$${}^*A + B \rightarrow A^+ + B^- \qquad \text{Electron transfer}$$

1.2.1.1. Selection of a dye

There are several major points which should be considered when selecting a dye for DSSCs, these include:

1) Binding of the sensitized dye to the semiconductor oxide surface, to facilitate subsequent injection of electrons into the conduction band.
2) Relative energies of dye (donor) and semiconductor (acceptor) orbitals.
3) Regeneration of dye sensitizer.
4) The extinction coefficient of the dye should be high and absorbance should occur across the whole visible spectrum.
5) The dye needs to be stable for a minimum 10^8 redox turnovers.

Which are discussed in detail below:

1) Binding of the dye sensitizer to the semiconductor oxide surface, with subsequent injection of electrons into the conduction band:

The dye must adhere to the semiconductor surface through linkages on the dye molecule. Without this, the dye would not be able to inject electrons into the conduction band of the semiconductor efficiently, hence the current and the voltage produced would be low. The current is dependent on the coating of the dye on the semiconductor surface, and the voltage is dependent on the redox potential of the electrolyte and the Fermi level of the semiconductor.[2] There are numerous ways in which transition metal complexes can be functionalised onto a metal oxide surface, these include:[28]

- covalent linkage, which is a direct link between the complex and the metal oxide.
- electrostatic interactions.
- hydrogen bonding.
- hydrophobic interactions.
- van der Waals forces.
- physical entrapment.

Currently, the most widely used covalent linker is a carboxylic acid functionality as it is the cheapest and easiest to synthesise. There are numerous possibilities for the binding of a carboxylic acid to a semiconductor (metal oxide), as illustrated in Figure 1-4.

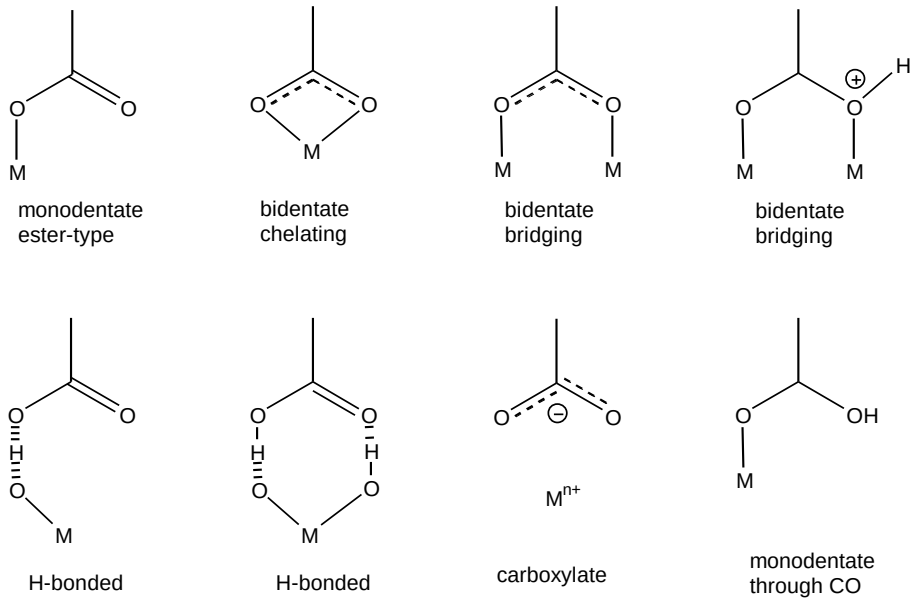

Figure 1-4 Possible modes of binding of the carboxylic acid functionality to metal oxide surfaces.[43-44]

The most commonly used method for the adsorption of the dye onto the semiconductor is by immersion of the semiconductor substrate into a solution of the dye. The substrate is left in the solution for 24 hours in the dark. Subsequently it is washed with ethanol and air dried, before being assembled into a DSSC.

The most efficient linkers will be those that form a covalent bond between the dye and semiconductor as this allows for direct electron transfer. Apart from carboxylate, other common linkers include silyl (–O–Si–), amide (–NH–(C=O) –), sulphide (–S–) and phosphonato (–O– (HPO_2)) which are all capable of forming stable linkages.[4, 45-46] The silyl, carboxylic acid or phosphonic acid groups are all able to react with the surface via hydroxyl groups on the oxide,[28, 44] for example:

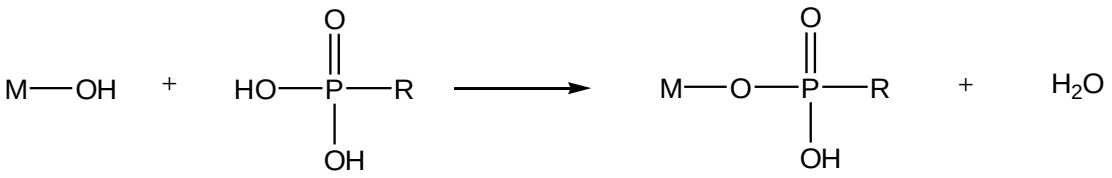

However, common carboxylate and phosphonate linkages are not stable in all solvents, with desorption from the semiconductor surface occurring in aqueous solution at pH > ~4 and pH > ~7 respectively, and in organic solvents this linkage is even weaker.[17, 47-48] Silanes on the other hand are stable in a wider range of solvents, including organic solvents, and over a wider range of pH conditions.

Electrons can be injected into the conduction band of the semiconductor once the dye is excited. According to *Marcus Theory* the rate of electron transfer depends on:[49-50]

a) the physical distance between the acceptor and the donor; the shorter the distance, the greater the efficiency of electron transfer. Hence, it is crucial to ensure that the metal centre is close spatially to the semiconductor surface to improve the efficiency of electron transfer.
b) a decrease in ΔG - If the reaction becomes exergonic, it releases energy spontaneously, this is observed when the Gibbs free energy is negative. This will lead to an increased efficiency of electron transfer.
c) the reorganization energy – the energy required to reorganise the system geometry. There needs to be minimal reorganisation from initial to final atomic coordinates when changing the electronic state in the overall redox cycle.

At present, carboxylate linkages are by far the most common,[43] with the current commercial dyes, in particular the **N3** and **N719** dyes (Figure 1-5), incorporating this linkage. The dye sensitizers **N3** and **N719** both contain the same Ru(II) complex, the difference simply being the accompanying cation, with **N3** effectively having H^+ (on the carboxylate groups) and **N719** having its anionic charge counter-balanced by the tetrabutylammonium cation. The cation in **N719** is used to preserve the deprotonated form of the carboxylic acid so as to enhance surface binding.[38, 51]

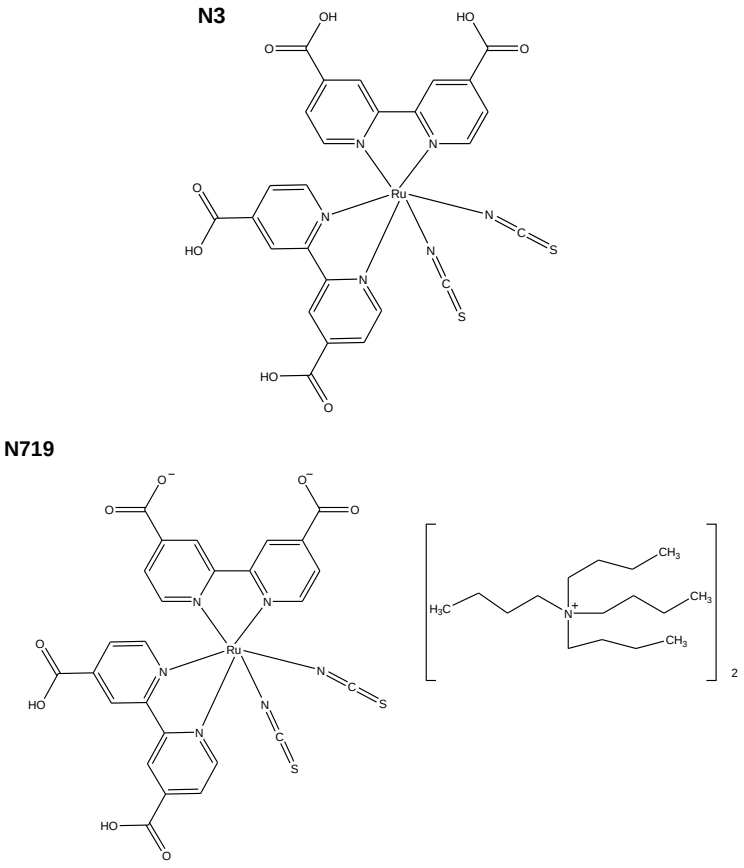

Figure 1-5 N3 and **N719** Commercial Dyes[38]

2) Relative energies of dye (donor) and semiconductor (acceptor) orbitals:

The injection of electrons occurs because the excited state of the dye is higher in energy than the conduction band edge of the semiconductor.[2, 6] The energy gap between the t_{2g} and e_g orbitals of coordinated metal ions falls within the visible, ultraviolet and near infrared regions of the electromagnetic spectrum.[52] Strong field ligands (strong π-acceptor ligands) that is, those to the right hand side of the Spectrochemical series, (Figure 1-6) result in a large gap between the t_{2g} and e_g. Hence, these ligands are the more desirable when designing complexes to be used as dyes.[53]

$\pi - donor\ \ ligands$ $\sigma - donor\ \ ligands$

$$I^- < Br^- < SCN^- < Cl^- < S^{2-} < NO_3^- < F^- < OH^- < C_2O_4^{2-} < H_2O$$

$$< NCS^- < py \approx NH_3 < en < bipy \approx NO_2^- \approx phen < PR_3 < CN^- < CO$$

weak $\pi - acceptor\ \ ligands$ strong $\pi - acceptor\ \ ligands$

Figure 1-6 The Spectrochemical series[52]

The Ru(III)/Ru(II) reduction potential for a *tris*-bipyridine system $[Ru(bipy)_3]^{2+}$ is +1.25V-+1.30V vs. NHE (Normal Hydrogen Electrode).[2, 39] This potential can be increased or decreased by tuning the metal centre with appropriate ligands. For example, the oxidation potential of the *bis-bipy* ruthenium system with two Cl^- ions, $[Ru(bipy)_2Cl_2]$, is lowered to approximately +0.35V vs. NHE, whereas the incorporation of two CO groups has the reverse effect, and an increase of the reduction potential to +1.9V vs. NHE is observed (Figure 1-7).[39]

The commercial **N3** dye contains two N-bound thiocyanate ligands, the purpose of which is to tune the metal t_{2g} orbitals and to stabilise the positive hole that is generated after electron injection.[54] The thiocyanate groups are thought to be the least chemically-stable component on the current dye. However, dye molecules that do not contain the thiocyanate ligand have much lower electron transfer efficiencies.[55]

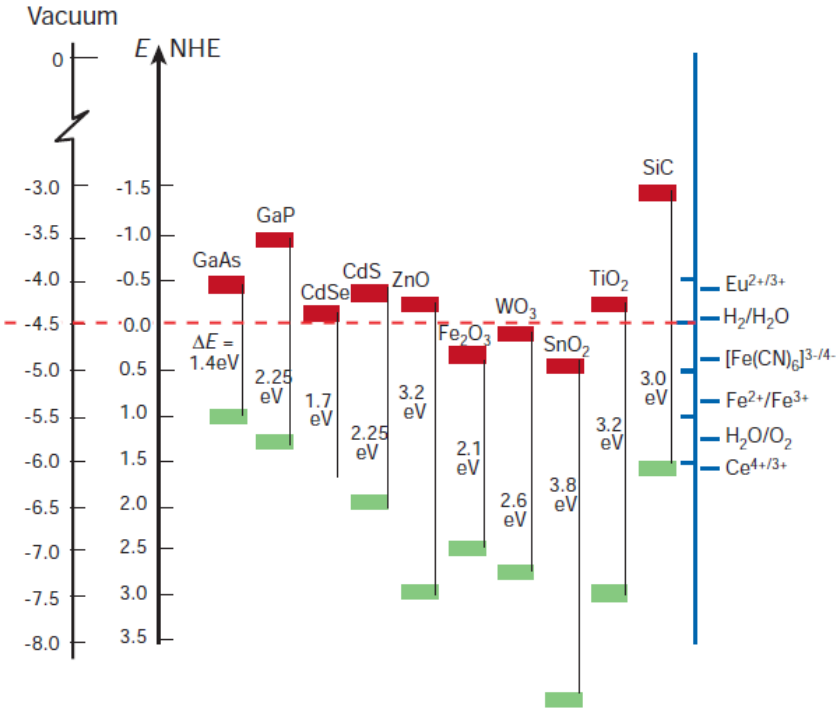

Figure 1-7 Band gap positions of semiconductors in contact with an aqueous electrolyte at pH 1.[6, 8]

3) Regeneration of the dye sensitizer

The regeneration of the dye is a crucial step in the operation of the solar cell, as this can determine the efficiency of the dye. Therefore the dye must undergo a facile, reversible redox process. When the Ru^{2+} dye injects an electron into the semiconductor it becomes oxidised to Ru^{3+}, and to complete the cycle the Ru^{2+} form needs to be regenerated. This is commonly achieved through a reducing agent in the cell electrolyte. Regeneration of the dye through a separate redox-couple prevents the electron donated to the conduction band being recaptured by the oxidised dye.[7]

When selecting an appropriate redox couple/reducing agent, several criteria must be met, which include:[2]

a) it must be soluble in a variety of organic solvents.
b) both the reduced and oxidised form must be stable.
c) it should be able to undergo a minimum of 10^8 turnovers.
d) it should be as optically transparent as possible, hence the molar extinction coefficient must be very low.

Redox active electrolytes are generally used as the reducing agents and have been successfully incorporated into DSSCs. There are three major types of electrolyte system; these include *liquid* (organic and ionic), *quasi-solid state* and *solid* electrolytes.[13] The most commonly used redox couple is a liquid electrolyte containing the triiodide/iodide couple (I_3^-/ I^-) E° = +0.54V (SHE).[2, 7, 13, 38] The iodide ion is a very effective reducing agent, and its incorporation into DSSCs has given the highest efficiency observed of approximately 10%.[38]

$$I_3^- + 2e^- \longleftrightarrow 3I^-$$
$$\tfrac{1}{2}\ I_2 + e^- \longleftrightarrow I^-$$

Like the dye, the iodide must also be regenerated. This occurs through the reduction of the triiodide ion at the counter-electrode (See Figure 1-8).[7] There is also the possibility that the iodide may become activated through interactions between the coordinated *bipy* ligand of the dye and the iodide.[56]

a)

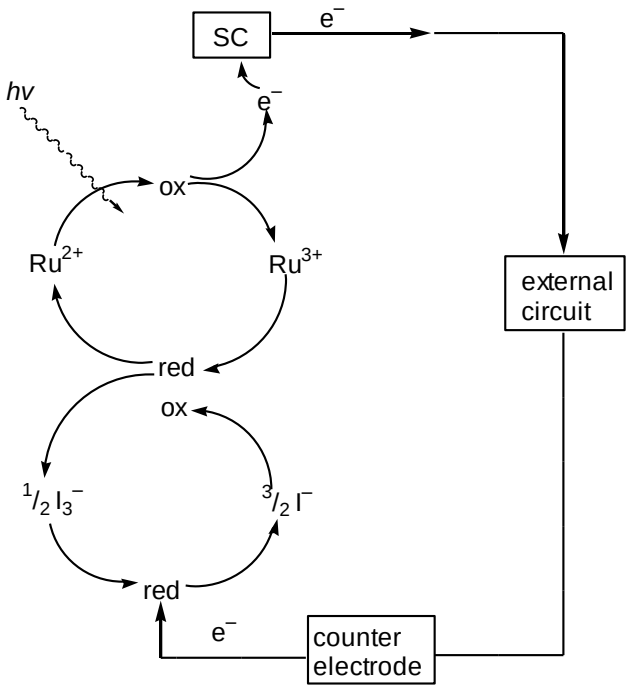

b)

$$SC\ (semiconductor - conduction\ band)$$
$$\uparrow$$
$$Ru^{2+} \xrightarrow{h\nu} Ru^{3+} + e^-$$
$$Ru^{3+} + I_3^- \longrightarrow Ru^{2+} + \tfrac{3}{2} I_2$$
$$(I^- \longrightarrow \tfrac{1}{2} I_2)$$

Figure 1-8 Regeneration of dye sensitizer - a) schematic of redox cycle, and b) essential chemical redox reaction.

4) The extinction coefficient of the dye should be high, and absorbance should occur across the whole visible spectrum.

The dye should be able to collect the maximum amount of photonic energy from the radiation available at the Earth's surface; the likelihood of this can be increased if the dye is able to absorb all wavelengths in the visible spectrum, but ideally all wavelengths under 920nm (see Figure 1-9 for the ideal spectrum of a dye molecule). In addition to this, the molar extinction coefficient, which is directly related to the ability of the dye solution to absorb light, should be high.[5, 9, 21] This can be achieved by altering the energy levels of the metal complex. There are two ways in which the

energy levels of MLCT transitions can be altered. The first includes the introduction of a ligand which contains a low lying π^* orbital. This allows for MLCT to reach higher wavelengths on the electromagnetic spectrum, hence the $d\pi \rightarrow \pi^*$ bands shift into the red region. The π^* orbital can be lowered by introducing electron-withdrawing groups on the ligand; this may involve altering the substituents on the ligand. The second includes the introduction of a strong electron donor ligand, which destabilises the t_{2g} metal orbitals.[21, 57]

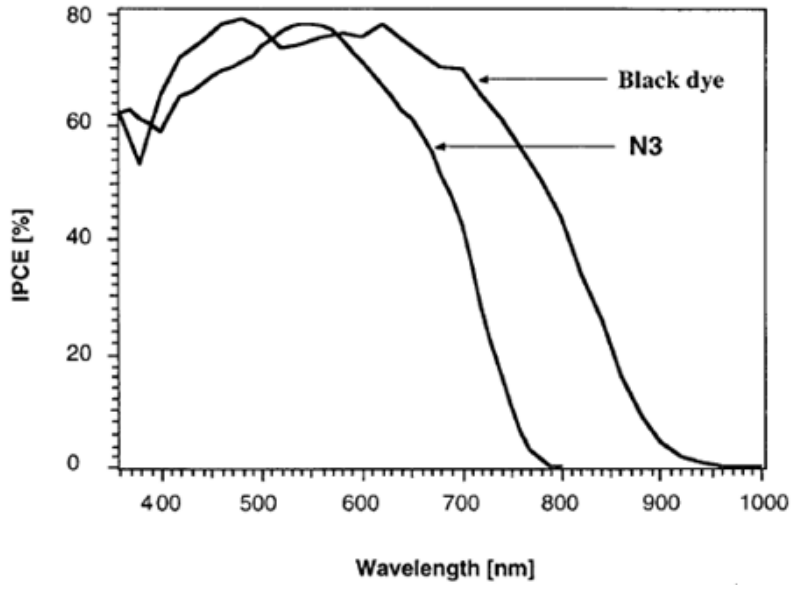

Figure 1-9 Spectral response curve of **N3** and **black dye**.[5]

As mentioned earlier, the most efficient dye sensitizer to-date is the **N3** dye. A comparison of the **N3** dye, [Ru(*dcbipy*)$_2$(NCS)$_2$], with the tris-complex [Ru(*dcbipy*)$_3$]$^{2+}$, shows that the absorption in the red region is higher in the former, although the reduction potential of the (Ru(III)/Ru(II)) couple is sacrificed.[38] Another quite successful Ru(II)-based sensitizer incorporates a tridentate terpyridine, rather than a bipyridine. The "**black dye**", as it is known, consists of one 4 ,4',4''-tricarboxylic acid-2,2':6',2''-terpyridine molecule and three thiocyanate anions (Figure 1-10). The absorption spectrum of the **black dye** is compared with that of **N3** in Figure 1-9, where it can be seen that the **black dye** has a high absorbance across the entire visible spectrum,[16] but its extinction coefficient was found to be lower, leading to a less-efficient DSSC.[38] This arises because absorbance (*A*) is given by the

product $\varepsilon \times c \times l$ (ε = molar extinction coefficient of the molecule, c = concentration, l = path length) and on a mol for mol basis, a greater absorbance is associated with a larger ε.

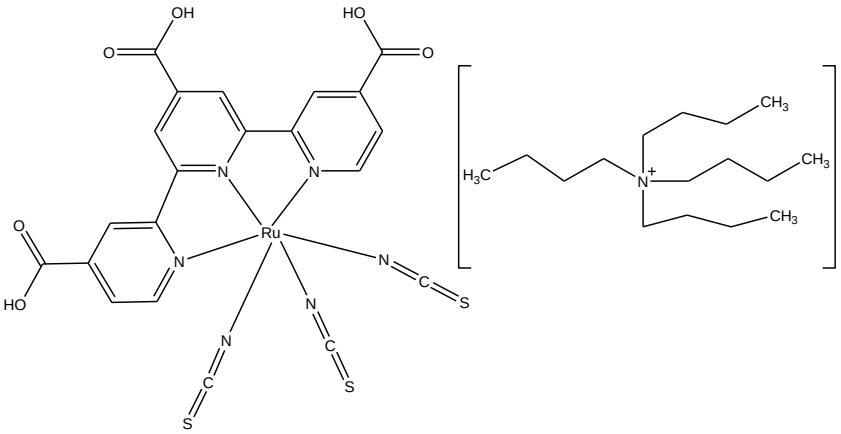

Figure 1-10 Black dye

5) The dye needs to be stable for a minimum of 10^8 redox turnovers

For the DSSC to be economically viable, the sensitizer must be chemically robust. It has been estimated that if the dye material is stable to 10^8 redox turnovers it can then be considered as a possible candidate for a commercial DSSC.

1.2.1.2. Alternative Metals for Dye Formulation

While ruthenium dyes have been investigated extensively, other transition metals have not been explored to the same extent. Iron(II) and osmium(II), which are similar to ruthenium(II) in being d^6 metals, have been investigated briefly.[1, 10, 24, 58-62] There are several advantages in using osmium polypyridine complexes compared to ruthenium analogues, in that the ligand field splitting is substantially greater, and as a result, the photostability of osmium is greater.[2] However, there are still very few osmium polypyridine complexes being incorporated in DSSCs, because despite the advantages of osmium, there are also many limitations. A key issue is that the regeneration of the osmium redox couple (Os(III)/Os(II)), using an iodide electrolyte, is not as efficient as ruthenium, therefore alternative electrolytes would need to be explored.[63]

The potential of transition metals other than d^6 metals is also of great interest, in particular d^{10} metals. Both copper(I) d^{10} and ruthenium (II) d^6 offer similar photophysical properties that can be used for solar energy conversion, see Figure 1-11. One attractive advantage of copper is cost. In 2011 the cost of ruthenium was approximately 6,500 USD per kilogram whilst copper was only 6.60 USD per kilogram, the prices for both have doubled since 2009.[64] In addition to this, copper is far more abundant in the earth's crust at 68,000 ppb by weight compared to ruthenium which is rare, at only 1 ppb.[20]

Therefore, copper(I) polypyridine complexes have been investigated recently as alternative dyes.[22, 27, 40, 65-68] Most first-row transition metal complexes tend to have short-lived MLCT excited states and so are not suited to DSSC use. However, copper(I) differs from the other first-row transition metal ions in that the *d* shell is full (Cu(I) = d^{10}), subsequently preventing non-radiative decay. Hence, the MLCT excited states persist for a substantially longer time, although because of the full *d* shell, Cu(I) cannot undergo MC electronic transitions (Figures 1-11 and 1-12).[22, 27] Therefore, there are only two possible ways in which electrons of a copper polypyridine complex can become excited, that is MLCT and LC, whilst in ruthenium polypyridine complexes there are three. The photophysical properties of copper(II) complexes, with a d^9 electronic configuration, are characterised by ultra-short life-times which can be difficult to detect. This generally means Cu(II) species would be unsuitable as dye sensitizers. The photophysical properties of Cu(II) complexes arise through *d*-*d* metal-centred transitions, which do not occur in the +1 oxidation state because of the full *d* orbital manifold.[27]

A key feature of copper(I) is that fewer coordination sites to the metal centre are available, when compared to ruthenium(II) (typically four versus six coordination). This 'simpler' structure allows for structural distortion in both ground and excited states, which in turn allows the fine tuning of photophysical and electrochemical properties.[27, 40] The selection of the ligand is also important since the nature, size and position of substituents can have drastic effects on the absorption properties, as well as on the ground state geometry, which can range from nearly tetrahedral (D_2d symmetry) to flattened tetrahedral (D_2 symmetry).[27, 40]

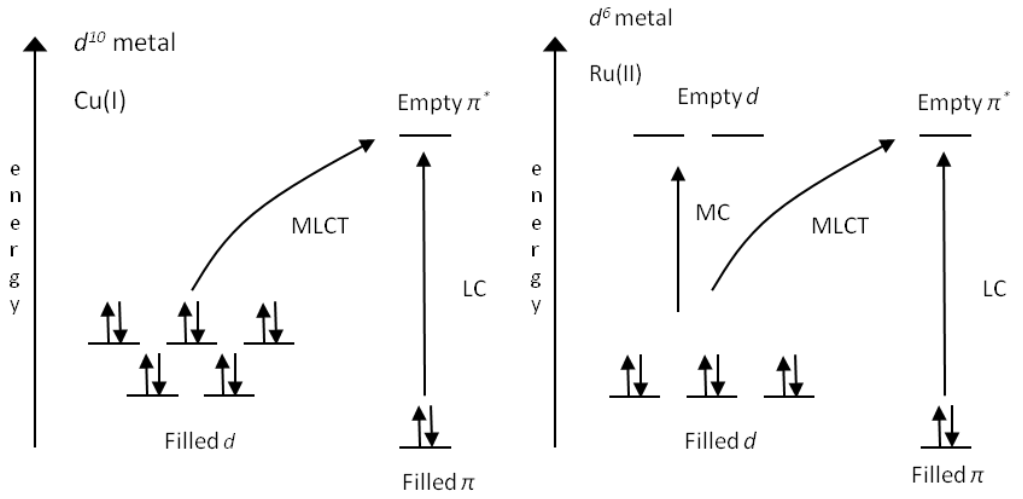

Figure 1-11 MO diagrams comparing d^6 to d^{10} metal complexes

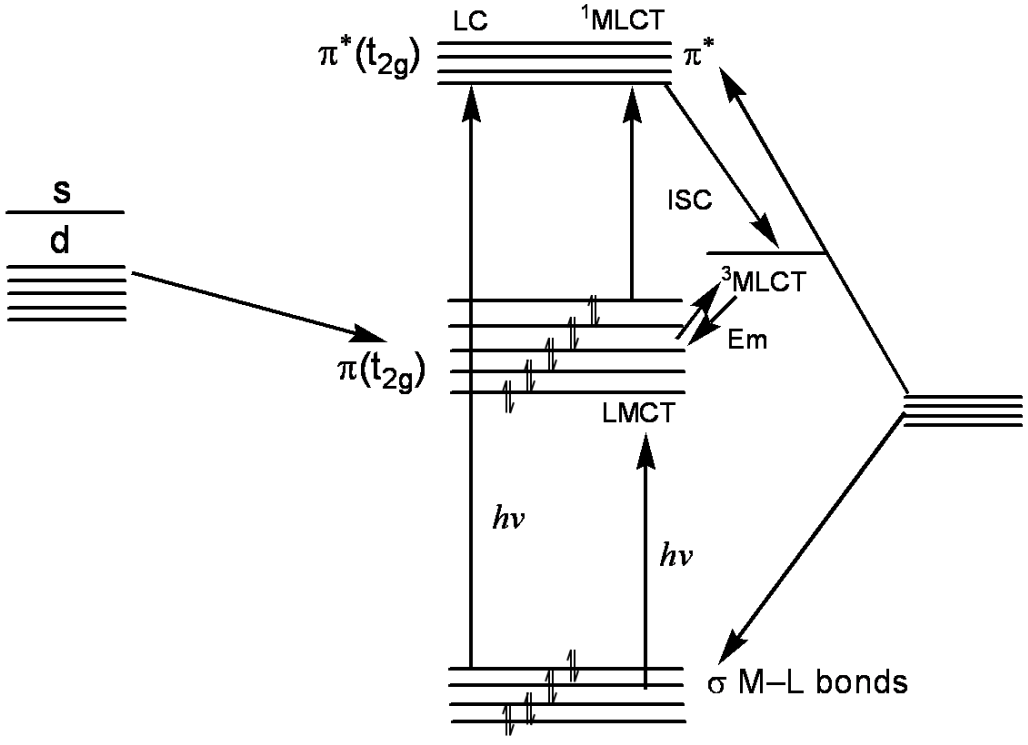

Figure 1-12 MO diagram of d^{10} metal

Possibly as a consequence of their more "open" structure, copper(I) complexes are highly susceptible to aerial oxidation, transforming to copper(II) complexes in the process. For example, the oxidation of Cu(*phen*)$_2^+$ would result in a small energy gap, and hence a short-lived excited state which would render it a less useful complex from a photophysical point of view.[69] However, there are several ways in which this type of oxidation can be prevented. Incorporation of bulky protecting groups in the 6 and 6' positions of the bipyridine ligand, or the 2 and 9 positions of phenanthroline, can prevent geometric changes (prevent expansion of the coordination sphere), hence the copper can be stabilised in the +1 oxidation state.[22] Methyl substituents in the 2 and 9 positions of *phen* (neocuproine (*neo*) = 2,9-dimethyl-1,10-phenanthroline (*dmp*)) are considered to be the best option as they are not too bulky, but still provide protection to the metal from aerial oxidation. The bulky substituents also limit the access of oxygen to the Cu(I) centre and so protect the metal from oxidation.

McMillin *et al.* [70-71] were successful in isolating copper(I) complexes which were similar to the conventional ruthenium complexes. In particular, McMillin found that Cu(*dmp*)$_2^+$ in DCM solution was photoluminescent at room temperature.[72] The luminescence was found to arise from two MLCT excited states, hence the singlet ^{1}MLCT and the triplet ^{3}MLCT. However, the observation of particular interest is that the majority of the luminescence at room temperature can be attributed to the triplet state, but it is the luminescence observed in the singlet state which is responsible for the emission observed.[72] Upon excitation of the copper(I) centre the lowest state (^{3}MLCT) is populated and the metal centre changes its oxidation state from +1 to +2.[40] Copper(I) complexes with 2, 9– disubstituted forms of phenanthroline (dimethyl (*dmp*), di-*tert*-butyl (*dbp*), di-*sec*-butyl (*dsbp*), diphenyl (*dpp*), and di-(2-methylphenyl)(*dop*)) have displayed MLCT transitions as well as weak luminescence, and ligands of this type can enhance the emission quantum yield (See Figure 1-13).[73-74] This is quite beneficial, as low quantum yield efficiency has been a major issue regarding Cu(I) complexes.[71, 75]

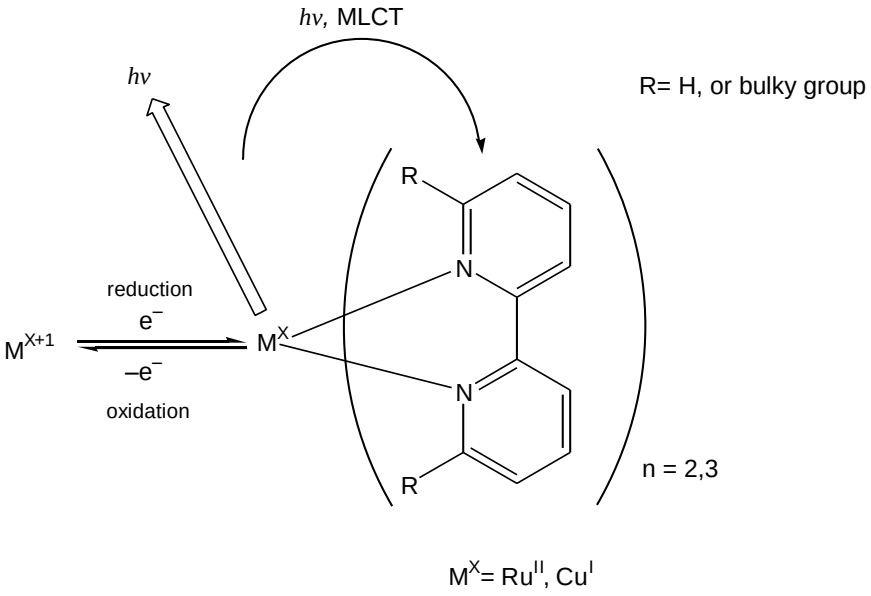

Figure 1-13 Key electrochemical, synthetic and photophyscial properties properties of Ru(II) and Cu(I)[22]

Other mononuclear copper(I) complexes, which do not require protecting groups, incorporate the π-acceptor ligands, phosphanes (PR_3).[73, 76-82] In the Spectrochemical series (Figure 1-6), phosphane groups are situated to the right hand side, hence they are able to create the desired large band-gap between the t_{2g} and e_g orbitals. This is advantageous, and copper(I) complexes which contain phosphane ligands can also possess photoluminescent properties.[81-83]

The reversible (Ru^{3+}/Ru^{2+}) redox potential in ruthenium complexes is a critical factor in selecting appropriate dye molecules, as this enables the system to be regenerated by the judicious choice of an appropriate electrolyte. Similarly, copper complexes with bipyridine coordination can also have reversible redox properties (Cu^{2+}/Cu^{+}) in an accessible voltage range, with a reduction potential of +0.69 V vs. NHE for a *bis*-phenanthroline system $[Cu(dpp)]^{+}$ (Figure 1-14).[84]

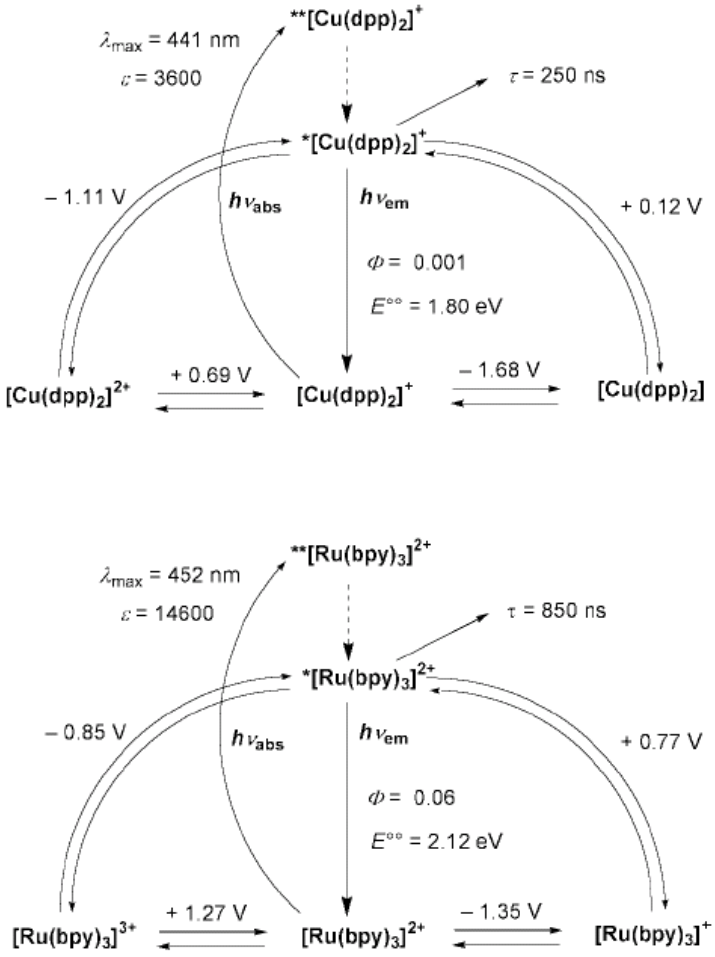

Figure 1-14 Comparison between the photophysical and electrochemical properties of $[Cu(dpp)_2]^+$ and $[Ru(bipy)_3]^{2+}$. (where Φ = quantum yield efficiency, $E^{\circ\circ}$ = excited state electrochemical potential, * = lowest lying electronically excited state, and ** = spin-allowed electronically excited state populated by excitation)[40]

Like mononuclear copper (I) complexes, dinuclear and polynuclear complexes can also possess the desired photochemical and photophysical properties required for dye purposes.[83, 85-87] Moreover, with such polymetallic species it is often not necessary to have the protecting groups required in mononuclear complexes.[69, 74, 87]

However, despite the advantages of copper in cost and abundance; reports of copper dyes in DSSC applications are quite limited.[3, 20, 22, 65-66, 88-91] Recently, Bessho *et al.* investigated several copper(I) complexes $[Cu(L)_2][PF_6]$ (where L = 6,6'-dimethyl-4,4'-dicarboxylic acid- 2,2'-bipyridine or 6,6'-dimethyl-4,4'-dibut-2-enoic acid- 2,2'-bipyridine) for use in DSSCs. These complexes contained bipyridine ligands with

methyl protecting groups in the 6- and 6'- positions and carboxylic acid anchoring groups in the 4- and 4'- positions, see Figure 1-15.[65] The voltage, current and efficiency of these DSSCs were compared to the commercially available N719 dye (Figure 1-5). However, the carboxylic analogues of the dyes were found to be four times lower in efficiency and current, and the voltage was ~30% lower. Although these efficiencies are lower, when the price of ruthenium is compared to copper the drop is not that significant, and therefore copper is still considered a viable alternative with potential for improvement.

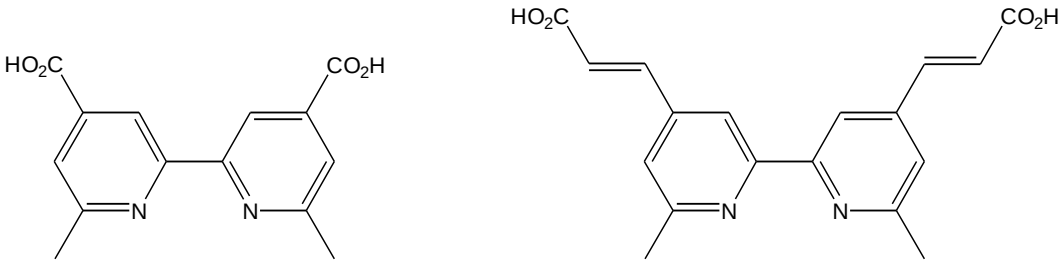

Figure 1-15 Substituted bipyridine ligands coordinated to copper[65]

1.2.2. Semiconductor substrate material

To utilise the photo-chemical and photo-physical properties of ruthenium or copper complexes as dye sensitizers, the dyes must be attached to a semiconducting surface, as described earlier in this chapter. Therefore another critical component of the DSSC is the semiconducting substrate. In order to be considered as possible candidates for solar harvesting, semiconducting surfaces must be sufficiently stable, such that they do not undergo decomposition under illumination.[37, 92-93] There are several metal oxide films which are suitable for this application, these include TiO_2, SnO_2, $SrTiO_3$, and WO_3,[37, 94] together with other oxide, sulphide or selenide substrates such as: ZnO, V_2O_5, Ag_2O, ZnS, CdS, PbS, Cu_2S, MoS_2 and CdSe. Other materials such as Cd_3P_2 and HgI_2 may also be used as semiconducting surfaces.[8] The band positions of some of these semiconductors in contact with an aqueous electrolyte solution at pH 1 are shown in Figure 1-7.[6, 8] In particular, TiO_2, ZnO and WO_3 exhibit exceptional photoelectrochemical properties. They are also highly porous, making them excellent candidates for modification with redox couples and sensitizers.[95]

A semiconductor with a conduction band gap greater than 1.7eV is referred to as a wide band-gap semiconductor, and those of the order of 3eV have been found to be the most effective for DSSC (Figure 1-7). In this case, the electron-hole pairs can only be produced by short wavelength light in the UV range, <400nm.[1, 92] Sunlight has very little light in this range and so cannot be utilised at these short wavelengths. As described earlier in this chapter, to allow for a wider range of wavelengths, in particular those in the visible and near-infrared ranges, to be absorbed, sensitization of the semiconductor needs to occur. Sensitization can be achieved by allowing an electron to be injected into the conduction band or a hole created in the valence band by an additional redox active species (e.g. the metal dyes).[1, 96]

To date, TiO_2 has been the most widely used semiconducting surface for DSSCs, due to its high abundance, relatively low cost, non-toxicity, ease of production and chemical inertness.[2, 18, 97] The anatase form of TiO_2 is a wide band-gap (3.2eV) indirect semiconductor.[97] Thus, the TiO_2 semiconducting surface only absorbs photons in the ultraviolet region, which only represents a small fraction of the solar energy reaching the earth. Sensitization of the surface extends the useful wavelengths into the visible wavelength region. Dye molecules which are *panchromatic*, that is they are able to absorb visible light of all colours,[2] and have an appropriate redox potential, are commonly used as sensitizers, as described in previous sections of this chapter.

To conduct electrons, the semiconductor film must be *n*-doped, although there is the possibility that quenching of the sensitizer can occur through energy transfer from the presence of conduction band electrons.[7] This can be improved through the use of nanocrystalline oxide films with particle sizes less than 1000 nm, and a porous structure, both of which increase surface activity quite significantly.[97]

More recently, interest has been shown in WO_3 as a substrate, since it is an intrinsic semiconductor and is able to absorb some visible light directly. Therefore higher currents may be observed. However, WO_3 does have a more acidic surface and an increased positive conduction band edge position in comparison to TiO_2 and ZnO.[98]

The energy of the conduction band of the semiconductor substrate is a key factor, and must be higher than the required redox level in order for reduction of the dye by the electrolyte.[8] It has been found that approximately 60% of the electrons are injected from the singlet state, and 40% from the triplet state of the ruthenium dye.[99]

The semiconducting substrates which will be investigated in this thesis include TiO_2 and, where possible, WO_3. The TiO_2 substrates were purchased from Dyesol, whereas the WO_3 samples were prepared by the School of Electrical and Computer Engineering at RMIT University.[98]

1.3. Concepts and work in this thesis

The overall aim of the work described in this thesis was to further extend the use of ruthenium and copper coordination compounds in dye-sensitized solar cells. To this end, a number of intermediate goals needed to be achieved:

- Synthesize several ruthenium dye materials
- Explore alternative dye materials, especially those based on the replacement of ruthenium by copper.
- Investigate the use of various ligands based on pyridyl functionalities
- Characterise the complexes synthesised through various analytical and spectroscopic techniques
- Test the efficiency of the dye materials within solar cells
- Explore any anomalies observed

Metal complexes of either ruthenium(II) or copper(I) with the N-heterocyclic ligands 2,2'-bipyridine, 1,10-phenanthroline, di-2-pyridyl ketone and their derivatives will be investigated in this thesis. The coordination chemistry of the amine ligands has been studied extensively and reviewed.[1, 27, 42] Throughout this thesis the ligands will be abbreviated to *bipy*, *phen*, and *dpk*, and their derivatives appropriately labelled. The bonding in a coordination complex is formed by an electron pair from the ligand being donated to an empty orbital on the transition metal (ruthenium or copper),[52] to form a donor-covalent, or coordinate bond, represented as $L{:}\rightarrow M^{n+}$.

Syntheses of the metal complexes are described in more detail in Chapter 2. Attempts were made to "tune" the complexes to improve their absorption of visible light and adsorption onto the semiconductor surface. The ruthenium complexes were modified by replacing *bipy* groups with chloro- or thiocyanato- groups. Exploration of various functional groups for adsorption purposes were also investigated, in particular carboxyl-, phosphonate- and silyl- linkages. The carboxyl-analogue can be purchased through Dyesol, however the phosphonate- and silyl- analogues required synthesis.

As mentioned throughout this chapter, copper is a viable alternative to ruthenium, therefore an investigation of various copper(I) complexes will be explored for use as potential dyes. However, the chemistry of copper(I) compared to ruthenium(II) is quite different, therefore the ligands which were suitable for ruthenium cannot necessarily be directly coordinated to copper(I). One of the main reasons is that copper(I) complexes readily oxidise to copper(II), but this can be avoided if the copper centre is protected. Hence, an investigation into copper(I) complexes which are redox stable and exhibit photochemical and photophysical properties will be explored and will be followed by an investigation of copper(I) complexes coordinated to *phen* or *dpk* functionalised with a variety of different anchoring groups.

The overall aim of the work described in this thesis was to isolate and characterise a range of complexes which exhibit appropriate photochemical properties for use in DSSCs. In particular, ruthenium and copper coordination complexes, with bipyridine or bipyridine derivatives. As part of this study, copper(I) and (II) 1H-[1,10]-phenanthrolin-2-one complexes are reported in Chapter Three. The reaction of copper(I) salts with di-2-pyridyl ketone in various ketone solvent systems are described in Chapter Four. Chapter Five deals with ruthenium(II) complexes with a range of anchoring groups, which have been incorporated into DSSC solar cells.

CHAPTER 2

Materials and Methods

2.1. Materials

Unless otherwise stated, all chemicals used in the synthetic procedures were of at least analytical reagent grade and used without further purification. The following chemical reagents were obtained from the supplier as indicated:

2.1.1. Common Solvents

All solvents marked $^{\alpha}$ were collected under argon from a solvent drying system operating with a J-Kem scientific pressure pump and a Dry Fast vacuum pump.

Acetaldehyde (CH_3CHO) Chem Supply
Acetone (CH_3COCH_3) Merck Chemicals
Acetophenone ($CH_3COC_6H_5$) BDH Chemicals
Benzene (C_6H_6) Aldrich Chemicals
Chlorobenzene (C_6H_5Cl) Ajax Chemicals – Chlorobenzene was dried over $CaCl_2$ and collected in a pressure equalising funnel. The dry solvent was used immediately.
Chloroform ($CHCl_3$) Chem Supply
Cyclohexanone ($C_6H_{10}O$) Ajax Chemicals
$^{\alpha}$ Dichloromethane (CH_2Cl_2) Chem Supply
$^{\alpha}$ Diethyl ether ($C_2H_5OC_2H_5$) Chem Supply
$^{\alpha}$ Dimethylformamide (C_3H_7NO) Ajax Chemicals

Ethanol (CH_3CH_2OH) Merck Chemicals

Hydrochloric acid (32%, HCl) Ajax Chemicals

Methanol (CH_3OH) Merck Chemicals

Methyl ethyl ketone ($C_2H_5COCH_3$) Mallinckrodt Baker

Methyl isobutyl ketone ($(CH_3)_2CHCH_2COCH_3$) Mallinckrodt Baker

Milli-Q Water (H_2O) – Ultrapure Milli-Q water was collected from a Milli-Q-plus 185-system operating with Millipore Purification Packs.

2-Pentanone ($CH_3COCH_2CH_2CH_3$) Fluka

3-Pentanone ($CH_3CH_2COCH_2CH_3$) H&W

Sulphuric Acid (98%, H_2SO_4) Ajax Chemicals

$^{\alpha}$ Tetrahydrofuran (C_4H_8O) Merck Chemicals

$^{\alpha}$ Toluene ($C_6H_5CH_3$) Ajax Chemicals

2.1.2. Chemical Reagents

(3-aminopropyl)triethoxysilane (≥ 98%, $H_2N(CH_2)_3Si(OC_2H_5)_3$) Sigma Chemicals

Ammonium hexafluorophosphate (95+ %, NH_4PF_6) Aldrich Chemicals

Ammonium hydroxide (28%, NH_4OH) Aldrich Chemicals

2,2-Bipyridine (99+ %, $C_{10}H_8N_2$) Aldrich Chemicals

Bromine (99%, Br_2) BDH Chemicals

n-butyllithium in hexane (1.567M, C_4H_9Li) Aldrich Chemicals

Copper(I) iodide (≥ 98%, CuI) Ajax Chemicals

Copper(I) thiocyanate (99%, CuNCS) Aldrich Chemicals

Copper(II) chloride (99%, $CuCl_2$) BDH Chemicals

Copper(II) nitrate trihydrate (99%, $Cu(NO_3)_2 \cdot 3H_2O$) BDH Chemicals

4,4'-Dibromo-2,2'-bipyridine ($C_{10}H_6N_2Br_2$) Carbosynth

4,4'-Dicarboxylic acid-2,2'-bipyridine ($C_{12}H_8N_2O_4$) Dyesol

Di-2-pyridylketone (99%, $C_{11}H_8N_2O$) Aldrich Chemicals

Hypophosphorous acid (50wt.% in H_2O, H_3PO_2) M&B Chemicals

Iodine (99%, I_2) BDH Chemicals

Lithium chloride (99%, LiCl) Merck Chemicals

Neocuproine (2,9-dimethyl-1,10-phenanthroline) (99%, $C_{14}H_{12}N_2$) Sigma Chemicals

1,10-phenanthroline (99+ %, $C_{12}H_8N_2$)Aldrich Chemicals

Potassium chloride (KCl) BDH Chemicals

Potassium iodide (KI) Ajax Chemicals

Ruthenium(III) chloride hydrate (99.9 %-Ru, $RuCl_3 \cdot xH_2O$) Strem Chemicals

Sodium hydroxide (NaOH) Ajax Chemicals

Sodium sulphite (97%, Na_2SO_3) Univar Chemicals

Sodium thiocyanate (99%, NaNCS) Unilab Chemicals

Tetraethylorthosilicate (99%, $Si(OC_2H_5)_4$) Sigma Chemicals

Tetrakis(triphenylphosphine)palladium(0) (99.9+ %, $Pd(P(C_6H_5)_3)_4$) Strem Chemicals

Thionyl chloride (≥ 98%, $SOCl_2$) Merck Chemicals

Triethanolamine (≥ 98%, $(HOCH_2CH_2)_3N$) BDH Chemicals

Triethylamine (≥ 99%, $(C_2H_5)_3N$) BDH Chemicals

Triethylphosphite (98%, $(C_2H_5O)_3P$) Aldrich Chemicals

Triisopropyl phosphite (90+ %, $((CH_3)_2CHO)_3P$)) Alfa Aesar Chemicals

Triphenylphosphine, (≥ 98%, $(C_6H_5)_3P$) BDH Chemicals

2.2. Methods

2.2.1. Preparation of Ligands

2.2.1.1. 1-(3'-aminopropylsilatrane)

1-(3'-aminopropylsilatrane) was synthesised following the procedure of Semenov.[100]

A mixture of 3-aminopropyl(triethoxy)silane (8.84g, 0.04mol) and triethanolamine (5.69g, 0.04mol) was heated (~70°C) in a flask fitted with a Dean-Stark apparatus, and the ethanol produced was removed as it formed. The product was recrystallised twice, from toluene and then chloroform, to give a pale yellow powder in 62% yield.

Chemical Equation:

$H_2N(CH_2)_3Si(OCH_2CH_3)_3 + (HOCH_2CH_2)_3N \rightarrow H_2N(CH_2)_3Si(OCH_2CH_2)_3N + 3CH_3CH_2OH$

IR (KBr): *v* = 3411 (b), 2954 (m), 2900 (m), 1660(m), 1576 (m), 1494 (b), 1124 (m), 1096 (m), 946 (s), 917 (s), 778 (m) cm^{-1}. (where b = broad, m = medium and s = strong)

^1H NMR ($CDCl_3$, 300 MHz): δ 0.4 (t, 2H, *J* = 5 Hz, $–CH_2–Si–$), 1.53 (m, 2H, $–CH_2–$), 2.60 (t, 6H, *J* = 4.5 Hz, $–CH_2–N$), 2.79 (t, 2H, *J* = 3.5 Hz, $CH_2–NH_2$), 3.75 (t, 6H, *J* = 2.5 Hz, $CH_2–O–$) ppm. (where t = triplet, and m = multiplet)

2.2.1.2. 2,2'-bipyridine-4,4'-dicarboxylic acid bis[(3-silatranylpropyl) amide] (*bipy-sil*)

2,2'-bipyridine-4,4'-dicarboxylic acid bis[(3-silatranylpropyl)amide] (*bipy-sil*) was synthesised following the procedure of Brennan *et al.*[48]

2,2'-bipyridine-4,4'-dicarboxylic acid (371mg, 1.52mmol) and thionyl chloride (4mL, 55mmol) were refluxed under nitrogen for 3 hours, and any remaining unreacted thionyl chloride was removed under vacuum. To this, a solution containing triethylamine (450µL, 3.23mmol) and dichloromethane (5mL, 78mmol) was added. This mixture was then transferred to a solution of toluene (15mL) containing 3-aminopropylsilatrane (712mg, 3.06mmol) and heated at 60°C for 1 hour, and then stirred at ambient temperature for 12 hours. The solvent was removed under vacuum and the dark yellow product purified by column chromatography on silica gel (9 $CHCl_3$: 1 CH_3OH) to give a white powder in 10% yield.

Chemical Equation :

$$[C_5H_3N.COOH]_2 + SOCl_2 \rightarrow [C_5H_3N.COCl]_2$$

$$(CH_3CH_2)_3N \text{ in } CH_2Cl_2 \quad \downarrow \quad H_2N(CH_2)_3Si(OCH_2CH_2)_3N \text{ in } (C_6H_5)CH_3$$

$$[C_5H_3N(CONH(CH_2)_3Si(OCH_2CH_2)_3N)_2]_2$$

IR (KBr): *v* = 3456 (b), 2937 (m), 2891 (m), 1659 (s), 1540 (s), 1463 (s), 1280 (s), 1119 (s), 1094 (s), 757 (s) cm^{-1}.

^{1}H NMR (DMSO-d_6, 300 MHz): δ 0.35 (t, 4H, J = 6 Hz, –CH_2–Si–), 1.50 (m, 4H, –CH_2–), 2.66 (t, 12H, J = 5 Hz, –CH_2–N), 2.84 (t, 4H, J = 4 Hz, CH_2–NH_2), 3.75 (t, 12H, J = 4 Hz, CH_2–O–), 7.8 (m, 2H, Ar-H), 8.05 (s, 2H, Ar-H), 8.6 (m, 2H, Ar-H) ppm. (where s = singlet)

2.2.1.3. 1-ethoxysilatrane

1-ethoxysilatrane was prepared using a similar procedure to that described in 2.2.1.1, however a large excess of benzene was added to act as an azeotropiser. A mixture of tetraethylorthosilicate (8.33g, 0.04mol), triethanolamine (5.69g, 0.04mol) and benzene (20mL) were heated (~70°C) in a flask fitted with a Dean-Stark apparatus; the benzene-ethanol azeotrope produced was removed as formed. The product was recrystallised twice from toluene and then chloroform to give a yellow solid in 73 % yield.

Chemical Equation:

$$(CH_3CH_2O)_4Si + (HOCH_2CH_2)_3N \xrightarrow{C_6H_6} CH_3CH_2OSi(OCH_2CH_2)_3N$$

^{1}H NMR ($CDCl_3$-d_6, 300 MHz): δ 1.10 (t, 3H, J = 6 Hz, CH_3–), 2.6 (t, 6H, J = 4 Hz, CH_2–N), 3.9 (m, 2H, CH_2–O), 3.9 (m, 6H, O–CH_2) ppm.

2.2.1.4. 1-chlorosilatrane

1-chlorosilatrane was prepared following the procedure of Kazakova *et al.*[101]

1-ethoxysilatrane (220mg, 1mmol) was reacted with excess thionyl chloride (0.4mL, 5mmol) under a nitrogen atmosphere for 4 hours. The excess thionyl chloride was removed under reduced pressure, and the product recrystallised from DCM and recovered as a white powder in 80% yield.

Chemical Equation:

$$CH_3CH_2OSi(OCH_2CH_2)_3N + SOCl_2 \longrightarrow ClSi(OCH_2CH_2)_3N$$

^{1}H NMR ($CDCl_3$-d_6, 300 MHz): 2.55 (t, 6H, J = 7 Hz, CH_2–N), 3.9 (m, 6H, O–CH_2) ppm.

2.2.2. Synthesis of Silatrane Ligands

2.2.2.1. Attempted Direct Linkage of Silatrane to *bipy*: Grignard Method

In a 250mL two-neck round bottom flask* fitted with a reflux condenser, a rubber septum and a stir bar, a mixture of 1-ethoxysilatrane (1.33g, 6mmol), anhydrous THF (10mL) , freshly washed magnesium turnings (121.5mg, 5mmol) and a small crystal of iodine[#] was heated to 70°C under a nitrogen atmosphere. Then, a concentrated THF solution containing 4,4'-dibromo-2,2'-bipyridine (314mg, 1mmol) was added dropwise via syringe over half an hour. The mixture was allowed to reflux for an additional 3 hours. The solvent was removed under reduced pressure, and hexane (30mL) added to the crude product. The resulting mixture was filtered, and an off-white precipitate formed within a day. Spectroscopic examination (NMR, IR) of the white precipitate indicated that starting material was isolated.

* glassware was flame dried before use.

[#] the same method was used with dibromoethane (375mg, 2mmol).

2.2.2.2. Attempted Direct Linkage of Silatrane to *bipy*: Palladium Method

Anhydrous toluene (33 mL) containing 4,4'-dibromo-2,2'-bipyridine (500mg, 1.6mmol), 1-ethoxysilatrane (1.5g, 7mmol), triethylamine (1.0mL, 7mmol), triphenylphosphine (2.1 g, 8mmol) and $Pd(PPh_3)_4$ (0.37 g, 0.32 mmol) were refluxed for 18 h under nitrogen. The solution was filtered and distilled. A milky-white liquid product was isolated. Spectroscopic examination (NMR) of the milky-white liquid indicated that starting material was isolated.

2.2.2.3. Attempted Direct Linkage of Silatrane to *bipy*: Butyl-lithium Method

An attempt was made to synthesise 4,4'-disilatrane-2,2'-bipyridine following the procedure of Reidmiller *et al.*[102] with some modification.

In a 100mL two-neck round bottom* flask fitted with two rubber septums and a stir bar under a nitrogen atmosphere, a solution of 4,4'-dibromo-2,2'-bipyridine (100mg, 0.32mmol) in anhydrous diethyl ether (5mL), a solution of *n*-butyllithium in hexane (0.2mL, 1.567M, 0.32mmol) was added dropwise while cooling to –78°C. The resulting solution was stirred and maintained at –78°C for 1 hour. A pre-cooled (–78°C) solution of 1-ethoxysilatrane (140mg, 0.64mmol) in anhydrous diethyl ether (5mL) was added to the former solution slowly via cannula. The resulting solution was stirred and maintained at –78°C for 1 hour, after which the solution was allowed to warm to room temperature. The solvent was evaporated and pentane (5mL) added to the residue. The solution was filtered and the product isolated by distillation. A yellow liquid product was isolated. Spectroscopic examination (NMR) of the yellow liquid indicated the presence of aromatic and silatrane peaks, although not in correct ratios.
*glassware was flame dried before use.

2.2.2.4. Attempted Direct Linkage of Silatrane to *bipy*: 1-chlorosilatrane

An attempt was made to synthesise 4,4'disilatrane-2,2'-bipyridine following the procedure of Anderson *et al.*[103] with some modification.

In a 100mL two-neck round bottom* flask fitted with two rubber septums and a stir bar under a nitrogen atmosphere, a solution of 4,4'-dibromo-2,2'-bipyridine (100mg, 0.32mmol) in anhydrous diethyl ether (5mL), a solution of *n*-butyllithium in hexane (0.2mL, 1.567M, 0.32mmol) was added dropwise while cooling to –78°C. The resulting solution was stirred and maintained at –78°C for 1 hour. A pre-cooled (–78°C) solution of 1-chlorosilatrane (133mg, 0.64mmol) in anhydrous

diethyl ether (15mL) was added to the former solution slowly via cannula. The resulting solution was stirred and maintained at –78°C for 1 hour, after which the solution was allowed to warm to room temperature. The solution was filtered and the product isolated by distillation. A yellow-brown liquid product was isolated. Spectroscopic examination (NMR) of the liquid indicated that only the starting materials had been recovered.

*glassware was flame dried before use.

2.2.2.5. N-(trimethylsilyl)pyridine-3-carboxamide

N-(trimethylsilyl)pyridine-3-carboxamide was prepared following the procedure of Gilg *et al.*[104-105]

A mixture of nicotinamide (250mg, 2mmol), chlorotrimethylsilane (224mg, 2mmol), and hexamethyldisilizane (2mL) were refluxed for five hours. A pale yellow powder was isolated in 65% yield.

Chemical Equation:

$$[C_5H_4N.CONH_2] + ClSi(CH_3)_3 \xrightarrow{[(CH_3)_3Si]_3NH} [C_5H_4N(CONSi(CH_3)_3)]$$

^{1}H NMR (DMSO-d_6, 300 MHz): -0.1 (s, 3H, J = 6 Hz, CH_3–Si), 0.1 (s, 3H, CH_3–Si), 0.3 (s, 3H, CH_3–Si), 7.23 (m, 1H, Ar–H), 8 (m, 1H, Ar–H), 8.6 (dd, 1H, J = 5 Hz, 4.5Hz, Ar–H), 8.9 (d, 1H, J = 3 Hz, Ar–H) ppm. (where d = doublet and dd = doublet of doublets)

2.2.2.6. Attempted Amide Linkage: 1-chlorosilatrane

An attempt was made to synthesise N-(1-silatranyl)nicotinamide following the procedure of Gilg *et al.*[104-105] with some modification.

A mixture of nicotinamide (125mg, 2mmol), 1-chlorosilatrane (214mg, 1mmol), and hexamethyldisilizane* (2mL) were refluxed for five hours. A brown powder was isolated, which on spectroscopic examination (NMR) was identified as starting material was isolated.

*The same method was used with toluene, benzene and chlorobenzene with similar results.

2.2.2.7. 4,4'-di(trimethylsilyl)-2,2'-bipyridine

4,4'-di(trimethylsilyl)-2,2'-bipyridine was synthesised following the procedure of Anderson *et al*.[103] with some modification.

In a 100mL two-neck round bottom* flask fitted with two rubber septums and a stir bar under a nitrogen atmosphere, a solution of 4,4'-dibromo-2,2'-bipyridine (100mg, 0.32mmol) in anhydrous diethyl ether (5mL), a solution of *n*-butyllithium in hexane (0.2mL, 1.567M, 0.32mmol) was added dropwise while cooling to –78°C. The resulting solution was stirred and maintained at –78°C for 1 hour. A pre-cooled (–78°C) solution of TMS-Cl (70mg, 0.64mmol) in anhydrous diethyl ether (15mL) was added to the former solution slowly via cannula. The resulting solution was stirred and maintained at –78°C for 1 hour, after which the solution was allowed to warm to room temperature. The solution was filtered and the product isolated by distillation. A yellow-brown liquid product was isolated. Spectroscopic examination (NMR) of the liquid indicated that 4,4'-di(trimethylsilyl)-2,2'-bipyridine was isolated in 12% yield.

*glassware was flame dried before use.

Chemical Equation:

$$[C_5H_3BrN]_2 \xrightarrow[(CH_3CH_2)_2O]{\text{1.BuLi 2. ClSi(CH}_3)_3} [C_5H_3N(Si(CH_3)_3)]_2$$

^{1}H NMR (DMSO-d_6, 300 MHz): 0.4 (s, 9H, CH_3–Si), 7.2 (d, 1H, J = 3.5 Hz, Ar–H), 7.6 (d, 1H, J = 3 Hz, Ar–H), 8.5 (m, 2H, Ar–H), 8.7(s, 2H, Ar–H) ppm.

2.2.2.8. Attempted Ester Linkage: 1-ethoxysilatrane

An attempt was made to synthesise 4,4'-dicarboxysilylestersilatrane-2,2'-bipyridine following the procedure of Chen *et al*.[106] with some modification.

In a two neck round bottom flask fitted with a Dean-Stark *dcbipy* (100mg, 0.4mmol), 1-ethoxysilatrane (90mg, 0.4mmol) and chlorobenzene (5mL) were refluxed for 3 hours under nitrogen. The ethanol and chlorobenzene were removed by azeotropic distillation. The pale yellow precipitate that formed was recrystallised from a 1:1 DCM/hexane solution. However, spectroscopic examination (NMR, IR) indicated that only starting material was isolated.

2.2.2.9. 2,2'-bipyridine-4,4'-(diethyl phosphonate) (*depbipy*)

2,2'-bipyridine-4,4'-(diethyl phosphonate) was synthesised following the procedure of Kanaizuka.[12]

A mixture of anhydrous toluene (33mL), 4,4'-dibromo-2,2'-bipyridine (1.00g, 3.17mmol), triethylphosphite (1.86mL, 14mmol), triethylamine (2.0mL, 14mmol), triphenylphosphine (4.17g, 16mmol) and $Pd(PPh_3)_4$ (0.73g, 0.64mmol) were refluxed for 14 hours under nitrogen. The mixture was transferred to a separating funnel and washed with aqueous ammonia (1M, 15mL) and then with Milli-Q water (15mL), and dried over $MgSO_4$. The solvent was removed under vacuum and the product purified by column chromatography on silica gel (99 CH_2Cl_2/ 1 CH_3OH), to give a white powder in 76% yield.

Chemical Equation:

$$[C_5H_3BrN]_2 \xrightarrow[Pd(PPh_3)_4,\ (C_6H_5)CH_3]{(CH_3CH_2)_3N,\ (CH_3CH_2O)_3P,\ (C_6H_5)_3P} [C_5H_3N(PO(OCH_2CH_3)_2]_2$$

IR (KBr): ν = 3455 (b), 2149 (m), 1968 (m), 1637 (s), 1435 (s), 1398 (s), 1365 (s), 1227 (m), 1043 (m), 567 (m) cm^{-1}

^1H NMR ($CDCl_3$, 300 MHz): δ 1.37 (t, 12H, J = 6 Hz, $–CH_3$), 4.20 (m, 8H, $–CH_2–$), 7.28 (s, 2H, Ar–H), 7.73 (dd, 2H, J = 4 Hz, 4.5Hz, Ar–H), 8.82 (m, 2H, Ar–H) ppm.

2.2.3. Preparation of Copper(I) and (II) Ophen complexes

2.2.3.1. Synthesis of $[Cu^{(I)}_2(Ophen)_2]$ (1) and the Cu(II) intermediates $[Cu^{(II)}(phen)_2(H_2O)] . (NO_3)_2$ (2) and $[Cu^{(II)}_2(Ophen)_2(phen)_2] . (NO_3)_2 . 9H_2O$ (3)

$[Cu^{(I)}_2(Ophen)_2]$ **(1)** was synthesised, as described below, following the procedure of Zhang,[107] with some modification.

A mixture of $Cu(NO_3)_2.3H_2O$ (0.12g, 0.5mmol), 1,10-phenanthroline (0.162g, 0.9mmol) and water (Milli-Q, 10mL) was adjusted to pH 9 with 2M NaOH solution. The blue suspension was then sealed in a Teflon-lined stainless steel autoclave (20mL)*, heated at 150°C for 120 hours under autogeneous pressure, and then allowed to cool slowly in the oven for 6 hours. This synthesis was repeated several times. The expected dark-blue block-like crystals of $[Cu^{(I)}_2(Ophen)_2]$ **(1)** were isolated from an emerald-green supernatant, on a number of occasions. However, in several cases only an emerald-green solution, similar in appearance to the supernatant from $[Cu^{(I)}_2(Ophen)_2]$, was obtained. This was stored in a sealed glass vial and allowed to crystallise at ambient temperature, yielding a mixture of light-green, $[Cu^{(II)}(phen)_2(H_2O)](NO_3)_2$ **(2)** (21% Yield), and emerald-green, $[Cu^{(II)}_2Ophen)_2(phen)_2] (NO_3)_2 . 9H_2O$ **(3)** (4% Yield), crystals after 7 days. The crystals were separated manually, whilst viewing under an optical microscope.

***** This type of vessel was used for all hydrothermal reactions. It is a stainless steel screw-top autoclave, which contains a Teflon cup lining, including a lid which holds approximately 20mL of solution, see Figure 2-1. The appropriate mixture is added to

the Teflon cup in the autoclave, the Teflon lid is then placed on top and finally the screw-top lid of the autoclave screwed on. The autoclave is then placed into a pre-heated oven under autogeneous pressure, for several days. The autoclave is cooled slowly in the oven before being opened.

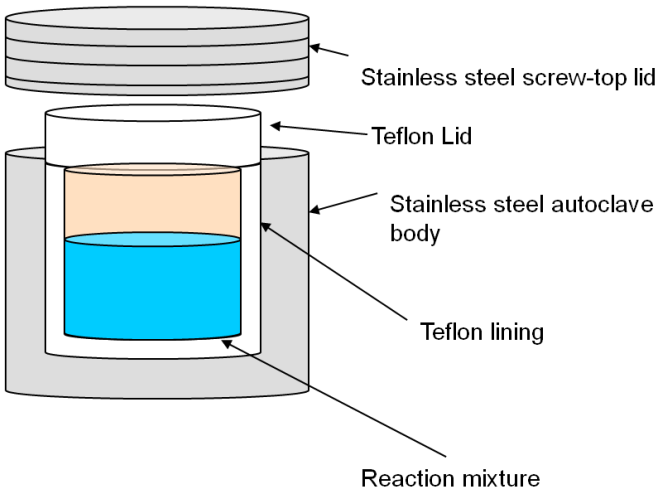

Figure 2-1 Schematic of Autoclave

Chemical Equation: See Scheme 3-5.

FT-IR data: See section 3.3.1 for a detailed discussion and interpretation.

$[Cu^{(I)}{}_2Ophen)_2]$ **(1)**: IR (KBr): *v* = 3415 (m), 1620 (s), 1562 (s), 1512 (s), 1485 (s), 1384 (s), 1128 (m), 843 (s), 731 (m) cm^{-1}.

$[Cu^{(II)}(phen)_2(H_2O)](NO_3)_2$ **(2)**: IR (KBr): *v* = 3407 (m), 1519 (s), 1428 (s), 1385 (s), 862 (s), 722 (m) cm^{-1}.

$[Cu^{(II)}{}_2(Ophen)_2(phen)_2]$ **(3)**: IR (KBr) : *v* = 3413 (m), 1621 (s), 1517 (s), 1483 (s), 1384 (s), 847 (m), 720 (b) cm^{-1}.

2.2.4. Preparation of complexes of Copper(I) and (II) with *dpk* and ligands derived from *dpk*

2.2.4.1. Synthesis of $[Cu^{(I)}(dpk)(NCS)]_n$ (4)/(5) and $[Cu^{(II)}_2(dpk.acetone)_2(NCS)_2]$ (6)

CuSCN (0.12g, 1mmol) and NaSCN (0.81g, 10mmol) were dissolved in a 1:3 aqueous-acetone (20mL) solution. The resulting pink solution was filtered, and to this *dpk* (0.37g, 2mmol) in acetone (5mL) was added. The mixture was stirred and heated gently (approx. 40°C) for 10 minutes. A combination of black block-like and black needle-like crystals, $[Cu^{(I)}(dpk)(NCS)]_n$ **(4)/(5)** were isolated from a purple-red supernatant in 70% yield within 2 hours. When $[Cu^{(I)}(dpk)(NCS)]_n$ was left to stand in the supernatant at ambient temperature for three days, large green block crystals of $[Cu^{(II)}_2(dpk.acetone)_2(NCS)_2]$ **(6)** formed in 15% yield, and the supernatant changed to a dark green colour.

Chemical Equation: See Scheme 4-1.

FT-IR data: See section 4.3.1.2 for a detailed discussion and interpretation

$[Cu^{(I)}(dpk)(NCS)]_n$ **(4)/(5)**: IR(KBr): ν = 3426 (m), 2091 (s), 1685 (s), 1581 (s), 1304 (s), 1278 (s), 935 (s) 750 (s), 663 (s) cm^{-1}.

$[Cu^{(II)}_2(dpk.acetone)_2(NCS)_2]$ **(6)**: IR(KBr): ν = 3420 (m), 2075 (s), 1711 (b), 1594 (s), 1465 (s), 1432 (s), 1101 (s), 1090 (s), 760 (m), 557 (s) cm^{-1}.

2.2.4.2. Synthesis of $[Cu^{(I)}_2(dpk)_2I_2]$ (7)

$[Cu_2(dpk)_2I_2]$ **(7)** was prepared using the same procedure as 2.2.4.1, except CuI (0.19g, 1mmol) and KI (1.66g, 10mmol) were used in place of CuSCN and NaSCN. A red-brown solution formed when CuI and KI were dissolved in the aqueous-acetone solution (20mL), and black block crystals were isolated from a brown supernatant in 60% yield after standing overnight.

Chemical Equation: See Scheme 4-3.

FT-IR data: See section 4.3.3.1 for a detailed discussion and interpretation.

$[Cu^{(I)}_2(dpk)_2I_2]$ **(7)**: IR(KBr): ν = 3414 (m), 1662 (s), 1579 (s), 1304 (s), 1276 (s), 1009 (s), 934 (s) 746 (s) 662(s)

2.2.4.3. Synthesis of $[Cu^{(II)}(dpk)_2(NCS)_2]$ (8) and $[Cu^{(II)}(dpk.H_2O)_2](NCS)_2$ (9)

$[Cu^{(II)}(dpk)_2(NCS)_2]$ **(8)** and $[Cu^{(II)}(dpk.H_2O)_2](NCS)_2$ **(9)** were prepared using the same procedure as 2.2.4.1, except methyl ethyl ketone (MEK) was used in place of acetone. A brown solution formed when CuNCS and NaNCS were dissolved in a 1:6 aqueous-MEK solution (20mL) (Note - MEK does not have the same miscibility in water as acetone and therefore the same solvent ratio could not be used as in 2.2.4.1). A combination of green block-like crystals of $[Cu^{(II)}(dpk)_2(NCS)_2]$ **(8)** in a 5% yield, and purple block-like crystals of $[Cu^{(II)}(dpk.H_2O)_2](NCS)_2$ **(9)** in a 50% yield, were isolated within one week, as the supernatant changed colour to green.

Chemical Equation: See Scheme 4-4.

FT-IR data: See section 4.3.5.2 for a detailed discussion and interpretation.

$[Cu^{(II)}(dpk)_2(NCS)_2]$ **(8)**: IR(KBr): ν = 3459 (b), 2060 (s), 1626 (m), 1310 (s), 1282 (s), 939 (s), 757 (s), 686 (s), 667 (s) cm^{-1}.

$[Cu^{(II)}(dpk.H_2O)_2](NCS)_2$ **(9)**: IR(KBr): ν = 3464 (b), 2086 (s), 2051 (s), 1681 (s), 1597 (s), 1309 (s), 1282 (s), 934 (s), 757 (s), 687 (s), 668 (s) cm^{-1}.

2.2.4.4. Synthesis of $[Cu^{(II)}(pic)_2]Na_2(NCS)_2.2H_2O$ (10), $Na_2[Cu^{(II)}(pic)_2(NCS)_2](H_2O)_2$ (11) and $[Cu^{(II)}(pic)_2]\cdot Na_2[Cu^{(II)}(pic)_2(NCS)_2]$ (12)

$[Cu^{(II)}(pic)_2]Na_2(NCS)_2.2H_2O$ **(10)**, $Na_2[Cu^{(II)}(pic)_2(NCS)_2](H_2O)_2$ **(11)** and $[Cu^{(II)}(pic)_2]\ Na_2\ [Cu^{(II)}(pic)_2(NCS)_2]$ **(12)** were prepared using the same procedure as 2.2.4.1, except acetophenone was used in place of acetone, and the crystals were isolated from two different experiments. A brown solution formed when CuNCS and NaNCS were dissolved in a 1:20 aqueous-acetophenone solution (20mL) (Note - acetophenone is only slightly miscible in water therefore the ratio was adjusted to 1:20). The resulting brown solution was filtered, and to this *dpk* (0.37g, 2mmol) in acetophenone (5mL) was added. The mixture was stirred and heated gently (approx. 60°C) for 10 minutes. A combination of blue prism crystals of $[Cu^{(II)}(pic)_2]Na_2(NCS)_2.2H_2O$ **(10)** and $Na_2[Cu^{(II)}(pic)_2(NCS)_2](H_2O)_2$ **(11)** in an *in-situ* 1% yield were isolated within five weeks from a brown supernatant (The crystals could not be separated, and differences between crystals could only be identified through single-crystal XRD, therefore the yield was calculated by averaging the total mass between the two molecular weights. The ratio between the two crystals is unknown; hence the yield is only an estimate.). In a separate experiment, blue block-like crystals of $[Cu^{(II)}(pic)_2]\ Na_2\ [Cu^{(II)}(pic)_2(NCS)_2]$ **(12)** were isolated within three months in 2% yield from a brown supernatant.

Chemical Equation: See Scheme 4-9.

FT-IR data: See section 4.3.6.1 for a detailed discussion and interpretation.

$[Cu^{(II)}(pic)_2]Na_2(NCS)_2.2H_2O$ **(10)** and $Na_2[Cu^{(II)}(pic)_2(NCS)_2](H_2O)_2$ **(11)**: IR(KBr): ν = 3456 (b), 2075 (s), 1650(s), 1606(s), 1380(s), 1362(s), 1296(s), 1051(s), 767(s), 695(s) cm^{-1}.

$[Cu^{(II)}(pic)_2]$ Na_2 $[Cu^{(II)}(pic)_2(NCS)_2]$ **(12)**: IR(KBr): ν = 3461 (b), 2084 (s), 2062 (s), 1640 (s), 1596 (s), 1446 (s), 1362 (s), 1270 (s), 1220 (s), 1095 (s), 1039 (s), 757 (s), 688 (s) cm^{-1}.

2.2.5. Preparation of complexes of Ruthenium (II) with bipy and ligands based on bipy.

2.2.5.1. Synthesis of *cis*- $[Ru(bipy)_2Cl_2]$

$[Ru(bipy)_2Cl_2]$ was synthesised following the procedure of Sprintschnik *et al*.[108]

$RuCl_3.xH_2O$ (1.95g, 9.4mmol) and *bipy* (2.34g, 14.98mmol) were refluxed in anhydrous DMF (75mL) under N_2 for 3 hours. Most of the solvent was distilled off and the resulting solution was cooled slowly overnight. The cooled solution was treated with acetone (75mL) and kept at 0°C overnight. The solution was filtered and the precipitate suspended in a 1:1 aqueous-ethanol solution (150mL) and refluxed for 1 hour, the solution was filtered from insoluble materials, and then excess lithium chloride (5g, 118mmol) was added to the filtrate. The ethanol was distilled off and the aqueous solution placed in an ice-bath until a precipitate formed. A dark red-purple microcrystalline product was isolated in 65-70% yield.

Chemical Equation: Scheme 5-2

IR(KBr): ν = 3460 (b), 1602 (s), 1465 (s), 1445 (s), 1441 (s), 1315 (s), 1268 (s), 1159 (s), 1019 (s), 769 (s) cm^{-1}.

^{1}H NMR (D_2O/DMSO-d_6, 300 MHz): δ 7.47 (d, 4H, J = 4Hz, Ar–H), 7.99 (m, 8H, Ar–H), 8.40 (d, 4H, J = 3.5Hz, Ar–H) ppm.

2.2.5.2. Synthesis of [Ru(*bipy*)$_2$(*dcbipy*)](PF$_6$)$_2$ (13)

Two synthetic methods were investigated for the synthesis of [Ru(*bipy*)$_2$(*dcbipy*)](PF$_6$)$_2$.

The first [Ru(*bipy*)$_2$(*dcbipy*)](PF$_6$)$_2$ synthesis followed the procedure of Browne *et al*.[109]

[Ru(*bipy*)$_2$Cl$_2$] (260mg, 0.5mmol) and *dcbipy* (122mg, 0.5mmol) were refluxed under subdued light in a 1:1 aqueous-ethanol solution (20mL) for four hours. The red reaction mixture was cooled to room temperature and filtered. To the filtrate a saturated NH_4PF_6 solution (2mL) was added. The resulting solution was acidified to pH 2, and the precipitate collected and washed with diethyl ether and recrystallised from a 1:1 aqueous-methanol solution. A red microcrystalline product was isolated in 58% yield.

The second, and higher yielding, [Ru(*bipy*)$_2$(*dcbipy*)](PF$_6$)$_2$ synthesis followed the procedure of Terpetschnig *et al*.[110]

[Ru(*bipy*)$_2$Cl$_2$] (200mg, 0.4mmol), *dcbipy* (150mg, 0.6mmol) and $NaHCO_3$ (200mg, 2.4mmol) were refluxed in a 1:4 aqueous-methanol solution for 8 hours. The solution was cooled in an ice-bath and the pH adjusted to 4 with H_2SO_4 (2M). The precipitate was filtered, and to the filtrate a saturated NH_4PF_6 solution (2mL) was added, this was then cooled in an ice-bath. A red microcrystalline product was isolated in 71% yield.

Chemical Equation: Scheme 5-2

FTIR data: See Section 2.2.6 for a detailed discussion.

IR(KBr): ν = 3463 (b), 2936 (m), 1739 (s), 1608 (m), 1470 (s), 1449 (s), 1236 (m), 850 (s), 764 (s), 559 (s) cm^{-1}.

A minimum of 128 scans was collected for each of the ^{1}H NMR spectra, due to the complexes being sparingly soluble in the deuterated solvents. Consequently the ^{13}C NMR data obtained was quite poor due to the extremely high signal to noise ratio and has not been included. The solvent peaks in all of the spectra are due to a ^{1}H impurity in $CDCl_3$: ($CHCl_3$ δ=7.26 ppm), d_6-DMSO (HDMSO δ=2.50 ppm), and D_2O (HDO δ=4.79 ppm), have been removed and where possible an additional smoothing process has been applied to reduce the background noise.

For identification purposes, the protons on *dcbipy* and *bipy* have been labelled as in Figures 2-2 and 2-3 respectively.

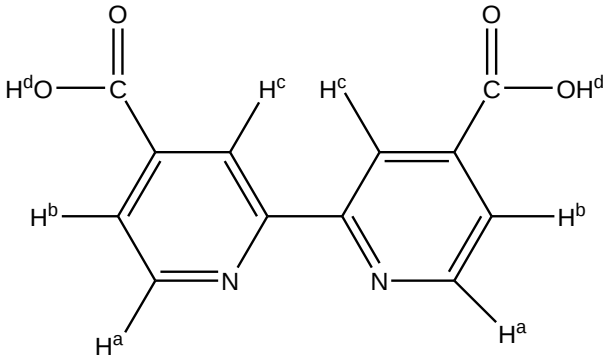

Figure 2-2 Location of protons on *dcbipy*

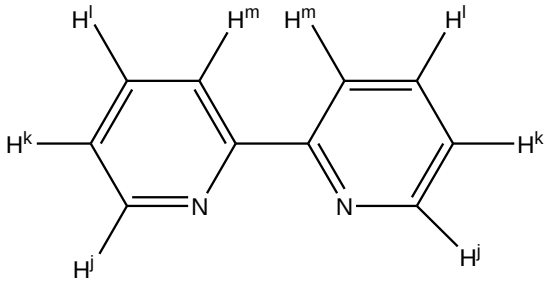

Figure 2-3 Location of protons on *bipy*

The ^{1}H NMR spectrum of complex **(13)**, $[Ru(bipy)_2(dcbipy)](PF_6)_2$, in both D_2O and DMSO-d_6 (see Figure 2-4 for full spectrum), shows five distinct sets of peaks in the aromatic region of the spectrum δ7-9 ppm, which correspond to all the protons on the *bipy* and *dcbipy* ligands.

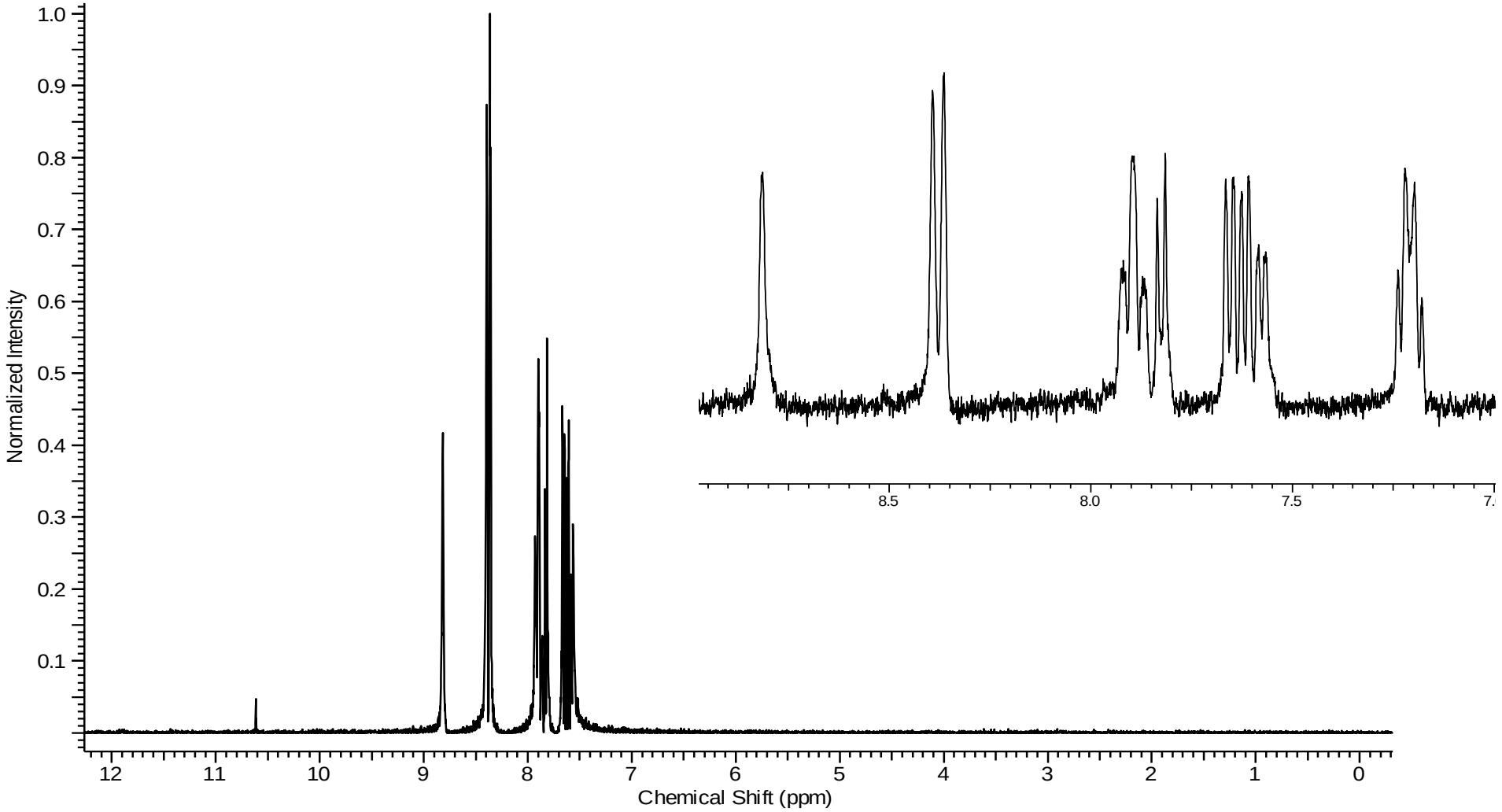

Figure 2-4 ^{1}H NMR of [Ru(*bipy*)$_2$(*dcbipy*)](PF$_6$)$_2$ **(13)**

The aromatic peaks appear to be a series of triplets and quartets as well as one singlet peak. The singlet peak at δ8.82 ppm is assigned to the proton, H^c, on the *dcbipy* ligand. When compared to the spectrum of the uncoordinated *dcbipy* ligand, the singlet peak in the complex shifted to δ7.91 ppm; indicating that an upward chemical shift has occurred when the ligand becomes coordinated. The remaining peaks overlap one another therefore making it difficult to separate and identify which are due to protons on the bipy ligand or the *dcbipy* ligand. The high chemical shift of the aromatic protons is characteristic of shifts influenced by nitrogen in the pyridine ring.

There is also a small peak at δ10.60 ppm which may arise from the proton H^d, located on the carboxylic acid. The integrated area of this peak compared to the aromatic region area, is substantially less than expected (in total there are 24 protons in this complex, two of which are from the carboxylic acid, therefore these protons should contribute to 8.3% of the total area, however this was not found to be the case with only 1% of the total area arising from this peak, the low area may be due to deprotonation). The ^1H NMR data for complex **(13)** is summarised in Table 2-1.

Table 2-1 Assigned protons for complex **(13)**

Proton*	Chemical Shift (ppm)	Splitting	Coupling Constant (Hz)
H^a	7.82	doublet	7
H^b	7.65	doublet	6
H^c	8.82	singlet	n/a
H^d	10.6	singlet	n/a
H^j	8.37	doublet	7
H^k	7.90	multiplet	n/a
H^l	7.90	multiplet	n/a
H^m	7.60	doublet	5

*As labelled in Figures 2-2 and 2-3.

^{1}H NMR (D_2O/ DMSO-d_6, 300 MHz): δ 7.20 (q, *J* = 5Hz, Ar–H), 7.55 (dd, *J* = 2Hz, 5Hz, Ar–H), 7.60 (d, 4H, *J* = 5Hz, Ar–H), 7.65 (d, 2H, *J* = 5Hz, Ar–H), 7.82 (d, 2H, *J* = 7Hz, Ar–H), 7.90 (m, 4H, Ar–H), 8.37 (d, 4H, Ar–H), 8.82 (s, 2H, Ar–H), 10.6 (s, 2H, –OH) ppm.

2.2.5.3. Synthesis of [Ru(*bipy*)$_2$(*dpbipy*)](PF$_6$)$_2$ (14)

[Ru(*bipy*)$_2$(*dpbipy*)](PF$_6$)$_2$ was prepared using the second method in procedure 2.2.5.2, except *depbipy* (190mg, 0.6mmol) was used in place of *dcbipy*, and $NaHCO_3$ was not added. The diethyl ester was hydrolysed by adjusting the pH to 4 with HCl (4M). A red microcrystalline product was isolated in 40% yield.

Chemical Equation: Scheme 5-2

The FT-IR spectrum of complex **(14)** shows well resolved peaks with characteristic stretching and bending bands of the phosphonate functional group. The *v*(P=O) stretching frequency bands are observed at 1024 and 1120 cm^{-1} and the δ(O-P-O) bending frequency bands at 538 cm^{-1}.[111] The aromatic stretches are also observed in the region: 1589 cm^{-1} (C=C) and 1541 cm^{-1} (C=N). A sharp intense peak at 1438cm^{-1} is due to aromatic C-H bending.

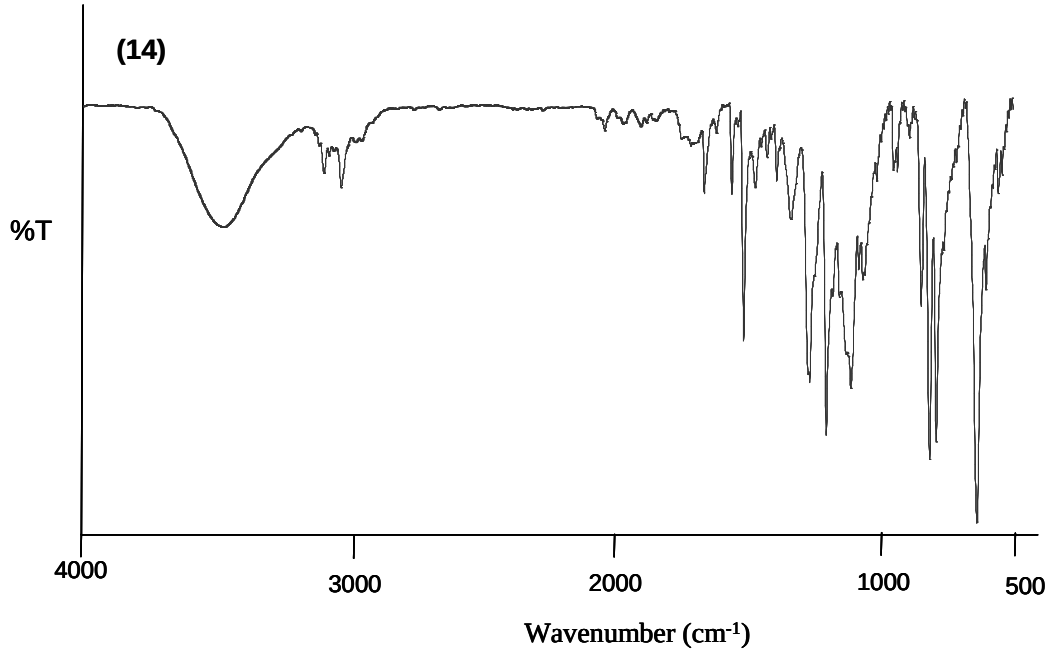

Figure 2-5 FTIR spectrum of $[Ru(bipy)_2(dcbipy)](PF_6)_2$ **(14)**

IR(KBr): *v* = 3484 (b), 2993 (m), 1891 (s), 1589 (s), 1541 (s), 1485 (s), 1439 (s), 1191 (s), 1121 (s), 1027 (s), 723 (s), 698 (s) 538 (s) cm^{-1}.

For identification purposes the protons on *dpbipy* have been labelled as in Figure 2-6.

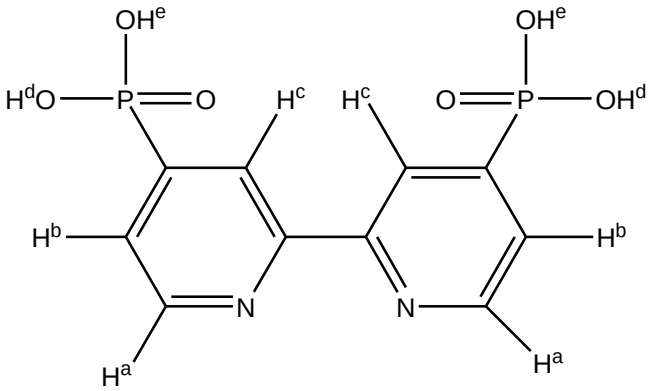

Figure 2-6 Location of protons on *dpbipy*

The ^1H NMR spectrum of complex **(14)**, $[Ru(bipy)_2(dpbipy)](PF_6)_2$ in both D_2O and DMSO-d_6 (See Figure 2-7 for full spectrum) exhibited distinctive aromatic shifts from approximately δ7-9 ppm similar to that observed in complex **(13)**. All the peaks in the aromatic region are observed as multiplets apart from one singlet at δ8.54 ppm, which is due to the proton labelled H^c, as there are no neighbouring protons to split this proton, see Figure 2-6.

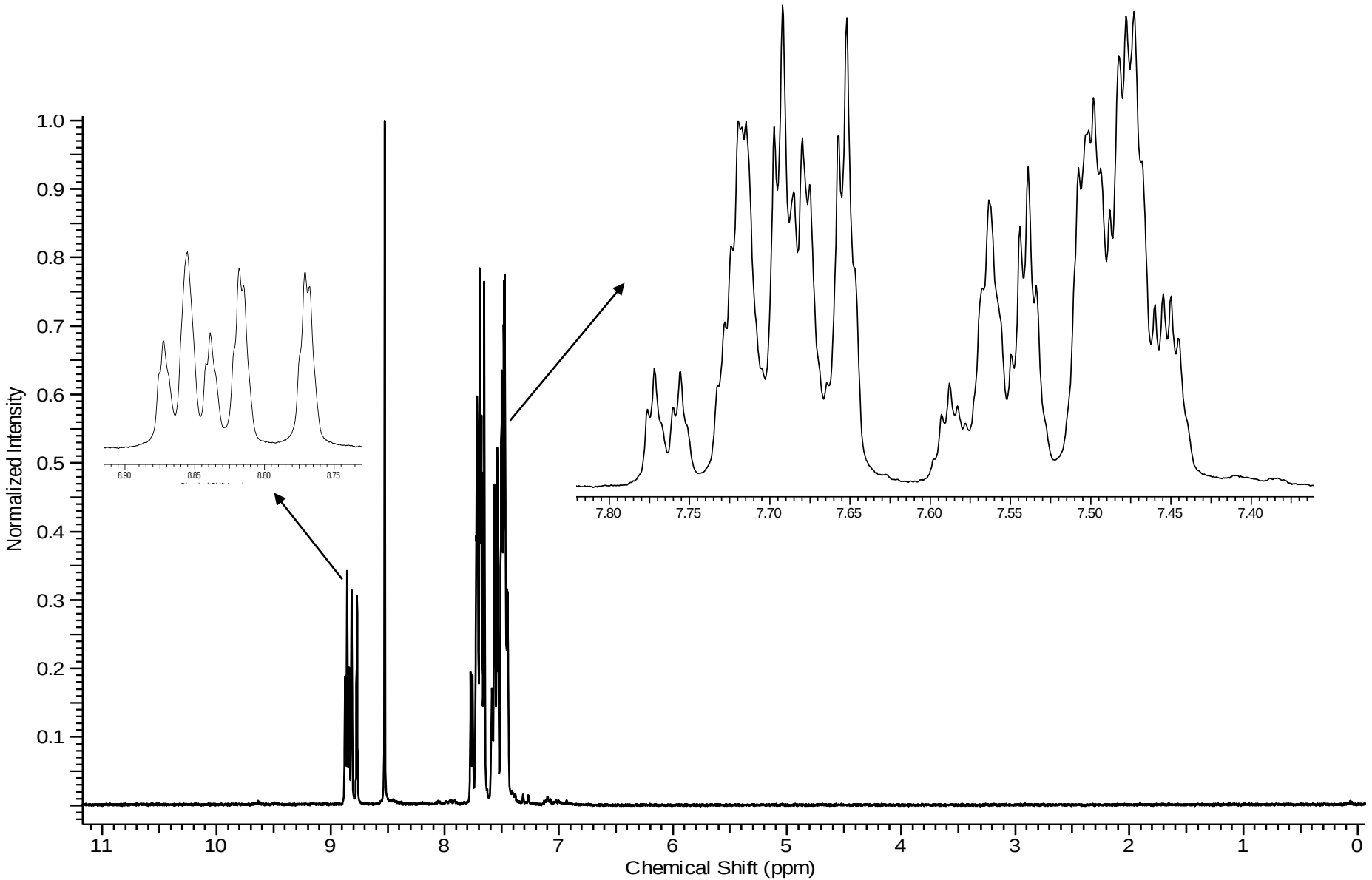

Figure 2-7 ^{1}H NMR of [Ru(*bipy*)$_2$(*dpbipy*)](PF$_6$)$_2$ **(14)**

Once again, compared to the uncoordinated *depbipy* ligand, there is an upward shift from δ7.3 ppm to δ8.54 ppm which is indicative of the *dpbipy* ligand being coordinated. Similar to the ^{1}H NMR of complex **(13)**, the aromatic region is quite complex, and in this case more so than before. Therefore the separation of protons on the *bipy* from those on the *dpbipy* is difficult. In addition to this, the two *bipy* ligands do not appear to be in the same environment due to the multiple splitting of the peaks.

At δ7.76 ppm and δ8.79 ppm there are two sets of doublets which appear in the exact same splitting order and when integrated have the exact same area, but are slightly shifted, to those observed in the uncoordinated *depbipy* ligand. This may be an influence of the phosphorus, as it was not observed in the other spectra. There is no indication of the protons located on the phosphonic acid, H^d and H^e, in the spectrum, as a chemical shift at ~ δ2 ppm would indicate their presence. This may be due to proton exchange with D_2O. See Table 2-2 for a summary of the proton NMR assignments.

Table 2-2 Assigned protons for [Ru(*bipy*)$_2$(*dpbipy*)](PF$_6$)$_2$ **(14)**

Proton*	Chemical Shift (ppm)	Splitting	Coupling Constant (Hz)
H^a	8.79	doublet of doublets	1.5, 9
H^b	7.76	doublet of doublets	2, 6
H^c	8.54	singlet	n/a
H^d	Not observed	not observed	n/a
H^e	Not observed	not observed	n/a
H^j	7.5-7.75	multiplet	n/a
H^k	8.85	triplet	6
H^l	7.5-7.75	multiplet	n/a
H^m	7.5-7.75	multiplet	n/a

*As labelled in Figures 2-3 and 2-6.

^{1}H NMR (D_2O/ DMSO-d_6, 300 MHz): δ 7.45-7.52 (m, Ar–H), 7.53-7.60 (m, Ar–H), 7.65-7.75 (m, Ar–H), 7.76 (dd, 2H, *J* = 2Hz, 6Hz, Ar–H), 8.54 (s, 2H, Ar–H), 8.79 (dd, 2H, *J* = 1.5Hz, 9Hz, Ar–H), 8.85 (t, *J* = 6Hz, Ar–H) ppm.

The ^{31}P NMR spectrum (solvents used - D_2O and DMSO) of complex **(14)** (See Figure 2-8 for spectrum from δ 100 to δ -100 ppm (Note – The PF_6^- chemical shift occurs at ~ δ -144 ppm, hence it is not displayed in the spectrum below) exhibited one peak at δ -14.26 ppm. The expected chemical shift of phosphates ($PO(OR)_3$) is from δ -10 ppm to δ -40 ppm, and the chemical shift of a phosphate with an R-group ($RPO(OR)_2$) is from δ 20 ppm to δ -20 ppm, hence the observed peak falls within these ranges.[112]

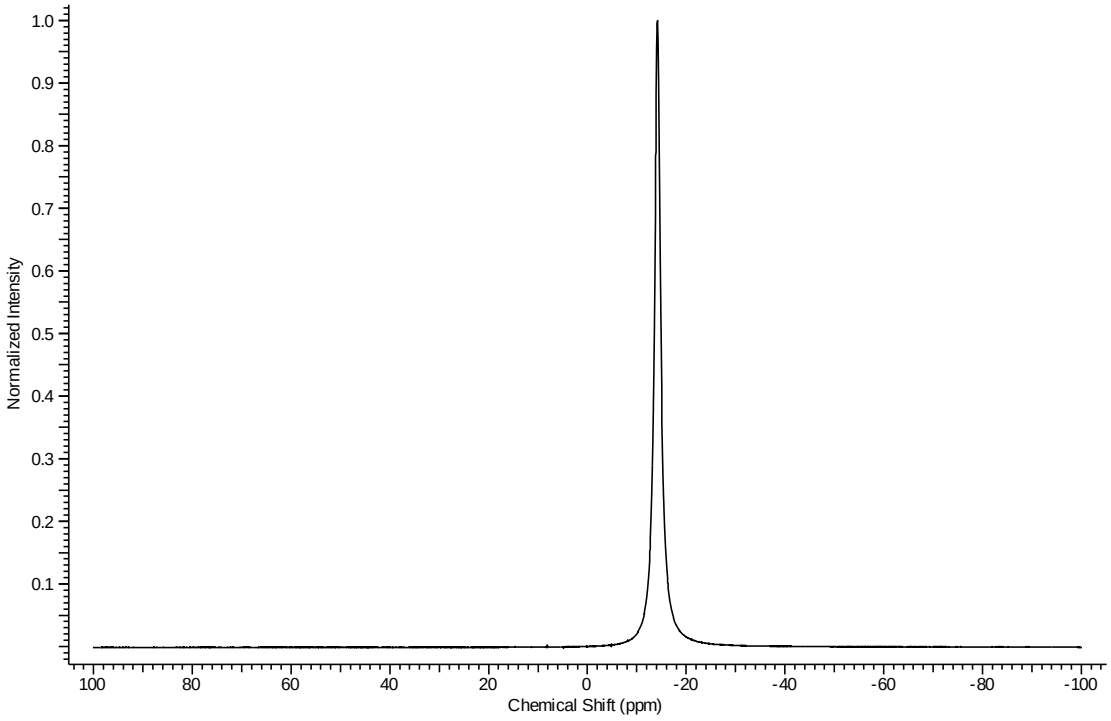

Figure 2-8 ^{31}P NMR of $[Ru(bipy)_2(dpbipy)](PF_6)_2$ **(14)**

^{31}P NMR (D_2O/ DMSO-d_6, 121.45 MHz): δ -10 (s, 2P, –P–) ppm.

2.2.5.4. Synthesis of $[Ru(bipy)_2(bipy\text{-}sil)](PF_6)_2$ (15)

$[Ru(bipy)_2(bipy\text{-}sil)](PF_6)_2$ was synthesised following the procedure of Brennan *et al.*[48]

$[Ru(bipy)_2Cl_2]$ (32mg, 0.06mmol) and *bipy-sil* (48mg, 0.07mmol) dissolved in DMF (3mL) were heated to 90°C under N_2 in subdued light for 72 hours. Most of the solvent was removed under vacuum and water (2mL) added. The resulting solution

was filtered, and to the filtrate was added a saturated NH_4PF_6 solution (0.4mL). The solution was then extracted with ethyl acetate and the solvent recovered by distillation. A red powder was isolated in 42% yield.

Chemical Equation: Scheme 5-2

FTIR data: See Section 2.2.6 for a detailed discussion.

IR(KBr): ν = 3367 (b), 2961 (m), 2896 (m), 1663 (s), 1551 (s), 1462 (s), 1277 (s), 1066 (m), 918 (s), 802 (s) cm^{-1}.

For identification purposes the protons on *bipy-sil* have been labelled as in Figure 2-9.

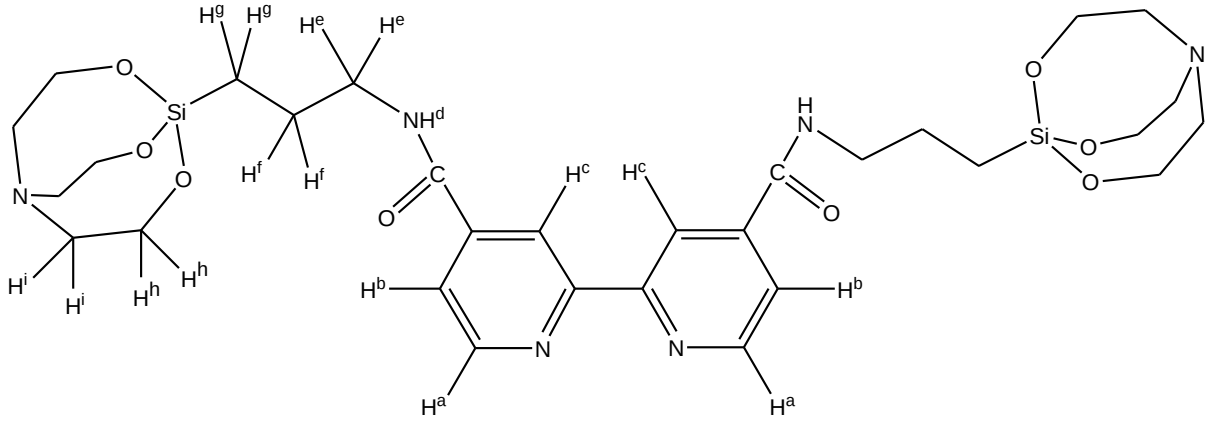

Figure 2-9 Location of protons on *bipy-sil*

The ^{1}H NMR spectrum of complex **(15)**, $[Ru(bipy)_2(bipy\text{-}sil)](PF_6)_2$ in both D_2O and DMSO-d_6 (See Figure 2-10 for full spectrum and Figure 2-11 for expanded areas), contains the expected aromatic peaks from δ 7-9 ppm, two of which appear to be singlets, and the remaining multiplets. In total, complex **(15)** contains 58 protons, 22 of which are aromatic protons (38%), and the remaining 36 from the anchoring propyl-silatrane (62%). The overall integrated area of the aromatic region was found to be 38% and the propyl-silatrane 62%, which is in excellent agreement with the expected values. However, the integrated area of the propyl protons (12 protons - ~20%) was found to be slightly lower than expected at 14%.

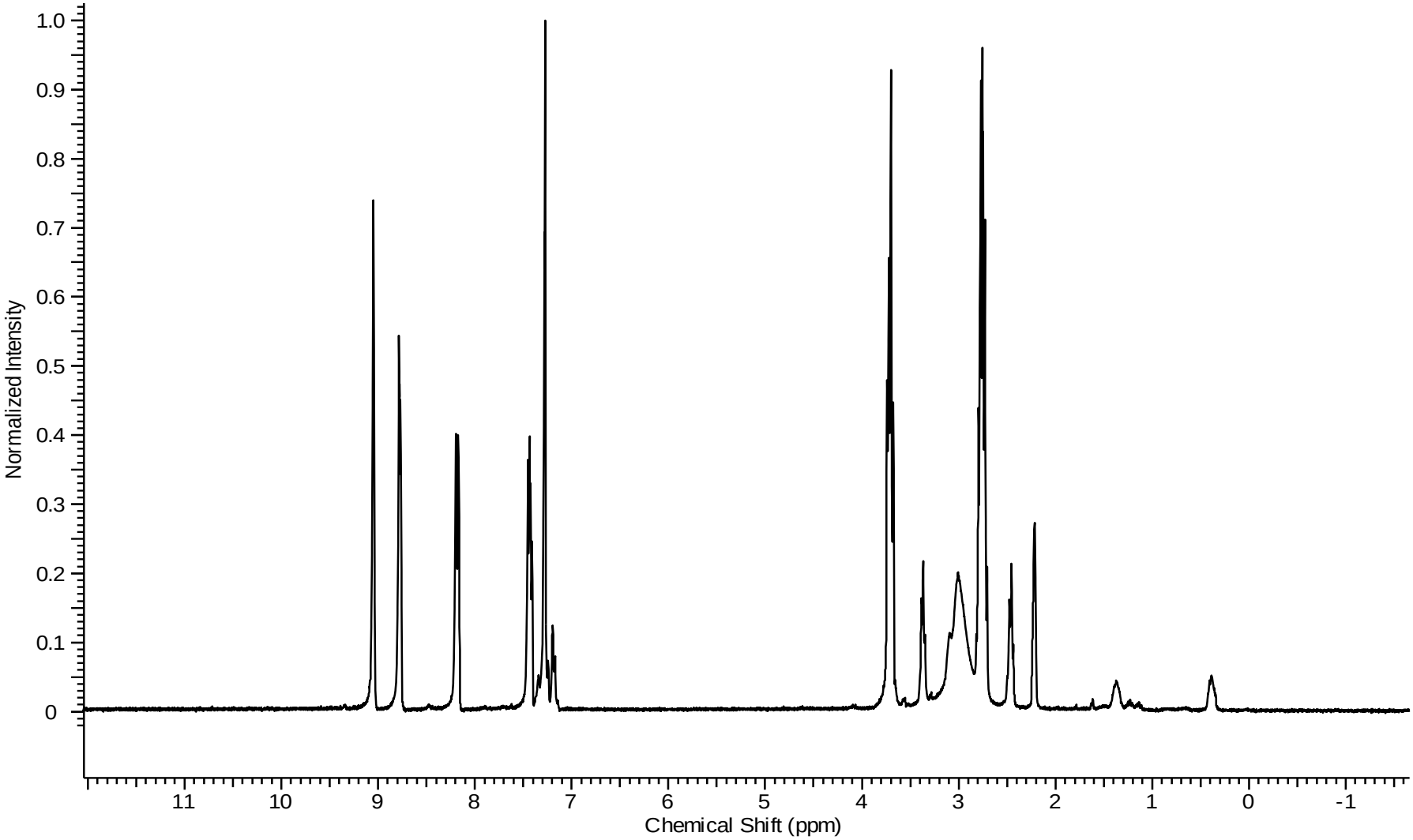

Figure 2-10 ^{1}H NMR of [Ru(*bipy*)$_2$(*bipy-sil*)](PF$_6$)$_2$ **(15)**

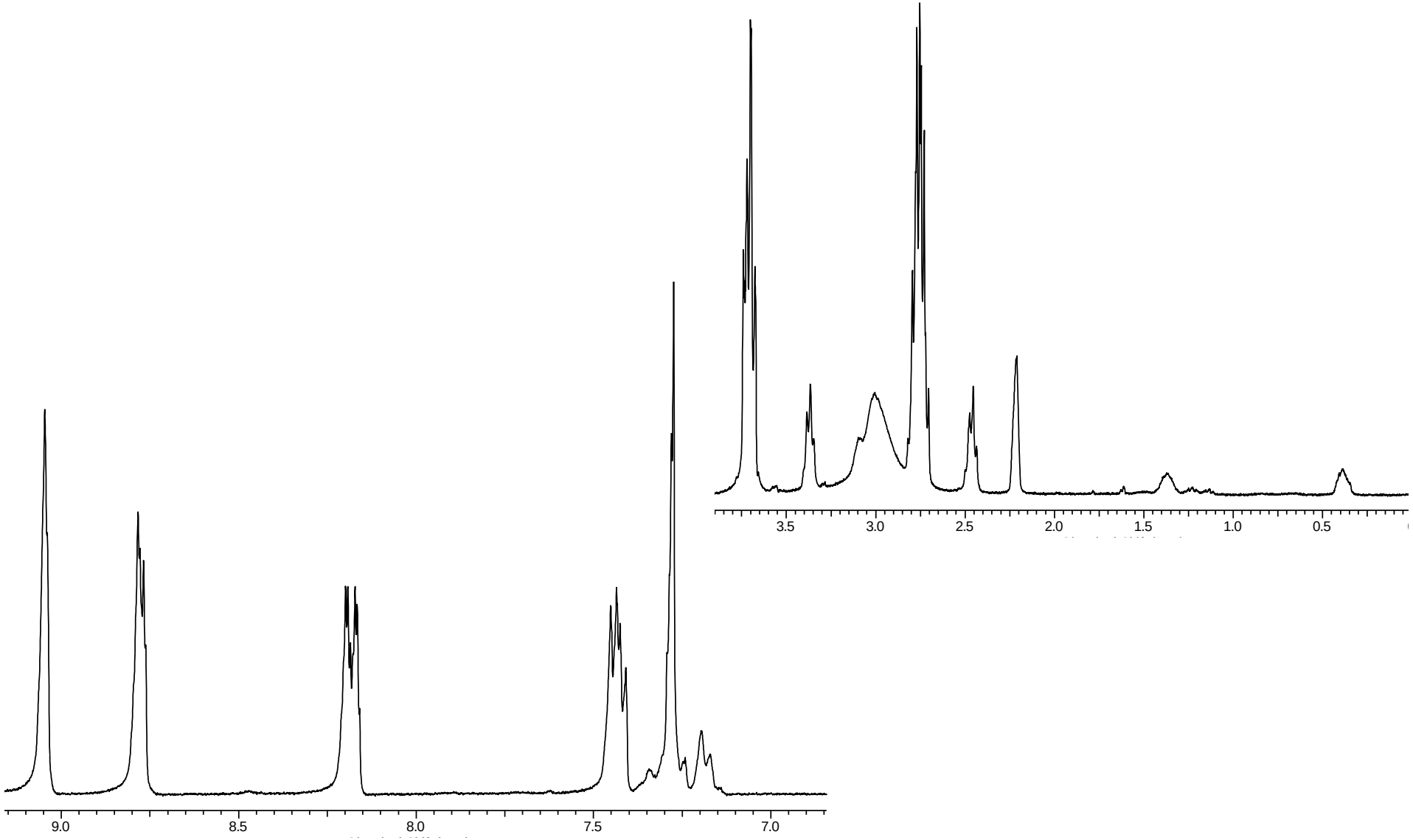

Figure 2-11 ^{1}H NMR of [Ru(*bipy*)$_2$(*bipy-sil*)](PF$_6$)$_2$ **(15)** (δ 0-4 ppm and δ 7-9.2 ppm)

There is one additional solvent peak in the spectrum which could not be removed at δ 2.23 ppm, which is due to HDMSO. See Table 2-3 for summary.

Table 2-3 Assigned protons for complex **(15)**

Proton*	Chemical Shift (ppm)	Splitting	Coupling Constant (Hz)
H^a	8.15	doublet	2
H^b	7.45	doublet	2.5
H^c	9.05	singlet	n/a
H^d	Not observed	not observed	n/a
H^e	2.75	uneven sextet	n/a
H^f	1.35	poorly split	n/a
H^g	0.30	poorly split	n/a
H^h	3.29 and 3.70	multiplet	n/a
H^i	2.45	triplet	6
H^j	8.77	multiplet	n/a
H^k	8.20	triplet	2
H^l	7.41	uneven doublet (may indicate overlap)	2
H^m	7.27	doublet	3

* As labelled in Figures 2-3 and Figure 2-9.

^{1}H NMR ($CDCl_3$, 300 MHz): δ 0.30 (m, 4H, –CH_2–Si), 1.35 (m, 4H, –CH_2–), 2.45 (t, 12H, *J* = 6Hz, –CH_2–N), 2.75 (m, 4H, –CH_2–NH), 3.29-3.70 (m, 12H, –CH_2–O), 7.27 (d, 4H, *J* = 3Hz, Ar–H), 7.41 (d, 4H, *J* = 2Hz, Ar–H), 7.45 (d, 2H, *J* = 2.5Hz, Ar–H), 8.15 (d, 2H, *J* = 2Hz, Ar–H), 8.20 (t, 4H, *J* = 2Hz, Ar–H), 8.77 (m, 4H, Ar–H), 9.05 (s, 2H, Ar–H) ppm.

2.2.5.5. Synthesis of *cis*- [Ru(*dcbipy*)$_2$Cl$_2$] (16)

[Ru(*dcbipy*)$_2$Cl$_2$] was synthesised following the procedure of Liska *et al.*[53]

$RuCl_3.xH_2O$ (60mg, 0.229mmol) and *dcbipy* (113mg, 0.463mmol) were refluxed in DMF under N_2 for 8 hours. The resulting solution was cooled slowly overnight, and then filtered. The majority of the DMF solvent was evaporated off to leave approximately 1mL of solution. Acetone was then added dropwise until a dark-red precipitate formed. The powder was filtered off and dried under vacuum to give a 55% yield.

Chemical Equation: Scheme 5-1

FTIR data: See Section 2.2.6 for a detailed discussion.

IR(KBr): ν = 3467 (b), 3115 (m), 2475 (b), 1989 (m), 1725 (s), 1660 (m), 1463 (s), 1368 (s), 1309 (s), 1142 (s), 1070 (s), 1014 (s), 767 (s), 685 (s) cm^{-1}.

The ^{1}H NMR spectrum of complex **(16)**, [Ru(*dcbipy*)$_2$Cl$_2$] in D_2O (See Figure 2-12 for full spectrum) showed three peaks in the aromatic region, two of which were doublets and one a singlet. The chemical shift of the singlet, δ8.84 ppm, was found to be very similar to that observed in the spectrum of complex **(13)** with a shift at δ8.82 ppm. The two doublet peaks are caused by the H^a and H^b protons, the doublet at δ8.91 ppm is due to the proton, H^a, whereas the doublet at δ7.93 ppm is due to proton, H^b, however is there is also some additional fine coupling which may be caused by H^c. The reason for the higher chemical shift being observed for H^a is due to the closer proximity of the proton to the nitrogen of the ring. See Table 2-4 for a summary of the proton NMR data.

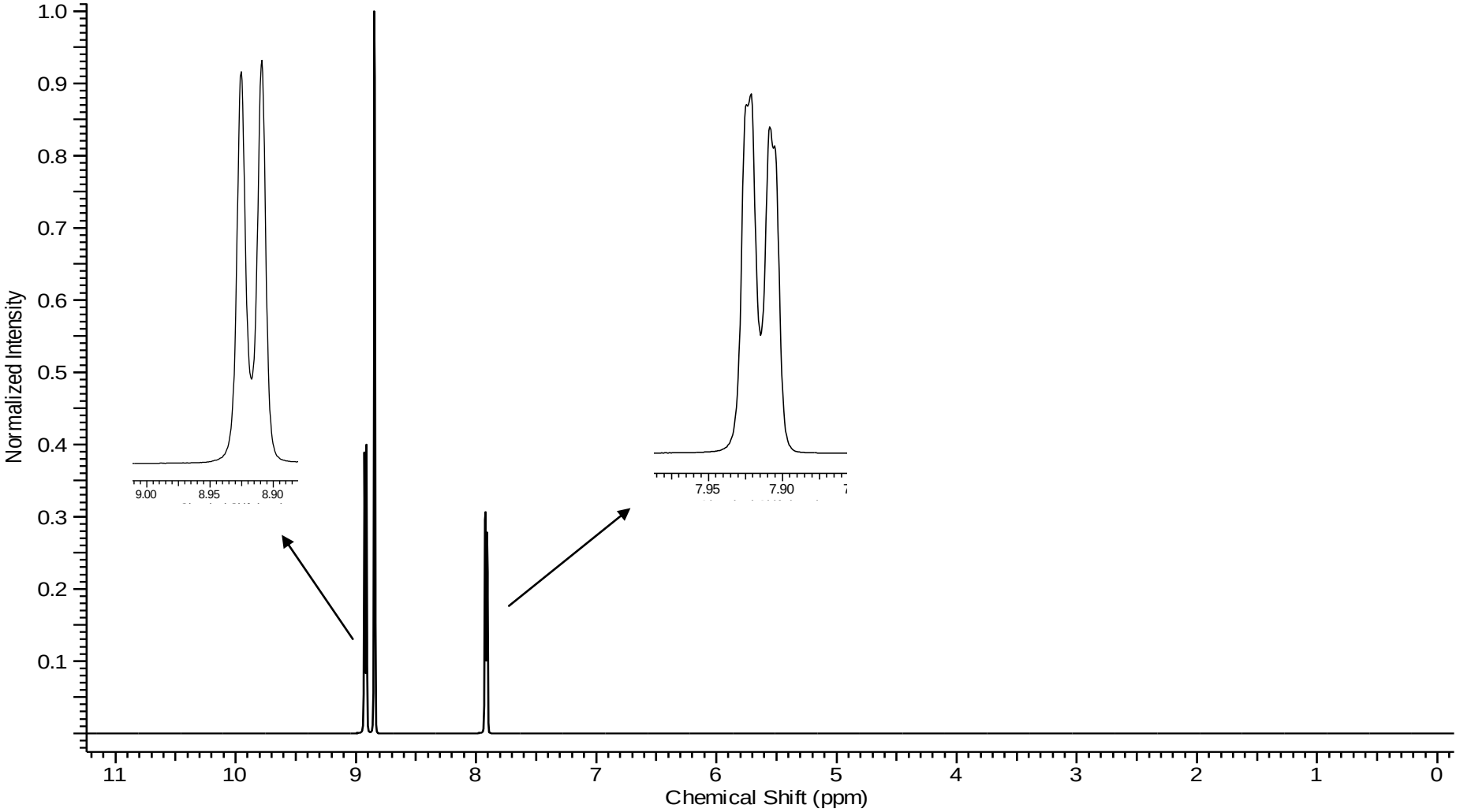

Figure 2-12 ^{1}H NMR of complex **(16)**

Table 2-4 Assigned protons for [Ru(*dcbipy*)$_2$Cl$_2$] **(16)**

Proton*	Chemical Shift (ppm)	Splitting	Coupling Constant (Hz)
H^a	8.91	doublet	5
H^b	7.93	doublet	4
H^c	8.84	singlet	n/a
H^d	not observed$^{\#}$	not observed	n/a

*As labelled in 2-2.

$^{\#}$ In D_2O, proton exchange can occur with –COOH to form –COOD and therefore the proton would not be observed.

^{1}H NMR (D_2O, 300 MHz): δ 7.93 (d, 4H, *J* = 4Hz, Ar–H), 8.84 (s, 4H, Ar–H), 8.91 (d, 4H, *J* = 5Hz, Ar–H) ppm.

The ^{1}H NMR spectra of complexes [Ru(*dcbipy*)$_2$Cl$_2$] **(16)** and [Ru(*dcbipy*)$_2$(NCS)$_2$] **(17)** were very similar. Thus, the FT-IR data was used to determine the inclusion of thiocyanate in the complex, (refer to section 2.2.6 for FT-IR data). This was also the case for the ^{1}H NMR spectra of complexes [Ru(*bipy-sil*)$_2$Cl$_2$] **(18)** and [Ru(*bipy-sil*)$_2$(NCS)$_2$] **(19)**.

2.2.5.6. Synthesis of *cis*-[Ru(*dcbipy*)$_2$(NCS)$_2$] 'N3 dye' (17)

[Ru(*dcbipy*)$_2$(NCS)$_2$] was synthesised following the procedure of Nazeeruddin *et al.*[113]

[Ru(*dcbipy*)$_2$Cl$_2$] (142mg, 0.214mmol) was dissolved in DMF (15mL) under subdued light. The carboxy groups were then deprotonated through the addition of NaOH (0.1M, 20mL, 2mmol). In a separate beaker, sodium thiocyanate (175mg, 2.26mmol) was dissolved in water (1-2mL), and then added to the DMF solution. The resulting mixture was refluxed and stirred for 6 hours under N_2. The solution was cooled slowly overnight, and the solvent removed under vacuum. The powder was dissolved in water and the suspension filtered through a sintered glass crucible. The pH of the

filtrate was lowered to 2.5 by addition of H_2SO_4 (2M), and cooled to 4°C for 18 hours. The solution was allowed to warm to room temperature and within several hours a microcrystalline solid formed. This was filtered and subsequently washed with water, acetone and anhydrous diethyl ether. [Ru(*dcbipy*)$_2$(NCS)$_2$] **(17)** was isolated as a dark red-microcrystalline powder 60% yield.

Chemical Equation: Scheme 5-1

FTIR data: See Section 2.2.6 for a detailed discussion.

IR(KBr): ν = 3449 (b), 2929 (b), 2119 (s), 2002 (s), 1722 (s), 1637 (m), 1553 (s), 1407 (s), 1379 (s), 1308 (s), 1324 (s), 1025 (s), 771 (s) cm^{-1}.

^{1}H NMR (D_2O, 300 MHz): δ δ 7.97 (d, 4H, J = 5Hz, Ar–H), 8.82 (s, 4H, Ar–H), 8.91 (d, 4H, J = 5Hz, Ar–H) ppm.

2.2.5.7. Synthesis of *cis*- [Ru(*bipy-sil*)$_2$Cl$_2$] (18)

[Ru(*bipy-sil*)$_2$Cl$_2$] was prepared using a similar procedure as 2.2.5.6, except *bipy-sil* (100mg, 0.1mmol) was used in place of *dcbipy*. A dark red microcrystalline product was isolated in 40% yield.

Chemical Equation: Scheme 5-1

FTIR data: See Section 2.2.6 for a detailed discussion.

IR(KBr): ν = 3423 (b), 2939 (m), 2892 (m), 1651 (s), 1551 (m), 1463 (s), 1281 (s), 1088 (s), 1022 (s), 916 (s), 759 (s) cm^{-1}.

Like the ^{1}H NMR spectra of the other complexes, [Ru(*bipy-sil*)$_2$Cl$_2$] **(18)** also exhibited distinct aromatic shifts (Figure 2-13).

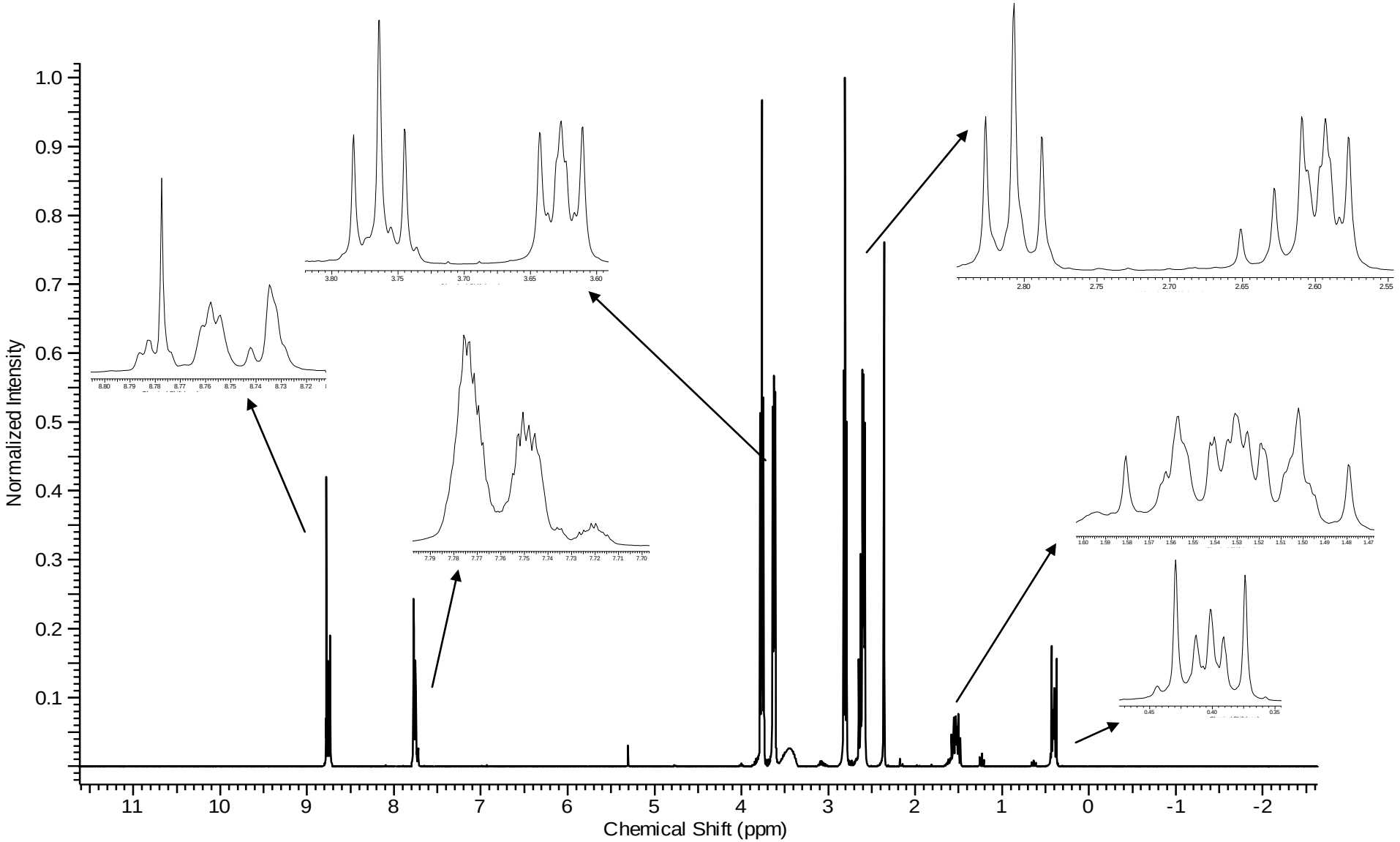

Figure 2-13 ^{1}H NMR of [Ru(*bipy-sil*)$_2$Cl$_2$] **(18)**

The absorptions at δ 7.70-7.80 ppm appear to be three sets of multiplets which may arise from the proton, H^b (See Figure 2-9), and the upward chemical shift at δ 8.72-8.80 ppm due to the proton, H^a. A singlet peak at δ8.78 ppm arising from the proton, H^c. Complex **(18)** contains a total of 84 protons, of which 12 (14%) are responsible for the aromatic protons, and the remaining 72 (86%) are from the propyl-silatrane. The measured integrated area is comparable to the number of protons with 11% of the area arising from the aromatic peaks, and the remaining 89% of the area arising from the aliphatic propyl-silatrane protons. However, even within the aliphatic region (from δ 0 to 4 ppm) there are some additional peaks which may be impurities contributing to the larger integrated area. There is one additional solvent peak in the spectrum which could not be removed at δ 2.37 ppm, which is due to DMSO.

The peaks in the NMR spectrum of **(18)** are better defined than those observed in complex **(15)**, $[Ru(\textit{bipy})_2(\textit{bipy-sil})](PF_6)_2$, due to its higher solubility (The PF_6^- salt of complex **(15)** is sparingly soluble). The chemical shifts in the spectrum of complex **(18)** are slightly different to those observed in complex **(15)** and are summarised in Table 2-5.

Table 2-5 Assigned protons for $[Ru(\textit{bipy-sil})_2Cl_2]$ **(18)**

Proton*	Chemical Shift (ppm)	Splitting	Coupling Constant
H^a	8.76	multiplet	n/a
H^b	7.75	multiplet	n/a
H^c	8.78	singlet	n/a
H^d	Not observed	not observed	n/a
H^e	2.81	triplet	6
H^f	1.54	multiplet	n/a
H^g	0.40	multiplet	n/a
H^h	3.70	2 sets of triplets	5
H^i	2.60	multiplet	n/a

* As labelled in Figure 2-9.

^{1}H NMR (DMSO-d_6, 300 MHz): δ 0.40 (m, 4H, –CH_2–Si), 1.54 (m, 4H, –CH_2–), 2.60 (m, 12H, –CH_2–N), 2.81 (t, 4H, *J* = 6Hz, –CH_2–NH), 3.70 (dt, 12H, *J* = 6Hz, –CH_2–O), 7.75 (m, 4H, Ar–H), 8.76 (m, 4H, Ar–H), 8.78 (s, 2H, Ar–H) ppm.

2.2.5.8. Synthesis of *cis*-[Ru(*bipy-sil*)$_2$(NCS)$_2$] (19)

[Ru(*bipy-sil*)$_2$(NCS)$_2$] was prepared using a similar procedure as 2.2.5.6, except [Ru(*bipy-sil*)$_2$Cl$_2$] was used in place of [Ru(*dcbipy*)$_2$Cl$_2$].

[Ru(*bipy-sil*)$_2$Cl$_2$] (60mg, 0.04mmol) was dissolved in DMF (5mL) under subdued light. In a separate beaker sodium thiocyanate (32mg, 0.40mmol) was dissolved in water (1mL), and then added to the DMF solution. The resulting mixture was refluxed and stirred for 6 hours under N_2. The solution was cooled slowly overnight, and the solvent removed under vacuum. The powder was dissolved in water and the suspension filtered through a sintered glass crucible. The solution was cooled to 4°C for 18 hours. The solution was allowed to warm to room temperature and within several hours a microcrystalline solid formed. This was filtered and subsequently washed with water, acetone and anhydrous diethyl ether. A dark red microcrystalline product was isolated in 35% yield.

Chemical Equation: Scheme 5-1

FTIR data: See Section 2.2.6 for a detailed discussion.

IR(KBr): *v* = 3419 (b), 3084 (b), 2945 (b), 2070 (s), 2000 (s), 1950 (s), 1664 (s), 1555 (s), 1470 (s), 1407 (s), 1104 (b) cm^{-1}.

^{1}H NMR (DMSO-d_6, 300 MHz): δ 0.39 (m, 4H, –CH_2–Si), 1.55 (m, 4H, –CH_2–), 2.62 (m, 12H, –CH_2–N), 2.80 (t, 4H, *J* = 5.5Hz, –CH_2–NH), 3.68 (m, 12H, –CH_2–O), 7.78 (m, 4H, Ar–H), 8.76 (m, 4H, Ar–H), 8.82 (s, 2H, Ar–H) ppm.

2.2.6. FTIR discussion for *dcbipy* and *bipy-sil* complexes

The FT-IR spectra of [Ru(*bipy*)$_2$(*dcbipy*)](PF$_6$)$_2$ **(13)**, [Ru(*dcbipy*)$_2$Cl$_2$] **(16)** and [Ru(*dcbipy*)$_2$(NCS)$_2$] **(17)**, shown in Figure 2-14, display well-resolved peaks, and the fundamental frequencies due to aromatic C=C (~1580 cm^{-1}) and C=N (~1550 cm^{-1}) stretches, as well as the carboxyl C=O band at ~1700 cm^{-1} ($^{\#}$) observed in the uncoordinated *dcbipy* ligand, are also seen in the coordinated ruthenium complexes. The FT-IR spectra of **(16)** and **(17)** are similar, which is not surprising, with the main difference between the two being two bands seen at 2000 and 2090 cm^{-1} (*), assigned to the two *cis*- N-coordinated thiocyanate ligands in complex **(17)**.

The FT-IR spectra of complexes [Ru(*bipy*)$_2$(*bipy-sil*)](PF$_6$)$_2$ **(15)**, [Ru(*bipy-sil*)$_2$Cl$_2$] **(18)** and [Ru(*bipy-sil*)$_2$(NCS)$_2$] **(19)** presented in Figure 2-15, all exhibit an N–H stretching frequency at ~3300-3450 cm^{-1} (3367 cm^{-1} for **(15)**, 3423 cm^{-1} for **(18)** and 3419 cm^{-1} for **(19)** ($^{\#}$)). This wide band is due to a combination of the amide N–H bond and the tertiary amine from the silatrane.[111] The Si–O stretching frequency is observed in all three complexes at ~1100 cm^{-1}, (1066 cm^{-1} for **(15)**, 1116 and 1088 cm^{-1} for **(18)** and 1104 cm^{-1} for **(19)** (^)) although a split-band is observed in **(18)**, a much broader band is observed in the spectra of the other two complexes. This may be due to solid-state splitting, or the bands in complex **(18)** being better resolved. The spectrum of **(19)** exhibits three bands in the ν(SC≡N) region at 1950, 2000 and 2070 cm^{-1} (*); the bands at 2070 and 2000 cm^{-1} are comparable to the ν(SC≡N) bands seen in the *cis*-[Ru(*dcbipy*)$_2$(NCS)$_2$] **(17)**, which may mean that the band at 1950 cm^{-1} is due to a *trans* isomer of [Ru(*bipy-sil*)$_2$(NCS)$_2$].

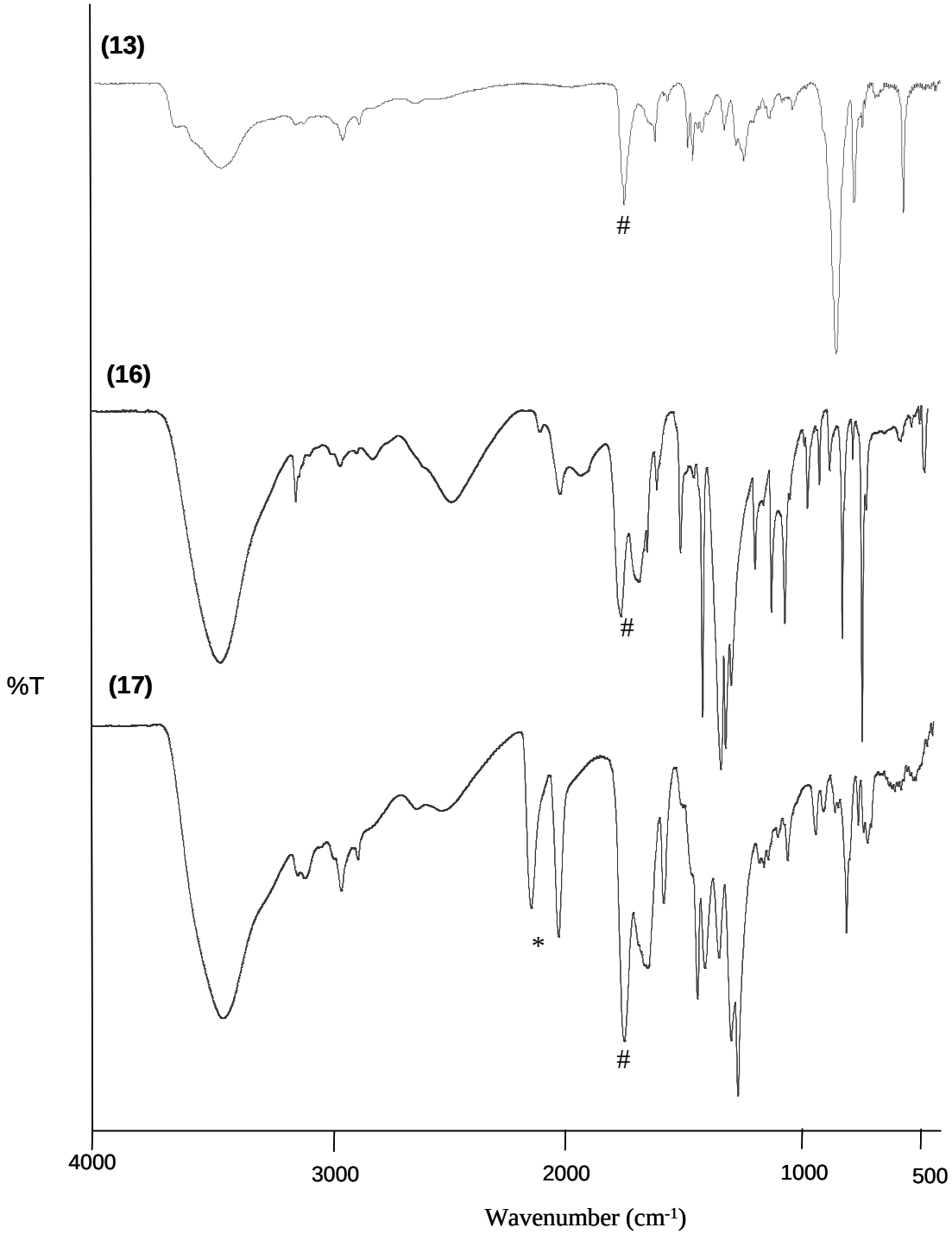

Figure 2-14 FTIR spectra of complexes [Ru(*bipy*)$_2$(*dcbipy*)](PF$_6$)$_2$ **(13)**, [Ru(*dcbipy*)$_2$Cl$_2$] **(16)** and [Ru(*dcbipy*)(NCS)$_2$] **(17)** (where * = 2000 and 2090 cm^{-1} and $^{\#}$ = ~1700 cm^{-1}).

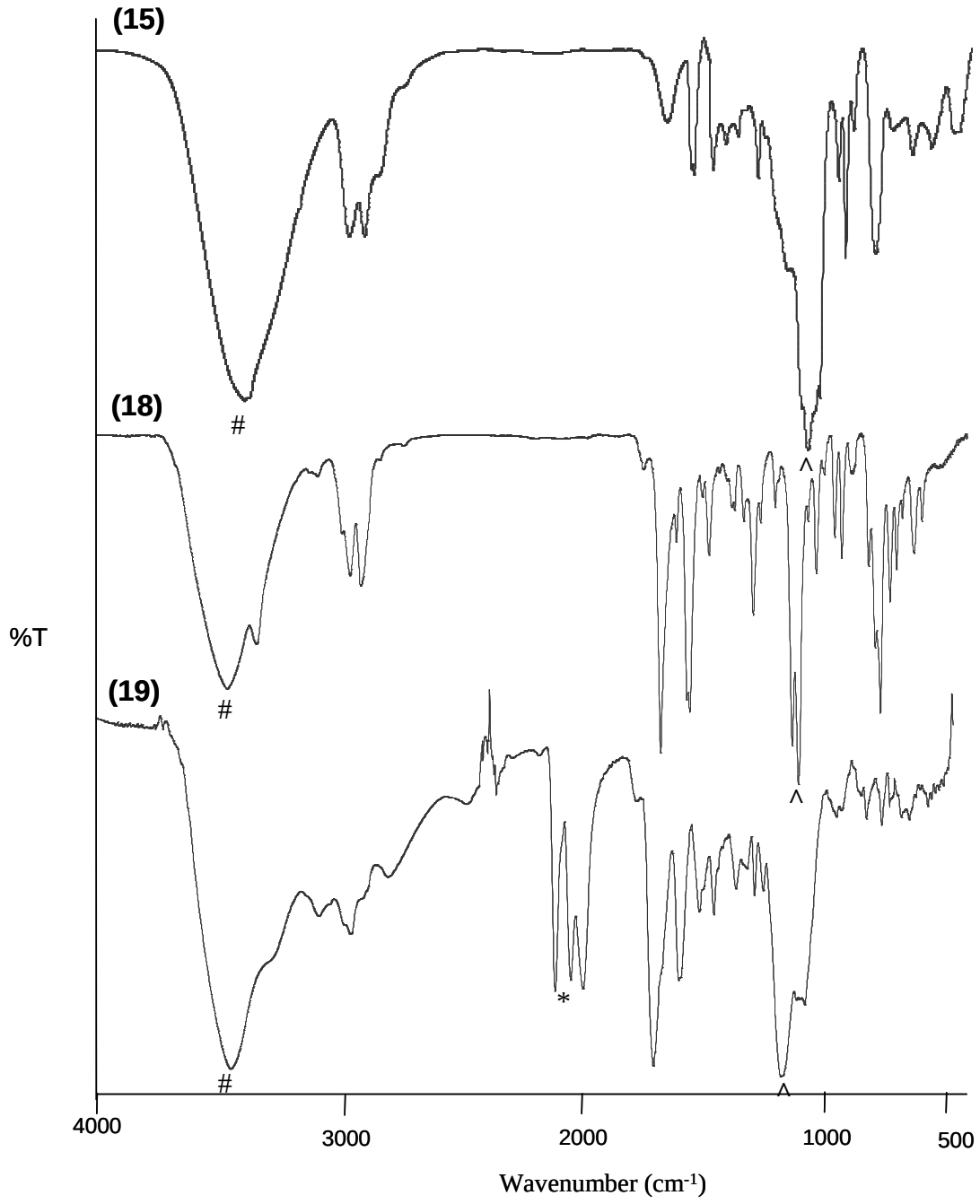

Figure 2-15 FTIR spectra of complexes [Ru(*bipy*)$_2$(*bipy-sil*)](PF$_6$)$_2$ **(15)**, [Ru(*bipy-sil*)$_2$Cl$_2$] (**18)** and [Ru(*bipy-sil*)$_2$(NCS)$_2$] **(19)** (where # = ~3300-3450 cm^{-1}, * = 1950, 2000 and 2070 cm^{-1} and ^ = ~1100 cm^{-1}).

2.2.7. Preparation of semiconductors (TiO_2 and WO_3)

The TiO_2 substrates were purchased from Dyesol: they consist of a glass substrate whose dimensions are 190mm x 260mm x 20mm, and have a TiO_2 coated area of 100mm x 70mm. The WO_3 substrates were prepared by the School of Electrical and Computer Engineering at RMIT University.[98] The dimensions of the glass substrates were 190mm x 140mm x 20mm, and had a WO_3 coated area of radius 25mm.

2.2.7.1. Annealing of TiO_2 and WO_3 substrates

The glass platelets of TiO_2/WO_3 substrates were placed in a tube furnace open to the air. The substrates were then heated slowly (2°C/min) from room temperature to 450°C, and held at 450°C for an hour and then cooled at a rate of 2°C/min.

2.2.8. Preparation of test batch solar cells (TiO_2 and WO_3)

Dyes containing ruthenium complexes prepared in-house and possessing carboxylic or phosphonic linkages were coated on to the annealed semiconductor substrate by immersion in a 0.3mM (acetonitrile or ethanol) solution of the dye, for 24 hours. Dyes containing a silyl linkage were adhered to the semiconductor by immersing the oxide substrate in a 0.3mM DMF solution of the dye and heating (~70°C) for 1 hour, in subdued light. In both cases a thin coloured film formed on the semiconductor, which was subsequently washed with ethanol and air dried.

Two holes were then drilled into a second FTO-glass plate (FTO – fluorine doped tin oxide), the counter electrode; this was done to allow the injection of the liquid electrolyte. A heat-activated gasket (Surlyn®-30), with a film thickness of 30μm was then placed around the dye-coated surface. The second FTO-glass plate was then placed on top and heated to approximately 100°C. The liquid electrolyte, I^-/I_3^- was then injected into the cell through the pre-drilled holes, approximately 1 drop in each

hole. The holes were then sealed with a heat activated gasket. See Figure 2-16 for solar cell schematic.

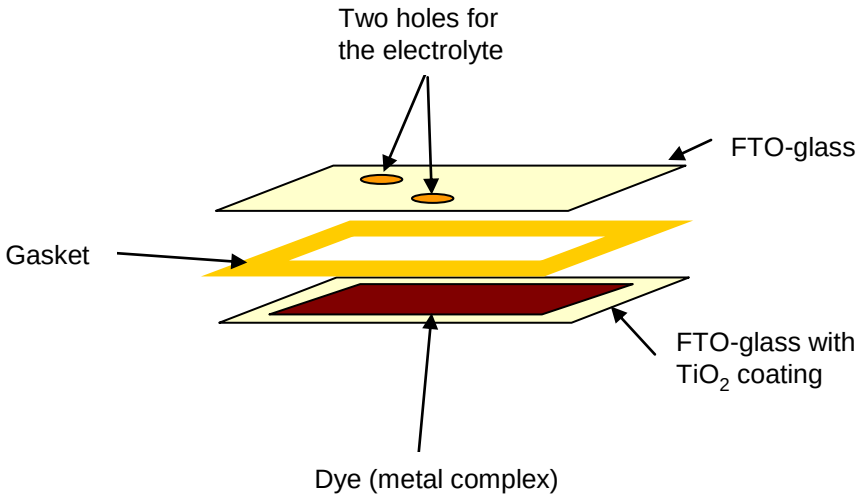

Figure 2-16 Schematic of DSSC

2.3. Instrumental Measurements

2.3.1. Fourier Transform Infrared Spectroscopy (FT-IR)

Stretching and bending vibrations within a molecule show characteristic absorption bands in the infra-red region. An FT-IR spectrum of these absorption bands can be used to identify functional groups within the molecule.

FT-IR absorption spectra were obtained on a Perkin Elmer Spectrum 100 spectrometer using KBr discs. The discs were prepared by grinding the sample (1-2mg) and IR grade KBr (100mg, into a homogeneous powder using a mortar and pestle. The powder was then placed in a die press (Specac 13mm) and compacted under vacuum for approximately 5 minutes using 8 tonne of pressure. The spectra were collected using the following conditions: scan range 4000-400cm^{-1}; number of scans 8; single beam; resolution: 4cm^{-1}.

2.3.2. Magnetic Moments and Susceptibility

The presence of unpaired electrons in a molecule gives rise to *paramagnetism* which is one of the more common forms of magnetism. Substances which do not contain unpaired electrons are termed *diamagnetic* and are repelled from a magnetic field. Measurements of the magnetic susceptibility (χ) of a sample allow its magnetic moment to be determined. The magnetic susceptibility of a sample is a measure of the intensity of magnetisation in the sample compared to the strength of the field.[114] (See theory in sections 3.3.3 and 4.3.2.2 for more detail)

The superconducting quantum interference device (SQUID) magnetometer currently is the most sensitive instrument used for magnetic measurements. It operates by measuring the electrical effect on a field due to a magnetised substance as it is moved through a superconducting coil. The electromotive force (e.m.f) that is generated is proportional to the magnetic moment of the sample.[115]

Variable-temperature magnetic susceptibilities were measured on powdered 20 mg samples using a Quantum Design MPMS5 SQUID magnetometer in a field of 1 T. Samples were contained in gel capsules that were held in the centre of a soda straw, and in-turn were fixed to the end of the sample rod. The instrument was calibrated against the accurately known susceptibilities of a standard Pd pellet (Quantum Design) and that of $CuSO_4 \cdot 5H_2O$.

2.3.3. Microanalysis for Carbon Hydrogen and Nitrogen

Elemental analysis for C, H, and N, was performed by the Campbell Microanalytical Laboratory at the University of Otago, New Zealand.

2.3.4. Nuclear Magnetic Resonance (NMR) Spectroscopy

NMR is a phenomenon that arises from the existence of nuclear spin. Measurements are obtained by immersing the sample in a strong homogenous magnetic field which allows the energy levels of the nucleus to split. Transitions between the levels are achieved by radio frequency radiation and the differences in the energy levels produce the resonances seen in the spectrum. An NMR spectrum allows the electronic environment of atoms to be assigned from the resonance frequencies.

In this work, the samples were prepared using deuterated solvents: typically 20mg of sample was dissolved in the appropriate solvent (either D_2O, $CDCl_3$ or DMSO-d6 $(CD_3)_2SO$) and placed in a 5mm diameter glass NMR tube. The samples were run on a Bruker AVANCE 300 MHz NMR spectrometer. Each sample was locked and shimmed for spectral optimization. Spectra were measured at a frequency of 300MHz for ^{1}H, 75.45 MHz for ^{13}C and 121.45 MHz for ^{31}P.

2.3.5. Single-Crystal X-Ray Diffraction (XRD)

Single crystal XRD allows the position and nature of atoms within a crystal to be determined, and hence the unit cell dimensions, bond lengths and bond angles of a crystalline substance can be assigned.[116] This process occurs when X-rays are directed at a single crystal, and when the geometry of the incident X-ray satisfies the Bragg equation, as expressed by Equation 2-1, constructive interference occurs, which is caused by the X-ray wavelengths being in-phase when reflected from a given crystal plane. A detector collects the entire diffraction pattern of reflections.

Equation 2-1

$$2d \sin\theta = n\lambda$$

(d = spacing between the planes in the atomic lattice, θ = Bragg angle, the angle between the incident ray and the scattering planes, n = an integer, λ = wavelength of incident light)

Single crystal data was collected and integrated using either a Bruker Smart Charge-Coupled Device (CCD) area detector system at 130 K using Mo Kα radiation, or an Oxford dual Supernova detector system at 130 K using Mo Kα or Cu Kα radiation. The structures were solved by direct methods, using SHELXS-97,[117] and refined using SHELXL-97.[117] A mixed strategy was used for the refinement of hydrogen atoms. Hydrogen atoms attached to carbon were placed in calculated positions with a C–H distance of 0.93 Å, whilst hydrogen atoms attached to oxygen were located from difference Fourier maps, and refined without constraint. Where large amounts of disordered solvent were present, a process known as the SQUEEZE[118] routine was applied which removes the disordered solvent and allows a satisfactory refinement to be obtained. Molecular graphics were performed using ZORTEP,[119] SHELXTL[120] and Mercury[121] programs.

2.3.6. Ultraviolet-Visible (UV-Vis) Spectroscopy

Ultraviolet-visible spectroscopy records the amount of light absorbed by a molecule within the ultraviolet and visible region. The UV-vis spectra allow the λ_{max} to be assigned, as well as the identification of absorption bands arising from electronic transitions within the molecule. The molar extinction coefficient of the molecule (ε) can also be calculated from the spectra using the Beer-Lambert Law, as expressed by Equation 2-2.

Equation 2-2

$$A = \varepsilon \times c \times l$$

(A = absorbance, ε = molar extinction coefficient, c = concentration, l = path length)

In this work, samples were prepared by dissolving 50-100 mg of sample in 25mL of an appropriate solvent (water, ethanol, DMF, or acetonitrile). The samples were measured in a 1cm path-length quartz UV cell, on a Varian Cary 50 spectrophotometer. Spectra were obtained over the wavelength range 200-800 nm, at a scan rate of 60 nm/min.

2.3.7. Fluorescence Spectroscopy

Fluorescence spectroscopy determines whether the sample has photoluminescent properties. The sample is excited at a specific wavelength, and if the sample is photoluminescent an emission spectrum will be collected.

Solid-state fluorescence measurements were carried out using a Fluorolog-3 fluorescence spectrometer from Jobin–Yvon–Horiba fitted with a 450W Xe lamp. The powdered samples were loaded evenly into the sample cavity of the solid sample holder and the fluorescence emission spectra were collected between 350 and 800 nm,* at an angle 45° to the incident beam, using an excitation wavelength from 200-450 nm,* and a slit width from 1-5 nm.* All spectra were collected at room temperature.

* This varied with samples.

2.3.8. Solar Cell Testing Unit

In electrochemical measurements of cell arrangements, the current, *I*, is defined as the flow of electric charge (coulomb/sec), and in the case of DSSCs it gives an indication of the efficiency of electron transfer between the dye and the semi-conductor substrate. The voltage, *V*, is the energy carried by the charge (Joule/coulomb) and in DSSCs it is the difference between the Fermi level (which is the energy of the electrons in a semiconductor under illumination) compared to the Nernst potential of the electrolyte redox couple.[2]

An indication of the efficiency of the cell to deliver useful energy can be obtained from the product, $V(\mathit{joule}/\mathit{coulomb}) \times I(\mathit{coulomb}/s) = \mathit{joule}/s$, which gives the electrical power output of the cell (1 Watt = 1J/s). This is incorporated in equation 1.3 in the Introduction.

All cells containing the metal complex "dye" were tested on a custom-made solar cell testing station.[98] The station comprised an ABET Technologies LS-120 solar light

source fitted with an AM 1.5 filter, where the illumination power density was calibrated to 90mW/cm^2. Voltage and current measurements were collected using a Keithly 2602 sourcemeter. The incident-photon-to-electron conversion efficiency (IPCE) measurements were conducted using a 1000W Xe lamp and a monochromator, according to the protocol described by Zheng *et al.*[98]

CHAPTER 3

Copper 1H-[1,10]-phenanthrolin-2-one Coordination Complexes

3.1. Summary

This study investigated the use of several N-heterocyclic ligands to modify the photonic properties of metal centres. In this chapter, the preparation of the ligand 1H-[1,10]-phenanthrolin-2-one (*HOphen*) was undertaken to explore the behaviour of its complexes with copper. The absorption and luminescent behaviour of the copper(I) complex, $[Cu_2(Ophen)_2]$ **(1)**, was subsequently investigated to determine whether the complex could be used in solar energy capture. Complex **(1)** exhibited a broad peak in the visible region and fluorescence in the solid state, hence it appeared a promising candidate for use in DSSC.

While investigating the synthesis and properties of $[Cu_2(Ophen)_2]$ **(1)**, which is a dinuclear complex of copper(I) with 1H-[1,10]-phenanthrolin-2-one (*HOphen*), two additional products, **(2)** and **(3)**, were isolated. Complex **(2)**, ($[Cu(phen)_2(H_2O)].(NO_3)_2$) containg Cu(II) is a polymorph of a previously described material, and complex **(3)**, also containing Cu(II) is a novel dinuclear, anti-ferromagnetic complex with the formula, $[Cu_2(Ophen)_2(phen)_2].(NO_3)_2.9H_2O$.

The observation of **(2)** and **(3)** suggests a possible variation to the proposed Gillard mechanism for the formation of covalent hydrates in bidentate N-heterocycles, in which the attacking nucleophile may be the OH^- ligand in the deprotonated form of **(2)**, $[Cu(phen)_2(OH)]^+$, rather than free OH^-. All of the compounds were prepared by thermal reaction at 150°C in an aqueous solution containing copper(II) nitrate and 1,10-phenanthroline, with the pH of the solution being adjusted to approximately 8 using 1M sodium hydroxide.

3.2. Introduction

Bidentate N-heterocycles such as phenanthroline (*phen)* are important building blocks for the preparation of coordination compounds[40, 71] and metallo-supramolecular assemblies.[122-126] These materials form stable and well-defined metal-ligand combinations that result in predictable 3-dimensional arrangements and hence are an important aid in the rational design of materials with specific architectures and properties.

In addition, N-heterocyclic ligands often confer useful photonic behaviour on metal centres and so this aspect was also to be explored. A further unusual property of N-heterocycles such as *bipy* and *phen* is the fact that they have frequently been reported to form "covalent hydrates" **(CH)** as outlined in Scheme 3-1. Subsequent oxidation to a hydroxy-pyridine **(HP)** allows tautomeric conversion to the more stable 1(H)-one.

To this end, recent reports of the synthesis of a novel chelating/bridging ligand, 1H-[1,10]-phenanthrolin-2-one (*HOphen*),[107] are particularly significant. This ligand tends to produce polynuclear clusters such as those observed in: $[Cu_2(Ophen)_2]$ (**1**),[107, 127] $[Cd_3Cl(Ophen)_5].1.5H_2O.2CH_2Cl_2$,[128] $[Zn_4O(Ophen)_4(OAc)_2].4H_2O.2CH_2Cl_2$,[129] and $[Ag_2(Ophen)_2]$,[130] which offer even greater structural rigidity and predictability as building blocks in supramolecular chemistry. *HOphen* is also of importance, as the free ligand is fluorescent and emits purple-blue light with an emission maximum at λ=401nm, and forms complexes with d^{10} metals,[128-129] with photoluminescent properties in the blue/green region, tuneable with metal type. Such complexes are promising as blue emitters in full-colour electroluminescent displays.

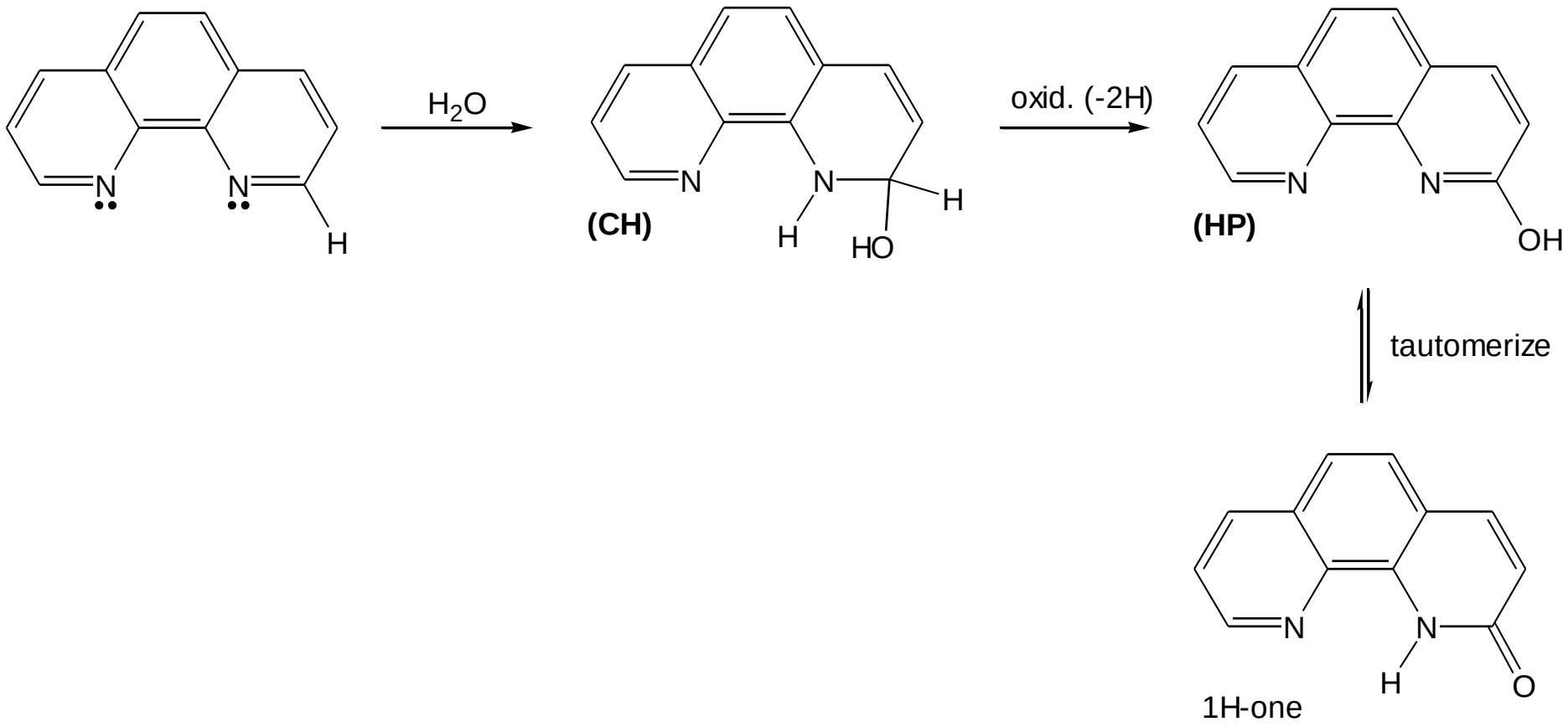

Scheme 3-1 Formation of a covalent hydrate **(CH)** and hydroxy-pyridine **(HP)** derivatives of *phen.*

In the present work, the anion, $^{-}$*Ophen*, was considered a promising ligand which might coordinate to copper as either a tridentate ligand in mononuclear complexes, or act as a bridging ligand, to enhance the photochemical behaviour of metal centres.

The most reliable source of *HOphen* is the synthesis first reported by Zhang *et al.*,[107, 127] who unexpectedly generated the ligand *in-situ* by reaction of a basic solution of copper(II) nitrate with *phen* under hydrothermal conditions, to produce the neutral, dinuclear Cu(I) compound, $[Cu_2(Ophen)_2]$ (**1**). The pure ligand was isolated by de-metallation with ammonium sulphide. Since this report of the stereospecific hydroxylation of *phen* (and *bipy*) in the presence of copper(II) ions, there has been considerable conjecture regarding an appropriate mechanism for the reaction, as there are at least three possibilities:

1. Direct nucleophilic attack on the coordinated N-heterocycle by *free* OH^-;
2. Direct nucleophilic attack on the ligand by *metal-co-ordinated* OH^-; or
3. An *E2 elimination/addition*, whereby OH^- attack generates a pyridyne intermediate from the N-heterocycle followed by water addition.

This latter mechanism is comparable to the Dow Chemical hydrothermal process for the industrial preparation of phenol from chlorobenzene.[131]

Gillard[132] and Constable[52] have previously suggested that N-coordination of pyridine-type ligands to metal ions is analogous to quaternisation by a proton (H^+) or an alkylating agent, allowing the positive charge from the metal centre to be delocalised over the pyridine ring, leaving the 2- and 4-carbon atoms susceptible to nucleophilic attack as demonstrated in Scheme 3-2.

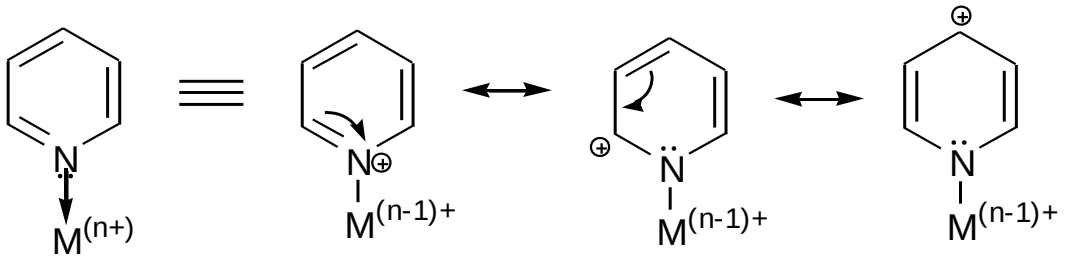

Scheme 3-2 A valence bond representation of a coordinated pyridine. (Apart from the simple e^- withdrawing inductive effect of the metal cation, the donor-covalent bond between N and M^{n+} can also be considered to form a shared covalent bond, effectively placing positive charge on the N-atom. The positive charge is delocalised into the ring with the 2- and 4-positions developing electrophilic character, making them susceptible to nucleophilic attack).[52, 127]

In aqueous media this can result in the promotion of hydroxylation of the heterocyclic ring and the formation of a 'covalent hydrate' (**CH**) (hydration across a –C=N– bond) to give –C(OH)–NH which can then release a proton to form the conjugate pseudo-base (**CB**) or undergo an intramolecular shift (**IMS**) to form the metal-hydroxy species (Scheme 3-3). In subsequent steps, the covalent hydrate can be aromatized by oxidation (-2H) giving rise to the 2- or 4- substituted hydroxy-pyridine (**HP** in Scheme 3-3), in a reaction exactly analogous to the Chichibabin reaction in which sodamide ($NaNH_2$) aminates the 2-position of pyridine by direct reaction.[52]

At the time of Gillard's publication,[132] an unambiguous mechanism could not be proposed due to a lack of structural evidence. One suggestion was for a nucleophile such as OH^- to attach itself to the metal centre, and in the case of $[M(phen)_2]^{2+}$ form a five-coordinate complex (similar to the **DH, IMS** structure in Scheme 3-4), rather than bind to the N-heterocycle to form a covalent hydrate (**CH**).[52, 133]It was not until several decades later, when Zhang and co-workers[107, 127-130] synthesized a range of d^{10} complexes with hydroxylated *phen* ligands (*HOphen*), that the Gillard mechanism (Schemes 3-3 and 3-4) was invoked as a viable rationalisation for the formation of such hydroxylated heterocycles.

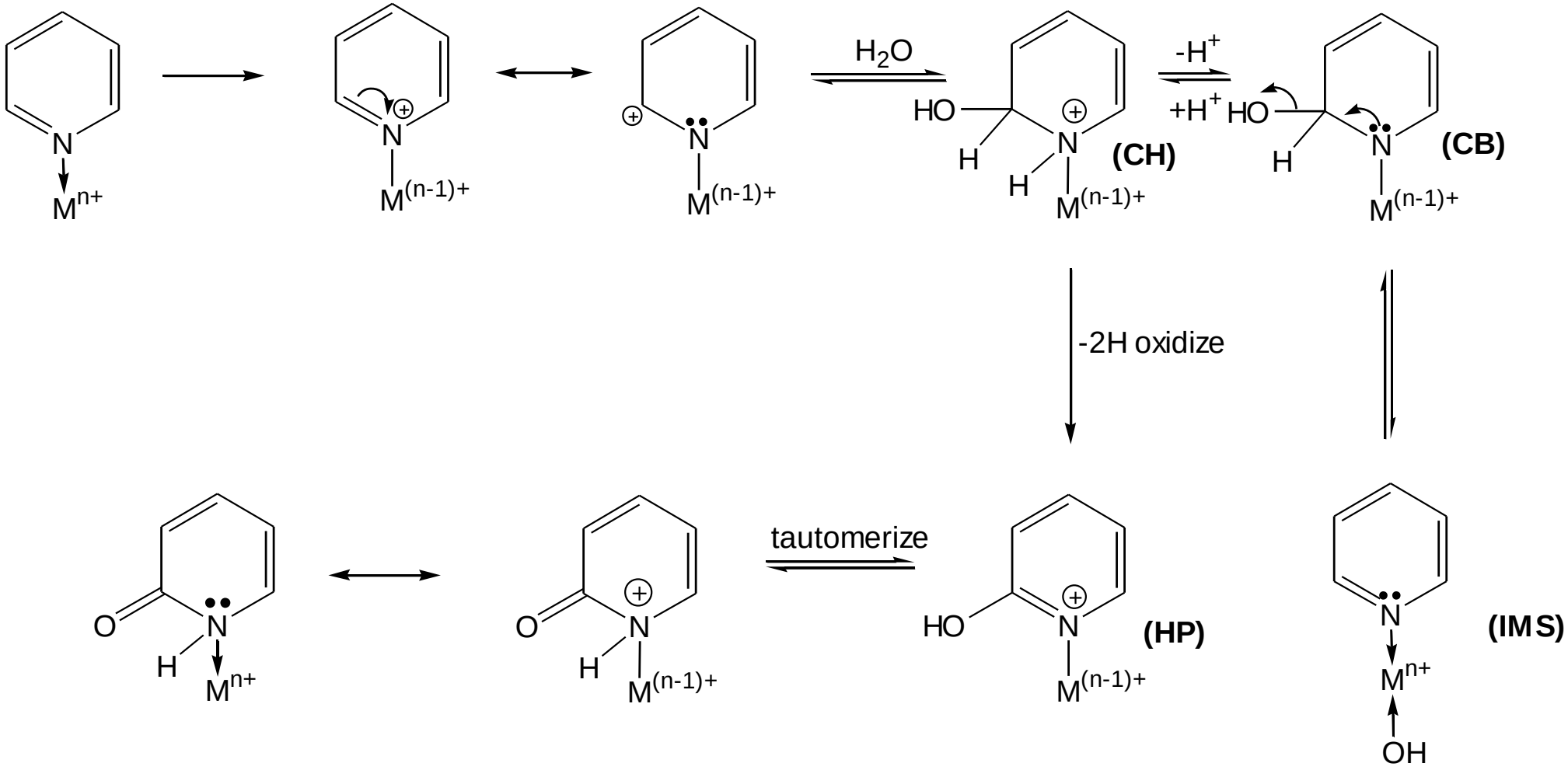

Scheme 3-3 Proposed Gillard Mechanism.[132]
CH = Covalent Hydrate, **CB** = Conjugate Base, **HP** = Hydroxy Pyridine, **IMS** = Intramolecular Shift

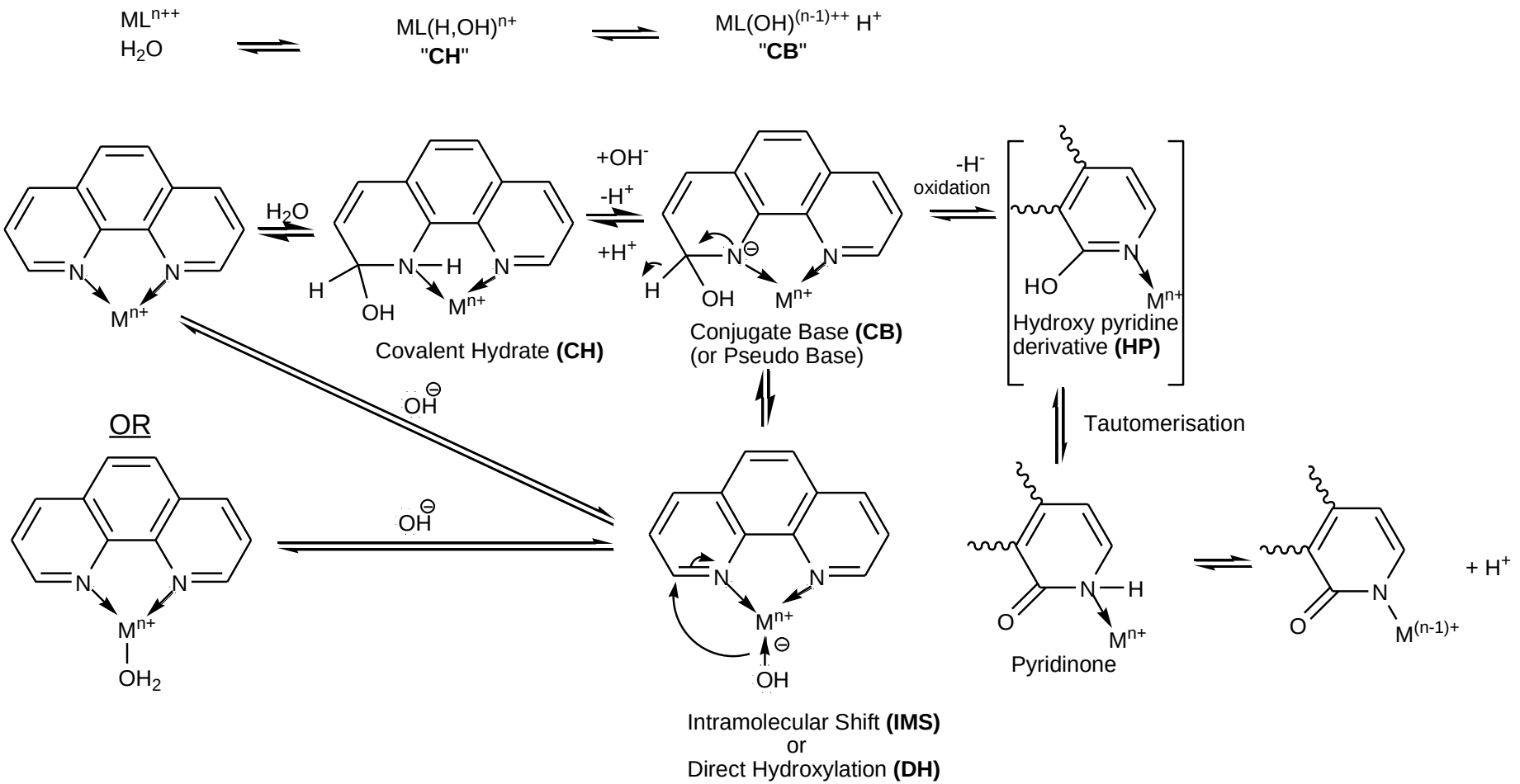

Scheme 3-4 Equilibria demonstrating the formation of a covalent hydrate and its conjugate base. The conjugate base can either be oxidized to the hydroxypyridine (**HP**) species, or it may undergo an intramolecular shift of the hydroxyl group to form the metal hydroxy species ($ML(OH^-)^{n+}$) (**IMS/DH**).

In this present study, two further compounds that were observed during the hydrothermal reaction have been isolated and characterised. This has allowed an alternative mechanism for the reaction to be proposed.

3.3. Results and Discussion

3.3.1. Structural Characterisation of Compounds (1), (2) and (3).

The hydrothermal reaction between copper(II) nitrate and phenanthroline under slightly basic conditions yielded products **(1)**, **(2)** and **(3)**, as outlined in Scheme 3-5:

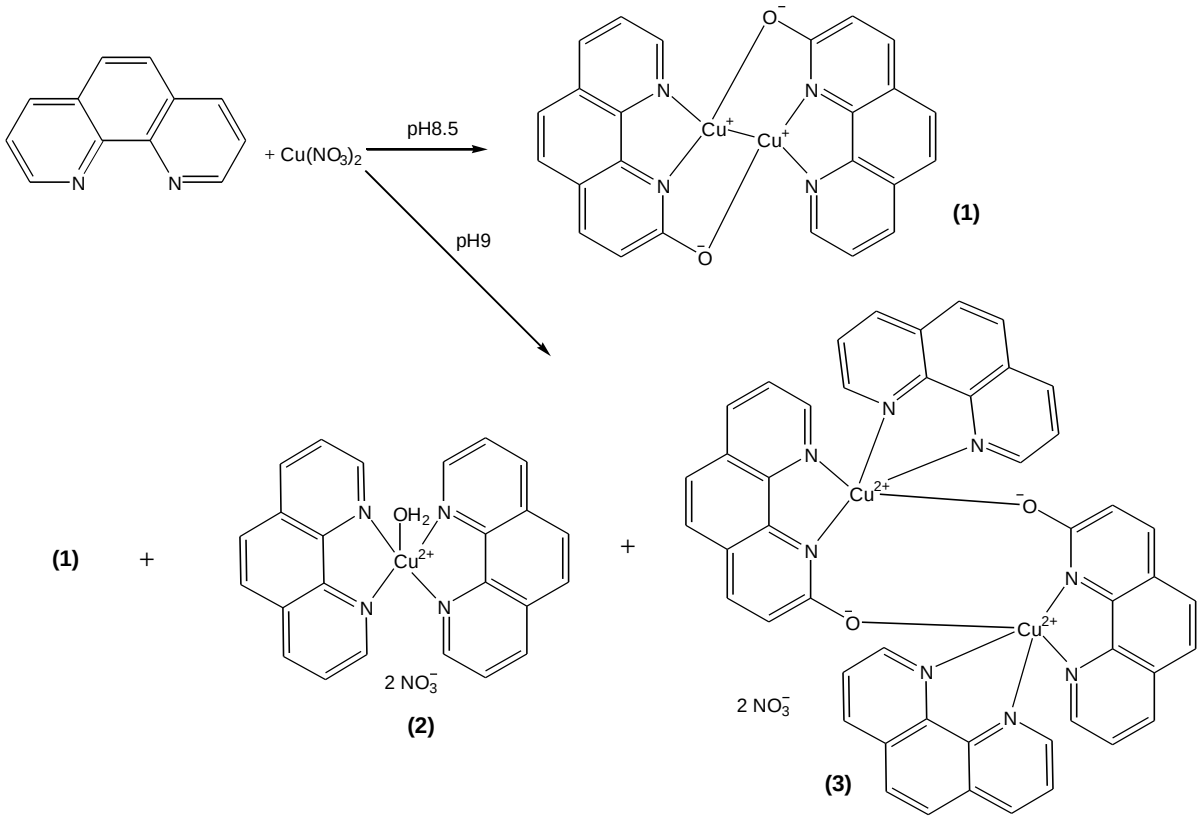

Scheme 3-5 Overall reaction for the formation of compounds **(1)**, **(2)** and **(3)**

Preparation of the desired dinuclear copper(I) complex **(1)** via the method published by Zhang and co-workers[107] was generally successful, with blue-black, block-like crystals of $[Cu^{(I)}_2(Ophen)_2]$ **(1)** isolated from an emerald-green supernatant in 35-45% yield. As mentioned earlier, product **(1)** has been identified previously by Zhang and

co-workers, [107] where three polymorphs (α, β, and γ) were isolated. Two (α, and β) contained copper centres in identical environments and the other (γ) had two different copper environments.

The elemental analysis of $[Cu_2(Ophen)_2]$ **(1)** presented in Table 3-1 suggests a Cu : *Ophen* ratio of 1:1, which is in agreement with the empirical formula.

Table 3-1 Elemental Analysis of **(1)**

Complex		% C	% H	% N
$Cu_2(C_{12}H_7N_2O)_2$	Found	55.63	2.65	10.78
$C_{24}H_{14}N_4O_2Cu_2$ (Mr=517.47g/mol)	Calc	55.70	2.73	10.83

Repeat attempts of this synthesis were found to be extremely pH dependent. To this end, the pH was varied from 7–14 to determine the optimal reaction conditions. At lower pH (7–8) it was observed that $[Cu(phen)_2(H_2O)]^{2+}$ **(2)** was formed rather than the $Ophen^-$ analogue. This was not surprising as $[Cu(phen)_2(H_2O)]^{2+}$ readily forms without pH manipulation. Yields, however, did vary, with pH 7 giving greater yields of $[Cu(phen)_2(H_2O)]^{2+}$ than pH 8. The pH reported by Zhang[107] was 8–8.5, however at this pH no hydroxylated *phen* species were isolated, suggesting that it may require increasing the pH further to promote hydroxylation. This was found to be the case, because at pH 9, slightly higher that initially reported by Zhang, [107] the desired hydroxylated *phen* species was isolated. Increasing the pH further was unsuccessful as at pH values greater than 10, the conditions were far too basic. At pH 10, the starting solution (i.e. before hydrothermal reaction) was similar to that observed in a pH 7–9 solution, whereby a light-blue opaque solution formed upon addition of the sodium hydroxide, but no copper complexes were isolated. At pH values greater than 11 the starting solution was dark blue and opaque, and once again no copper complexes were isolated. These observations suggested that the optimal pH value to ensure *phen* hydroxylation and subsequent deprotonation of the *HOphen* in good yield, was pH 9, which is in accord with the expected weak acid behaviour of *HOphen* (Scheme 3-6). *HOphen* contains the weakly acidic phenol group ($pK_a \approx 10$)

and would have acid dissociation constants similar to the related model compound, 8–hydroxyquinoline which has pK_a values of 4.85 (NH^+) and 9.95(OH).[134]

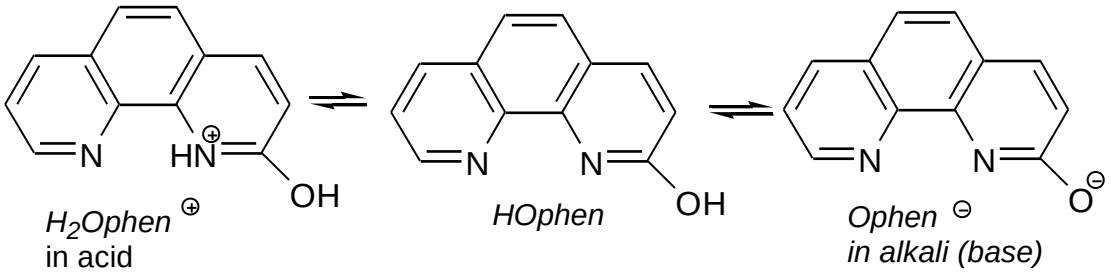

Scheme 3-6 Deprotonation equilibria for *HOphen.*

In addition to varying the pH, the effect of varying the mole ratio of copper(II) nitrate to phenanthroline was also studied. Phenanthroline in a slight excess was found to produce the highest yield of $[Cu_2(Ophen)_2]$ **(1)**, see Table 3-2.

Table 3-2 Molar ratios of $Cu(NO_3)_2$ to phenanthroline and their corresponding yields of $[Cu_2(Ophen)_2]$

Molar Ratio $Cu(NO_3)_2$: *phen*	Yield(%)
1:1	35
1:1.5	45
1:2	35
1:3	30

In work by Zheng and co-workers,[128, 130] the free *HOphen* ligand was isolated via a demetallation reaction with ammonium sulphide. In the present work, $[Cu^{(I)}{}_2(Ophen)_2]$ **(1)** (400mg) in methanol was treated in a similar manner until the precipitation of black CuS ceased. The solution was filtered and the mother liquor allowed to stand, whereby a yellow precipitate of *HOphen* formed (~50mg) after two weeks, which was characterised by FTIR, see Figure 3-1.

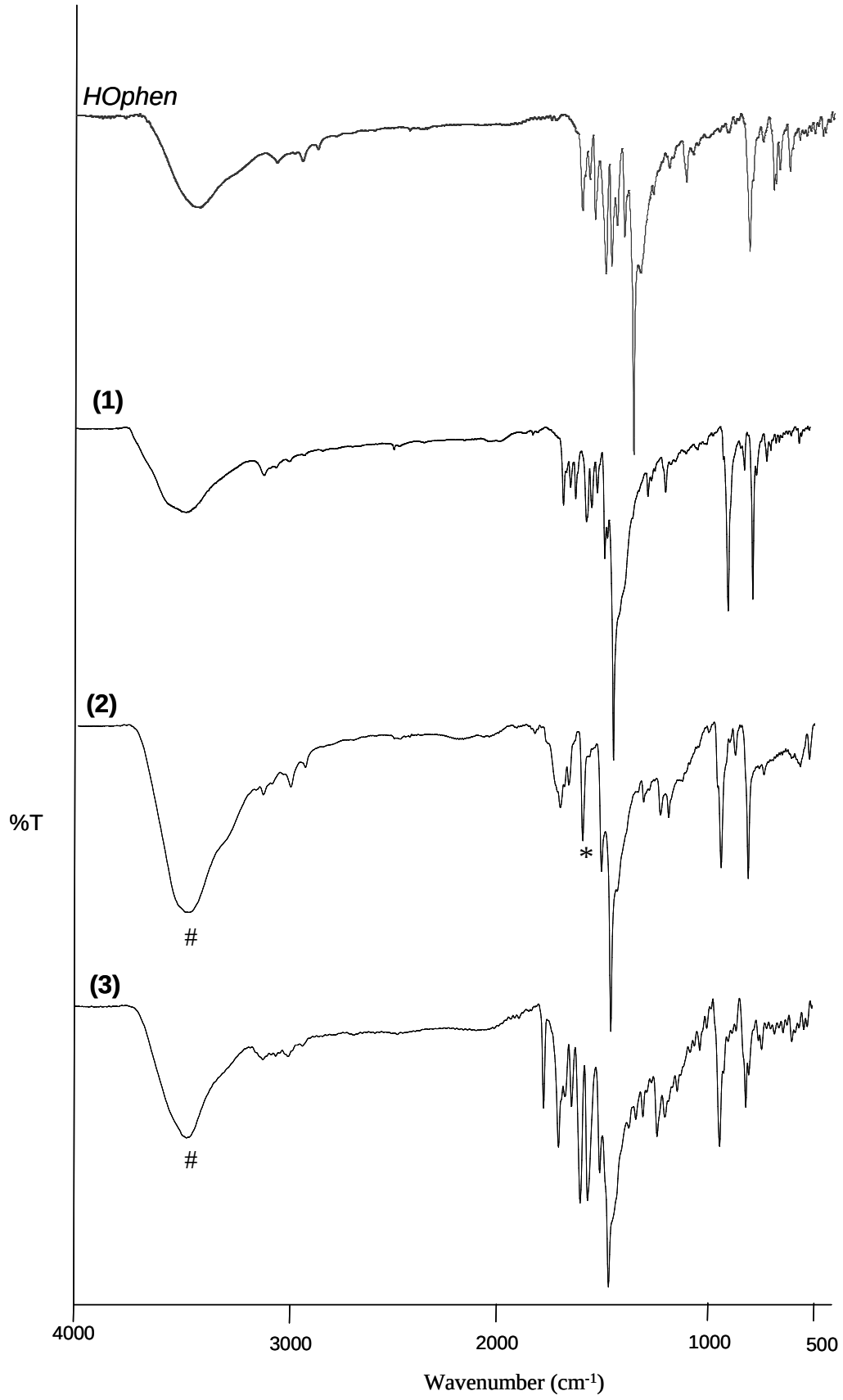

Figure 3-1 FTIR spectra of *HOphen* ligand, $[Cu_2(Ophen)_2]$ **(1)**, $[Cu(phen)_2(H_2O)]^{2+}$ **(2)** and $[Cu_2(Ophen)_2(phen)_2]^{2+}$ **(3)**, (where # = ~3500 cm^{-1} and * = 1600 cm^{-1}).

In preliminary studies aimed at preparing **(1)**, a series of ambient pressure and variable temperature experiments, including reflux, and reflux under N_2, were attempted, but with little success. In all cases $[Cu^{(II)}(phen)_2(H_2O)](NO_3)_2$ **(2)** was isolated, clearly indicating that elevated temperature and pressure conditions were required for the formation of hydroxylated ligand species. Hence, all the complexes reported in this section were prepared by hydrothermal autoclave synthesis.
Products **(2)** and **(3)** were isolated as light-green and emerald-green crystals in 20–25% and 3–5% yield respectively from an emerald green supernatant. Their presence indicates that they may be intermediates in the Gillard mechanism.[132] The colours of the materials isolated in these reactions suggested that copper was present in the +1 state in **(1)** and the +2 state in **(2)** and **(3)**.

The FT-IR spectra of **(1)**, **(2)** and **(3)** shown in Figure 3-1 display well resolved peaks due to the ligands, and the fundamental frequencies due to aromatic C=C and C=N stretches observed in the uncoordinated phenanthroline ligand are also seen in the coordinated *Ophen* and *phen* copper complexes. The FTIR spectra are quite similar with only minor differences observed between **(1)** and **(2)**, with the coordinated water in **(2)** exhibiting a strong δ (H–O–H) band at 1600 cm^{-1} (*), and a broad ν(H–O) stretching band at ~3500 cm^{-1} ($^{\#}$) in **(2)** and **(3).**

The compositions of **(2)** and **(3)** were confirmed by single crystal x-ray diffraction, which also provided unambiguous structural characterisation of each compound.

The structure of $[Cu^{(II)}(phen)_2(H_2O)](NO_3)_2$ **(2)** has been previously determined by Nakai and Deguchi (1975),[135] and by Catalan *et al.* (1995),[136] with *R*-factors of 11.8% (293K) and 4.2% (293K) respectively. The structure was re-determined here with an *R*-factor of 2.67% (130K).

The crystals of **(2)** exhibit monoclinic, C2/c symmetry. The asymmetric unit consists of half the metal complex and one nitrate anion giving the empirical formula $[Cu_{0.5}(C_{12}H_8N_2)(H_1O_{0.5})]N_1O_{1.50}$. Each copper atom has distorted trigonal bipyramidal geometry, coordinating four nitrogens from two *phen* ligands (Cu–N = 1.996–2.059 Å), and an oxygen from a water molecule (Cu–O = 2.051Å), with the 2+ charge

counter-balanced by two nitrate anions. Thus the molecular unit of **(2)** has composition: $[Cu(phen)_2(H_2O)].(NO_3)_2$ **(**Figures 3-2 and 3-3**)**. One nitrogen from each *phen* ligand coordinates to the copper in the axial positions, with a Cu–N distance of 1.996 (2) Å, while the other nitrogens and oxygen occupy the equatorial positions, with a Cu–N distance of 2.059(2) Å and Cu–O distance of 2.051(3) Å.

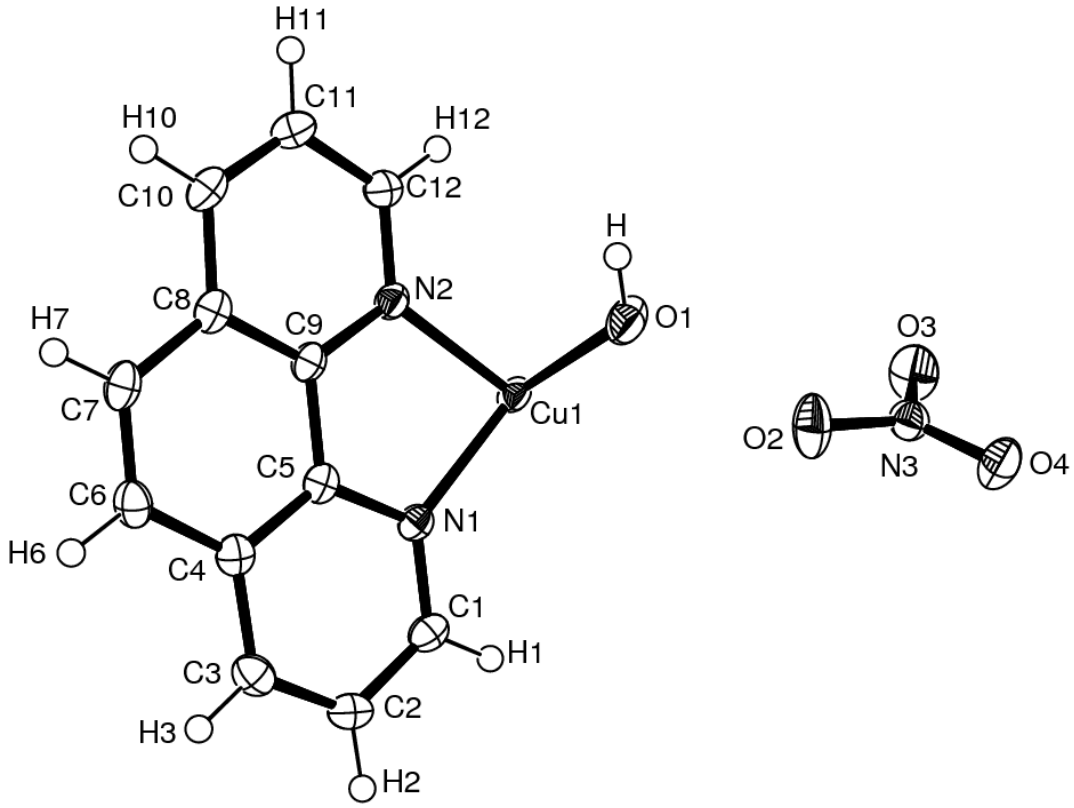

Figure 3-2 ORTEP Diagram of the asymmetric unit of $[Cu(phen)_2(H_2O)]^{2+}$ $(NO_3^-)_2$ **(2)**.

In the crystal lattice, the complex exists as zigzag ribbons of alternating $[Cu(phen)_2(H_2O)]^{2+}$ cations which are held together by a network of hydrogen bonds and Offset-Face-to-Face (OFF) π- π interactions that run along the *c*-axis. This type of π- π interaction is characteristic of *phen* in $M(phen)_n$ complexes, and Dance *et al.* [137] noted that OFF π- π interactions occur more frequently than edge-to-face (EF) interactions. The OFF interactions between the N1N2 *phen* rings are perfectly parallel and each *phen* is engaged in OFF π- π interactions with two *phen* ligands from two neighbouring molecular units. The interplanar distances of the OFF interactions are

3.259Å and 3.338Å, which is in accordance with the values of similar interactions observed by Dance *et al.*[137] The copper cations are associated with the nitrate anions through H-bonds (2.664–3.049Å) (Figure 3-3**)**. H-bonds also occur between the methine CH of the *phen* rings and the coordinated water molecule.

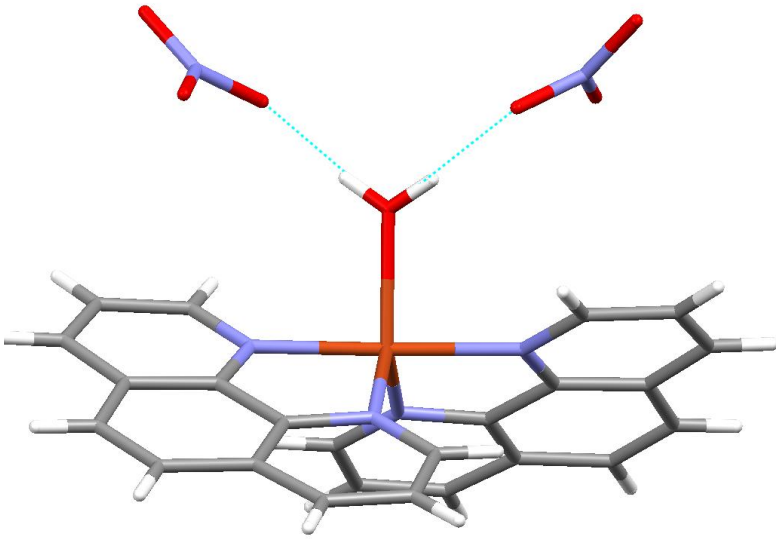

Figure 3-3 Molecular unit of **(2)** showing H-bonding interaction between coordinated water and counter-balancing nitrate anions.

Compound **(2)** is in fact a polymorph of the Nakai (CCDC code APENCU)[135] and Catalan (CCDC code APENCU01)[136] structures, and both possess very similar unit-cell dimensions as seen in Table 3-3.

Table 3-3 Summary of single crystal xrd data for compounds **(2)**, **(3) APENCU**[135] and **APENCU01**.[136]

	(2)	**APENCU**[135]	**APENCU01**[136]	**(3)**
Empirical formula	C_{24} H_{18} Cu N_6 O_7	C_{24} H_{18} Cu N_6 O_7	C_{24} H_{18} Cu N_6 O_7	C_{48} H_{39} Cu_2 N_{10} O_{17}
Molecular weight	565.98	566.0	566.0	1154.97
Crystal Class	monoclinic	monoclinic	monoclinic	triclinic
Space Group	C2/c	C2/c	Cc	P-1
a, Å	19.375(5)	22.58(2)	22.640(5)	14.063(5)
b, Å	7.469(5)	7.23(1)	7.254(2)	14.257(5)
c, Å	15.775(5)	16.59(2)	16.604(3)	15.012(5)
α, (°)	90.000(5)	90	90	114.293(5)
β, (°)	100.782(5)	123.6(1)	123.76(2)	95.803(5)
γ, (°)	90.000(5)	90	90	111.651(5)
V, Å ^{3}	2242.5(18)	2256	2267.08	2433.5(15)
Z	4	4	4	2
Crystal description	Slab, green		Blue, elongated prisms	Green, block
T/K	130(2)		298	130(2)
λ (Mo-Kα)/Å	0.71073			0.71073
Number of reflections	5686		2929	2604
Size(mm)	0.15×0.4×0.45		0.9×0.45×0.12	0.2×0.3×0.4
$R_1[F^2>2\sigma(F^2)]$	0.0267	0.118	0.0424	0.0698
wR[F^2]	0.0776		0.0588	0.1889
S	1.064		0.63	1.006

The difference between the unit cell *'a'* dimension and the *β* angle for compound **(2)** compared to the previous structures calls for comment. Compound **(2)** can transform to the alternative monoclinic space group setting, *I2/a* with similar dimensions to the earlier structures (*a* and *c* change as a result of this transformation, but *b* stays the same). However that would require the earlier structures to be incorrectly reported as *C2/c* (*Cc*) when they should be *I2/a (Ia)*. Also the transformation does not affect the *b*-axis, and in **(2)** the *b* dimension is 7.469Å whereas the corresponding values in the previously reported structures are 7.23Å (APENCU) and 7.25Å (APENCU01) and therefore significantly different (Figure 3-4). Nevertheless, the overall unit cell volume is essentially the same for all three polymorphs and indicates that subtle changes in molecular packing can accommodate the change in angle and unit cell dimensions.

The bond lengths and angles observed for APENCU and APENCU01 are quite similar, but differ from those in **(2)**, which is summarised in Table 3-4. The Cu–O distance in **(2)** is 2.052 Å compared to the APENCU and APENCU01 distances of 2.181 Å and 2.189 Å, respectively. This can also been seen by comparing the angles of the *phen* planes in the complex with APENCU and APENCU01 which are 40.57° and 40.59° respectively, whilst **(2)** is 54.97°. The equatorial N–Cu–N angle also increased substantially, with the angle observed in **(2)** being 124.58° and the corresponding angle for APENCU and APENCU01 being 139.60° and 139.65° respectively. The large difference between the bond lengths and angles has been observed previously in work done by Hathaway *et al.*[138] with two $[Cu(phen)_2(H_2O)](Y)_2$ complexes (where Y= $CF_3SO_3^-$ or ClO_4^-). Hathaway found that elongation of the Cu–O distance increased the angles between the *phen* planes and the equatorial N–Cu–N angle, and assigned different stereochemistries to the two complexes. The complex with shorter Cu–O distance and smaller equatorial N–Cu–N angles was best described as a regular trigonal bipyramid (RTB) and the other as a square-based pyramid distorted trigonal bipyramid (SBPDTB), with distortion from the former suggested to occur because of vibronic coupling.[138]

a)

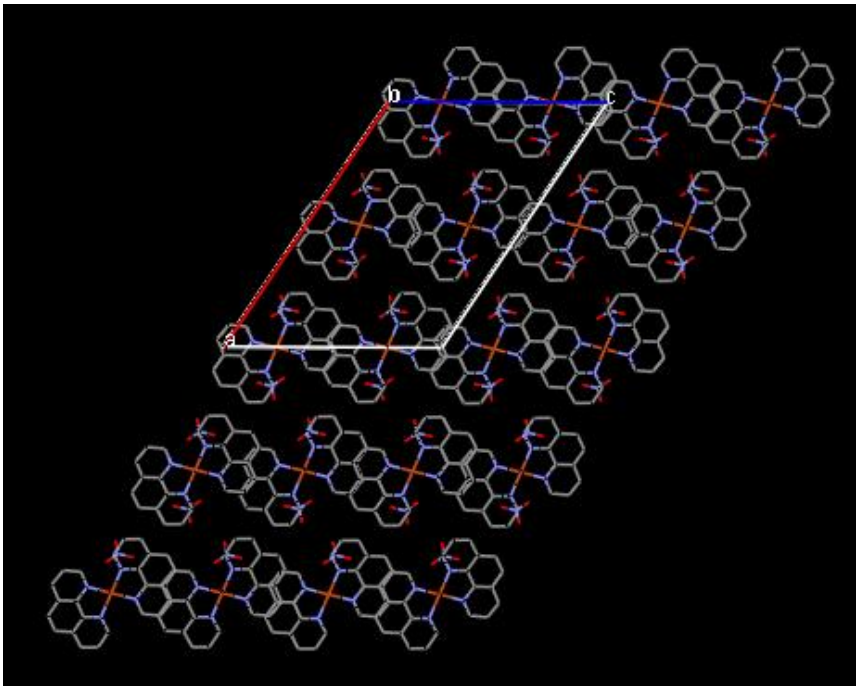

b)

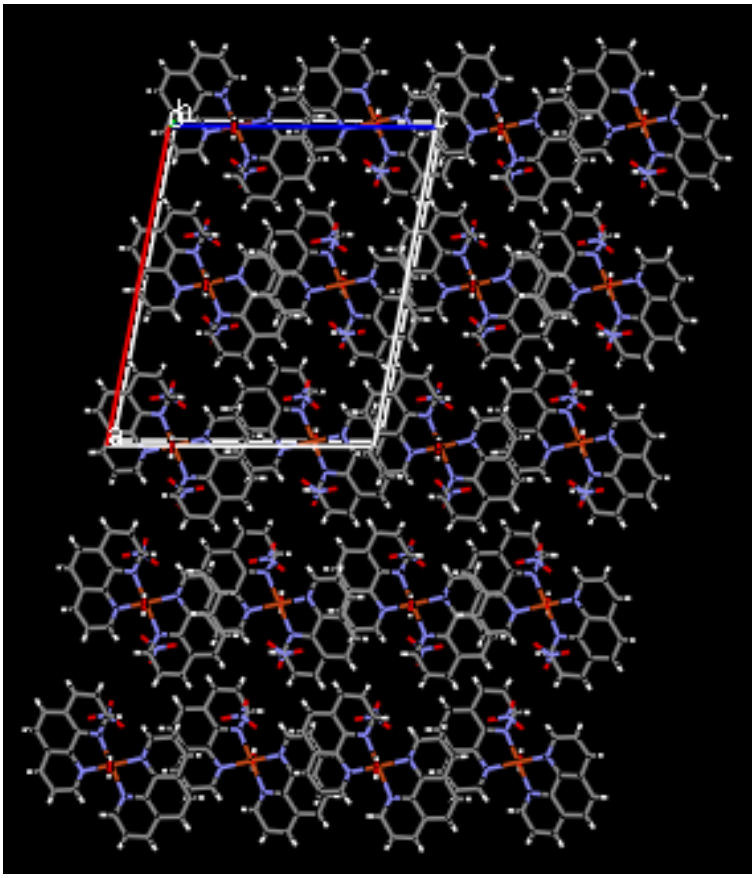

Figure 3-4 Packing of **a)** APENCU,[135] and **b)** complex **(2)**, viewed along *b*-axis.

Table 3-4 Significant bond lengths and bond angles for compounds **(2)**, **APENCU**[135] and **APENCU01**.[136]

	(2)		**APENCU**[135]		**APENCU01**[136]	
	(Å)	**(°)**	**(Å)**	**(°)**	**(Å)**	**(°)**
Cu1 – O1	2.052(3)		2.181(3)		2.189(4)	
Cu1–N1	2.058(16)		1.994(2)			
Cu1–N2	1.996(17)		2.031(3)		1.980(5)	
Cu1–N3					2.010(5)	
Cu1–N4					2.018(5)	
Cu1–N5					2.037(4)	
N1–Cu–O1		117.74(5)		85.49		
N2–Cu–O1		89.32(4)		110.20		
N1–Cu–N2 bite		81.95(6)		83.00		
N1–Cu–N2'		98.70(6)		100.15		
N1–Cu–N1'		124.53(9)		170.97		
N2–Cu–N2'		178.63(8)		139.60		
N2–Cu–N3						82.1(2)
N2–Cu–N4						172.2(2)
N2–Cu–N5						99.1(2)
N3–Cu–N4						101.5(2)
N3–Cu–N5						139.6(2)
N4–Cu–N5						82.7(2)
N2–Cu–O1						84.9(3)
N3–Cu–O1						113.0(3)
N4–Cu–O1						87.4(3)
N5–Cu–O4						107.2(3)

The crystals of **(3)** exhibit triclinic, *P-1*, symmetry and contain the novel compound $[Cu^{(II)}_2(Ophen)_2(phen)_2](NO_3)_2$. The asymmetric unit, and, in this case the molecular unit, consists of a hetero-ligand dinuclear copper(II) complex of formula $[Cu_2(Ophen)_2\,(phen)_2].(NO_3)_2.9H_2O$ (Figure 3-5), with two of these units per unit cell. The unit cell dimensions are a = 14.063 (5) Å, b = 14.258 (5) Å and c = 15.012 (5) Å. The two copper centres are crystallographically independent of one another, they are both five-coordinate and have trigonal-bipyramidal coordination with the Cu_2 dimeric unit bridged via two deprotonated phenolic hydroxy groups, one on each $^{-}$*Ophen* ligand. The latter, together with two nitrate anions, counter-balance the charge of the two copper(II) ions. The voids in the global packing of **(3)** contain two nitrate anions and nine water molecules; however the water molecules and nitrate ions were found to be statically and dynamically disordered, therefore they were removed via the SQUEEZE routine.[118] Without the removal of these species the *R*-factor would be considerably higher and a successful structure determination may not have been possible, hence it enables refinement and good-quality data to be used.

Each copper(II) ion is coordinated by two N atoms from a *phen* ligand (Cu–N = 1.992 – 2.068Å), two N atoms from an $^{-}$*Ophen* ligand (Cu–N = 1.965–2.170Å) and one oxygen (Cu–O = 1.976–1.980Å) from a deprotonated phenolic hydroxy (phenoxy) group on the neighbouring $^{-}$*Ophen* ligand, hence forming an –N=C–O^{-} bridge between the two copper centres, supported by an OFF π-π interaction between the two co-ordinated *phen* groups **(**Figure 3-5**)**. The close proximity of the two metal centres, with a Cu^{2+} – Cu^{2+} non-bonding distance of 3.102Å, is short enough to suggest the possibility of a magnetic interaction between the two unpaired electrons on the Cu_2 unit.

The Cu–N distances for the $^{-}$*Ophen* ligands are considerably different (Cu–N = 1.965–2.170Å), with the shorter distance being observed on the nitrogen adjacent to the coordinating hydroxy group. The axial positions on Cu1 are occupied by N2 ($^{-}$*Ophen*) and N4 (*phen)* and on Cu2 are occupied by N5 (*phen*) and N7 ($^{-}$*Ophen*). Siginifcant bond lengths and bond angles are summarized in Table 3-5.

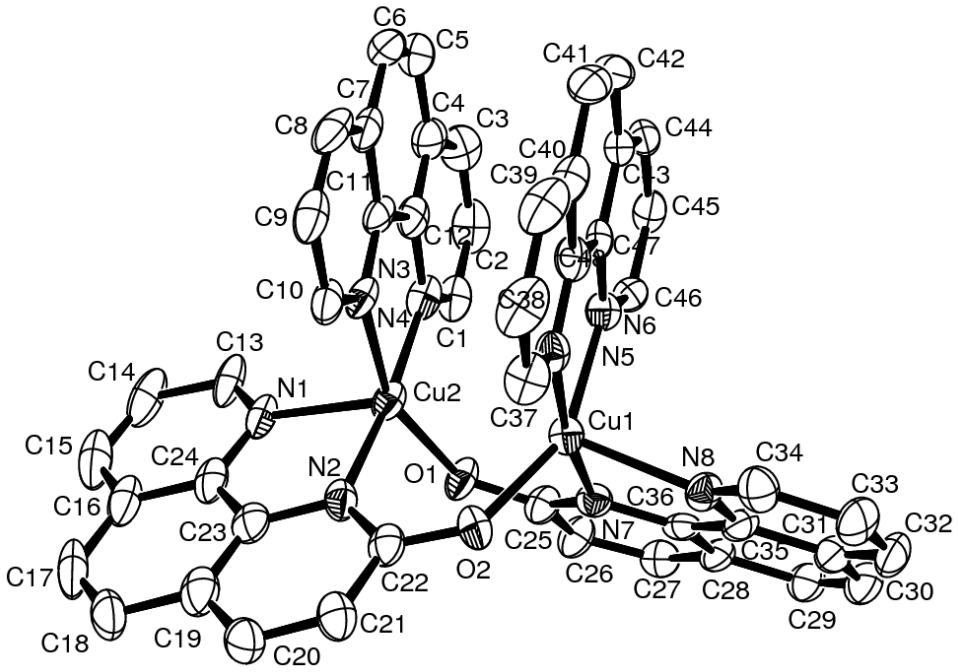

Figure 3-5 ORTEP Diagram of the asymmetric unit of $[Cu^{(II)}_2(phen)_2(Ophen)_2](NO_3)_2$ **(3)** (post application of SQUEEZE[118] routine to remove disordered water and nitrate anions).

In the crystal lattice this novel complex exists as layers of dinuclear copper complexes separated by layers of disordered water molecules and disordered nitrate anions, which are held together by a network of hydrogen bonds and OFF π- π interactions, which run along the *c*-axis as shown in Figure 3-6.

In the discrete Cu_2 dimeric unit an intramolecular OFF interaction occurs between the N3N4 and N5N6 coordinated *phen* rings which deviates from planarity by 6.65°, with a closest approach of 3.279Å between N4 and N6 (Figures 3-5, 3-6 and 3-7). In the crystal packing, intermolecular OFF interactions occur between the ⁻*Ophen* N1N2 ring, and between the *phen* N5N6 rings and between the ⁻*Ophen* N7N8 rings. All interactions are between perfectly parallel aromatic rings with interplanar distances of 3.551Å, 3.361Å and 3.282Å respectively. The cationic copper dimers are also associated with water molecules, through H-bonding (2.790–3.210Å) between the O atoms on the ⁻*Ophen* ligands and water, and between the methine CH groups of the N3N4 *phen* rings and the nitrate anions.

Table 3-5 Significant bond lengths and bond angles for compound **(3)** $[Cu^{(II)}_2(phen)_2(Ophen)_2](NO_3)_2$.

	(3)		
	(Å)		**(°)**
Cu1–O2	1.978(3)	N1–Cu2–O1	100.90(14)
Cu2–O1	1.977(3)	N2–Cu2–O1	94.85(16)
Cu2–N1	2.165(4)	N3–Cu2–O1	156.42(15)
Cu2–N2	1.968(4)	N4–Cu2–O1	91.08(16)
Cu2–N3	2.071(4)	N5–Cu1–O2	90.30(15)
Cu2–N4	1.992(4)	N6–Cu1–O2	153.99(15)
Cu1–N5	1.999(4)	N7–Cu1–O2	97.77(16)
Cu1–N6	2.068(4)	N8–Cu1–O2	104.08(15)
Cu1–N7	1.970(4)	C25–O1–Cu2	133.9(3)
Cu1–N8	2.168(4)	C22–O2–Cu1	135.3(3)
O1–C25	1.299(6)	N1–Cu2–N2 bite	81.83(17)
O2–C22	1.292(6)	N3–Cu2–N4 bite	81.32(16)
		N5–Cu1–N6 bite	81.07(16)
		N7–Cu1–N8 bite	81.44(16)
		N1–Cu2–N4	95.19(17)
		N2–Cu2–N3	93.91(16)
		N2–Cu2–N4	173.77(17)
		N5–Cu1–N7	171.73(16)
		N5–Cu1–N8	94.89(16)

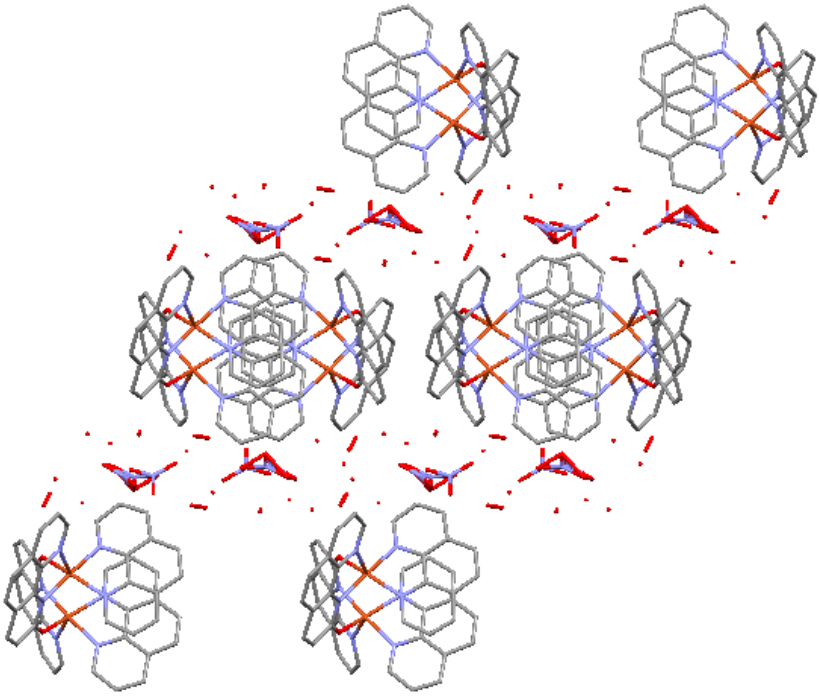

Figure 3-6 Packing of **(3)** $[Cu^{(II)}_2(phen)_2(Ophen)_2](NO_3)_2$ viewed along *c*-axis.

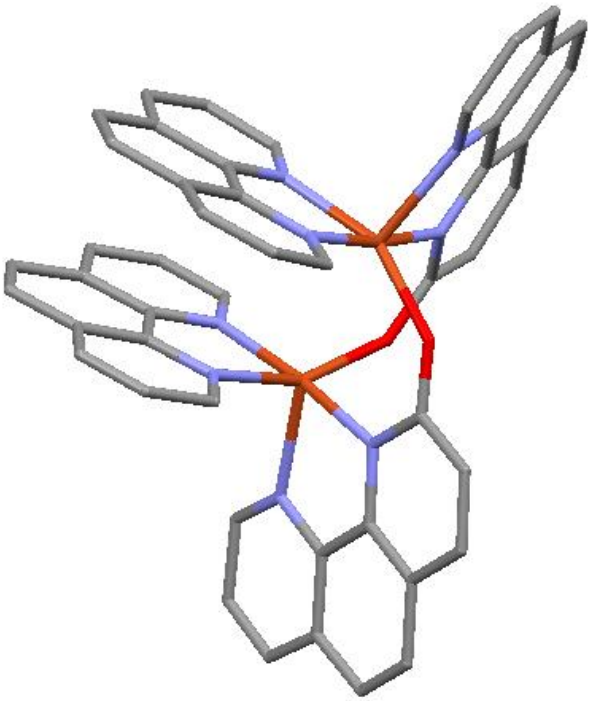

Figure 3-7 Intramolecular OFF π-π interaction in cation of complex **(3)** $[Cu^{(II)}_2(phen)_2\,(Ophen)_2]$

3.3.2. UV-Visible and Fluorescence Spectroscopic Properties

The UV-visble absorption spectra of complexes **(1)**, **(2)** and **(3)** in either a DMF or water solution are shown in Figure 3-8. The black crystals of complex **(1)**, $[Cu^{(I)}_2(Ophen)_2]$ gave a dark red solution when dissolved in DMF, and a broad absorption band was observed from 400–500nm with a λ_{max} at 445nm. This is indicative of a dark red copper(I) complex, with an absorption band shift into the blue region.

Generally the majority of copper(II) complexes are blue or green in visible light as a result of the selective absorption of energy in the 600–900nm region of the electromagnetic spectrum.[41] This is the case in both complex **(2)**, $[Cu^{(II)}(phen)_2(H_2O)]$ and **(3)** $[Cu^{(II)}_2(Ophen)_2(phen)_2]$; with **(2)** showing a broad band from 500 to 730nm, with a λ_{max} at 640nm, and **(3)** showing a broad band from 560 to 730nm, with a λ_{max} at 660nm.

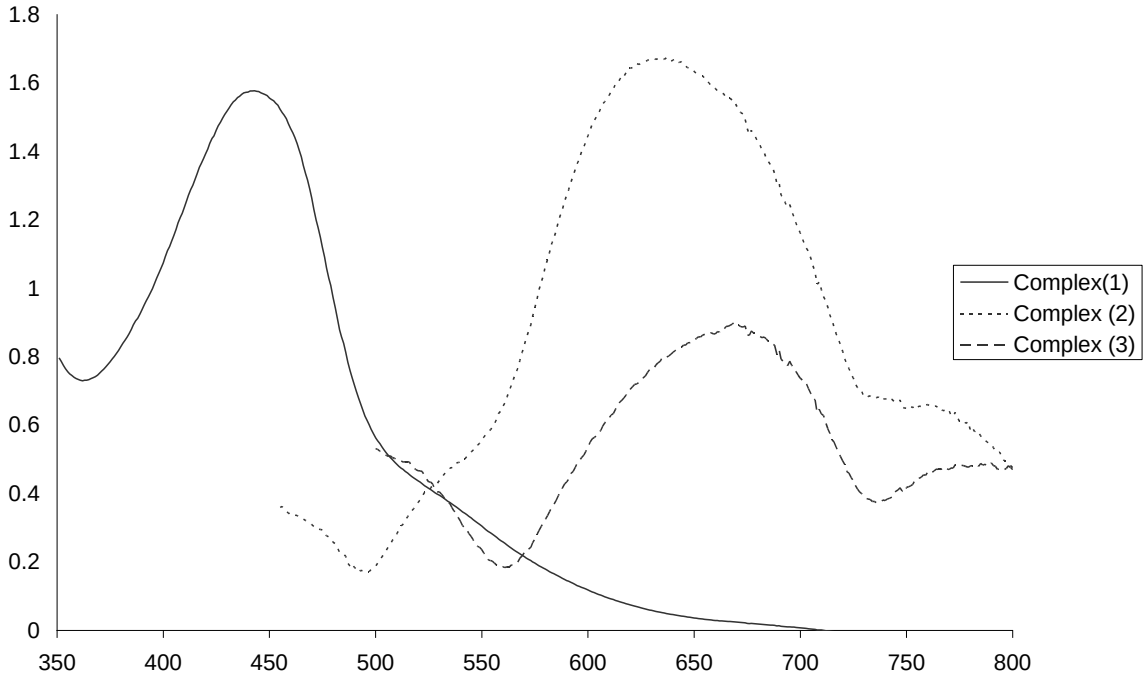

Figure 3-8 UV-Vis of complexes **(1), (2)** and **(3).**

Chen[107] performed photoluminescent studies on complex **(1)** in solution, but no luminescence was observed, indicating that the luminescence of complex **(1)** appears to be quenched when in solution.

In the present work, complex **(1)** exhibited luminescence in the solid-state when it was excited at 252nm, producing an emission band at 370 to 455nm with λ_{max} at 410nm (Figure 3-9), which is suggested to arise from an $^{-}$*Ophen* ligand-centred $\pi \rightarrow \pi^{*}$ transition.[40] Copper(I) complexes do not exhibit *d-d* transitions, due to the full d^{10} orbital manifold, hence its complexes are generally colourless, but ligand-to-metal charge transfer (LMCT) and metal-to-ligand charge transfer (MLCT) often leads to a red or orange coloured complex being observed due to a shift of the UV absorbance into the blue, see Figure 1-11.[41] Weak MLCT was observed when the solid was excited at 422nm, with a λ_{max} 480nm (Figure 3-10). Longer excitation wavelengths shift the emission further into the red region, together with a significant reduction in intensity, as seen when comparing Figures 3-9 and 3-10, where complex **(1)** was excited at 252nm and 422nm respectively.

It has been observed that the luminescence of copper(II) complexes is often quenched by the paramagnetic metal centre. This was found to be the case with complexes **(2)** and **(3)**, which exhibited no luminescent behaviour. As all of these copper complexes lacked fluorescent behaviour in solution, they were not considered for use in DSSC's, and their study was discontinued. However, further studies were conducted on metal complexes using different ligands.

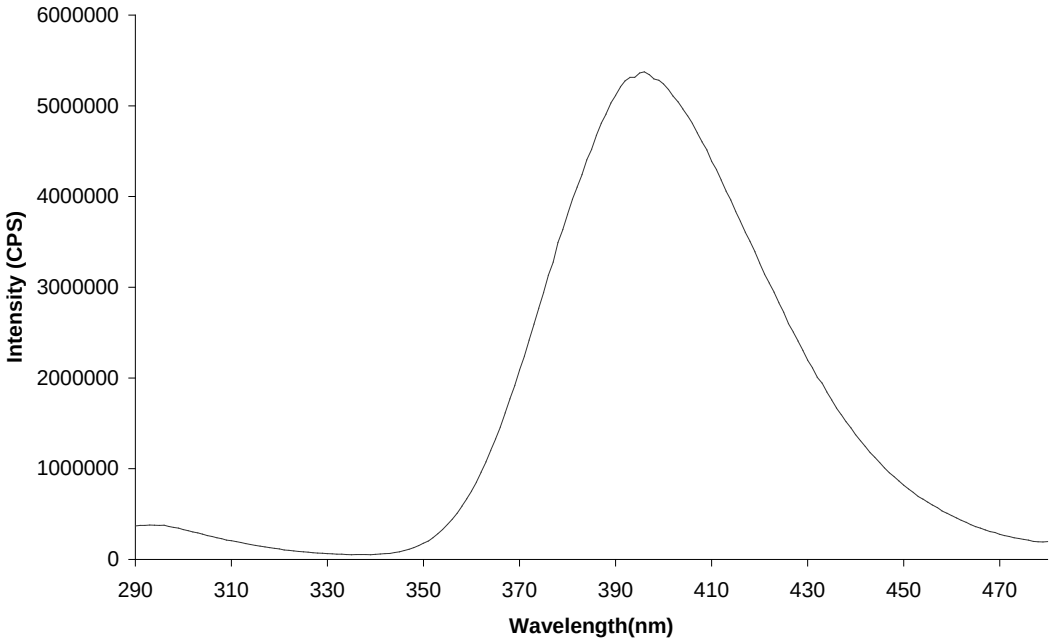

Figure 3-9 Photoluminescence spectrum of complex **(1)** (Solid-State). Excitation wavelength at 252nm. (CPS- Counts per Second)

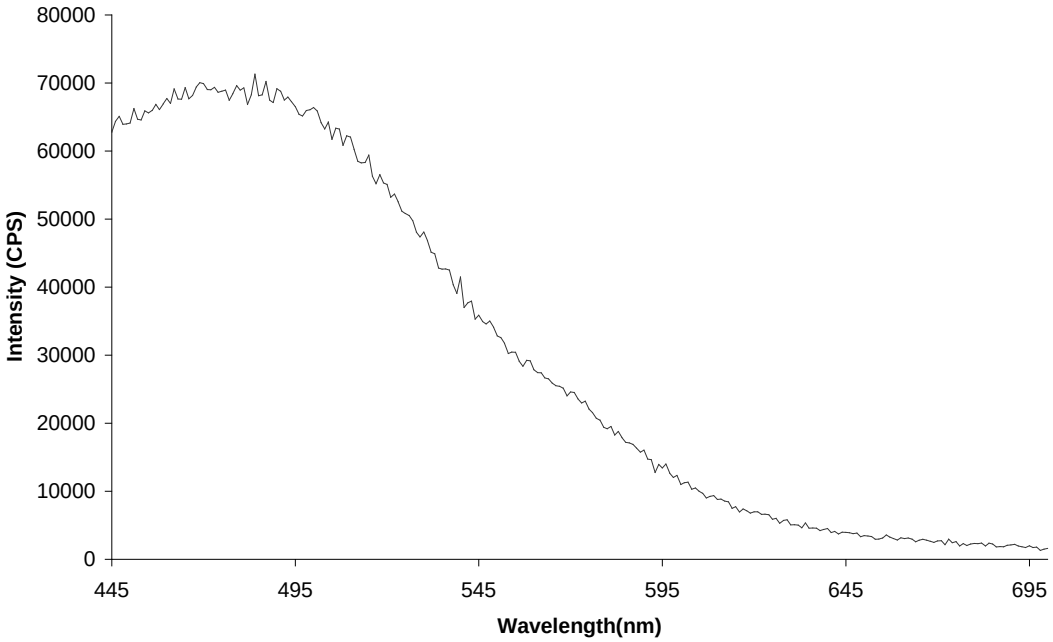

Figure 3-10 Photoluminescence spectrum of complex **(1)** (Solid-State). Excitation wavelength at 422nm (Note that this is 1% of the emission intensity when excited at 252nm, Figure 3-9).

3.3.3. Magnetic measurements

When a substance is placed in a magnetic field, the magnetic field intensity within the substance can either be lesser or greater than the intensity of the applied field. If the effective field is lower in the material, the substance is known as a *diamagnetic* species, and if it is greater within the material then it is termed *paramagnetic*.[114] The magnetisation (**M**) and susceptibility (χ) in diamagnetic samples are both negative, and consequently the sample is repelled weakly by the magnetic source. The net number of free electron spins in the sample is also zero due to all the electrons being paired. On the other hand, in paramagnetic samples unpaired electrons are present, **M** and χ are both positive and the sum of the magnetic dipoles causes the sample to be attracted to the magnetic source.[115] At low temperatures, thermal randomisation is minimized and spontaneous magnetic ordering of the dipoles can occur. If the dipoles are anti-parallel to one another and this is repeated throughout the sample it leads to anti-ferromagnetic behaviour, see Figures 3-11 and 3-12, although this can give way to paramagnetism as the temperature is raised due to thermal disruption of the ordering.

If strong coupling occurs, antiferromagnetic behaviour is observed and the susceptibility (and magnetic moment, μ) decreases as the temperature is lowered. If the dipoles align parallel then ferromagnetic behaviour is observed. Ferromagnetic ordering is less common compared to anti-ferromagnetic ordering, but the susceptibility of such samples can be up to eight orders of magnitude higher than similar paramagnetic species.[115] In the Cu^{II}–Cu^{II} dimers, **(3)**, observed here, the magnetic behaviour depends largely on the coupling (J) of the two single electron wavefunctions ψ (S_1) and ψ (S_2) present in the dimer, as shown schematically in Figure 3-12b. Where weak coupling is present, an essentially paramagnetic system is observed, which may exhibit some ferromagnetic behaviour as a result of magnetic dipole coupling in the bulk crystal. Table 3-6 summarises the essential characteristics of each type of magnetic behaviour.

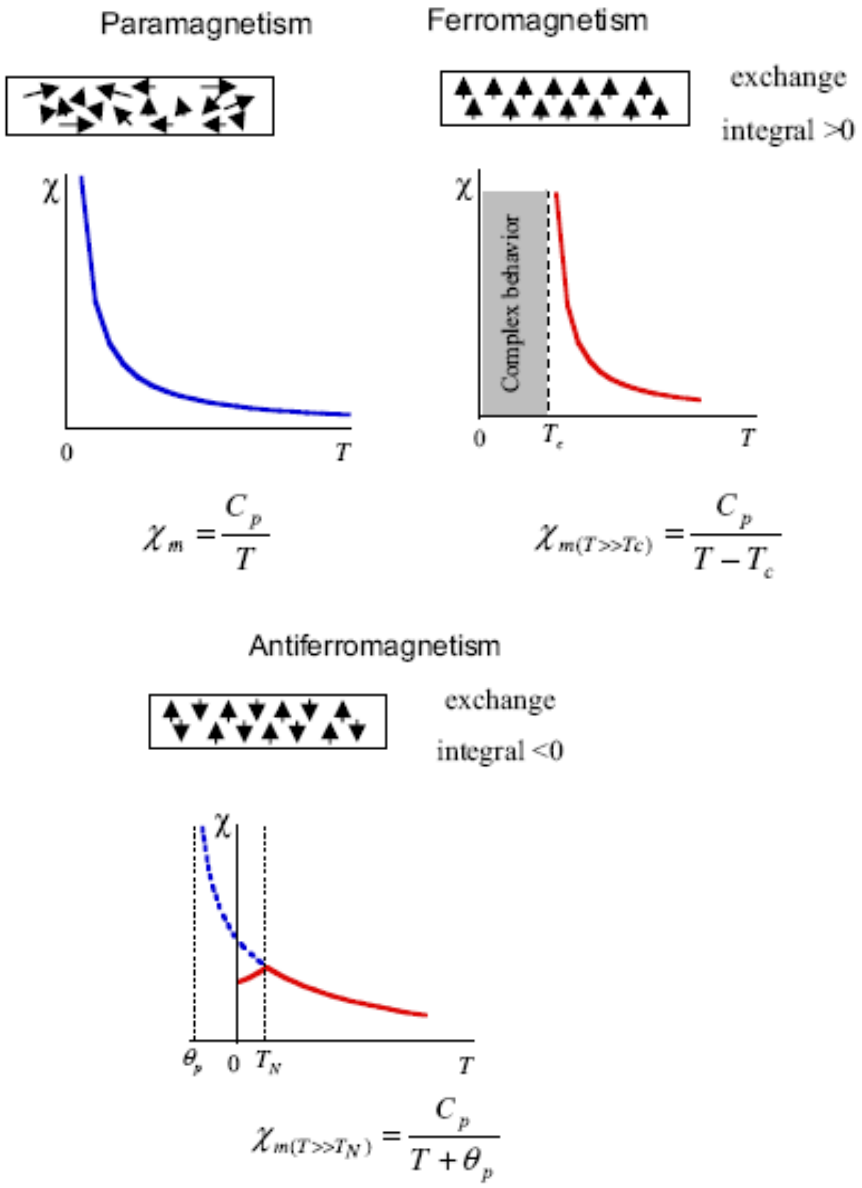

Figure 3-11 Magnetic Susceptibility (χ) versus Temperature (T) plot for various types of magnetic behaviour.[139]

a)

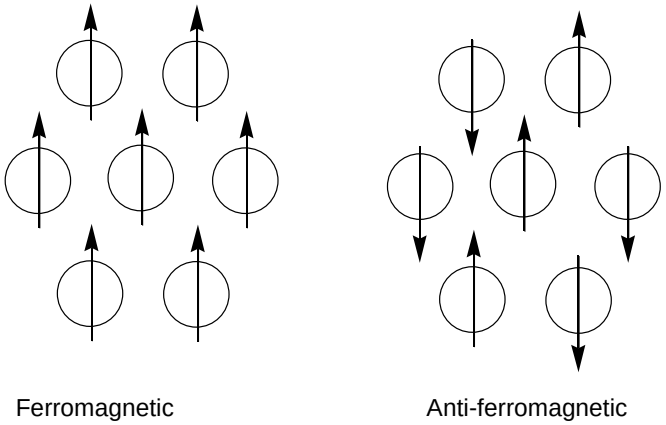

b)

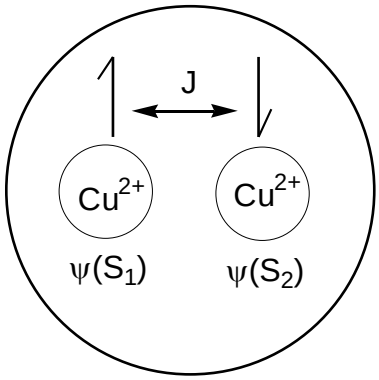

Figure 3-12 a) Magnetic ordering in ferromagnetic and anti-ferromagnetic solids and **b)** Coupling of the two single electrons in a Cu_2 dimeric unit = $J.S_1S_2$ (See Equation 3-3)(J = exchange integral).[115]

Table 3-6 The molar susceptibility of various types of magnetic behaviour at ambient temperatures.[115]

Magnetic behaviour	Molar Susceptibility Magnitude (α)	Dependence on temperature	Dependence on an applied field
Diamagnetism	-10^{-3}	×	×
Paramagnetism	1	✓	×
Anti-ferromagnetism	≤0.1	✓	✓
Ferromagnetism	10^{7}	✓	✓

Compound **(3)** $[Cu^{(II)}_2(Ophen)_2(phen)_2](NO_3)_2$ was found to be paramagnetic with an isotropic *g*-factor (g = 2.10) indicating that the signal originates from copper(II) centres. The effective magnetic moment was found to be $1.74\mu_B$ (μ_B = Bohr magneton, the unit of magnetic moment) per Cu ion at ambient temperature, as expected for non-interacting spin-free Cu(II) d^9 ions calculated according to Equation 3-1.[41]

Equation 3-1

$$\begin{aligned} &For\ Cu^{2+},\ d^9,\ n=1,\ so: \\ &\mu_{eff} = \sqrt{n(n+1)} \\ &\quad = \sqrt{3} \\ &\quad = 1.73\mu_B \end{aligned}$$

The χ_M versus T plot (Figure 3-13) shows that the compound obeys the Curie-Weiss law (Figure 3-11 and Equation 3-2) in the temperature range 80 to 310K:

Equation 3-2

$$\chi_{Molar} = \frac{C}{T}\ and\ \mu_{eff} = 2.84\sqrt{\chi_M \times T}$$

$$so\ \ \chi_M T = \left(\frac{\mu_{eff}}{2.84}\right)^2$$

However, at lower temperatures spin-pairing between the electrons on adjacent Cu(II) ions occurs as expected by Equation 3-3.

Equation 3-3 The modified Bleaney-Bowers relationship[115, 140]

$$\chi_{Cu} = \frac{Ng^2\beta^2}{kT}\left[3 + \exp\left|\frac{-2J}{kT}\right|\right]^{-1}\left|1-P\right| + \frac{Ng^2\beta^2 P}{4kT} + N\alpha$$

χ = magnetic susceptibility

N = Avogadro's number

g = spectroscopic splitting factor

β = the Bohr magneton

K = Boltzman constant

T = temperature

J = the exchange integral

P = the mole fraction of paramagnetic impurity

$N\alpha$ = the temperature independent paramagnetism

In the present case, $J = -44$ cm^{-1} for complex **(3)**, giving rise to typical 'copper acetate' anti-ferromagnetic behaviour ($J = -295$ cm^{-1} for copper-acetate)[115] for **(3)**. The lower exchange coupling for the present compound is consistent with the fact that the two Cu^{2+} centres are further apart (3.10 Å) than in the copper acetate–type derivatives (2.44 – 2.81 Å). In addition, in compound **(3)** the two Cu^{2+} centres are bridged by only *two* N=C–O$^-$ groups supported by *one* OFF π-π interaction, whereas in copper acetate, the two Cu^{2+} centres are bridged by *four* O=C–O$^-$, providing a more rigid framework with greater opportunity for super-exchange coupling between the adjacent Cu*(d_{x2-y2})* orbitals and the *p-π* orbitals on the bridging moieties. [115]

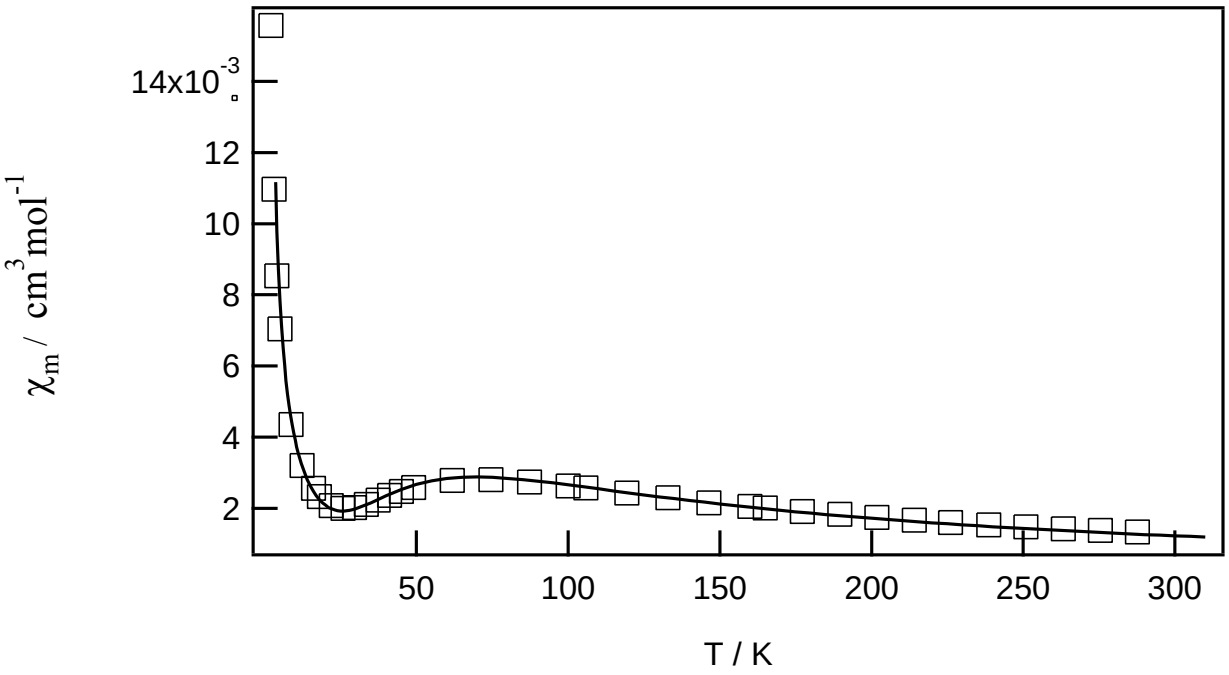

Figure 3-13 Plot of the molar susceptibility versus temperature (per 1Cu centre) for **(3)**.

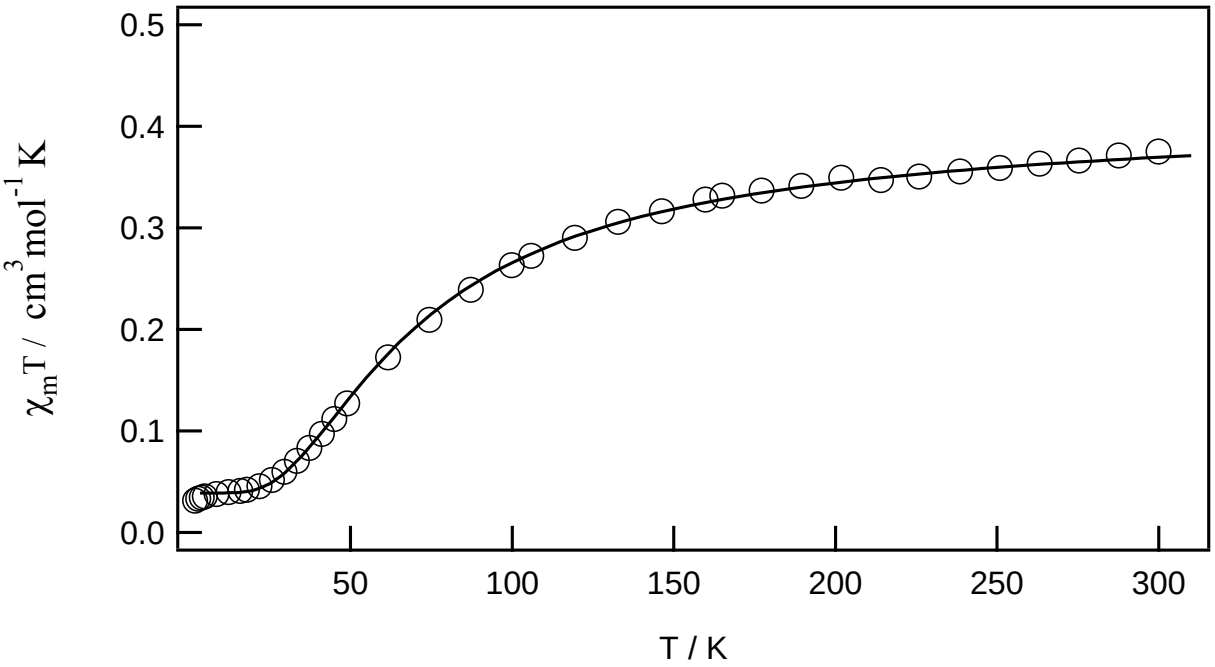

Figure 3-14 The product $\chi_M T$, which is proportional to μ_{eff} , versus temperature (per 1 Cu centre) for **(3)**.

The plot of molar susceptibility (χ_m) per Cu(II) versus temperature (Figure 3-13**)** also displays a maximum at ~60K which is indicative of weak to medium strength antiferromagnetic coupling occurring between the Cu(II) ions in the dinuclear complex (see Figure 3-11). The rapid increase seen below 10K is due to traces of monomer impurity in the sample. Calculations based on the magnetic data indicate there is a 9% monomer impurity in the Cu-dimer sample which is very common, this occurs because the ligand can also form a monomeric complex with paramagnetic behaviour. Monomer impurities of this type tend to have a dominant effect on antiferromagnetic exchange,[141] and the result does not mean that there is 9% impurity in the sample.

The rapid increase at low temperature also shows Curie dependence (Figure 3-11), which is a common observation in the purest dinuclear copper compounds. The corresponding plot of $\chi_m T$ which is proportional to the magnetic moment, μ_{eff} (see Equation 3-2) per Cu(II) versus temperature (Figure 3-14), has a value of 0.38 cm^{3}mol^{-1}K at 300K (equivalent to a $\mu_{eff} = 1.74\mu_B$) which decreases gradually at first, then quite rapidly to reach ~0.03 cm^3 mol^{-1} K at 2K (equivalent to a $\mu_{eff} \sim 0.49\mu_B$)

clearly illustrating the anti-ferromagnetic behaviour of **(3)**. The data fitted well to a $S = ½$ dimer model[140, 142] (See Equation 3-3) with best-fit parameters:

- $g = 2.09$
- $J = -44.2\ cm^{-1}$
- $N\alpha$ (temperature independent susceptibility, per Cu) = $65 \times 10^{-6}\ cm^3\ mol^{-1}$
- Fraction monomer 0.09

The negative J value indicates an anti-ferromagnetic interaction in **(3)** which causes both χ and μ_{eff} to decrease as the temperature is lowered, as seen in Figures 3-13 and 3-14.

Currently, applications of antiferromagnetic materials are quite limited and are generally restricted to use in data-storage systems and sensing.[114-115, 143-144] However, with the current surge in research into these materials the future may unveil more diverse applications.[143]

3.3.4. Mechanistic Considerations of the Hydroxylation reaction

Since Gillard[132] first reported the formation of 'covalent hydrates' by coordinated *phen* and *bipy* there has been considerable emphasis on obtaining structural evidence to support this claim and clarify the reaction mechanism. Gillard proposed that the free hydroxide ion attacks the 2- or 4-position of the coordinated pyridine to form a hydroxy-substituted 1,2- or 1,4-dihydropyridine (Schemes 3-2 and 3-3). Nucleophilic attack at these locations can also be seen on the basis of the charge density calculation in the free pyridine ligand (Figure 3-15),[52] and the reduction in the total charge density suggests that the pyridine molecule is likely to undergo nucleophilic attack. The formation of the hydroxyl species is suggested to provide an explanation for the observed pH dependence of a variety of reactions undergone by complexes of N-heterocycles.

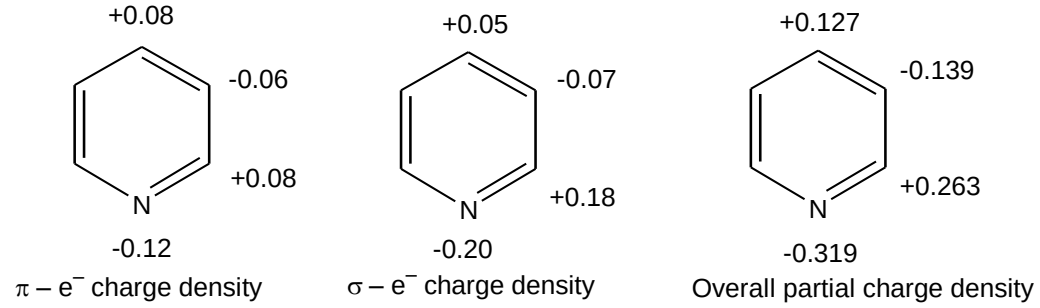

Figure 3-15 σ, π, and overall charge densities in the pyridine molecule [52]

Gillard suggested that with metal cations, pyridine-like ligands could form a 4 - or 6 - coordinate (depending on the metal centre) complex, and, on the basis of the valence-bond structures in Schemes 3-2 and 3-3, nucleophilic attack at the 2 or 4-position of the pyridine ring would be enhanced. However, during the course of the reaction, the site of addition of the nucleophile to the metal-pyridine complex may initially be at the metal, and not at the ligand[52] (see **DH, IMS** in Scheme 3-4). In other words, the first step in the mechanism may be the generation of a bound OH^- on the metal by either base assisted deprotonation of bound water, or the hydroxide ligand co-ordinating directly to the metal ion, instead of covalently-attaching to the pyridine ring. It is of course very difficult to distinguish between these two processes on the basis of kinetic or simple spectroscopic data, unless intermediates are isolated and characterised structurally.

The present work appears to have isolated such intermediates in the reaction of *phen* with Cu^{2+} under mildly alkaline hydrothermal conditions. Since it is known that hydrothermal reactions tend to follow a non-equilibrium course and slight changes in pH, temperature, time and reactant ratios can have an extreme effect on the outcome of the reaction, they provide conditions which allow the synthesis of compounds that cannot be achieved via bench-type reactions.

The observation of significant yields of **(2)**, $[Cu^{(II)}(phen)_2(H_2O)](NO_3)_2$, is not surprising since this compound has been reported to form readily by reaction of copper(II) nitrate with *phen* in aqueous solution, even without pH adjustment.[135-136] It therefore appears that the first stage of the hydroxylation process may involve

deprotonation of the coordinated water molecule on **(2)** to form a $Cu^{2+} - OH^{-}$ species **(DH, IMS** in Scheme 3-4**)**. This step could then be followed by either an ***intra***- or ***inter***-molecular nucleophilic attack at the 2-position of a co-ordinated *phen* ligand to give the **CB** or **CH**, depending on pH, as illustrated in Scheme 3-4. It is agreed that 'covalent hydrates' are formed during this reaction, but that they may form through an alternative route to that favoured by Gillard,[132] whereby, prior to nucleophilic attack on the 2-carbon, a five-coordinate complex in which the hydroxide is coordinated to the metal centre is formed, (see Scheme 3-7a for the ***intra***-molecular reaction, and Scheme 3-7b for the ***inter***-molecular mechanism).

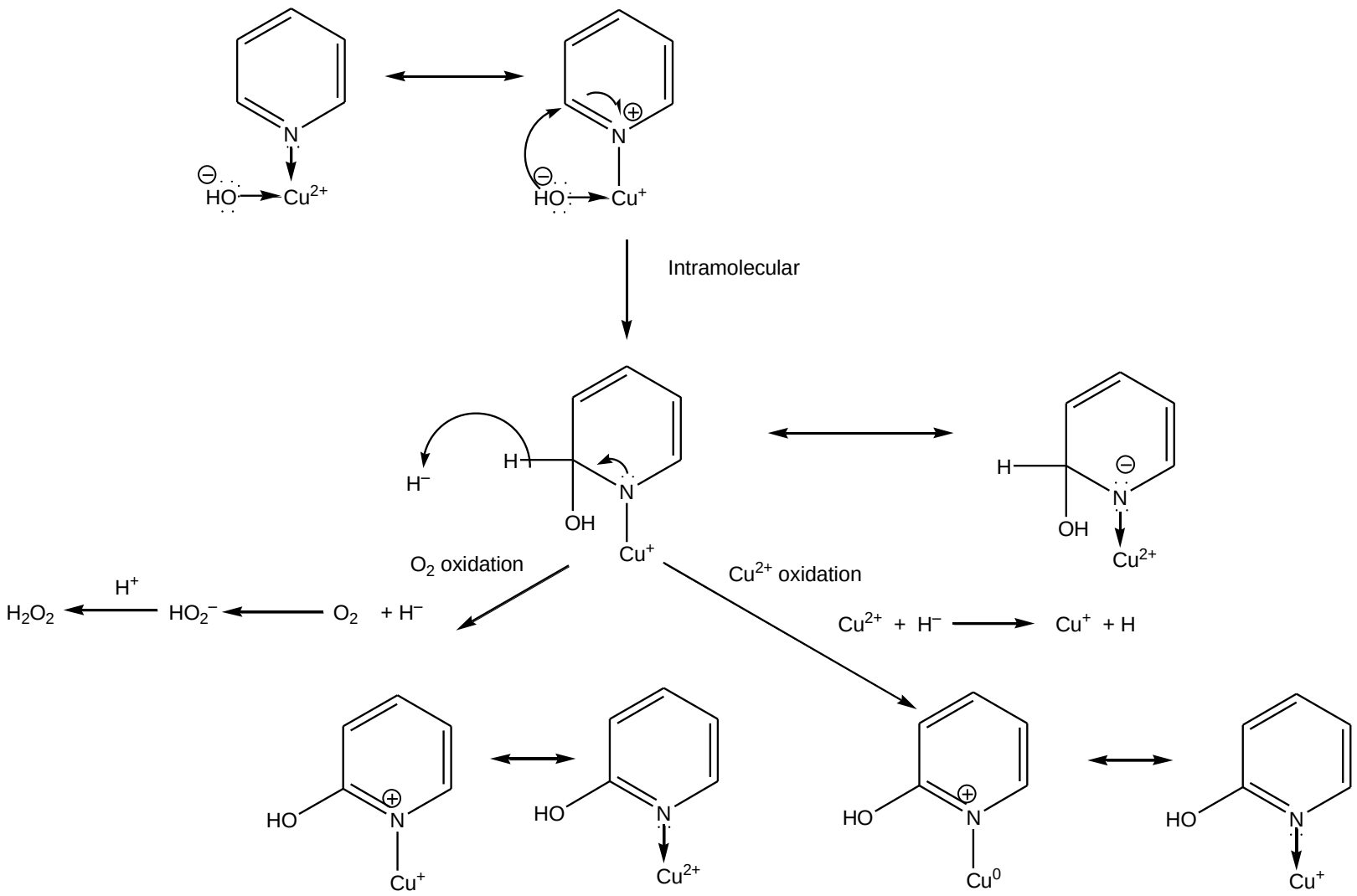

Scheme 3-7a Proposed Mechanism – Intramolecular Shift

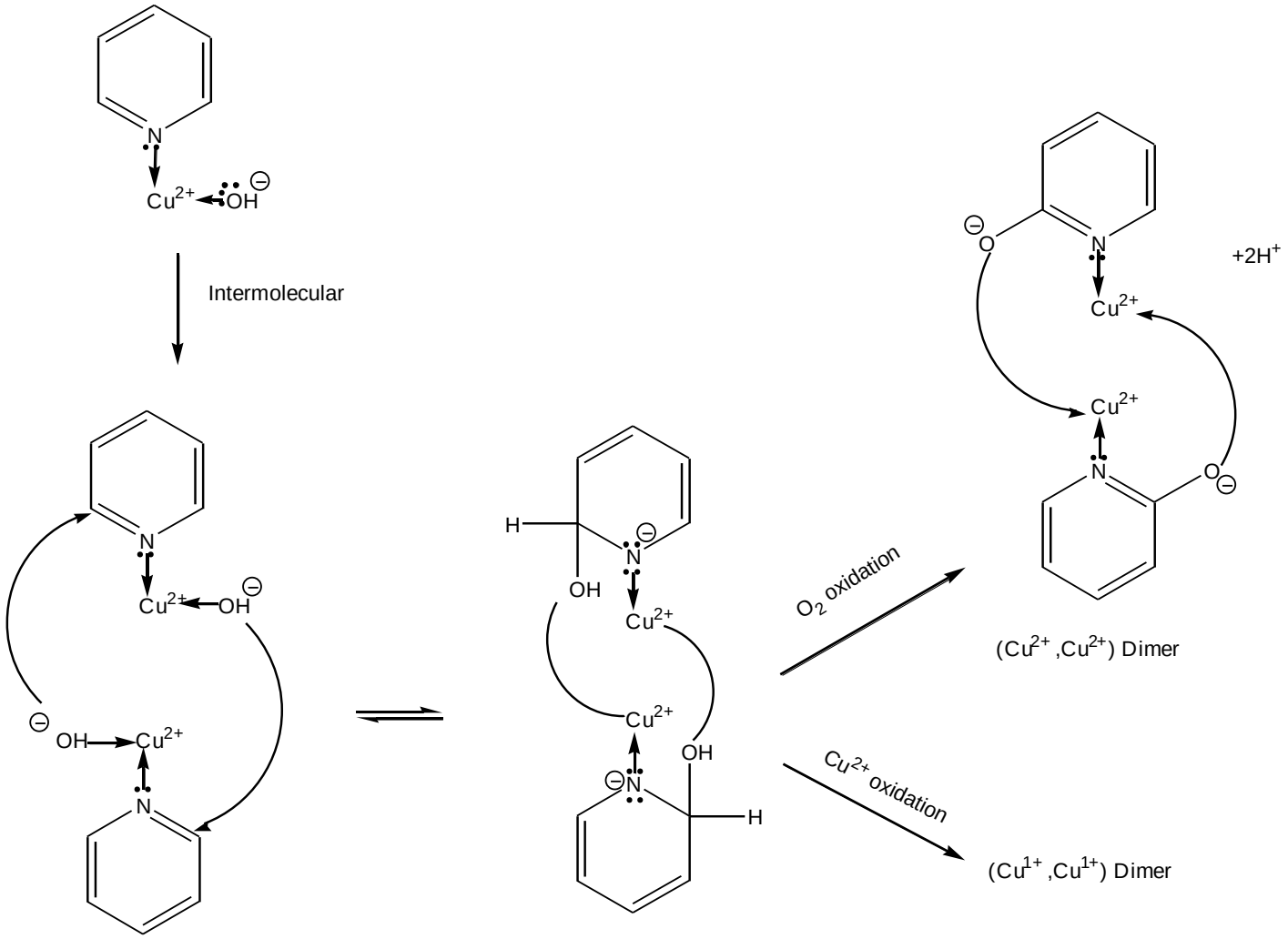

Scheme 3.7b Proposed Mechanism – Intermolecular Shift

Coordination of Cu^{2+} to the *phen* activates the ring towards attack by a nucleophile, and in the proposed mechanism it is the OH^- of the Cu^{2+}–OH^- moiety. Such a suggestion is attractive, because simultaneous binding of *phen* and OH^- to the same metal centre confers a kinetic advantage for the reaction by bringing the reactants into close proximity. If the attached OH^- reacts via an ***intra***-molecular process attacking at the 2-carbon of the *phen* ligand (Scheme 3-7a), it will produce the monomeric (**CB or CH**, Scheme 3-4) hydroxylated species. This can then be oxidised by either an external oxidant such as oxygen, to give a Cu(II) product, or undergo an internal electron transfer to give a Cu(I) product. Dimerisation of the Cu(II) intermediate yields **(3)**, whereas dimerisation and loss of one *phen* ligand gives **(1).** Reaction via an ***inter***-molecular process proceeds in a similar fashion (Scheme 3-7b), but gives rise to a dimeric species containing two hydroxylated *phen's*. Again oxidation by oxygen yields the Cu(II) compound **(3),** whereas oxidation by internal electron transfer leads to ligand (*phen*) release and the formation of the Cu(I) compound **(1)**. Thus, the proposed mechanism provides a rationale for all the products observed in the hydrothermal reaction.

3.4. Conclusion

During studies of the reaction of *phen* with copper nitrate under mildly alkaline hydrothermal conditions, several intermediate products were isolated. These included the expected, and previously reported, neutral Cu(I) homo-dimer $[Cu^{(I)}_2(Ophen)_2]$ **(1)**,[145] and the Cu(II) complex, $[Cu^{(II)}(phen)_2(H_2O)](NO_3)_2$ **(2)** [135-136] together with a novel dinuclear heteroleptic copper(II) complex, $[Cu^{(II)}_2(Ophen)_2(phen)_2](NO_3)_2.9H_2O$ **(3)**.

Compound **(2)** is a polymorph of a previously reported material, and following deprotonation of the coordinated water to produce a Cu^{2+} – OH^- species **(DH, IMS,** Scheme 3-4**)**, may be a key intermediate in the production of **(3)** and **(1)**, since it is always the primary species formed in an aqueous mixture of Cu^{2+} and *phen* under a variety of conditions.[135-136] Thus, an alternative mechanism leading to the formation of 'covalent hydrates' in the hydroxylation of N-heterocycles may be suggested in which the nucleophile that attacks at the 2-carbon of the *phen* ligand in the formation

of **(3)** and **(1)** is not free OH^-, but rather the OH^- coordinated to Cu(II) **(**The **DH, IMS** in Schemes 3-4, 3-7a and 3-7b). Nucleophilic attack is then accompanied by aerial oxidation to give the hetero-ligand Cu(II) dimer **(3)**. The Cu(I) dimer may be formed in a similar fashion, but via an internal electron transfer concomitant with ligand release, giving the Cu(I) product.

Magnetic susceptibility studies on **(3)** confirmed that both Cu cations were in the +2 oxidation state (paramagnetic at T > 80 K), and exhibit anti-ferromagnetic behaviour (suggested by the short Cu–Cu distance) at lower temperatures.

Although the work described here has enabled an alternative mechanism for the Gillard reaction to be proposed, this was not the main purpose of exploring the preparation and isolation of the $^-$*Ophen* ligand. The *HOphen* molecule is known to be luminescent as both a free ligand and also when coordinated to copper(I). Therefore its use as a ligand to form metal complexes for use in solar energy capture was of interest. Unfortunately, it was not possible to isolate sufficient quantities of the free *HOphen* ligand to enable reaction with ruthenium or other transition metals, and therefore the luminescent behaviour could only be tested when coordinated to copper(I). It was found that although the absorption spectrum of $[Cu^{(I)}{}_2(Ophen)_2]$ **(1)** exhibited a broad peak in the visible region, the luminescence was quenched in solution. In the solid-state, fluorescence emission was observed from 370 to 455nm with a λ_{max} at 400nm, which is toward the UV end of the visible spectrum. Excitation at longer wavelengths resulted in a shift further into the red region but the intensity of the emission was drastically reduced. Therefore, in terms of solar energy capture, complex **(1)** was not deemed suitable for further study. Neither of the Cu(II) complexes **(2)** and **(3)** exhibited any fluorescence. Subsequent chapters in this thesis detail the studies undertaken to prepare other metal complexes containing polypyridyl ligands with application to radiative energy capture.

CHAPTER 4

Di-2-pyridyl ketone complexes of Cu(I) and Cu(II) containing iodide and thiocyanate ligands.

4.1. Summary

For their use in DSSC's, metal complexes need to bind securely to the surface of the seminconductor substrate. The interaction of chemical species with a semiconducting surface such as a polar metal oxide can occur through several modes, one of the possibilities being through a dipole-dipole non-covalent interaction utilizing a carbonyl functionality. In this context, di-2-pyridyl ketone (*dpk*) was investigated as a possible candidate to assist with the binding of a metal complex to the surface of TiO_2 and WO_3.

Initial studies investigating the synthesis and properties of $[Cu^{(I)}(dpk)(NCS)]_n$ found two forms, **(4)** and **(5)**, of a polymeric complex of copper(I) with di-2-pyridyl ketone (*dpk*) and thiocyanate anions, in which the latter bridge to form a one-dimensional continuous polymer chain. When either **(4)** or **(5)** was allowed to stand in the acetone supernatant an additional product was isolated, which is a novel ferromagnetic dinuclear complex of formula, $[Cu^{(II)}_2(dpk.acetone)_2(NCS)_2]$ **(6)**.

A dinuclear copper(I) complex $[Cu^{(I)}_2(dpk)_2I_2]$ **(7)**, was also synthesised, which contains two, four-coordinate, copper(I) ions that are bridged through iodide ions. All compounds were prepared by reacting copper(I) salts of either thiocyanate or iodide with *dpk* in the presence of an excess of the sodium salt of thiocyanate or iodide, in an acetone/water solution, with mild heating (~40°C). The black colour of complexes **(4)**, **(5)** and **(7)** made them quite appealing for solar energy capture and their visible spectroscopic data indicated absorbance across the whole visible spectrum. In addition to this, the uncoordinated carbonyl group on the *dpk* of these complexes, provides a potential site for binding to metal oxide semiconductors.

On the basis of the reaction forming $[Cu^{(II)}_2(dpk.acetone)_2(NCS)_2]$ **(6)**, an investigation, using alternative ketones, led to the isolation of five further complexes two, **(8)** and **(9)**, from methyl ethyl ketone solution and three, **(10)**, **(11)** and **(12)** from acetophenone solution. Complex **(8)**, $[Cu^{(II)}(dpk)_2(NCS)_2]$ is a new compound, complex **(9),** $[Cu^{(II)}(dpk.H_2O)_2](NCS)_2.H_2O$, has been described previously.[146] Compounds **(10), (11)** and **(12)** contain the picolinate anion derived from pyridine-2-carboxylic acid (*pic*); **(10)** is composed of square planar $Cu(pic)_2$ with H_2O and a stoichiometric amount of 2 mole of Na^+ NCS^-, that is ordered electrostatically throughout the crystal lattice. Compound **(11)** contains the octahedral $[Cu^{(II)}(pic)_2(NCS)_2]^{2-}$ salt having 2 Na^+ ions and 2 water molecules bonded in the crystal lattice. Compound **(12)** is a mixed coordination copper(II) complex, $Na_2[Cu^{(II)}(pic)_2][Cu^{(II)}(pic)_2(NCS)_2]$ which contains the motifs of **(10)** and **(11)** in a composite structure. The formation of complexes **(10)**, **(11)** and **(12)** is suggested to arise from a novel Baeyer-Villiger rearrangement on both *dpk* and acetophenone.

4.2. Introduction

Coordination polymer networks can form through self-assembly reactions between metal salts and ligands. There has been particular interest in univalent group 11 metals, such as copper(I), as it readily coordinates to bidentate *N*-heterocyclic ligands.[147] This type of combination can lead to 1D-chain or 2D-sheet networks, with numerous types of structures, including the dimeric and polymeric structures, which have been observed with 2,2-bipyridine (*bipy*), 1,10-phenanthroline (*phen*) and

2,9-dimethyl-1,10-phenanthroline (*dmp*) in combination with thiocyanate, iodide and bromide, as shown schematically in Figure 4-1.

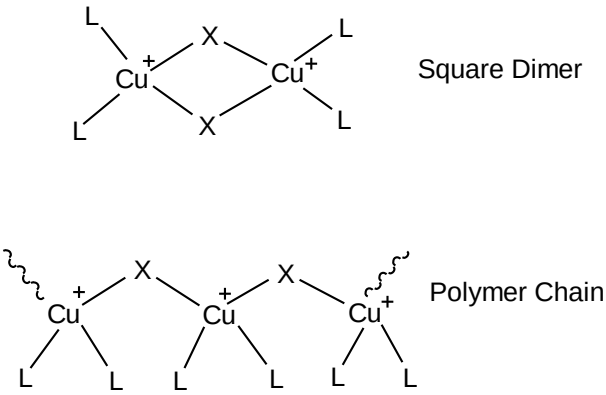

Figure 4-1 Dimer and polymer coordination combinations of copper(I) (where L= heterocyclic ligand, X=halide or pseudo halide) [147]

Polydentate heterocyclic ligands such as di-2-pyridyl ketone (*dpk*) are important building blocks for the preparation of coordination compounds, and metallo-supramolecular assemblies some of which may have application in solar energy capture.[25] The *dpk* ligand is extremely versatile since it has the ability to chelate through multiple donor sites. It is capable of behaving as a bidentate or tridentate ligand chelating through *N,N, N,O,* or *N,N,O*$^{-1}$ donor atoms respectively. [33, 146]

When *dpk* is coordinated to a metal centre the keto-carbonyl group becomes susceptible to nucleophilic addition. Subsequently, *dpk* can transform to a chemically modified ligand through *in-situ* processes, which are not readily achieved through conventional organic methods.[25] For example, in the presence of water the keto-carbonyl can undergo hydration forming a *gem-diol* (*dpk.*H_2O), or in the presence of alcohols (e.g. methanol) an "alcoholated" (*dpk.ROH*) hemi-ketal derivative can form, as indicated in Figure 4-2.[148] The resulting species can coordinate in either the protonated or deprotonated form, and thus the possibilities for *dpk* coordination are extensive.[25]

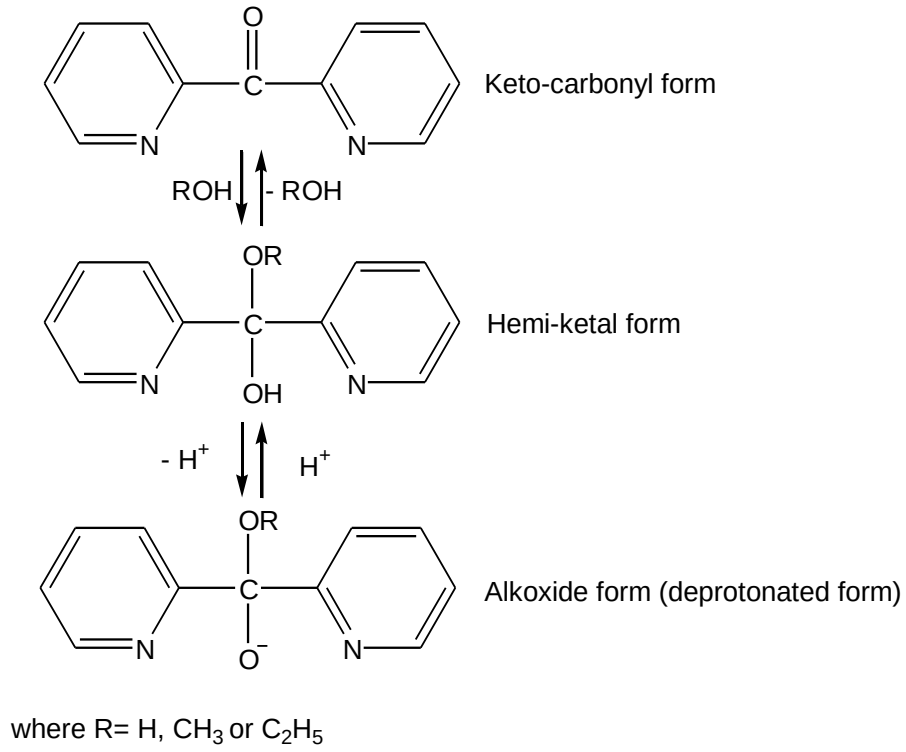

Figure 4-2 The hydrated/ alcoholated *dpk* derivative[33, 146]

Thus, in addition to metal co-ordination in a complex, the utilization of one or more of these features may provide an efficient binding mode for attaching a metal complex to a semi-conducting surface.

The reactivity of the carbonyl group is noteworthy, as generally ketones do not undergo hydration, except when the ketone moiety is adjacent to strongly electron-withdrawing groups. However, in the case of *dpk* the polarisation of the >C=O bond, assisted by the adjacent pyridyl groups, is sufficient to allow for facile hydration.[52, 146] The hydration of ketones is analogous to the hydrolysis of esters which initially occurs through a nucleophilic addition at the ester carbonyl group, forming a tetrahedral intermediate (Figure 4-3).[131] Likewise the hydration of the ketone produces a tetrahedral intermediate which can coordinate directly to a metal centre.

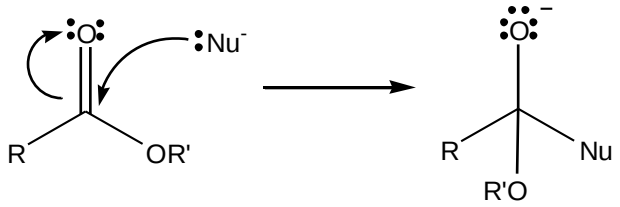

Figure 4-3 Nucleophilic substitution at an ester carbonyl

When deprotonated, the negatively-charged oxygen atom from a hydroxyl group may act as a bridge between metal centres, but the precise mechanism of coordination to the metal before, or after, hydration is unknown. If it occurs before hydration, then there is direct activation of the carbonyl towards nucleophilic attack, whereas if it occurs after hydration, it is due to the polarisation effect of the metal on the hydroxyl group.[52]

Hydrated and alcoholated derivatives of *dpk* are quite common, but recently more interest has developed in the use of other nucleophiles to attack the keto-carbonyl.[25] In particular, in the presence of a Ni(II) salt and acetonitrile *in-situ* cyanomethylation of the keto-carbonyl occurs to form the ligand *dpk*.MeCN,[149] and Abrahams *et al.* have observed nucleophilic attack using bisulfite and pyrazole.[150]

In-situ metal-promoted mixed aldol condensation reactions have been observed in basic solutions containing acetone, and an additional carbonyl group from either a ketone or aldehyde. A condensation reaction of this type has been reported recently by Hussain *et al.* who found that a new aldol ligand was generated when *o*-vanillin reacted with acetone in the presence of Dy(III) and potassium hydroxide.[151] Other transition metal promoted reactions have also been observed with *dpk*. For example in the presence of Co(II) or Ni(II) acetate, Wu *et al.* reported an *in-situ* nucleophilic addition of L-proline as a secondary amine to the keto-carbonyl.[152]

The Perlepes group have also explored the reactions of *dpk* extensively and have published a review summarising this work.[25] Recently, similar to Hussain, where acetone was able to form a nucleophilic enolate,[151] Perlepes observed a Ni(II)-promoted mixed aldol condensation between *dpk* and acetone in the presence of

potassium hydroxide, to form the novel ligand (*dpk.acetone*) observed here in compound **(6)** $[Cu^{(II)}_2(dpk.acetone)_2(NCS)_2]$. However, there has not been a detailed study reported of this work.

Both thiocyanate and iodide ions are efficient bridging ligands and form dimeric or polymeric complexes, making it possible to form neutral networks.[147, 153] Although several *N*-heterocyclic ligands, including 2,2'-bipyridine (*bipy*), 1,10-phenanthroline (*phen*) and 2,9-dimethyl-1,10-phenanthroline (*dmp*) have been incorporated into neutral copper(I) thiocyanate polymeric networks,[153-156] *dpk* analogues have not been explored in any detail. The study most relevant to the work reported here is that of Goher *et al*. who investigated complexes containing copper(I) with iodide and thiocyanate, and the uncoordinated, *N*-protonated *dpk* cation ($dpk.H^+$).[157]

This chapter concerns studies on the Cu-*dpk* system. The work describes eight new complexes and one previously published complex. Two of the complexes are copper(I) polymorphs, **(4)** and **(5)** $[Cu^{(I)}(dpk)(NCS)]_n$, another is an iodo-bridged copper(I) dimer **(7)** $[Cu^{(II)}_2(dpk)_2I_2]$, **(8)** $[Cu^{(II)}(dpk)_2(NCS)_2]$ is a mononuclear copper(II) compound containing *dpk*, **(9)** $[Cu^{(II)}(dpk.H_2O](NCS)_2$ is a mononuclear copper(II) compound containing *dpk* which has undergone hydration. Compound **(6)** is a copper(II) dimer resulting from a facile mixed-aldol reaction between the *dpk* ligand and acetone solvent promoted by Cu(II), in the presence of NaSCN (See Scheme 4-1), while **(10)**, and **(11)** are copper(II) complexes which contain the picolinate (*pic*) ligand, and **(12)** $[Cu^{(II)}(pic)_2].Na_2[Cu^{(II)}(pic)_2(NCS)_2]$ is a composite of **(10)** $[Cu^{(II)}(pic)_2]Na_2(NCS)_2.2H_2O$ and **(11)** $Na_2[Cu^{(II)}(pic)_2(NCS)_2](H_2O)_2$.

4.3. Results and Discussion

4.3.1. $[Cu(dpk)(NCS)]_n$

4.3.1.1. Polymorphs of $[Cu^{(I)}(dpk)(NCS)]_n$ (4) and (5)

Products **(4)** and **(5)** were prepared by reacting copper(I) thiocyanate and excess sodium thiocyanate with *dpk* in acetone and water, forming both black needle-like and block-like crystals of $[Cu(dpk)(NCS)]_n$ in good yield (70%), which could be separated manually on the basis of their crystalline form, see Scheme 4-1.

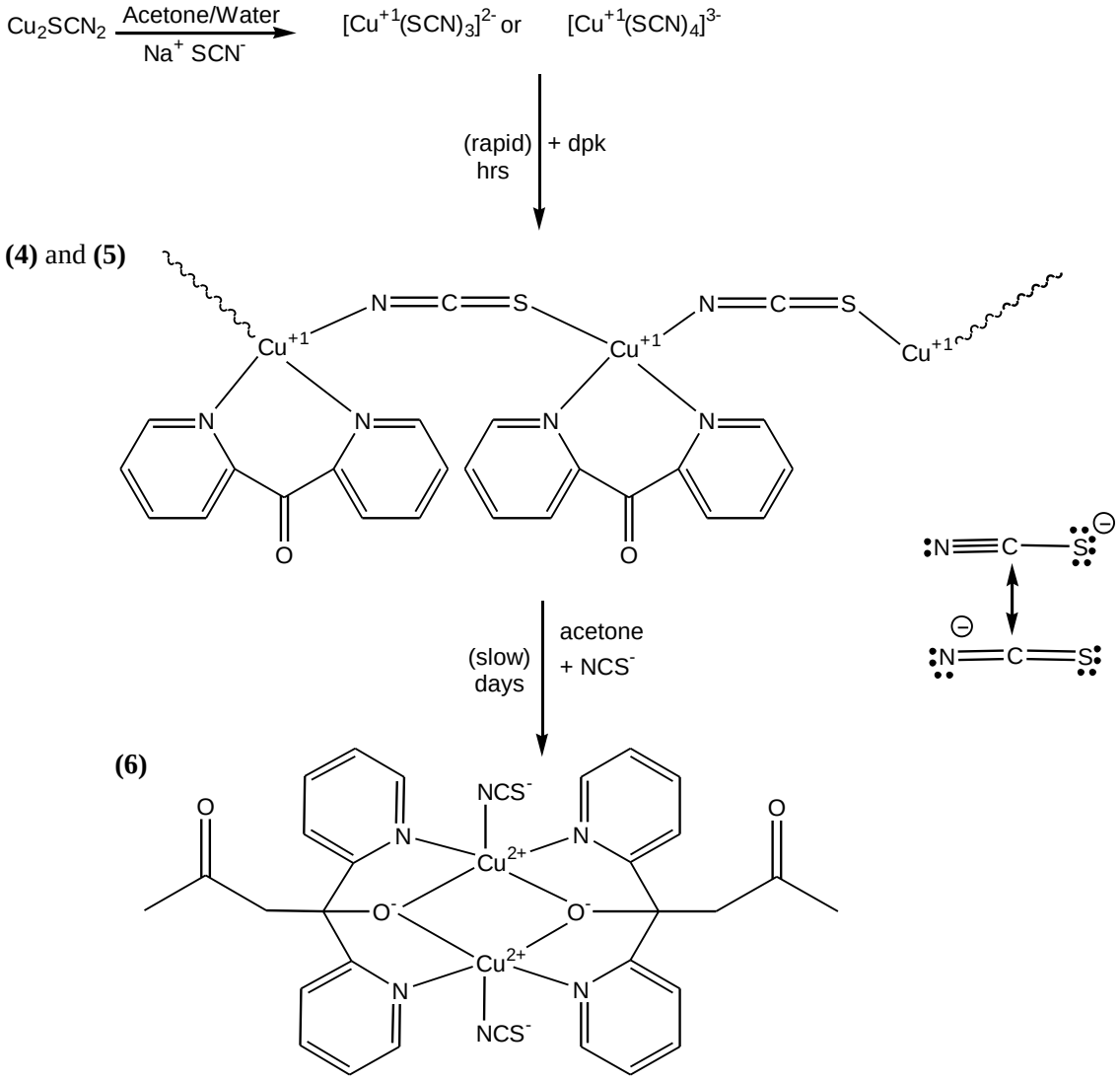

Scheme 4-1 Overall reaction for the formation of compounds **(4)**, **(5)** and **(6).**

4.3.1.2. FTIR of (4) and (5)

The black colour of compounds **(4)** and **(5)** $[Cu^{(I)}(dpk)(NCS)]_n$ suggested the copper was present in the +1 state. FT-IR spectra of **(4)** and **(5)** were identical, with the presence of coordinated NCS being indicated by a strong band at 2091cm^{-1} ($^{\#}$) and the presence of the carbonyl group (C=O) was inferred from a strong band at 1685cm^{-1} (*). This band was also observed in the free *dpk* ligand at 1682cm^{-1}, see Figure 4-4.

When products **(4)** and **(5)** were left in the supernatant liquid overnight they re-dissolved. This was accompanied by a change in colour of the supernatant from purple-red to dark green. The dark green supernatant was left to stand, and within two days product **(6)** was isolated as large, green, block-like crystals in 15% yield. The colour of this material suggested that the copper had oxidized and was now present in the +2 state. The FT-IR spectrum of **(6)**, shown in Figure 4-4, confirmed the presence of NCS with a strong band at 2076cm^{-1} ($^{\#}$), while a weak band at 1711cm^{-1} (*) indicated that a C=O group was also present.

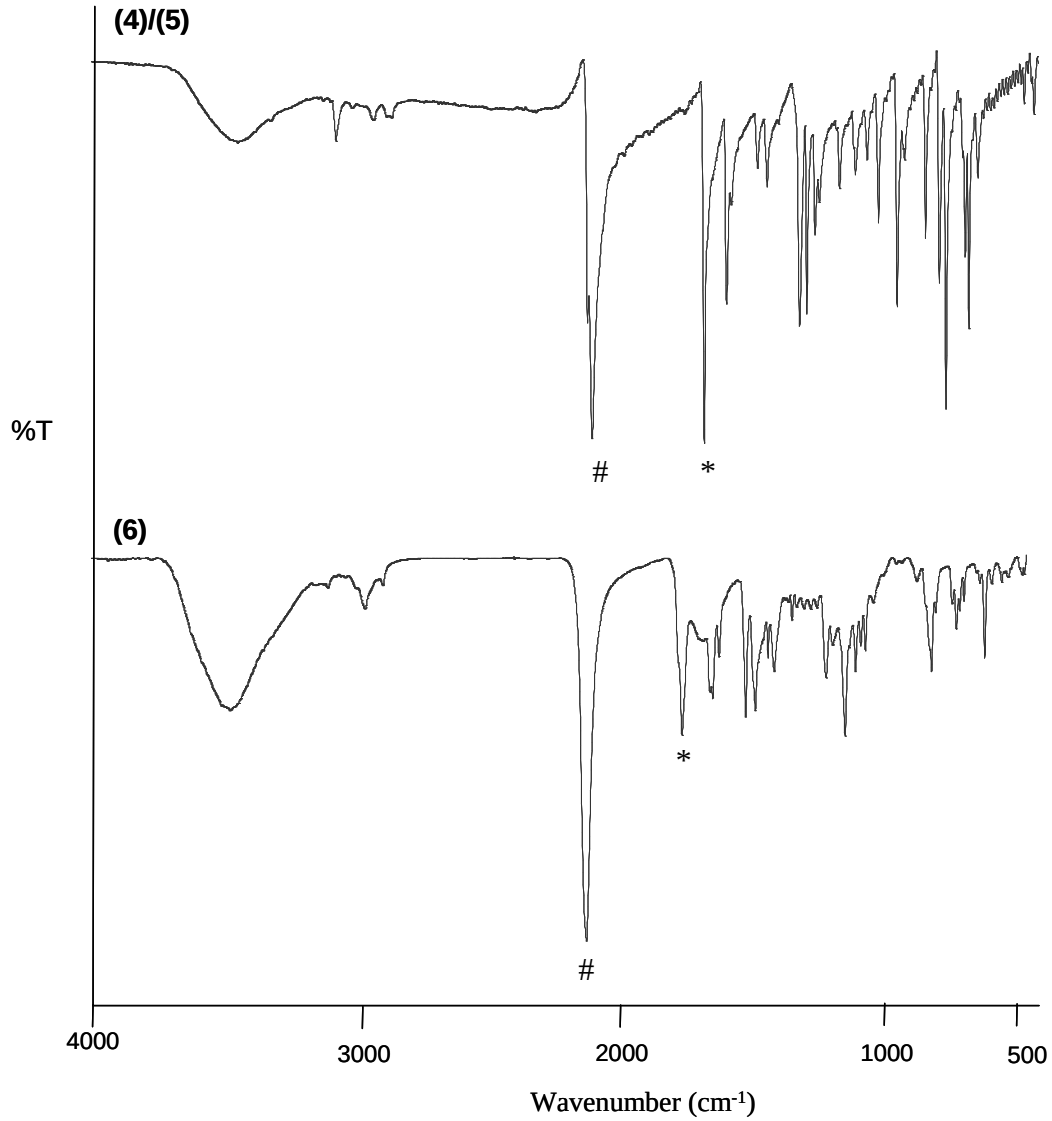

Figure 4-4 FTIR spectra of **(4)/(5)** $[Cu^{(I)}(dpk)(NCS)]_n$ and **(6)** $[Cu^{(II)}_2(dpk.acetone)_2(NCS)_2]$ (where $^{\#}$ = ~2080 cm^{-1} and * = ~1700 cm^{-1})

The compositions of **(4)**, **(5)** and **(6)** were confirmed by single-crystal X-ray diffraction, which provided unambiguous structural characterisation of each complex.

4.3.1.3. Crystal Structures – Polymorphs (4) and (5)

The chemical formulae of **(4)** and **(5)** are the same, $[Cu^{(I)}(dpk)(NCS)]_n$; however, the crystal packing is different with **(4)** exhibiting orthorhombic, *Pmna*, symmetry and **(5)** exhibiting monoclinic, *P21/n*, symmetry. Hence they are polymorphs (see the crystal data in Table 4-1). Both complexes contain a continuous chain of four-coordinated copper(I) species, which are bridged together through thiocyanate groups (both N- and S- donor) forming a one-dimensional linear polymeric network as shown in Scheme 4-1. The copper(I) cation is coordinated to three nitrogen atoms (two from a *dpk* ligand, and one from the bridging thiocyanate), and one sulphur atom from another bridging thiocyanate, forming a distorted tetrahedral structure. The cationic +1 charge on the copper is counter-balanced by the coordinated thiocyanate anion.

This type of coordination enables the copper to remain in its +1 oxidation state, which is beneficial for dye purposes. In addition to this, the carbonyl oxygen is not bound, which provides a potential site for binding to an oxide surface. Both of these points increase the likelihood for this complex to be used for solar energy capture.

The molecular unit of **(4)** and **(5)** has the composition $[Cu^{(I)}(dpk)(NCS)]_n$ illustrated in Figure 4-5; this is comparable to the *bipy*, *phen*, *dmp* and *dafone* (where *dafone* = 4,5-diaza-fluoren-9-one) Cu(I)-thiocyanate analogues previously reported. [146-147, 150, 154]

The monomeric unit of **(4)** contains mirror symmetry, with the copper, the thiocyanate ion and the carbonyl on the *dpk* ligand lying on the crystallographic plane. This type of mirror symmetry has been observed previously with $[Cu(dafone)(NCS)]_n$.[154]

Table 4-1 Summary of the single crystal data for compounds **(4)** to **(6)**.

	(4)	**(5)**	**(6)**
Empirical formula	$C_{12}H_8\,Cu\,N_3\,O\,S$	$C_{12}H_8\,Cu\,N_3\,O\,S$	$C_{67.5}\,H_{67}\,Cu_4\,N_{12}\,O_{10.5}\,S_4$
Molecular weight	305.81	305.81	1596.73
Crystal Class	Orthorombic	Monoclinic	Monoclinic
Space Group	Pmna	P21/n	P2(1)/c
a, Å	8.1396(2)	14.3219(9)	21.932(7)
b, Å	13.4112(3)	5.7110(3)	15.142(5)
c, Å	11.0248(2)	15.0857(9)	23.223(7)
α, (°)	90	90	90
β, (°)	90	109.377(7)	113.514(5)
γ, (°)	90	90	90
V, Å ^{3}	1203.49(5)	1164(12)	7072(4)
Z	4	4	4
Crystal, colour	Needle/ black	Block/ black	Block/green
Crystal size (mm)	0.17 x 0.11 x 0.07	0.04 x 0.03 x 0.02	0.40 x 0.50 x0.50
Temp (K)	130(2)	130(2)	130(2)
Rad wavelength / Å	1.54184	1.54184	0.71073
Radiation type	CuKα	CuKα	MoKα
θ min-max /°	3.29-72.40	3.69-67.45	1.65-27.68
Index ranges	$-9 \le h \ge 9$	$-16 \le h \ge 17$	$-28 \le h \ge 28$
	$-16 \le k \ge 16$	$-6 \le k \ge 6$	$-19 \le k \ge 19$
	$-13 \le l \ge 9$	$-13 \le l \ge 18$	$-29 \le l \ge 30$
No. of reflections	1235	2000	15959
$R_1[F^2 > 2\sigma(F^2)]$	0.0252	0.0732	0.0460
wR[F^2]	0.0666	0.1374	0.1051
S	0.955	0.779	0.846

In the crystal lattice, complex **(4)** exists as a one-dimensional copper(I) polymeric network, bridged through thiocyanate and further associated through edge-to-face (EF) π-π interactions and electrostatic dipole-dipole interactions. The thiocyanate bridging is almost linear with an N–C–S angle of 178.96°.

The EF interactions occur through the aromatic protons of the bound *dpk* ligand and the aromatic ring of identical neighbours at an angle of 65.11° (edge-tilted, T-shaped EF interactions)[158] and a distance of 2.940Å (H-to-ring centre distance), which is indicative of a weak interaction (ca. 2.5-2.7 Å strong interaction) in accordance with the classification of Jennings *et al.*[158] A dipole-dipole electrostatic interaction is observed between neighbouring keto-carbonyl groups, at a distance of 3.181 Å.

The slight negative charge on the oxygen atom causes charge repulsion between the keto-carbonyl groups on the *dpk*, which result in the carbonyl group deviating from the plane of the aromatic groups. The alternating spacial positions of the *dpk* ligands along the Cu-chain are reminiscent of the *syndiotactic* form of polypropylene,[131]as shown in Figures 4-6, 4-7 and 4-8. Significant bond angles and distances for compounds (**4)** and **(5)** are listed in Table 4-2.

a)

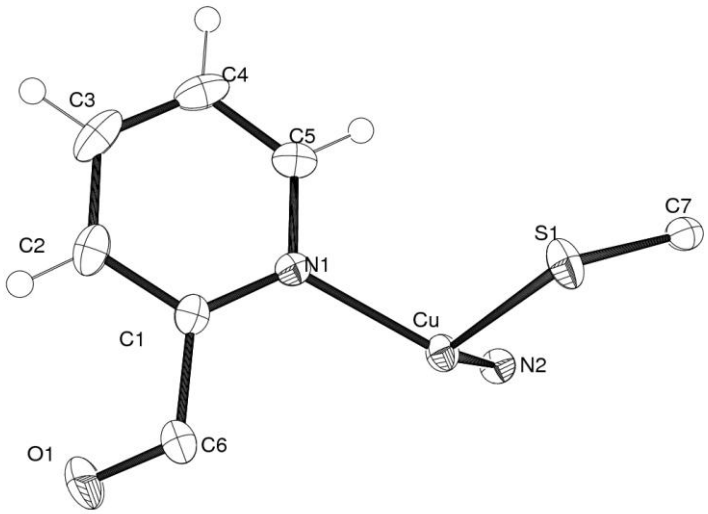

b)

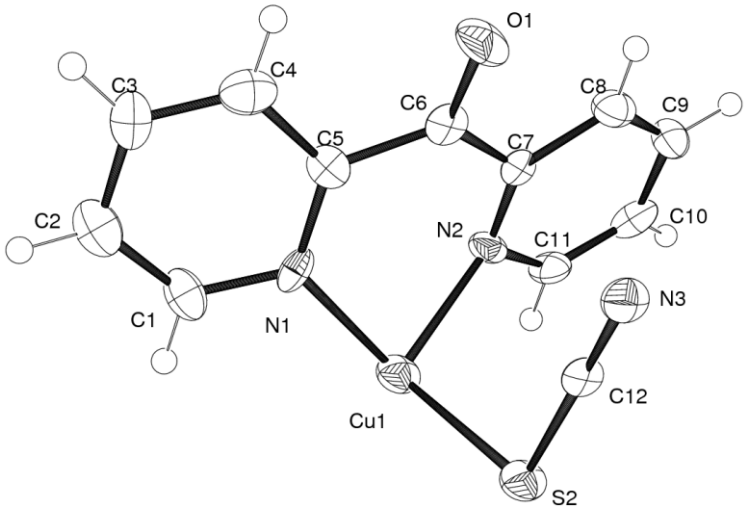

Figure 4-5 Asymmetric units of $[Cu^{(I)}(dpk)(NCS)]_n$

a) compound **(4)** and, **b)** compound **(5)**.

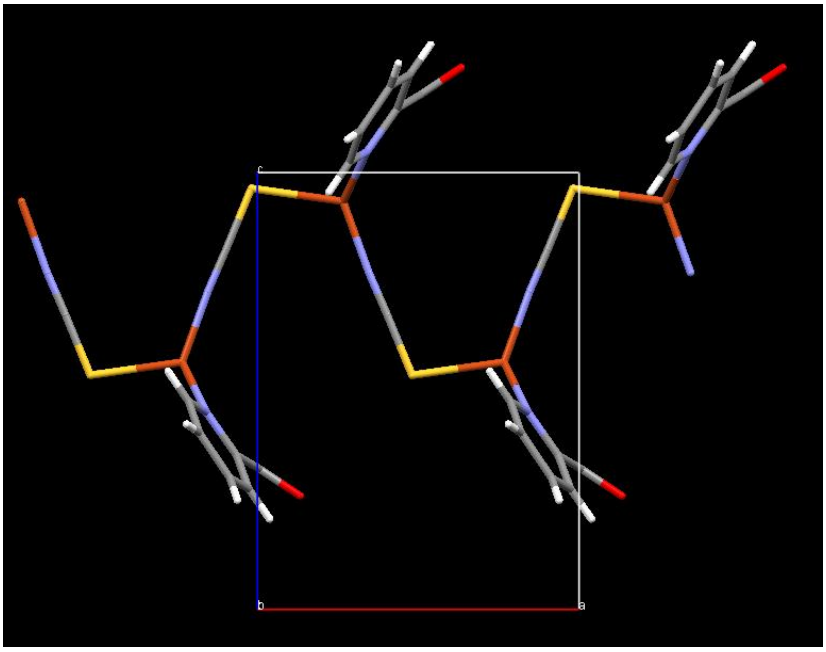

Figure 4-6 Packing of **(4)** $[Cu^{(I)}(dpk)(NCS)]_n$ along the *b*-axis "*syndiotactic*" form

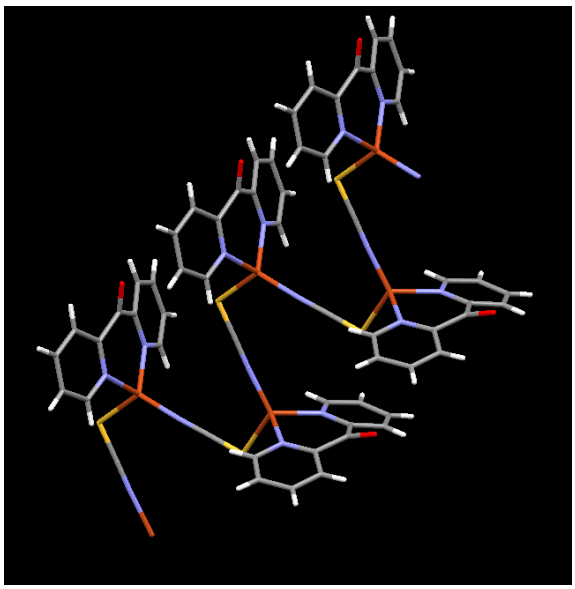

Figure 4-7 Packing of **(4)** $[Cu^{(I)}(dpk)(NCS)]_n$ side view "*syndiotactic*" form

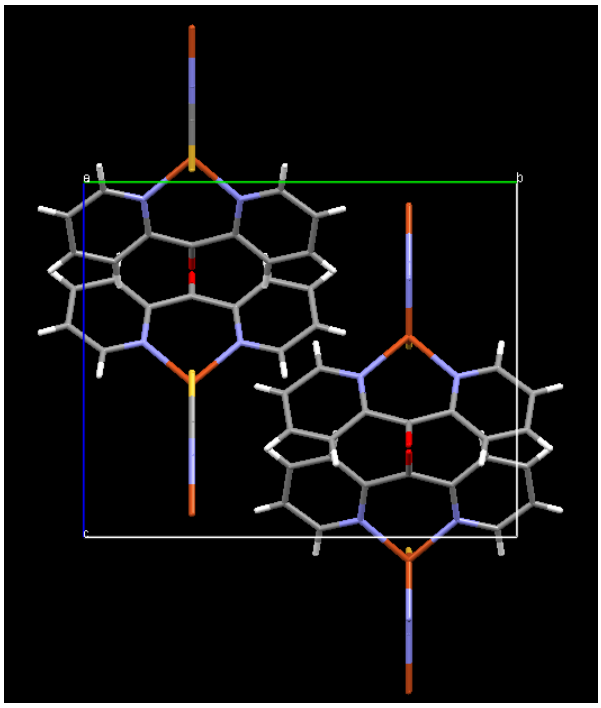

Figure 4-8 Packing of **(4)** $[Cu^{(I)}(dpk)(NCS)]_n$ along the *a*-axis

Compound **(5)** does not exhibit the mirror symmetry observed in **(4)**. However, similar to **(4)**, **(5)** exists as a one-dimensional copper(I) polymeric network bridged through thiocyanate anions in which the spacial distribution of ligands along the Cu-chain is akin to the *isotactic* form of polypropylene,[131] with all the *dpk* ligands located on the same side of the Cu-chain backbone, i.e. they have the same repeating stereo-configuration, see Figure 4-9.

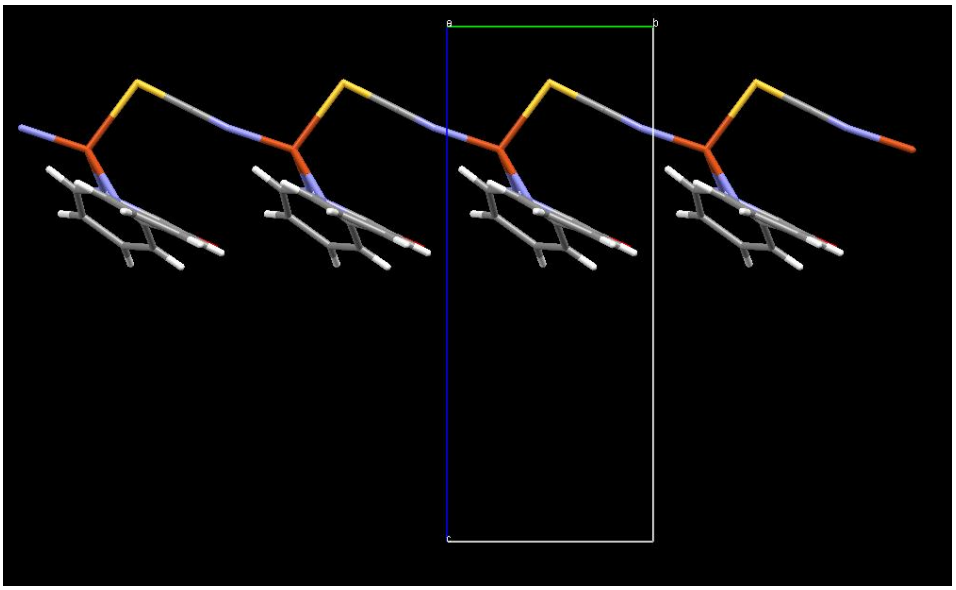

Figure 4-9 Packing of **(5)** $[Cu^{(I)}(dpk)(NCS)]_n$ along *a*-axis "*isotactic*" form

Table 4-2 Significant bond angles and distances for compounds **(4)** and **(5)** $[Cu^{(I)}(dpk)(NCS)]_n$

	(4)		**(5)**	
	(Å)	**(°)**	**(Å)**	**(°)**
Cu1-N1	2.051(1)		2.035(6)	
Cu1-N2	1.911(2)		2.063(9)	
Cu1-N3			1.919(8)	
Cu1-S2	2.347(7)		2.335(3)	
N2-C7	1.153(3)			
N3-C12			1.150(1)	
S2-C7	1.658(2)			
S2-C12			1.660(1)	
C6-O1	1.220(3)		1.220(1)	
Cu1-N1-C1		117.2(1)		116.38
Cu1-N2-C7		176.4(2)		
Cu1-N2-C11				120.0(6)
Cu1-N3-C12				171.5(8)
Cu1-S2-C7		104.42(8)		
Cu1-S2-C12				99.7(3)
N2-Cu1-S2		118.01(7)		
N3-Cu1-S2				107.6(3)
C5-C6-C5		125.6(2)		
C5-C6-C7				123.9(8)
N1-Cu1-N1		94.13(6)		
N1-Cu1-N2				90.0(3)

In the crystal lattice, complex **(5)** is associated through EF π-π interactions and H-bonding. The EF interactions occur between an N1 aromatic ring and the N1 aromatic protons on an identical neighbouring complex at a distance of 2.913Å and an angle of 65.91°. Interactions between the N2 ring and N2 aromatic protons are also observed at a distance of 2.914Å. Weak H-bonding is observed between the keto-carbonyl and the aromatic protons at a distance of 3.163 Å, as can be seen in Figure 4-10. Significant bond lengths and angles are listed in Table 4-2.

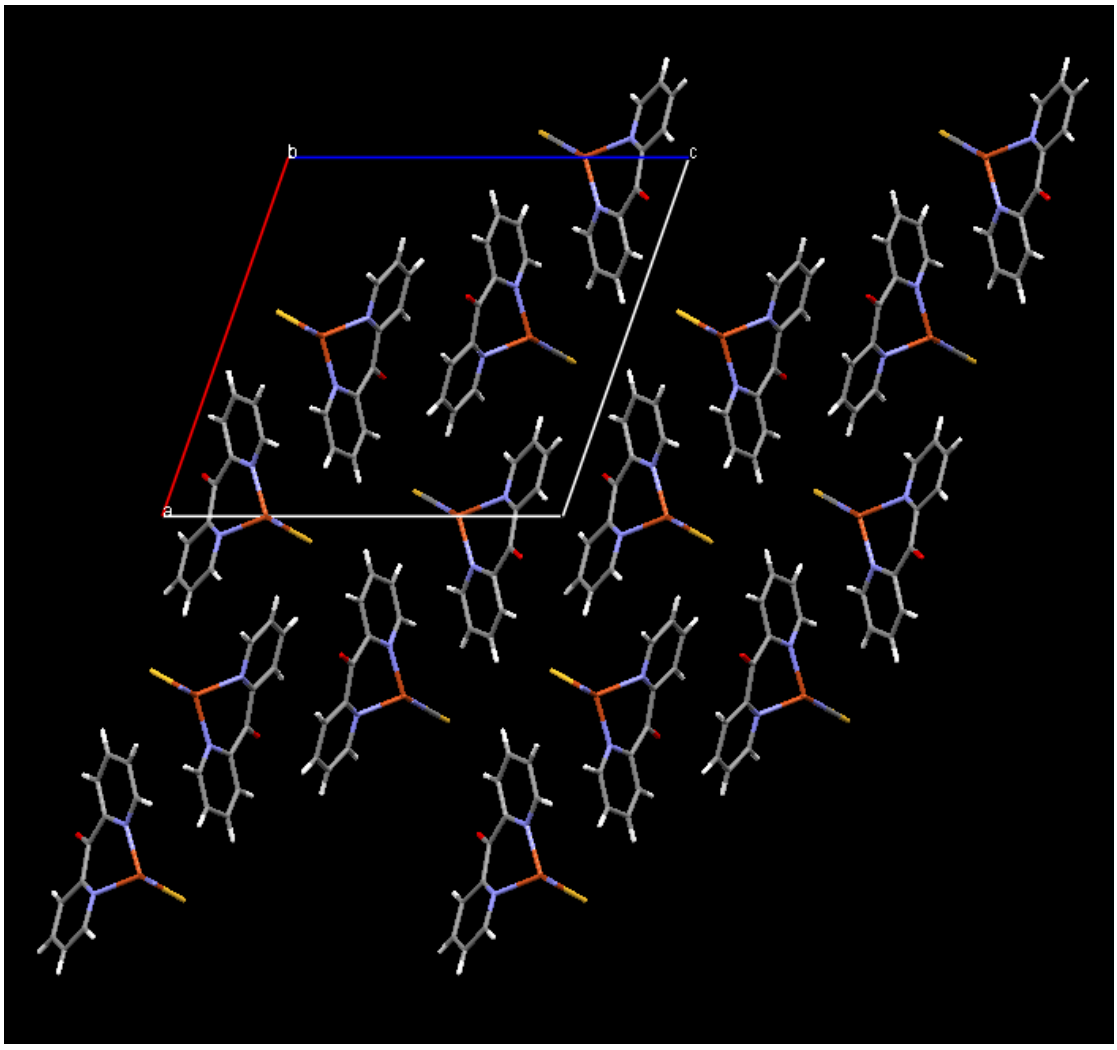

Figure 4-10 Packing of **(5)** $[Cu^{(I)}(dpk)(NCS)]_n$ along the *b*-axis

4.3.2. $[Cu^{(II)}_2(dpk.acetone)_2(NCS)_2]$ (6)

4.3.2.1. Crystal Structure - Complex (6)

The crystals of **(6)** exhibit monoclinic, *P21/c*, symmetry and the single crystal data is listed in Table 4-1. The complex is a novel structure containing a dinuclear copper(II) centre and has the formula $[Cu^{(II)}_2(dpk.acetone)_2(NCS)_2]$ (Figure 4-11). The molecular unit contains two five-coordinate copper(II) ions, with trigonal-bipyramidal coordination, which are bridged through a deprotonated hydroxyl group on each bridging *dpk.acetone* ligand, and also through the two nitrogen atoms on each ligand, resulting in *dpk.acetone* bridging chelation to copper using the N,N',O^- tridentate mode. The anionic charge on the deprotonated hydroxyl groups, along with two N-coordinating thiocyanate groups, counter-balance the cationic charge on the two copper(II) cations. Each copper(II) ion is coordinated by two N atoms from different *dpk.acetone* ligands (Cu-N = 1.979-2.212 Å), one N atom from a thiocyanate (Cu-N = 1.959-1.966 Å) and two O atoms from the deprotonated hydroxyl groups from different *dpk.acetone* ligands (Cu-O = 1.956-1.974 Å), with a Cu-Cu non-bonding distance of 2.872-2.896Å. The asymmetric unit comprises two dinuclear complexes with different symmetries.

In the crystal, the complex exists as ribbons of alternating dinuclear copper complexes, which are associated by a network of H-bonding through the deprotonated oxygen and the acetone-carbonyl to neighbouring aromatic protons and methylene acetone protons, as can be seen in Figure 4-12. The angle between the central carbon bridging the two pyridine rings has decreased (C-C-C ~ 108°) when compared to *dpk* complexes which contain a keto-carbonyl group (C-C-C ~ 125°). This angle change has been observed in other complexes where *dpk* has undergone hydration,[146] and is consistent with a change from a trigonal keto-group to a tetrahedral *gem-diol* (Figures 4-2 and 4-3). Table 4-3 lists the significant bond lengths and angles for compound **(6)**.

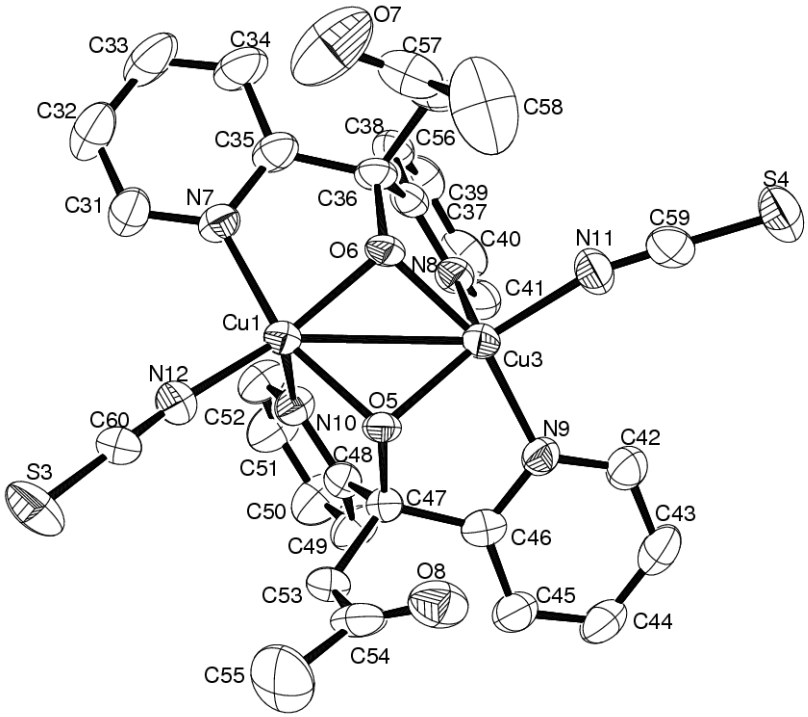

Figure 4-11 Molecular unit of complex **(6)** $[Cu^{(II)}_2(dpk.acetone)_2(NCS)_2]$

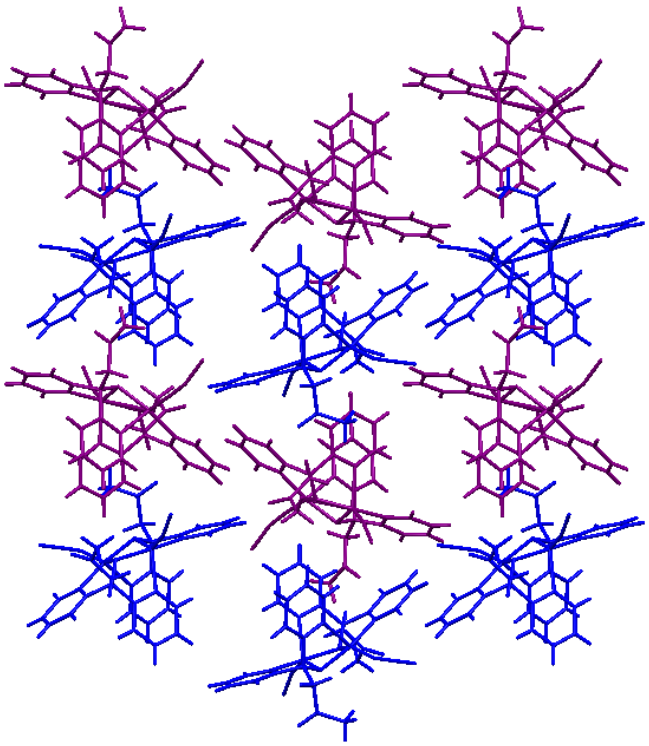

Figure 4-12 Packing of **(6)** $[Cu^{(II)}_2(dpk.acetone)_2(NCS)_2]$ along the *c*-axis, the purple and blue colours representing the alternating dinuclear copper complexes

Table 4-3 Significant bond lengths and angles for compound **(6)**, $[Cu^{(II)}_2(dpk.acetone)_2(NCS)_2]$

	(6)		
	(Å)		**(°)**
Cu1-N7	1.979(2)	Cu1-O5-Cu3 (bite)	95.10(8)
Cu1-N10	2.186(2)	Cu3-O6-Cu1 (bite)	95.01(8)
Cu1-N12	1.965(3)	N10-Cu1-N12	103.0(1)
Cu1-O5	1.956(2)	N11-Cu3-N9	97.3(1)
Cu1-O6	1.963(2)	N12-Cu1-O5	100.06(9)
Cu3-N8	2.212(2)	N7-Cu1-N10	103.2(1)
Cu3-N9	1.982(2)	N8-Cu3-O6	77.39(8)
Cu3-N11	1.959(3)	N8-Cu3-N11	96.5(1)
Cu3-O5	1.965(2)	N9-Cu3-O5	81.39(9)
Cu3-O6	1.961(2)	Cu2-O2-Cu4 (bite)	93.61(8)
Cu2-N1	1.994(2)	Cu4-O1-Cu2 (bite)	93.92(8)
Cu2-N3	2.208(2)	N1-Cu2-O1	80.91(9)
Cu2-N6	1.970(3)	N3-Cu2-N6	99.5(1)
Cu2-O1	1.972(2)	N4-Cu4-N5	98.0(1)
Cu2-O2	1.966(2)	N5-Cu4-N2	104.9(1)
Cu4-N2	2.171(2)	N6-Cu2-N1	97.9(1)
Cu4-N4	1.981(2)	O1-Cu4-N2	78.29(9)
Cu4-N5	1.959(3)	O2-Cu2-N3	77.51(8)
Cu4-O1	1.958(2)	O2-Cu4-N4	81.90(9)
Cu4-O2	1.974(2)	S1-C29-N5	179.4(3)
N11-C59	1.145(5)	S2-C30-N6	164.4(6)
C59-S4	1.636(4)	S3-C60-N12	179.5(3)
N12-C60	1.150(5)	S4-C59-N11	178.9(3)
C60-S3	1.631(4)		
N6-30	1.131(5)		
C30-S2	1.65(2)		
N5-C29	1.154(5)		
C29-S1	1.624(4)		

4.3.2.2. Magnetic measurements

The short non-bonding distance (2.874-2.893Å) between the Cu(II) centres in **(6)** suggests that magnetic interactions may be present. Thus, the magnetic moment and magnetic susceptibility were measured, and the results are presented in Figures 4-13 and 4-14.

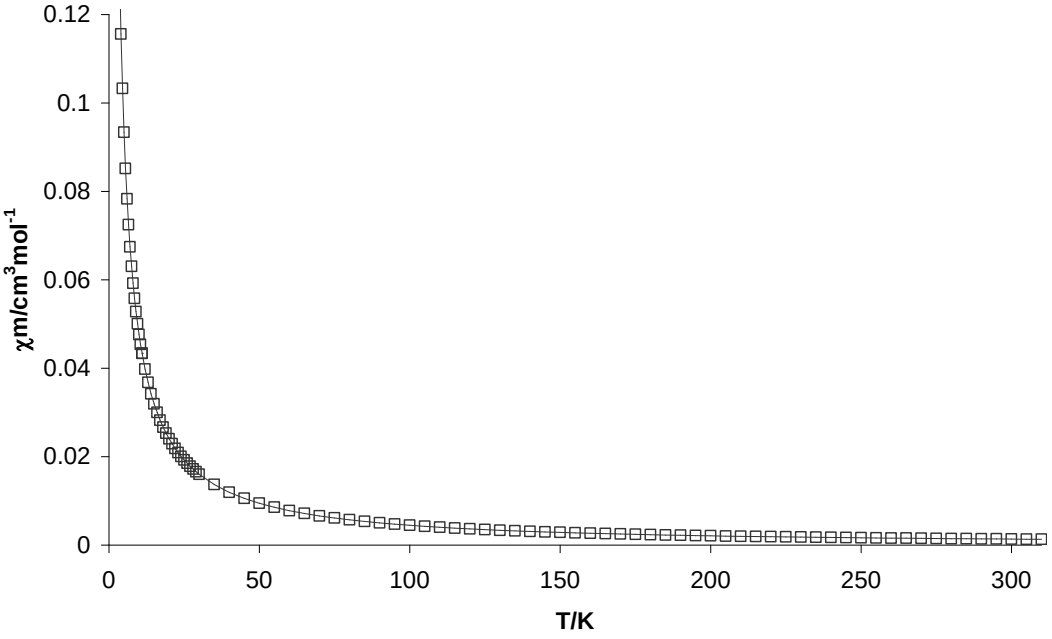

Figure 4-13 χ_m Vs T (per 1Cu centre) for **(6)** $[Cu^{(II)}_2(dpk.acetone)_2(NCS)_2]$.

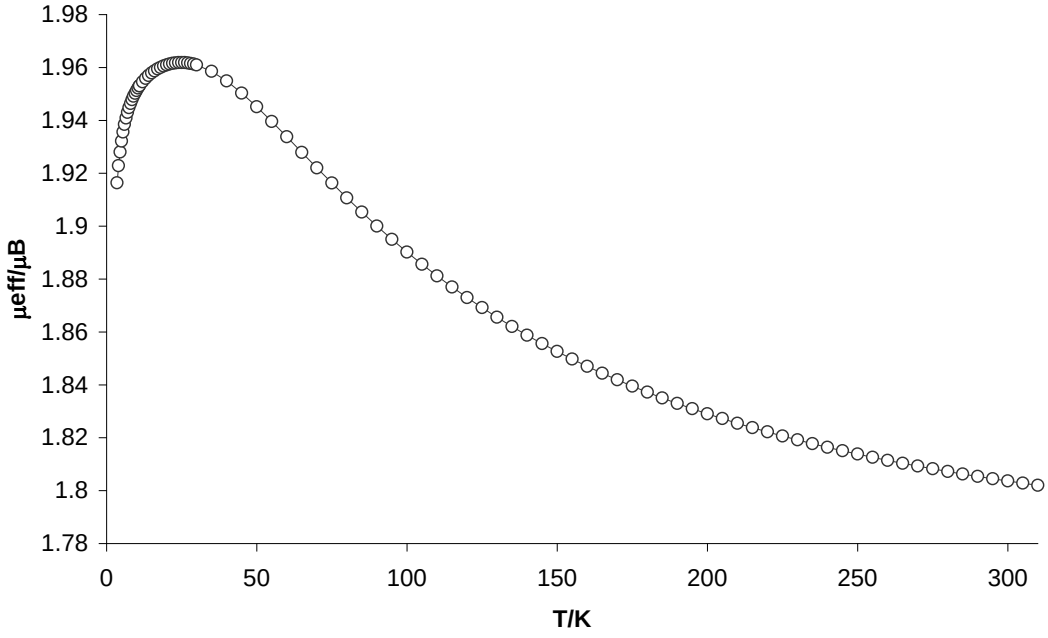

Figure 4-14 μ_{eff} Vs T (per 1Cu centre) for **(6)** $[Cu^{(II)}_2(dpk.acetone)_2(NCS)_2]$.

The susceptibility data in Figure 4-13 were fitted to the modified Bleaney-Bowers relationship[140] given in Equation 3-3 in Chapter 3, page 102. For a Cu(II) dimer, the spin Hamiltonian H equals $-2J\ S_1S_2$, where J is the exchange coupling parameter and $S_1 = S_2 = ½$ (two interacting local spins). [See Figure 3-12 in chapter 3]

At ambient temperatures **(6)** $[Cu^{(II)}_2(dpk.acetone)_2(NCS)_2]$ was found to be paramagnetic with an isotropic *g*-factor (g=1.97), which is similar to other copper complexes of *dpk* derivatives, where isotropic *g*-factors have been observed which vary from 2.00–2.06.[159-160] The room temperature susceptibility correlates with an effective magnetic moment of 1.81 μ_B per Cu(II) ion, as expected for non-interacting Cu(II) d^9 ions,[41] and it increased to 1.96 μ_B at 40K. Although the more usual magnetic behaviour in Cu(II) d^9 dimeric species is a spin-pairing anti-ferromagnetic interaction (J –ve) as described in the previous chapter,[161] the ferromagnetic interaction (J +ve) observed here is uncommon but not unique,[30-31, 162] and complex **(6)** represents a further example, see Table 4-4.

The μ_{eff} vs *T(K)* plot (Figure 4-14) shows an increase in μ_{eff} as the temperature is lowered which is characteristic of ferromagnetic coupling, and is confirmed by the positive J value of $+45.2cm^{-1}$. The rapid decrease in μ_{eff} at low temperatures (40K) is indicative of a weak intermolecular antiferromagnetic interaction; this has been accounted for by a Weiss-type correction (Θ), Equation 4-1.[32, 115] The data for **(6)** is comparable to the magnetic data observed in other ferromagnetic alkoxy-bridged[31, 162] and azido-bridged[30] complexes, with similar M-O-M angles and magnetic susceptibility plots, as listed in Table 4-4.

Equation 4-1 Curie-Weiss Law[115]

$$\chi = \frac{C}{(T - \Theta)}$$

χ = magnetic susceptibility

C = Curie constant

T = temperature

Θ = Weiss constant

Table 4-4 Magnetic behaviour of various copper dimers comparing their Cu-O-Cu angle and *J*-coupling value.

Ferromagnetic	**Cu^{2+}-O-Cu^{2+} (°)**	***J* (cm^{-1})**
(6) $[Cu_2(dpk.acetone)_2(NCS)_2]$	93.6-95.1	+45.2
Azido-bridged $[Cu_4L^{dur}(\mu_2N_3)_4](PF_6)_4 \cdot 4H_2O \cdot 6CH_3\text{-}CN]$ [30]	96.6-98.1	+94
$[Cu_2Lim(OAc)] \cdot 6H_2O$[162]	91.8-102.5	+49.2
Anti-ferromagnetic		
Hydroxo-bridged $[Cu_4L^{dur}(\mu_2\text{-}OH)_4](ClO_4)_4]$ [30]	95.7-97.9	-27
Cu acetate[41]	n/a	-295
(3) $[Cu_2(Ophen)_2(phen)_2](NO_3)_2$ (from Chapter 3)	n/a	-44

n/a = not applicable

L^{dur} = 1,2,4,5-tetrakis-(1,4,7-triazacyclonon-1-ylmethyl)benzene)

H_3Lim = 2-(2-hydroxyphenyl)-1,3-bis[4-(2-hydroxyphenyl)-3-azabut-3-enyl]-1,3 imidazolidine

The applications of ferromagnetic materials are extensive when compared to antiferromagentic materials, which are quite limited.[143] Some possible uses for ferromagnetic materials include sensing, data storage, molecular magnets, magnetic recording, permanent magnets, and electrical insulators.[115, 143]

4.3.2.3. Mechanistic Considerations

Many polymeric complexes of copper(I) have been synthesised previously, and in most cases their usefulness has been frustrated by insolubility. This was also the case with polymorphs **(4)** and **(5)** $[Cu^{(I)}(dpk)(NCS)]_n$, which were insoluble in a wide range of polar and non-polar solvents. However, when the insoluble copper(I) complexes were left in their mother liquor over several days, dissolution occurred, even under ambient laboratory conditions. The red, aqueous acetone solution that contained black crystals of **(4)** and **(5)** transformed into an emerald green solution in air, and deposited

the copper(II) complex **(6)** $[Cu^{(II)}_2(dpk.acetone)_2(NCS)_2]$ as green crystals. Unfortunately, despite favourable spectral properties and the potential for binding to metal oxide semiconducting surfaces, the instability of **(4)** and **(5)** in air indicated they were unsuitable for use as dyes in a DSSC.

In ketones, the hydrated *gem-diol* form and the carbonyl ketone are in equilibrium in an aqueous medium (Figure 4-2), with the equilibrium often favouring the ketone-form. However, strong electron-withdrawing substituents on the carbonyl group increase the electrophilic nature of the carbonyl carbon,[52] thus increasing its susceptibility to attack by weak nucleophiles such as water, and favouring the hydration reaction. It is also well-documented that, in the presence of divalent metal ions, *dpk* is able to undergo hydration across the keto-carbonyl group to form a *gem-diol*.[25, 33, 146] Hemiketals have also been known to form in alcoholic medium (Figure 4-2), where chelation to the metal centre occurs through N,N',O coordination, and the resultant -C–OH groups deprotonate to yield a mono-anionic ligand.[148]

Figure 4-11 illustrates that complex **(6)** has N,N',O^- coordination, but a *gem-diol* has not formed, rather the co-ordinated *dpk* has reacted with the acetone in solution which has been deprotonated to provide a carbanion nucleophile that can attack the metal-activated *dpk* carbonyl group and form an alkoxide, which has then become coordinated to the copper as the reaction sequence in Scheme 4-2 shows.

This reaction is analogous to an aldol condensation which occurs when a carbonyl group with an α-hydrogen atom undergoes proton abstraction by base to form an enolate ion, see Scheme 4-2. The enolate ion can then undergo a nucleophilic addition reaction to a second carbonyl group. This step is often followed by a relatively facile dehydration to generate an alkene, however in the present case the reactivity of the hydroxy group is masked when it becomes bound to the Cu^{2+} ion, thus blocking the dehydration process.[131]

The formation of **(6)** in significant yield (15%) is quite surprising under the mild conditions of the experiment, and it would appear that unreacted starting material contained in the mother liquor was responsible for initiation of the reaction. Indeed, a large excess of sodium thiocyanate was added to the reaction mixture to ensure that

the copper(I) thiocyanate remained soluble. Hence, it is suggested that it is the unreacted thiocyanate ion behaving as a weak base that is the most likely candidate to initiate the formation of the enolate. Hussain[151] and Perlepes[25] have used strong base to initiate the formation of enolates, but in the present work, we have observed similar results with a much weaker base.

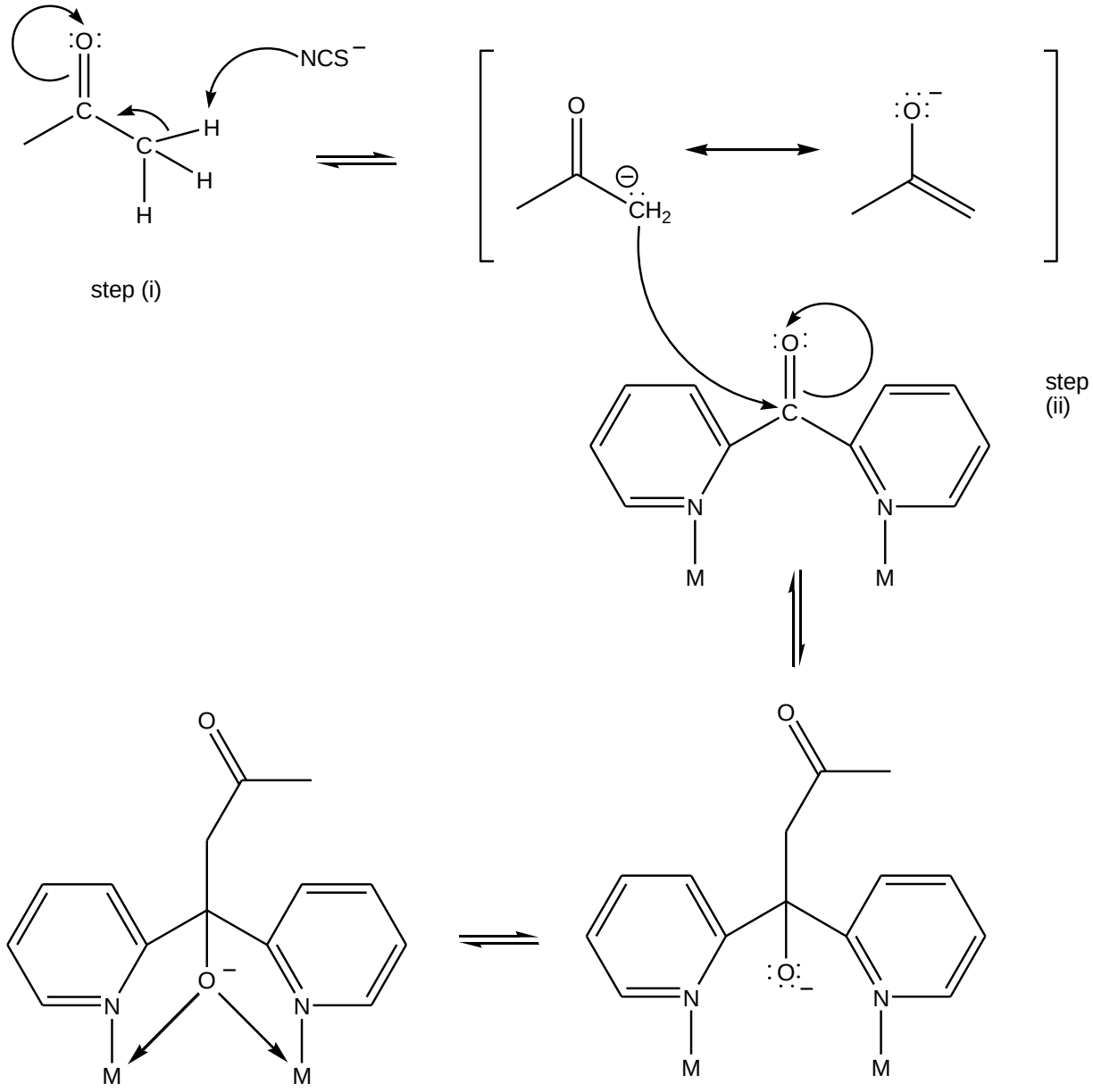

Scheme 4-2 Proposed mixed aldol condensation mechanism for conversion of **(4)/(5)** $[Cu^{(I)}(dpk)(NCS)]_n$ into **(6)** $[Cu^{(II)}_2(dpk.acetone)_2(NCS)_2]$ (Step (i) is the proton abstraction from acetone by the weak base NCS^-, Step (ii) is the nucleophilic attack on the carbonyl group of the *dpk*.)

4.3.3. $[Cu_2(dpk)_2I_2]$ (7)

Complex **(7)** was prepared in a similar manner to **(4)** and **(5)** $[Cu^{(I)}(dpk)(NCS)]_n$, with the iodo forms of the copper and sodium salt being used instead of the thiocyanate analogues (Scheme 4-3). The iodide ion was selected as a co-ligand since it is known to be an excellent bridging species.[26, 147, 163-164] However, instead of the infinite chain polymers formed by thiocyanate bridging in $[Cu^{(I)}(dpk)(NCS)]_n$, black block-like crystals of dimeric $[Cu^{(II)}{}_2(dpk)_2I_2]$ were obtained in good yield (60%). The black colour of the material suggested the copper remained in the +1 state.

As with complexes **(4)** and **(5)**, in complex **(7)** the copper was found in the +1 oxidation state and the oxygen was not bound to the metal centre. However, unlike complexes **(4)** and **(5)** which were found to unstable, complex **(7)** did not undergo any further reaction; hence it may be of sufficient stability to be considered as a dye for DSSC. Unfortunately, the insolubility of complex **(7)** in various solvents precluded fabrication into a solar cell.

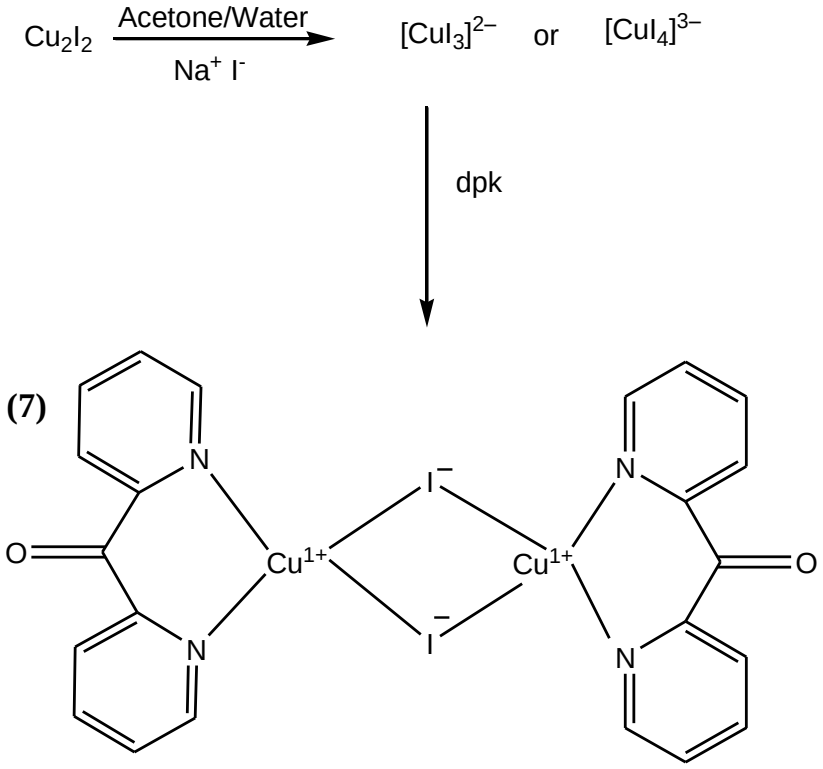

Scheme 4-3 Reaction summary for the formation of **(7)** $[Cu^{(I)}{}_2(dpk)_2I_2]$.

4.3.3.1. FTIR of Complex (7)

The FTIR spectrum of **(7)** $[Cu^{(I)}_2(dpk)_2I_2]$ confirmed the presence of a free carbonyl group (C=O) with a strong band at 1660cm^{-1} ($^{\#}$), the corresponding absorption in polymers **(4)** and **(5)** **(**$[Cu^{(I)}(dpk)(NCS)]_n$) occurs at 1685 cm^{-1} (*), as illustrated in Figure 4-15(a). The composition of **(7)**, was confirmed by single-crystal X-ray diffraction, which provided unambiguous structural characterisation of the complex. **(7)** is a new compound, which exists as a dinuclear copper(I) complex of formula $[Cu^{(I)}_2(dpk)_2I_2]$. The molecular unit contains two four coordinate copper(I) cations, with tetrahedral coordination, with the cationic charge counter-balanced by two bridging iodide anions.

Figure 4-15(b) is a comparison of the FTIR spectrum of the linear polymers, $[Cu^{(I)}(dpk)(NCS)]_n$ **(4)** and **(5)**, and the dimeric $[Cu^{(I)}_2(dpk)_2I_2]$ **(7)** which clearly shows the ν(N≡C–S) band (^) in **(4)** and **(5)** and the close correlation of the remaining *dpk* bands indicating similar structural motifs for the *dpk* in all these complexes, as confirmed by XRD.

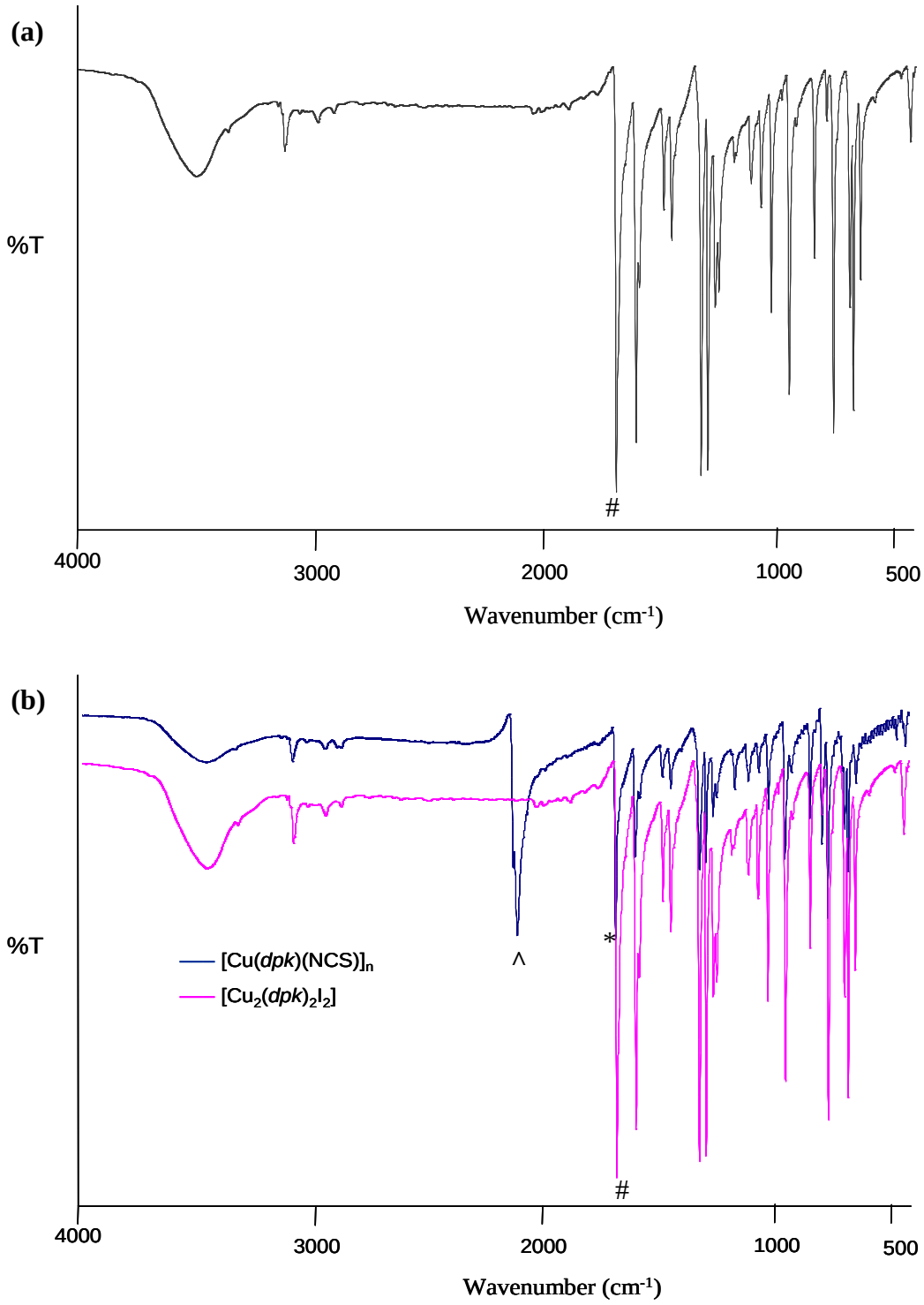

Figure 4-15(a) FTIR spectrum of $[Cu^{(I)}_2(dpk)_2I_2]$ **(7)** and

(b) comparison of FTIR of polymer $[Cu^{(I)}(dpk)(NCS)]_n$ **(4)** and **(5)** and the dimeric $[Cu^{(I)}_2(dpk)_2I_2]$ **(7)**. (All spectra obtained in KBr discs). (where ^ = 2076 cm^{-1}, * = 1685 cm^{-1} and # = 1660 cm^{-1}).

4.3.3.2. Crystal Structure – Complex (7) $[Cu_2(dpk)_2I_2]$

The crystals of **(7)** exhibit monoclinic, *P21/c*, symmetry and the single crystal XRD data is summarised in Table 4-5. In the solid crystal the compound exists as layers in which the complexes are associated with their identical neighbour through a combination of π- π interactions and hydrogen bonding. In addition, an intermolecular OFF π- π interaction with an interplanar distance of 3.473Å, which runs along the *b* axis (Figure 4-16), occurs between the N1 coordinated *dpk* rings. H-bonding is also observed between protons on the aromatic rings and the keto-carbonyl and iodide ions (O···H = 2.437 Å, I···H = 3.162 Å). Table 4-6 lists the significant bond lengths and angles for compound **(7)**.

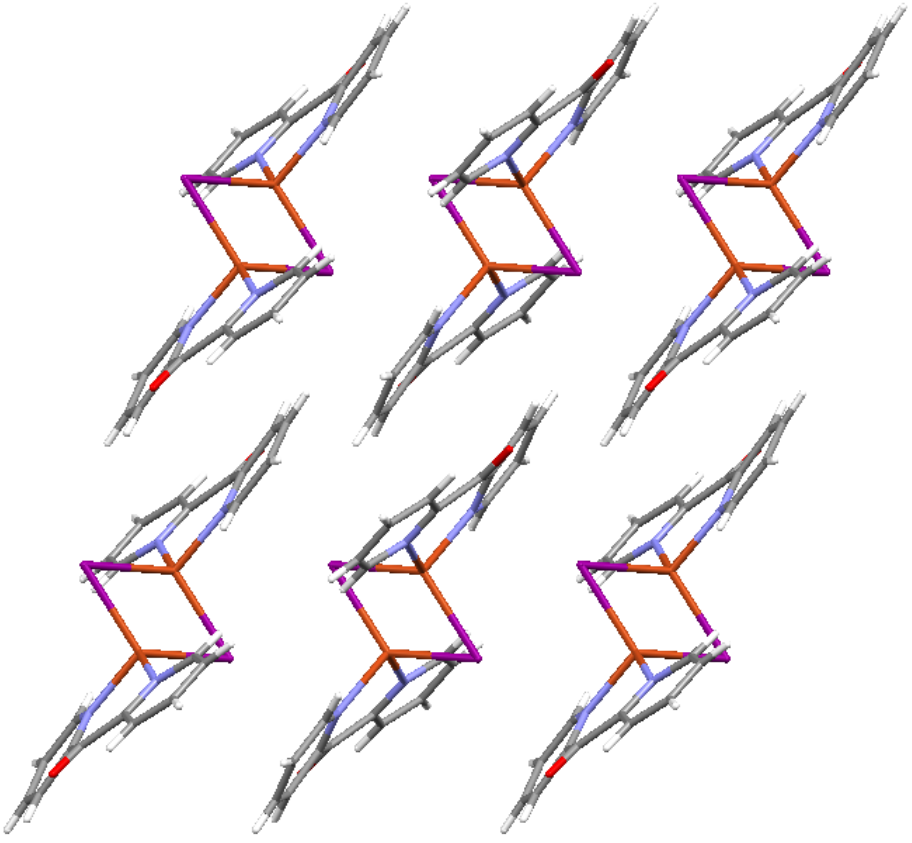

Figure 4-16 Packing of **(7)** along *b*-axis

Table 4-5 Summary of single crystal XRD data for compound **(7)** $[Cu^{(I)}_2(dpk)_2I_2]$

	(7)
Empirical formula	$C_{11}H_8$ Cu I N_2 O
Molecular weight	374.63
Crystal Class	Monoclinic
Space Group	P 21/c
a, Å	9.9663(7)
b, Å	9.4446(9)
c, Å	12.4390(10)
α, (°)	90
β, (°)	104.602(8)
γ, (°)	90
V, Å^3	1133.01(16)
Z	4
Crystal, colour	Prism/black
Crystal size (mm)	0.04 x 0.03x 0.02
Temp (K)	130(2)
Rad wavelength / Å	1.54184
Radiation type	CuKα
θ min-max /°	4.58-73.14
Index ranges	$-12 \leq h \geq 9$
	$-11 \leq k \geq 9$
	$-15 \leq l \geq 12$
No. of reflections	2150
$R_1[F^2 > 2\sigma(F^2)]$	0.0446
wR[F^2]	0.0995
S	0.695

Table 4-6 Significant bond lengths and angles for compound **(7)** $[Cu^{(I)}_2(dpk)_2I_2]$

	(7)	
	(Å)	**(°)**
Cu1-N1	2.033(9)	
Cu1-N2	2.037(9)	
Cu1-I1	2.622(2)	
Cu1-I1	2.597(1)	
C6-O1	1.24(2)	
N2-Cu1-N1		94.24(4)
C7-C6-C1		126(1)
Cu1-I1-Cu1		58.40(5)

The close proximity of the two Cu(I) ions in the $[Cu^{(I)}_2(dpk)_2I_2]$ **(7)** complex is in accord with values observed in many other Cu(I) dimers. For example, Cu(I) polynuclear compounds often exhibit short Cu-Cu distances ranging between 2.38 – 3.2 Å, as indicated in Figure 4-17.[41] The contact distance in **(7)**, (Cu···Cu = 2.547 Å), is comparable to that seen in other Cu^+/Cu^+ dimers; for example the Cu···Cu separation in $[Cu_2I_2(phen)_2]$ is 2.664Å.[26]

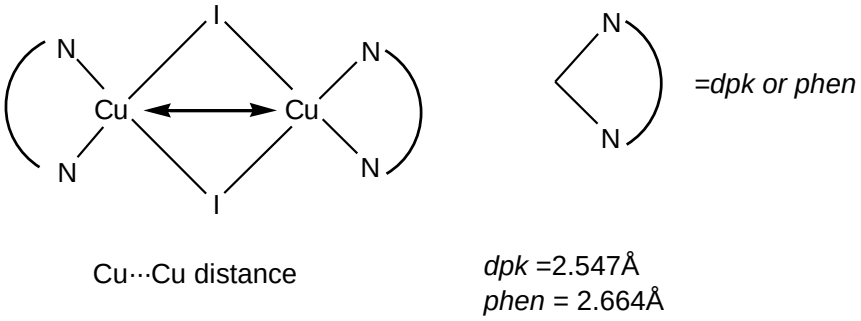

Figure 4-17 Cu···Cu distance in Cu_2 dimers.[26]

Each copper(I) ion is coordinated by two N atoms from *dpk* (Cu-N = 2.032-2.036Å), and two I atoms (Cu-I = 2.596-2.622Å). This type of Cu_2I_2 halide-bridged square dimer has been seen previously with other N-heterocyclic ligands.[26, 147, 163-164] In addition, other Cu_2X_2 (where X = F, Cl or Br) species which contain a halide-bridged

square dimer include $[Cu_2(bipy)_2Br_2]$ which has a Cu···Cu non-bonding distance of 2.85Å.[165] Larger distances between the non-bonding copper centres are observed when the copper ions are present in the +2 oxidation state, for example, $[Cu_2(dpk.H_2O)_2Br_2]$ has a Cu···Cu non-bonding distance of 4.090 Å.[166]

4.3.4. Spectroscopic Properties: UV-Visible /Fluorescence

UV-visible absorption studies of complexes **(4)** and **(5)**, ($[Cu^{(I)}(dpk)(NCS]_n$), were carried out in the solid-state, as they are unstable in solution and readily oxidise to copper(II). Both **(4)** and **(5)** are black in colour, and therefore, as expected, a broad absorption band across the entire visible spectrum was observed (Figure 4-18). The solid-state UV-Vis spectrum of complex **(7)**, $[Cu^{(I)}{}_2(dpk)_2I_2]$, (Figure 4-18) which is also black in colour, is very similar to that observed for **(4)** and **(5)**. The absorption spectrum of the green copper(II) complex **(7)** (Figure 4-19) was determined in DMF solution, and exhibited a broad absorbance beginning at 575nm with a λ_{max} at 675nm, and extending throughout the red region.

Fluorescence studies were also carried out in the solid state. Many copper(I) complexes with pyridine-type ligands exhibit luminescent behaviour, as reported in the previous chapter with $[Cu_2(Ophen)_2]$ **(1)**, and by McMillin *et al.* with the $[Cu(dmp)_2]^{2+}$ anion.[72] However, complexes **(4)** and **(5)** exhibited no emission in the visible region despite the copper being in the +1 oxidation state. Goher *et al.*[167] found similar non-emitting properties in the polymeric $[Cu(dpk.ox)(NCS)]_n$ complex (where *dpk.ox* = di-2-pyridylketone oxime). They suggested that this occurred due to the oxime group altering the energy levels of the aromatic rings. However, this cannot be the case here, and it seems more likely that the non-emitting properties of **(4)** and **(5)** may be due to the polymeric nature of the complexes giving rise to fluorescence quenching as a result of the close proximity of the copper(I) centres in the polymer. This latter suggestion is consistent with the observation of weak luminescence for the dimeric complex, $[Cu^{(I)}{}_2(dpk)_2I_2]$ **(7)**, which, when excited at 360nm, exhibits a broad emission at 400-550nm with a λ_{max} at 420nm, as illustrated in Figure 4-20.

While the spectroscopic data observed in complex **(7)** is favourable for dye species, its insolubility limits its use. The current method used to bind dyes to an oxide surface requires the dye to be in solution rather than as a solid. Other methods were investigated, which included embedding complex **(7)** into an oxide. However, the oxides tend to be annealed at high temperature (>450°C) and unfortunately the organic material in the complex, that is, the ligands, are not stable at this temperature and start to decompose at ~200°C. In addition to this, if the dye was embedded into the oxide surface the electrolyte would not be able to reduce the metal centre, hence there would be only one redox turnover, and for a dye to be commercially viable, 10^8 redox turnovers are required.

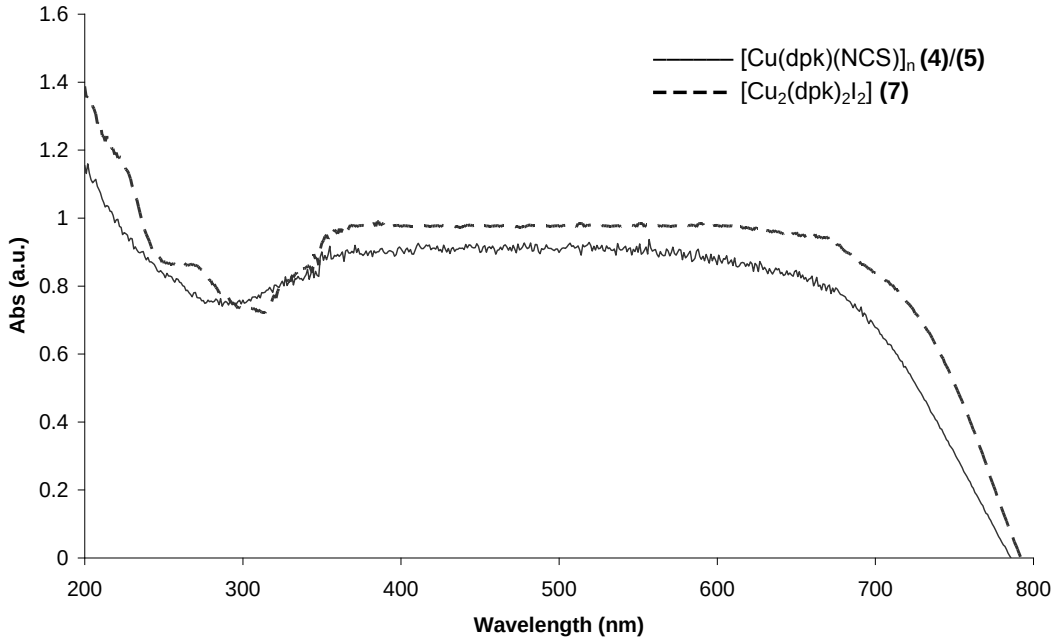

Figure 4-18 Solid-state UV-Vis spectra of complexes **(4)** and **(5)**, and **(7)**.

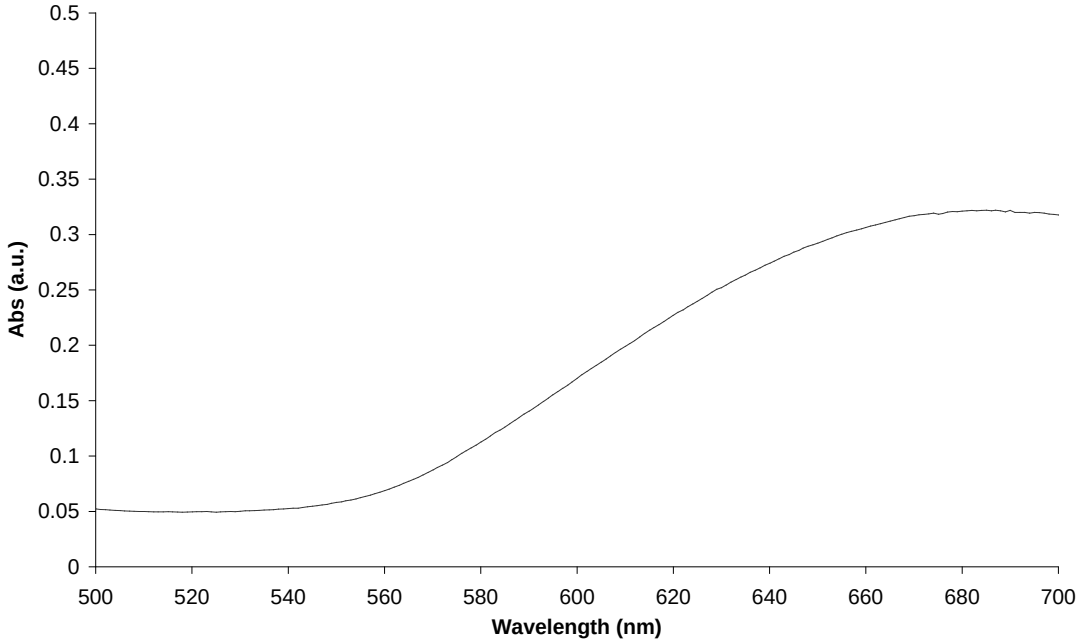

Figure 4-19 Solution UV-Vis spectrum of complex **(6)**, $[Cu^{(II)}_2(dpk.acetone)_2(NCS)_2]$.

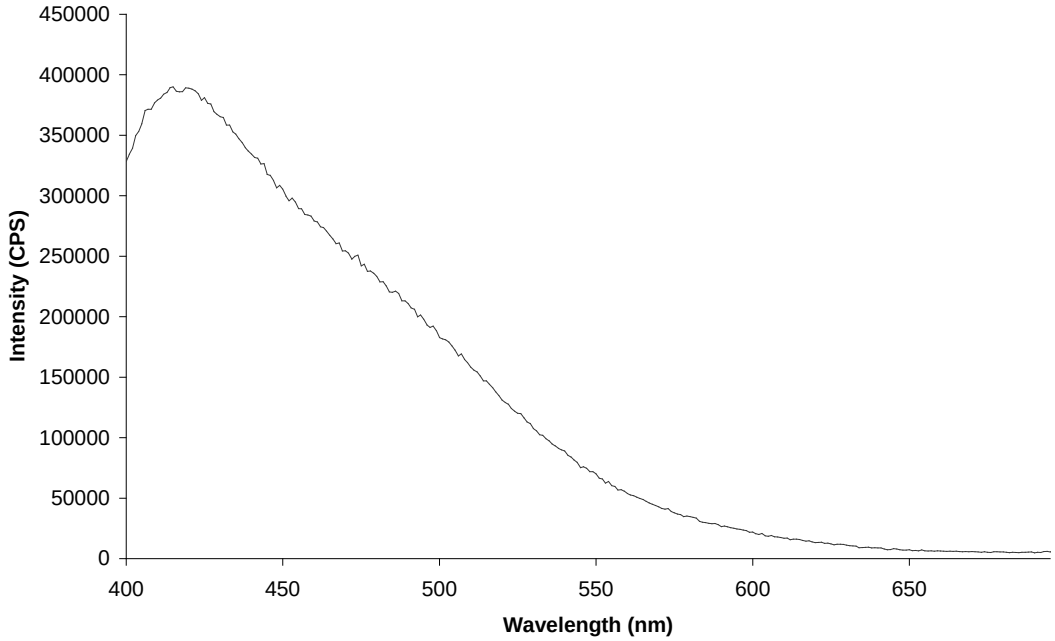

Figure 4-20 Solid-state luminescence spectrum of compound **(7)** $[Cu^{(I)}_2(dpk)_2I_2]$ excited at 360nm.

4.3.5. Complexes (8) and (9)

When *dpk* is coordinated to a transition metal via its two nitrogen atoms the carbonyl group in the ligand is known to be extremely susceptible to attack from various nucleophiles such as the action of acetone enolate (CH_3–CO–CH_2^-) described earlier, which resulted in the formation of **(6)** [$Cu^{(II)}_2$(*dpk.acetone*)$_2$$(NCS)_2$], from **(4)** and **(5)** **(**[$Cu^{(I)}$(*dpk*)$(NCS)]_n$). Thus, an investigation of the reaction of CuNCS with *dpk* in the presence of alternative ketones and aldehydes including acetophenone, cyclohexanone, methyl ethyl ketone, 2-pentanone, 3-pentanone, methyl isobutyl ketone and acetaldehyde (Table 4-7) was undertaken, to see whether similar reactions would occur.

Crystals were isolated from two of the ketone systems, methyl ethyl ketone (MEK) and acetophenone, and a powdered product was obtained from the 3-pentanone system. For the remaining carbonyl species, although colour changes were observed in solution, indicating that some reaction had occurred, no solid products were isolated. See Table 4-8 for a summary of the results.

Table 4-7 Chemical structure and miscibility in water for several ketone solvents.

Solvent	**Chemical Structure**	**Miscibility in water**
Acetone	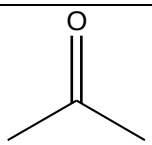	Yes
Acetophenone	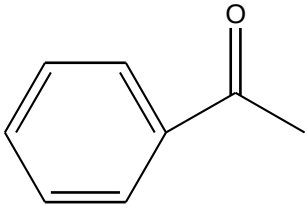	Slightly
Cyclohexanone	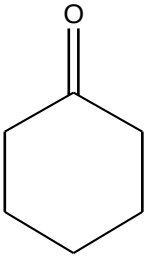	Slightly
Methyl ethyl ketone (MEK)	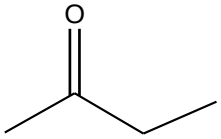	Yes
2-pentanone	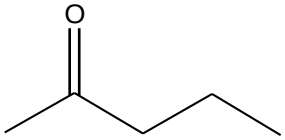	Slightly
3-pentanone	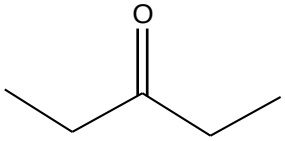	Slightly
Methyl isobutyl ketone (MIBK)	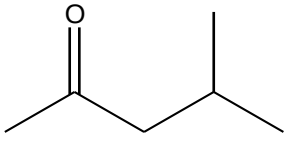	Slightly
Acetaldehyde	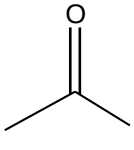	yes

Table 4-8 Summary of results for the interaction of CuNCS with *dpk* in the presence of various ketone solvents

Solvent	**Colour (mother liquor)**	**Product(s)**
MEK	Green	Green crystals formed initially. When left in the mother liquor purple crystals started to form.
Acetophenone	Initially red, then turned brown and subsequently olive green	A green ppt formed, (and blue crystals after three months).
Cyclohexanone	Brown	No solid product was isolated.
3-pentanone	Brown	A green ppt formed.
2-pentanone	Brown	No solid product was isolated.
MIBK	Green	Green needles formed, which decomposed when removed from the mother liquor.
Acetaldehyde	Green	No solid product was isolated

The structural results indicated that, unlike acetone, MEK and acetophenone did not undergo an aldol condensation to form an enolate ion. Possible reasons for acetone's lone success could be that it is completely miscible with water, it is a relatively small and non-bulky molecule compared to, for example acetophenone, and the symmetrical nature of acetone provides two methyl groups with α-hydrogens for nucleophilic attack.

Although all of these carbonyl compounds are known to undergo aldol condensations in the presence of a strong base, this was not observed under the mild reaction conditions used here.

4.3.5.1. Crystal Structures – Complexes (8) and (9)

Complexes **(8)** $[Cu^{(II)}(dpk)_2(NCS)_2]$ and **(9)** $[Cu^{(II)}(dpk.H_2O)_2](NCS)_2.H_2O$ were prepared in a similar manner to **(4)** and **(5)** ($[Cu^{(I)}(dpk)(NCS)]_n$), with methyl ethyl ketone being used as the co-solvent instead of acetone, as summarised in Scheme 4-4. A combination of green crystals of $[Cu(dpk)_2(NCS)_2]$ **(8)** and purple block-like crystals of $[Cu(dpk.H_2O)_2](NCS)_2.H_2O$ **(9)**, were isolated in a 1:10 ratio. The colour of the materials suggested the copper was present in the +2 state in both, and this was confirmed by single crystal x-ray diffraction.

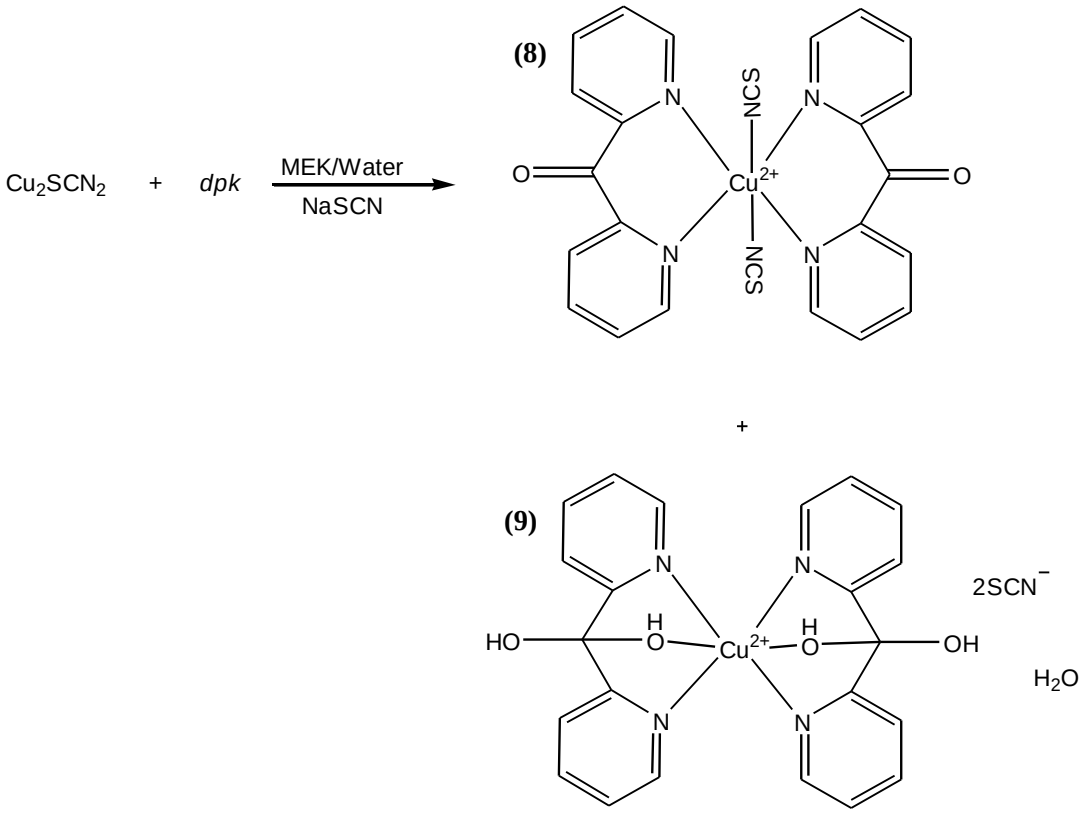

Scheme 4-4 Overall reaction for the formation of **(8)** and **(9)**

Thus, a copper(II) complex **(8)**, where the keto-carbonyl of the *dpk* ligand has not undergone hydration, was isolated from the MEK system. While this has been observed in other copper(I) complexes, (refer to complexes **(4)** and **(5)**), it is uncommon for copper(II). Two of the complexes reported previously in the literature are rather similar to **(8)** with halides instead of thiocyanate, but this work was completed in the 1960's and only chemical analysis and FT-IR data were presented to support the structural assignment.[168-170]

The manganese(II) analogue, $[Mn(dpk)_2(NCS)_2]$, of complex **(8)**, $[Cu(dpk)_2(NCS)_2]$, has been reported previously by Serna *et al.*[146] This work also included the isolation of a hydrated *dpk* complex when coordinated to copper, and is identical to complex **(9)**. Serna suggested one reason why the d^9 copper allowed hydration of the *dpk*, whereas the d^5 manganese did not, was the higher number of *d*-electrons present in the copper ion. This enables greater distortion of the octahedral geometry, caused by the Jahn-Teller effect,[41] and allows the stabilisation of the *gem-diol* through coordination to the copper ion (Cu-O bond). Mn(II) has a lower affinity for distorted octahedral geometry, which would be required to form the Mn-O bond.[131, 146] Therefore, as a result of the willingness of copper to distort its geometry, many d^9 copper complexes of *dpk*, either hydrated or alcoholated exist, and even in the case of compound **(6)** a transition metal promoted aldol condensation product is observed. It would be logical therefore to assume that Jahn-Teller distortion might also be observed in complex **(8)** however, this was found not to be the case with the carbonyl ketone remaining, rather than the formation of the *gem-diol*.

4.3.5.2. FTIR of (8) and (9)

The FT-IR spectrum of complex **(8)**, $[Cu^{(II)}(dpk)_2(NCS)_2]$, (Figure 4-21) shows a strong band at 2060cm^{-1} ($^{\#}$), indicative of N-coordinated thiocyanate, and a very weak band at 1626cm^{-1} (*) that suggests a carbonyl group (C=O) is also present, the corresponding absorption occurs at 1685cm^{-1} in complexes **(4)** and **(5)** ($[Cu^{(I)}(dpk)(NCS)]_n$) and 1660cm^{-1} in complex **(7)** $[Cu^{(I)}_2(dpk)_2I_2]$. The FT-IR spectrum of complex **(9)** $[Cu^{(II)}(dpk.H_2O)_2](NCS)_2.H_2O$ (Figure 4-21) shows a broad split band, at 2059 cm^{-1} and 2086 cm^{-1} ($^{\#}$) which is indicative of thiocyanate, which may be caused by solid-state splitting or distortion from regular octahedral symmetry brought about by the Jahn-Teller effect,[171] and the absence of a C=O peak at ~1630cm^{-1} (*).

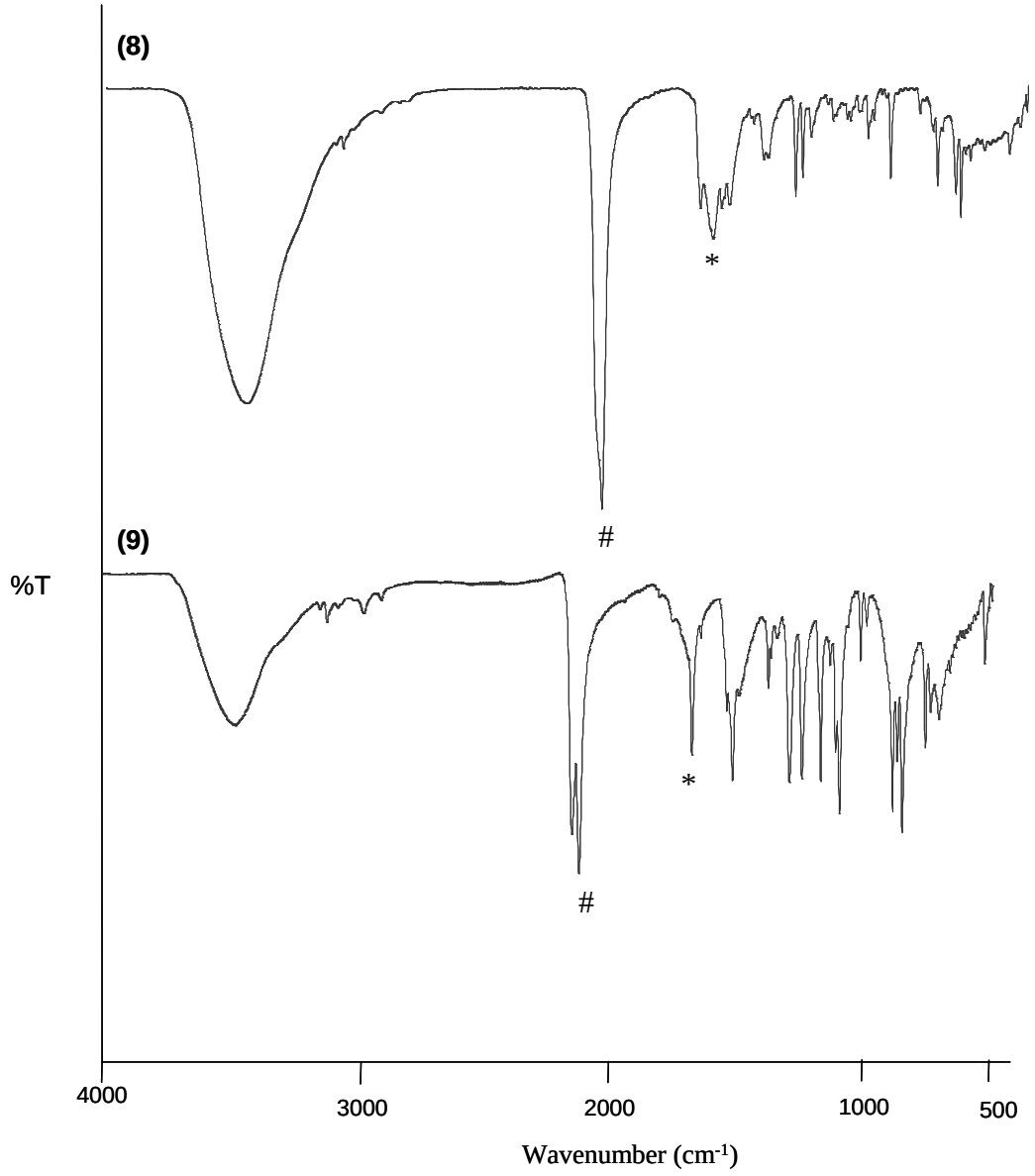

Figure 4-21 FTIR of complex **(8)** $[Cu^{(II)}(dpk)_2(NCS)_2]$, and **(9)** $[Cu^{(II)}(dpk.H_2O)_2](NCS)_2.H_2O$ (where # = ~2070 cm^{-1} and * = 1626 cm^{-1}).

4.3.5.3. Crystal Structures – Complexes (8) and (9)

The green crystals of **(8)** exhibit orthorhombic, *Fddd* symmetry with crystal data summarised in Table 4-9. The asymmetric unit consists of half the metal complex, giving the empirical formula $[Cu_{0.5}(C_{11}H_8ON_2)(NCS)]$ (Figure 4-22).

Table 4-9 Summary of single crystal XRD data for compounds **(8)**, **(9)** and **cuzu**[146]

	(8)	**(9)**	**cuzu**[146]
Empirical formula	$C_{24}H_{16}CuN_6O_2S_2$	$C_{24}H_{18}^{\#}CuN_6O_6S_2$	$C_{24}H_{24}^{\#}CuN_6O_6S_2$
Molecular weight	548.09	614.13	620.16
Crystal Class	Orthorhombic	Triclinic	Triclinic
Space Group	Fddd	P-1	P-1
a, Å	16.875(4)	7.884 (19)	7.914(3)
b, Å	21.566(5)	9.201 (2)	9.223(2)
c, Å	26.429(5)	9.411 (2)	9.429(2)
α, (°)	90	96.388 (4)	96.38(2)
β, (°)	90	95.478 (4)	95.54(2)
γ, (°)	90	96.456(4)	96.61(2)
V, Å^3	9618(3)	670.13	675.2(3)
Z	8	2	1
Crystal, colour	Block, green	Block, purple	Primatic, purple
Temp (K)	293(2)	293(2)	*
Rad wavelength /Å	1.5418	0.7107	*
Radiation type	CuKα	MoKα	*
θ min-max /°	3.72 – 73.01	2.19 - 27.52	1-30
Index ranges	$-20 \le h \ge 16$	$-9 \le h \ge 10$	*
	$-23 \le k \ge 21$	$-11 \le k \ge 11$	*
	$-32 \le l \ge 24$	$-12 \le l \ge 7$	*
No. of reflections	1984	2843	4123
$R_1[F^2 > 2\sigma(F^2)]$	0.0643	0.0737	0.0342
$wR[F^2]$	0.0838	0.2092	0.0946
S	0.695	0.759	1.089

* This information was not available in the CIF

In the crystal structure of complex **(9)** not all of protons have been assigned, whereas in **cuzu** they have been.

Each copper atom has octahedral stereochemistry, coordinating to six nitrogen atoms from two *dpk* ligands (Cu-N = 1.995-2.217Å) and two thiocyanate anions in a *cis* configuration (Cu–N = 2.148 Å), hence the +2 copper charge is counter-balanced by the coordinating thiocyanate anions, which are present in the *cis*-arrangement. Thus, the molecular unit of **(8)** has the composition *cis*-[Cu(*dpk*)$_2$(NCS)$_2$] (Figure 4-23). The thiocyanate anion is almost linear with an N–C–S angle of 172.91°. The C–C–C angle across the keto-carbonyl is 119.43°, as expected for an sp^2 hybridized trigonal carbon atom, and is similar to that observed in complexes **(4)** and **(5)**, and other complexes where the keto-carbonyl has not undergone hydration. The symmetry of complex **(8)** is demonstrated by the trans N1–Cu–N1 and trans N2–Cu–N3 (N2 from the coordinated *dpk* ligand and N3 from the coordinated thiocyanate anion) with both angles being almost linear at 178.39° and 177.00°, respectively. See Table 4-10 for a listing of the significant bond lengths and angles for complex **(8).**

In the crystal lattice, the complex exists as clusters that contain alternating [Cu(*dpk*)$_2$(NCS)$_2$] units, which are associated by a network of weak OFF π-π interactions. The OFF interactions are perfectly parallel and occur between the identical N1N1 aromatic *dpk* rings at a distance of 3.739 Å. This can be observed in the global packing of the complex, see Figures 4-24 and 4-25.

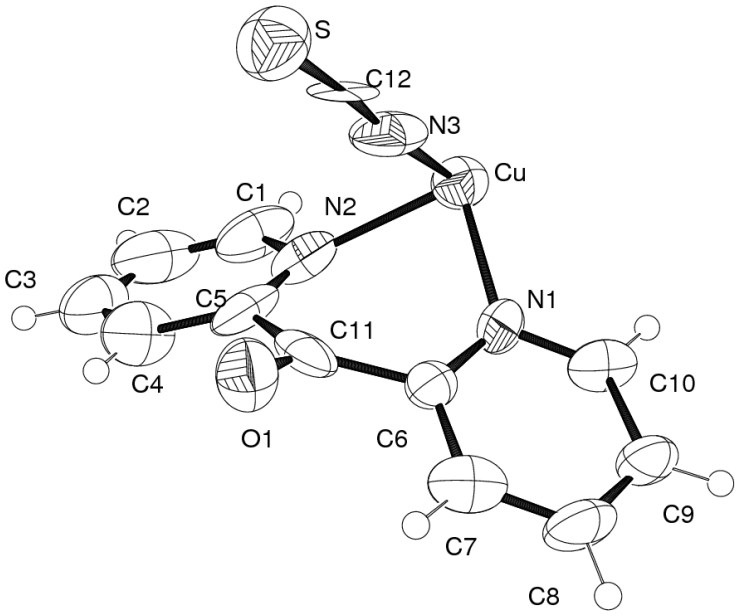

Figure 4-22 Asymmetric unit of **(8)** [Cu$^{(II)}$(*dpk*)$_2$(NCS)$_2$].

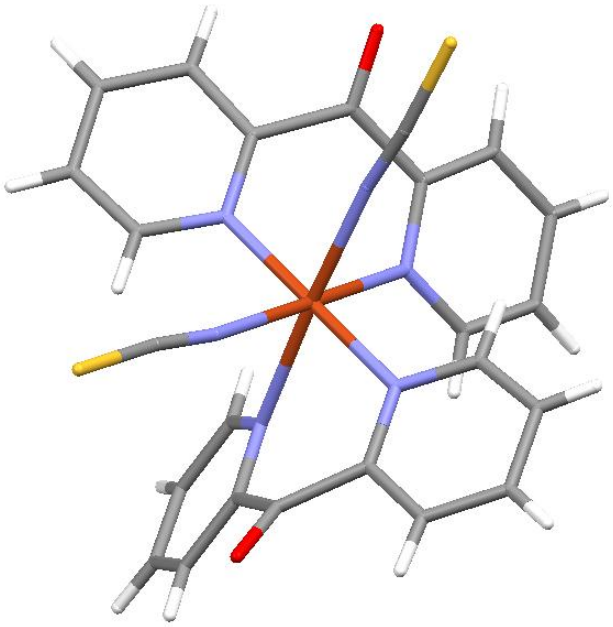

Figure 4-23 Complex **(8)** *cis*-[$Cu^{(II)}$(*dpk*)$_2$(NCS)$_2$] (green crystals)

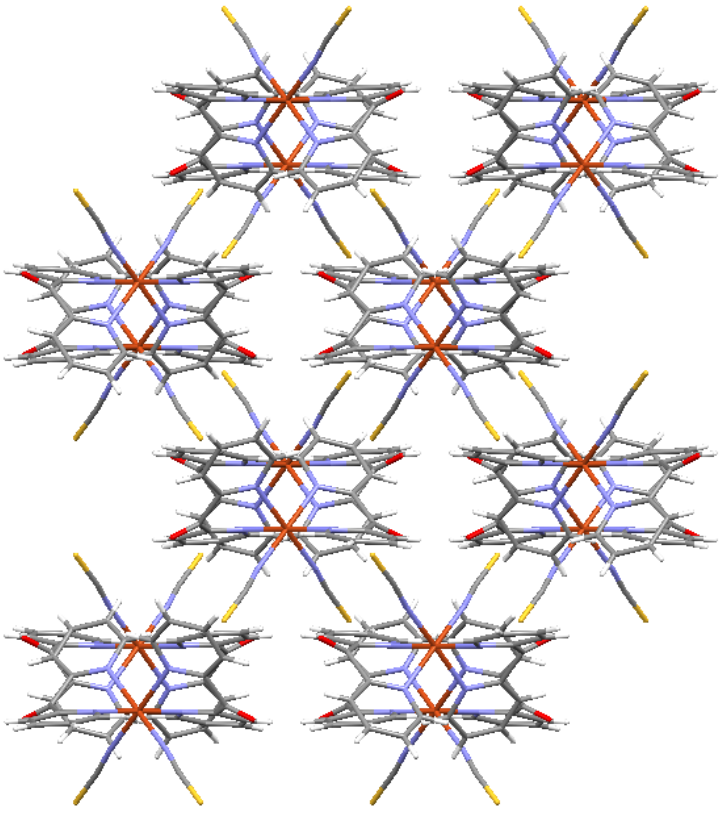

Figure 4-24 Packing along the *a*-axis of **(8)** [$Cu^{(II)}$(*dpk*)$_2$(NCS)$_2$].

Table 4-10 Significant bond lengths and angles for complexes **(8)**, **(9)** and **cuzu** (which is **(9)** prepared by Serna).[146]

	(8)		**(9)**		**cuzu**[146]	
	(Å)	**(°)**	**(Å)**	**(°)**	**(Å)**	**(°)**
Cu-N1	1.995(3)		2.016(3)		2.008(2)	
Cu-N2	2.217(3)		2.001(4)		2.012(2)	
Cu-N3	2.148(3)					
Cu-O1			2.395(5)		2.389(5)	
C11-O1	1.211(2)					
N3-C12	1.166(2)					
C12-S	1.649(2)					
N1-Cu-N2 (bite)		85.93				
C6-C11-C5		119.30				
S-C12-N3		172.94				
N3-Cu-N3		95.73				
N3-Cu-N2		176.95				
N2-Cu-N1		95.18				
O1-Cu-O1				180.00		180.0(4)
N2-Cu-N1 (bite)				87.14		87.21(6)
C7-C6-C5				108.3		108.3(1)
O1-Cu-N2				76.21		74.16(5)
O1-Cu-N1				74.65		76.12(5)
N2-Cu-N1				92.86		92.79(6)

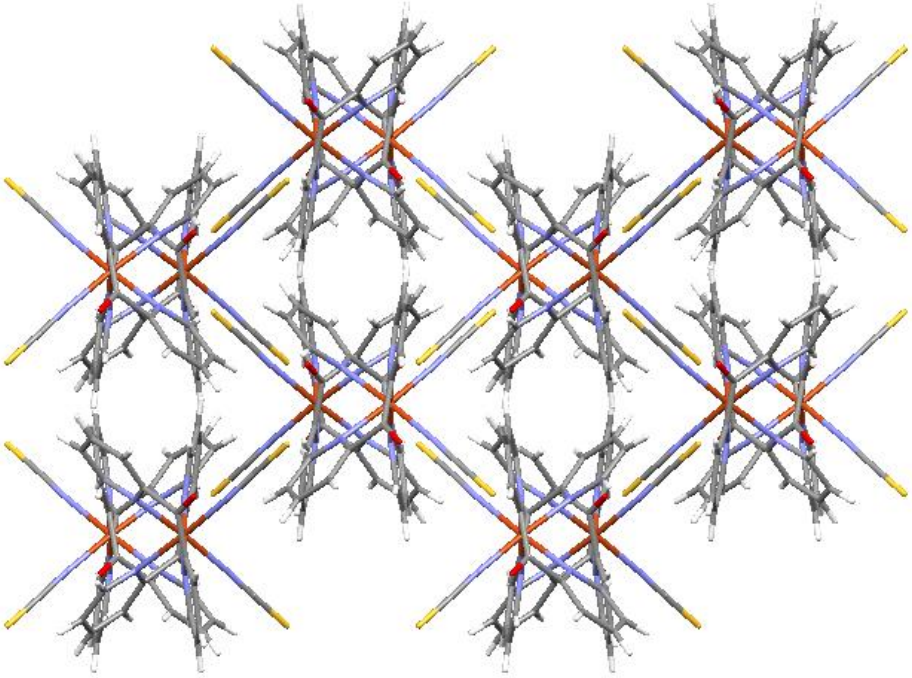

Figure 4-25 Packing along the *b*-axis of **(8)** $[Cu^{(II)}(dpk)_2(NCS)_2]$.

Complex **(9)** is a purple mononuclear octahedral copper(II) complex of formula $[Cu^{(II)}(dpk.H_2O)_2](NCS)_2.H_2O$ (Figure 4-26). This structure has been published previously by Serna *et al.*[146], (CCDC code **cuzu**). The unit cell volumes of the crystals are very similar with 670.13 $Å^3$ for **(9)** and 675.2 $Å^3$ for **cuzu**, as listed in Table 4-9.

The molecular unit contains one six-coordinate copper(II) ion, with octahedral coordination, for which the cationic charge is counter-balanced by two non-bonding lattice bound thiocyanate anions. The copper(II) cation is coordinated to four N-atoms from two $dpk.H_2O$ ligands (Cu–N = 2.007–2.016 Å) and two O-atoms from the same two $dpk.H_2O$ ligands (Cu–O = 2.395 Å). The symmetry of the octahedral complex is demonstrated by the N1–Cu–N1, N2–Cu–N2 and O1–Cu–O1 angles all being 180°. The N1–Cu–O1 angle of 74.65°, N2–Cu–O1 angle of 87.14° and the two N1–Cu–N2 angles of 87.14° and 92.86° indicate that there is some distortion from true octahedral symmetry. The crystals exhibit triclinic, *P-1*, symmetry and the complex exists as ribbons which are held together through a series of H-bonds between $dpk.H_2O$ and non-coordinated water (2.671–2.712 Å), see Figures 4-26, 4-27 and 4-28.

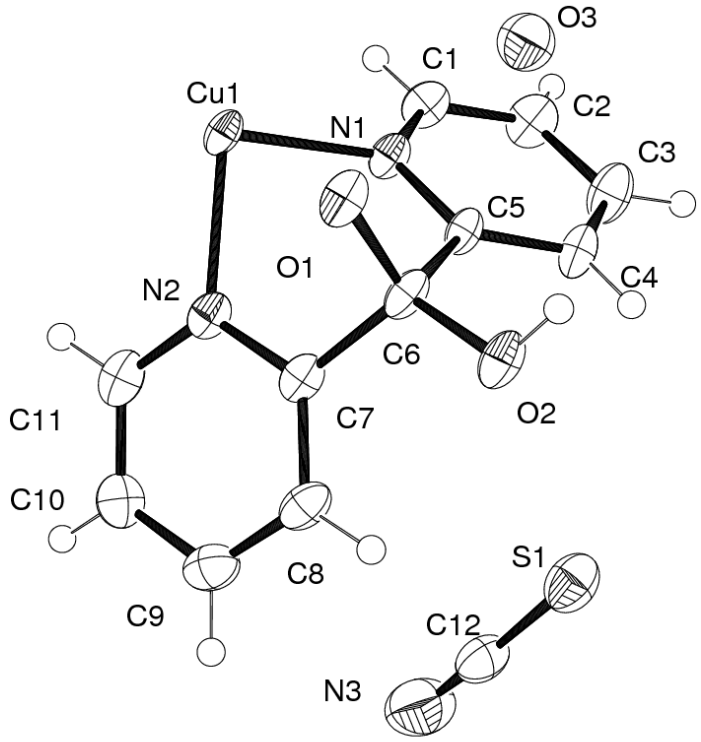

Figure 4-26 Asymmetric unit of complex **(9)** $[Cu^{(II)}(dpk.H_2O)_2](NCS)_2.H_2O$.

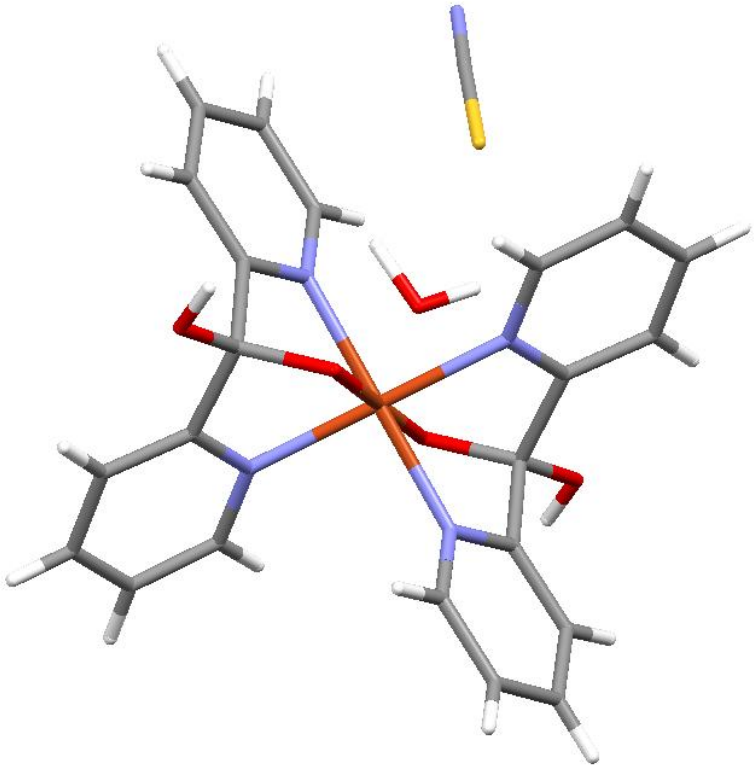

Figure 4-27 Complex **(9)** *trans*-$[Cu^{(II)}(dpk.H_2O)_2](NCS)_2$ (purple crystals)

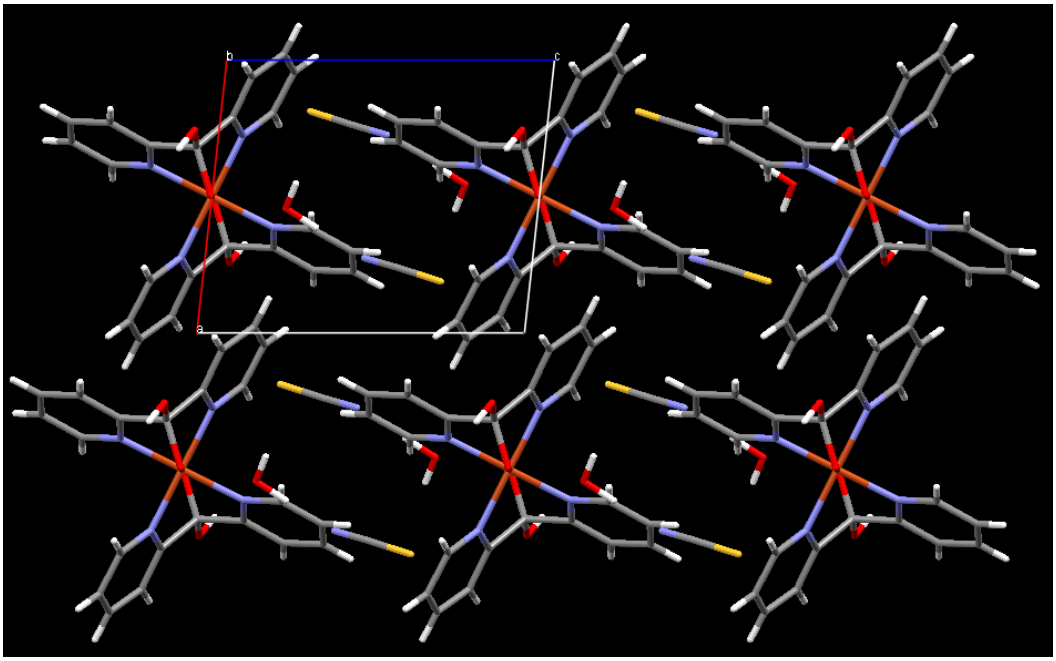

Figure 4-28 Packing of $[Cu^{(II)}(dpk.H_2O)_2](NCS)_2$ **(9)** along the *b*-axis

4.3.6. Picolinic Acid Complexes (10), (11) and (12)

Complexes **(10)**, **(11)** and **(12)** were prepared in a similar manner to **(4)** and **(5)** ($[Cu^{(I)}(dpk)(NCS)]_n$), but with acetophenone, Figure 4-29, being used instead of acetone. Over a period of five weeks complexes **(10)** $[Cu^{(II)}(pic)_2]Na_2(NCS)_2.2H_2O$ and **(11)** $Na_2[Cu^{(II)}(pic)_2(NCS)_2](H_2O)_2$ were isolated, whereas complex **(12)** $[Cu^{(II)}(pic)_2]\cdot Na_2\ [Cu^{(II)}(pic)_2(NCS)_2]$ formed over three months. All the complexes were obtained by allowing the metal-ligand-solvent mixture to evaporate slowly at ambient temperature. In the preparation, the only variable was the laboratory temperature, and while this should be constant, it can fluctuate between the summer and winter months. All three complexes contain the picolinate anion (2-carboxyl pyridine) "*pic*" as illustrated in Figure 4-29. Due to twinning; the single crystal data obtained for complex **(12)** was quite poor with a rather high R-factor of 9.84%. Despite repeated attempts, the preparation of further crystals of **(12)** was unsuccessful, although a physical mixture of crystals of its two components **(10)** and **(11)** were isolated in low yields (~1%), but without twinning. The slow evaporation of acetophenone appears to be a crucial factor, since in the formation of **(12)**, three months were required to obtain the crystals, whereas the isolation of **(10)** and **(11)** was achieved after a five week period.

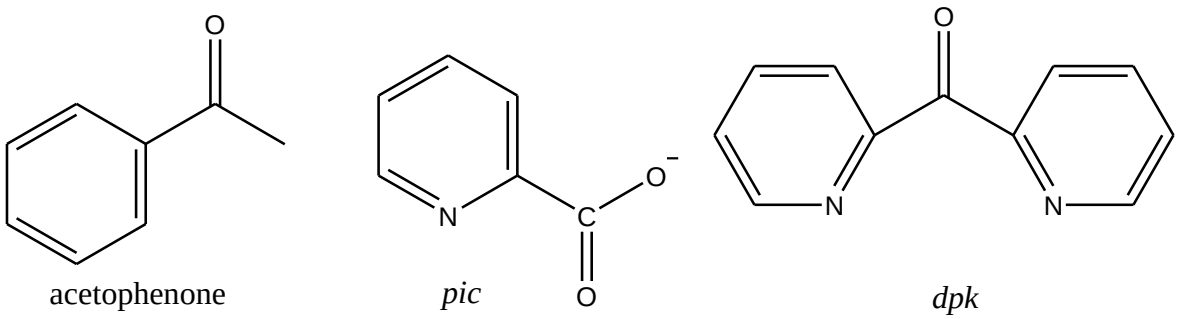

acetophenone *pic* *dpk*

Figure 4-29 Structures of acetophenone, *pic* and *dpk*.

4.3.6.1. FTIR of (10), (11) and (12)

The crystals of complexes **(10)** $[Cu^{(II)}(pic)_2]Na(NCS)_2$ and **(11)** $Na_2[Cu^{(II)}(pic)_2(NCS)_2].2H_2O$ could not be separated manually; so the FT-IR spectrum is a composite of the two complexes **(**Figure 4-30**)** and has a band at 2075cm^{-1} ($^{\#}$) indicative of S-coordinated thiocyanate, and a strong stretch at 1650cm^{-1} (*) which indicates the presence of a carbonyl group in a carboxyl group. The FT-IR spectrum of complex **(12)** is similar of that observed for **(10)** and **(11)**, with a split band at 2062 cm^{-1} and 2084 cm^{-1} ($^{\#}$) indicative of S-coordinated thiocyanate (attributed to solid-state splitting). A strong stretch at 1640 cm^{-1} (*) indicates the presence of a carbonyl group. The FT-IR spectra of all three complexes show *no evidence* for the presence of *dpk* and this was further confirmed by single-crystal data.

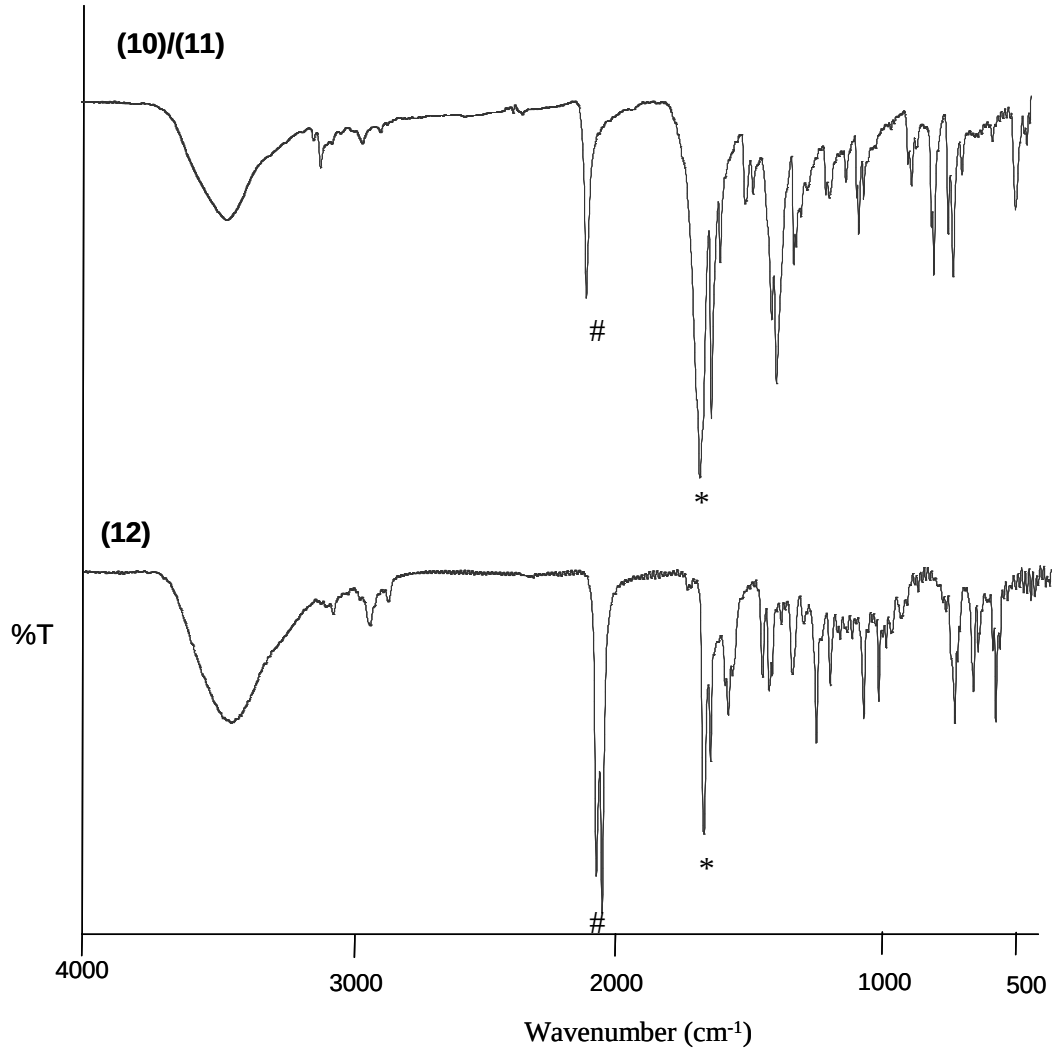

Figure 4-30 FTIR spectra of $[Cu(pic)_2]Na(NCS)_2$ **(10),** $Na_2[Cu(pic)_2(NCS)_2].2H_2O$ **(11)** and Na_2 $[Cu(pic)_2(NCS)_2]$ $[Cu(pic)_2]$ **(12)** (where # = ~2070 cm^{-1} and * = ~1645 cm^{-1}).

4.3.6.2. Crystal Structure – Complex (10)

Crystal data for **(10)**, **(11)** and **(12)** is summarised in Table 4-11. The crystals of **(10)** $[Cu^{(II)}(pic)_2]Na_2(NCS)_2.2H_2O$ exhibit triclinic, *P-1*, symmetry. The asymmetric unit of **(10)** consists of half a copper centre, one picolinate (*pic*) ligand, one sodium cation, one thiocyanate anion, one water molecule and a disordered benzoic acid molecule. The crystal structure shows no evidence of the *dpk* ligand in the structure, rather the ligand has undergone a unique C–C bond cleavage, which has not been reported previously in the literature, to form the 2-picolinate anion (*pic*) (Figure 4-29). The *pic* ligands chelate to Cu(II) ions and simultaneously bridge to sodium ions that are electrostatically ordered throughout the crystal lattice.

The disordered molecules appear to be benzoic acid which has arisen from oxidative cleavage of acetophenone (Figure 4-31). This is not surprising because the oxidant that cleaved the *dpk* would be able to do the same to any other ketone species in the reaction mixture. The disordered benzoic acid could not be removed using the SQUEEZE program as in previous structures, as the molecules are involved in the extended crystal structure.

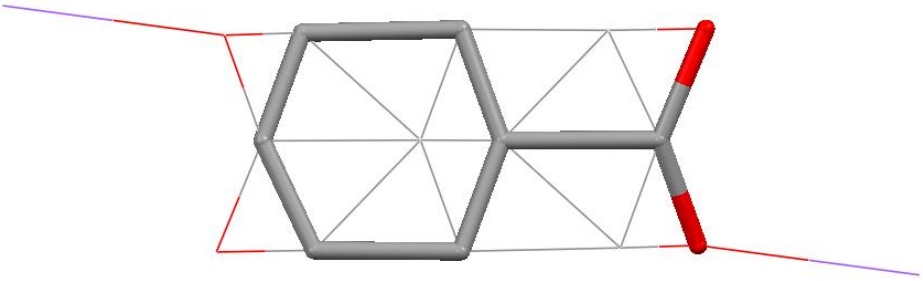

Figure 4-31 Disordered benzoic acid in **(10)**

Table 4-11 Summary of single crystal XRD data for compounds **(10)**, **(11)** and **(12).**

	(10)	**(11)**	**(12)**
Empirical formula	$C_7\ H_6\ Cu_{0.5}\ N_2\ Na\ O_5\ S$	$C_7\ H_7\ Cu\ N_2\ Na\ O\ S$	$C_{12}\ H_{0.33}\ Cu_{1.33}\ N_{0.67}\ Na_{0.67}\ O_2\ S_{1.33}$
Molecular weight	333.00	253.78	325.59
Crystal Class	Triclinic	Monoclinic	Triclinic
Space Group	P-1	C2/c	P-1
a, Å	7.580(3)	18.913(8)	7.734(15)
b, Å	10.008(4)	7.432(3)	9.540(10)
c, Å	10.200(5)	14.580(7)	11.364(19)
α, (°)	67.168(4)	90	95.460(11)
β, (°)	88.318(4)	105.632(5)	107.546(16)
γ, (°)	68.012(4)	90	109.798(13)
V, Å ^{3}	655.16(5)	1973.72(15)	733.8(2)
Z	2	8	3
Crystal, colour	Blue-block	Blue-block	Blue-platelet
Temp (K)	130.0	130.0	293(2)
Rad wavelength / Å	0.71073	1.54184	1.54184
Radiation type	MoKα	CuKα	CuKα
θ min-max /°	2.93-29.25	4.86-73.95	4.18-72.82
Index ranges	$-9 \le h \ge 9$	$-23 \le h \ge 22$	$-9 \le h \ge 9$
	$-11 \le k \ge 12$	$-9 \le k \ge 6$	$-9 \le k \ge 11$
	$-13 \le l \ge 13$	$-14 \le l \ge 18$	$-13 \le l \ge 14$
No. of reflections	2299	1779	2855
$R_1[F^2 > 2\sigma(F^2)]$	0.0404	0.0329	0.0984
wR[F^2]	0.1054	0.0887	0.3570
S	1.025	1.052	1.376

The empirical formula, without the disordered molecules, is ([$Cu_{0.5}(C_6H_4N_1O_2)$] Na (NCS) (H_2O)). The copper ion has square planar geometry, and is coordinated to two nitrogen atoms (Cu–N = 1.966 Å) and two oxygen atoms (Cu–O = 1.952 Å) from two identical *pic* ligands giving a molecular formula of Cu(*pic*)$_2$Na$_2$(NCS)$_2$.2H_2O for **(10)**. Table 4-12 contains a summary of significant bond lengths and angles for compounds **(10)**, **(11)** and **(12)**. The +2 charge on the copper ion and the +1 charge on the two sodium cations are counter-balanced by the two monoanionic *pic* ligands and the two thiocyanate anions.

In complex **(10)** it is interesting to note that the thiocyanate does not coordinate to the copper centre or assist in the bridging of the complex. Rather it is held by electrostatic interactions between the sodium cation and oxygen atoms from the *pic* (Na···O = 2.432–2.639 Å) and the disordered benzoic acid molecules (Na···O = 2.973Å) which form the continuous 2-D polymer network (Figures 4-32 and 4-33). The sodium cation also interacts with the nitrogen from the thiocyanate (Na···N = 2.321 Å) and a water molecule (Na···O = 2.315 Å), however they are not involved in the bridging.

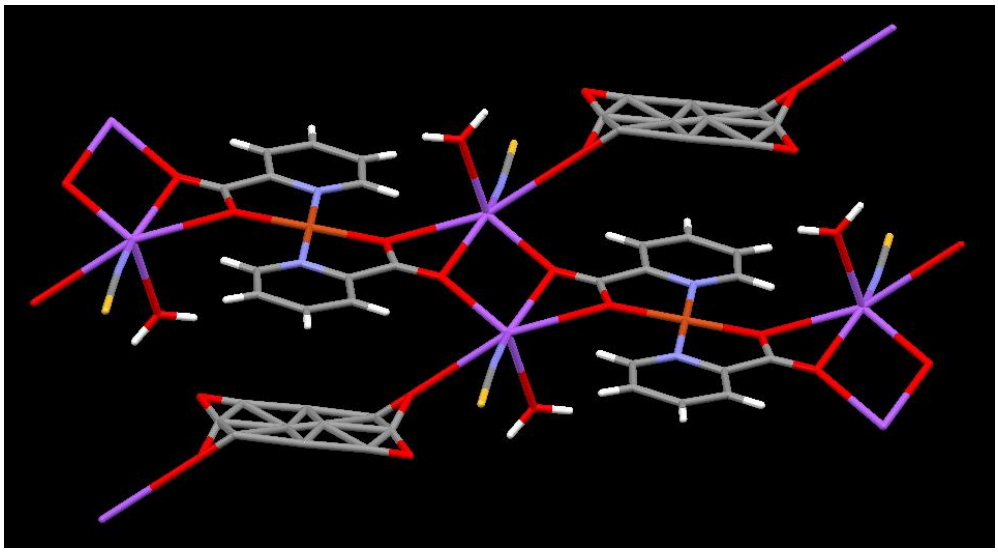

Figure 4-32 Complex **(10)** [Cu(*pic*)$_2$]Na$_2$(NCS)$_2$.$C_6H_5COOH.H_2O$

The N–Cu–O "bite" angle on the *pic* ligand is 83.56°, and N–Cu–O angle between the *pic* ligands is 96.44°. In addition to this, the angles across the copper centre, that is the N–Cu–N and O–Cu–O angles, are 180°, with the aromatic planes deviating slightly from one another with a distance of 0.197 Å, indicating the Cu^{2+} is exhibiting essentially square planar co-ordination.

Table 4-12 Significant bond lengths/interactions and angles for **(10)**, **(11)**, **(12)** and **WIGGOI** [172]

	(10)		**(11)**		**(12)**		**WIGGOI**[172]	
	(Å)	**(°)**	**(Å)**	**(°)**	**(Å)**	**(°)**	**(Å)**	**(°)**
Cu1–O1	1.952(2)		1.967(2)		1.988(5)		1.944(3)	
							1.952(3)	
Cu1–N1	1.966(3)		1.977(2)		1.939(8)		1.960(3)	
							1.970(3)	
Cu1–S1			2.960(7)		2.935(2)			
Cu2–O3					1.955(4)			
Cu2–N2					1.982(9)			
Na1···N3					2.39(1)		2.388(4)	
Na1···N2	2.322(4)		2.349(3)					
Na1···O1	2.637(3)		2.540(2)		2.566(5)		2.750(3)	
Na1···O2	2.557(2)		2.413(3)		2.474(7)		2.555(4)	
	2.433(3)		2.252(3)					
Na1···O3	2.316(3)		2.274(3)					
Na1···O4	2.973(9)				2.303(7)		2.355(4)	
N1-Cu1-N1		180.0(1)		180.0(9)		180.0(3)		175.8(1)
N2-Cu2-N2						180.0(3)		
O1-Cu1-O1		180.0(9)		180.0(9)		180.0(3)		171.8(1)
O3-Cu2-O3						180.0(2)		
S1-Cu1-S1				180.0(2)		180.0(7)		
O1-C6-C5						116.9(7)		124.1(4)
								125.4(4)
C7-S1-Cu1						94.9(3)		
N3-C7-S1						179.0(9)		
N2–C7–S1		178.9(3)		179.1(3)				
O1–Na–O2		51.68(9)		53.26(8)				
O2–Na–O2		78.2(1)		82.80(9)				
O1–Na–O4		159.7(2)						
O1–C6–O2		123.8(3)		124.0(3)				

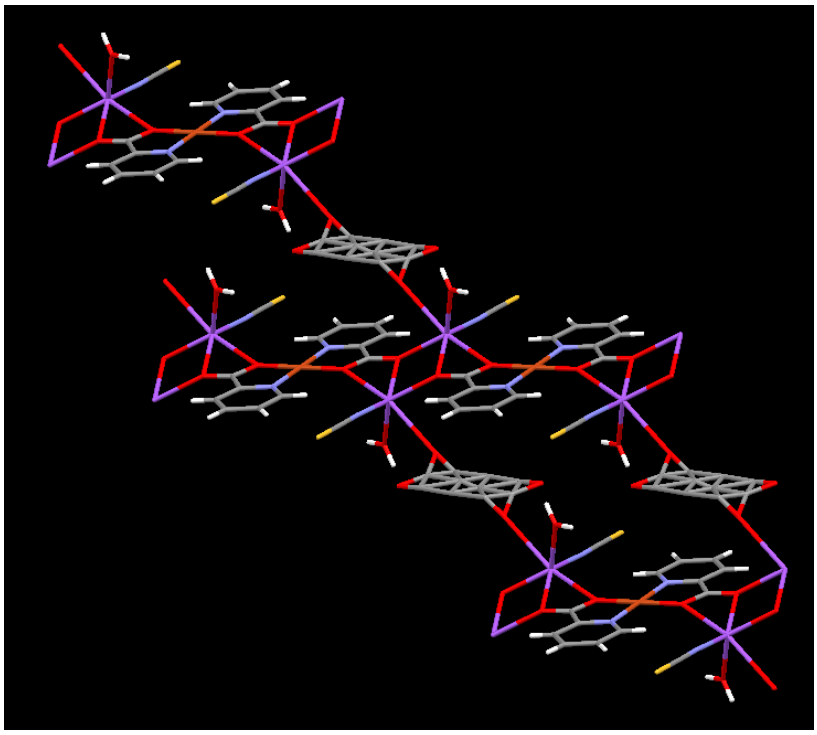

Figure 4-33 Packing of **(10)** $[Cu^{(II)}(pic)_2]Na_2(NCS)_2.2H_2O$ viewed along *a*-axis

4.3.6.3. Crystal Structure – Complex (11)

The crystals of **(11)** $Na_2[Cu^{(II)}(pic)_2(NCS)_2].2H_2O$ exhibit monoclinic, *C2/c* symmetry, and like **(10)**, the structure does not show evidence of *dpk*. The asymmetric unit of **(11)** contains half a copper centre, one *pic* ligand, one sodium cation, one thiocyanate anion and one water molecule. The empirical formula is thus $Na[Cu_{0.5}(C_6H_4N_1O_2)(NCS)](H_2O)$, so, the molecular unit of **(11)** has the composition: *trans*-$Na_2[Cu^{(II)}(pic)_2(NCS)_2](H_2O)_2$ (Figure 4-34). The copper centre has octahedral geometry, with the Cu(II) ion coordinated to two nitrogen atoms (Cu–N = 1.979 Å) and two oxygen atoms (Cu–O = 1.969 Å) from the *pic* ligand, and two sulphur atoms (Cu–S = 2.959 Å) from a thiocyanate anion in a *trans* configuration. See Table 4-12 for a listing of significant bond lengths and angles.. The +2 charge on the copper and the +1 charges on the two sodium cation are counter-balanced by the two anionic *pic* ligands and the two thiocyanate anions.

The N–Cu–O "bite" angle on the *pic* ligand is 83.27°, and the N–Cu–O, the angle between the two *pic* ligands is 96.73°, both of which are similar to that observed in complex **(7)**. The N–Cu–S and O–Cu–S angles were found to be 92.80° and 92.09°,

respectively. Similarly the angles across the copper centre, that is the N–Cu–N, O–Cu–O and S–Cu–S angles are 180°, with the aromatic planes deviating from one another with a distance of 0.283 Å, indicating the regularity of the octahedral stereochemistry about the copper(II) ion.

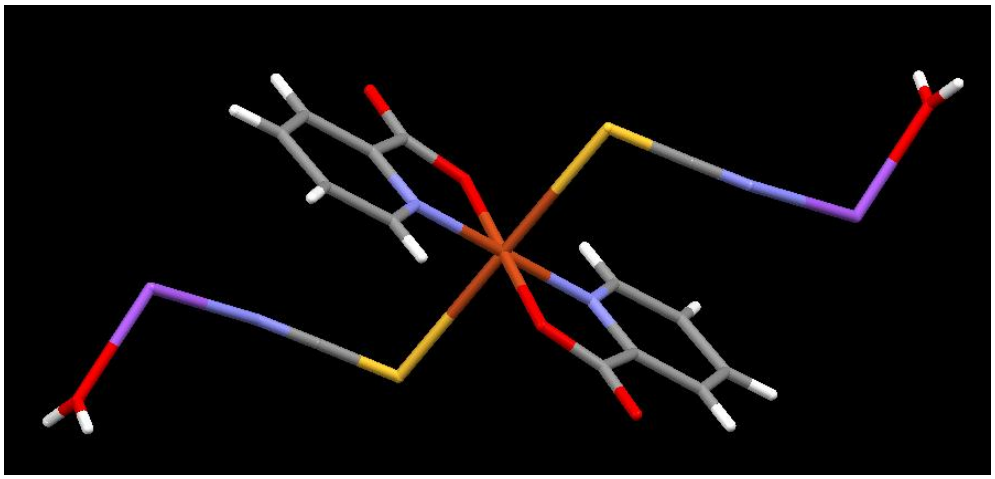

Figure 4-34 Molecular unit of **(11)** $Na_2[Cu^{(II)}(pic)_2(NCS)_2].2H_2O$.

Complex **(11)** exists as a 2-D network (Figures 4-35 and 4-36) held together through ionic sodium interactions, like those observed in complex **(10)** $[Cu^{(II)}(pic)_2]Na_2(NCS)_2.2H_2O$. In complex **(10)** there are six interactions to each sodium, however in complex **(11)** there are only five interactions per sodium and they occur between oxygen atoms on the *pic* ligand (Na···O = 2.252-2.539 Å) and the water (Na···O = 2.258 Å), as well as a nitrogen atom on the thiocyanate anion (Na···N = 2.348 Å).

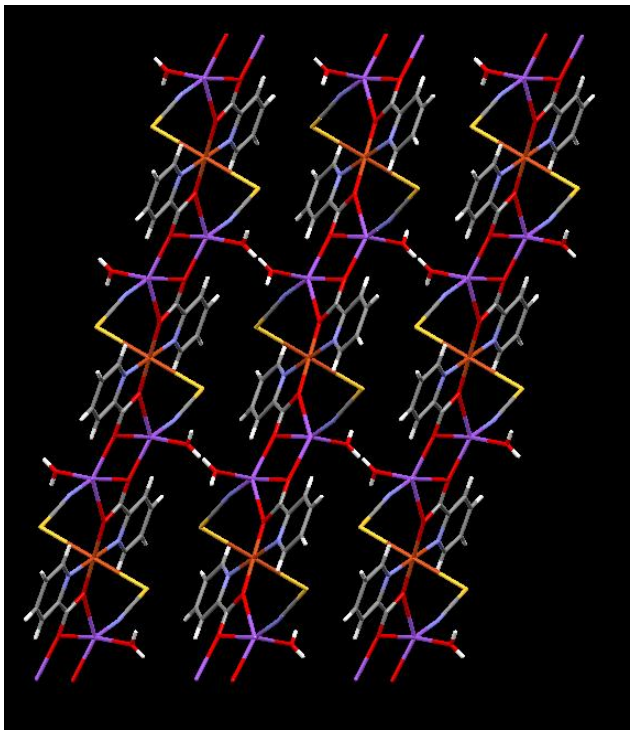

Figure 4-35 Packing of $Na_2[Cu^{(II)}(pic)_2(NCS)_2].2H_2O$ **(11)** viewed along *b*-axis

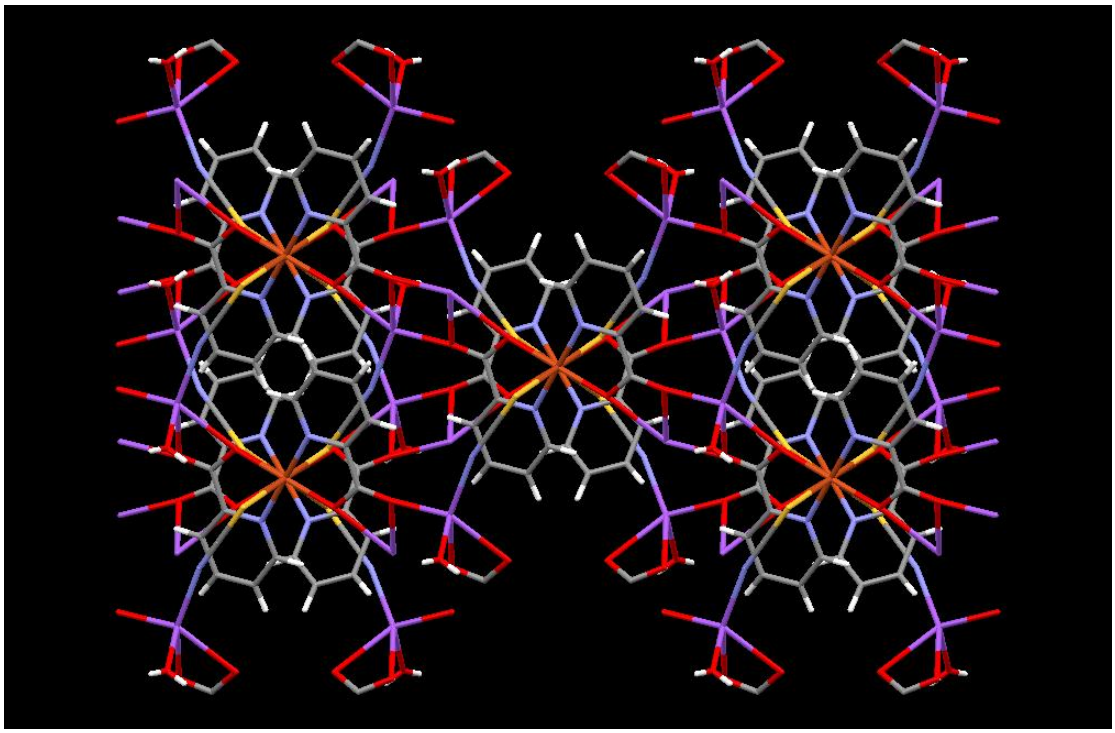

Figure 4-36 Packing of $Na_2[Cu^{(II)}(pic)_2(NCS)_2].2H_2O$ **(11)** viewed along *c*-axis

4.3.6.4. Crystal Structure – Complex (12)

The crystals of **(12)** $[Cu^{(II)}(pic)_2]\cdot Na_2$ $[Cu^{(II)}(pic)_2(NCS)_2]$ exhibit triclinic, *P-1* symmetry, the same as that observed for complex **(10)** $[Cu^{(II)}(pic)_2]Na_2(NCS)_2.2H_2O$, and, like **(10)** and **(11)** $(Na_2[Cu^{(II)}(pic)_2(NCS)_2](H_2O)_2)$, the structure again shows no evidence of *dpk*. Although, unlike **(10)**, which contains one square planar copper centre, or **(11)**, which contains one octahedral copper centre, **(12)** contains two crystallographically distinct copper centres, one square planar and the other octahedral, and is essentially a composite of **(10)** and **(11)**.

The asymmetric unit of **(12)** consists of half of each of the two copper complexes, and one sodium cation giving the empirical formula $[Cu_{0.5}(C_6H_4N_1O_2)(NCS)]Na\cdot Cu_{0.5}(C_6H_4N_1O_2)]$. The two copper centres are crystallographically distinct. The first Cu(II) ion has square planar geometry, coordinating to two nitrogen atoms (Cu–N = 1.982 Å) and two oxygen atoms (Cu–O = 1.955 Å) from two identical picolinate anionic ligands, which counter-balance the +2 charge on the copper.

The second Cu(II) ion has octahedral geometry, coordinating to two nitrogen atoms (Cu–N = 1.939 Å) and two oxygen atoms (Cu–O = 1.988 Å) from two identical picolinate ligands, and two sulphur atoms (Cu–S = 2.935 Å) from two thiocyanate anions confirming the IR data suggesting S–coordinated NCS^-. Each sodium cation is held by strong electrostatic interactions between four oxygen atoms (Na···O = 2.295–2.566 Å) from the picolinate ligands, as well as one nitrogen atom (Na···N = 2.388 Å) from a thiocyanate anion (See Table 4-12 for a summary of significant lengths and angles). The charges on the copper(II) and sodium cations are counter-balanced by the mono anionic picolinate ligands and thiocyanate anions.

Overall, the combination of the two copper centres observed in complex **(12)** appears to be a composite of complexes **(10)** and **(11)**. Thus, the molecular unit of **(12)** has the composition: $Na_2[Cu^{II}(pic)_2(NCS)_2][Cu^{II}(pic)_2]$, see Figures 4-37 and 4-38, which exists as a 3-D network held together through ionic sodium interactions. The N–Cu–O "bite" angles of the *pic* ligand (83.67° and 83.89°) are comparable to those observed in other copper complexes containing *pic* which have corresponding angles of 83.37°[173] and 83.47°.[174] The thiocyanate anion is almost linear with a N–C–S angle

of 178.96°, although the Cu–S–C angle, 94.86°, is close to a right angle. The N–Cu–N, O–Cu–O and S–Cu–S angles are all perfectly linear, with angles of 180°. The planes of the neighbouring *pic* ligands in both copper centres are co-planar, but the aromatic planes on neighbouring ligands differ slightly from one another with a distance of 0.100 Å and 0.113Å between them (See Figure 4-38).

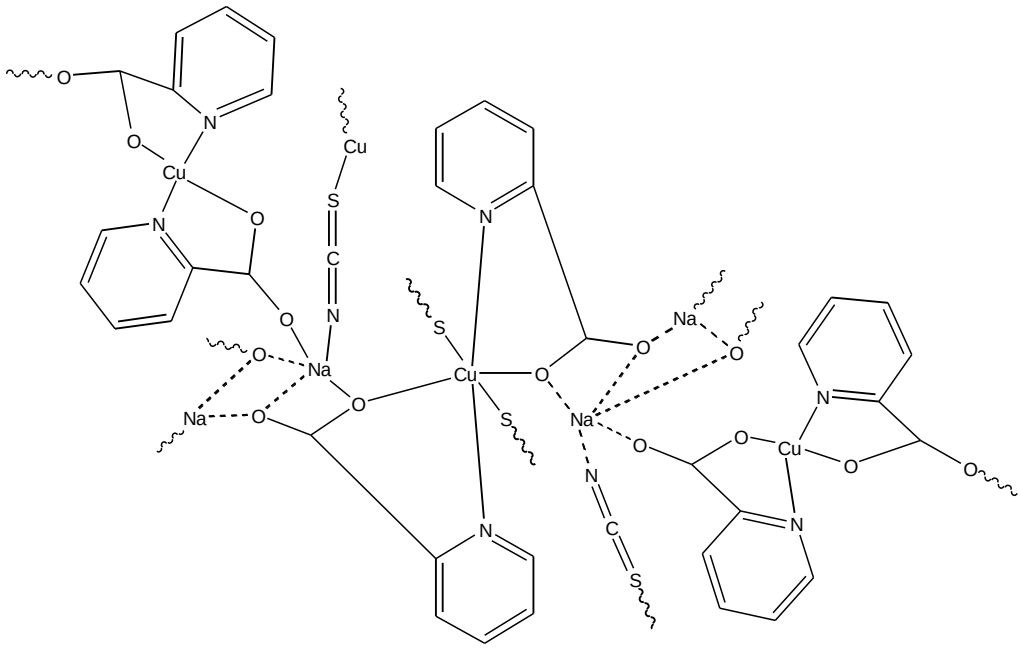

Figure 4-37 Interactions observed with neighbours in complex **(12)** $[Cu^{(II)}(pic)_2]\cdot Na_2\ [Cu^{(II)}(pic)_2(NCS)_2]$

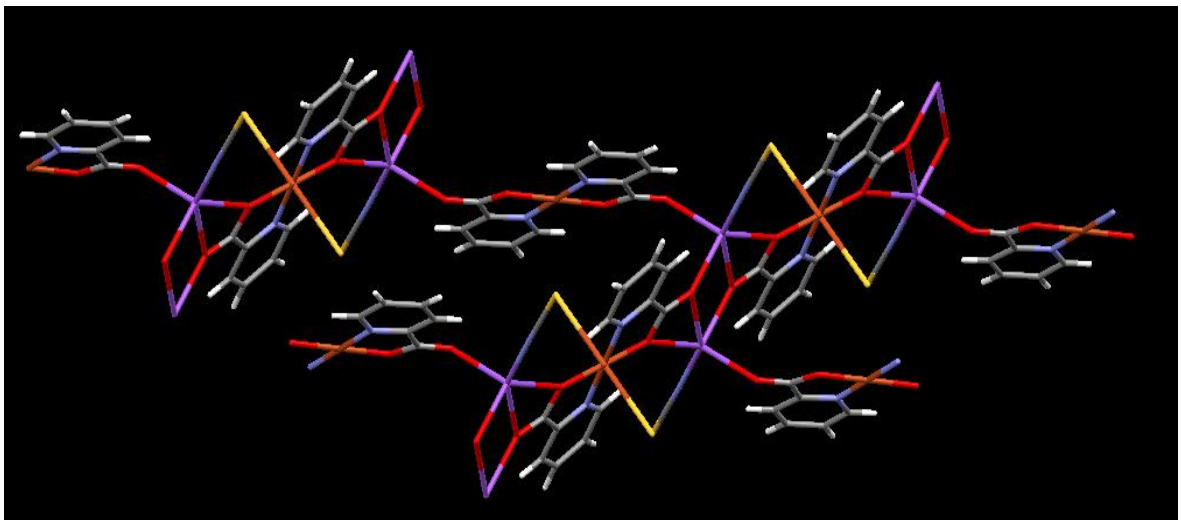

Figure 4-38 Packing of **(12)** $[Cu^{(II)}(pic)_2]\cdot Na_2[Cu^{(II)}(pic)_2(NCS)_2]$ viewed along *a*-axis

The adventitious incorporation of the sodium cation in the crystal lattice of a copper(II)-picolinic acid complex has been observed previously in the compound $NaCu(pic)_2(N_3)(H_2O)_2$ (CCDC code **WIGGOI**).[172] This complex was formed through the reaction of copper(II) nitrate with picolinic acid and sodium azide. Like the thiocyanate ion in complex **(12)**, the isostructural azide anion also acts as a bridging ligand, coordinating to the copper(II) ion and interacting with the sodium cation. The anionic *pic* ligand in **WIGGOI** also coordinates to the copper centre and has strong electrostatic interactions with the sodium. All bonds have comparable distances to those observed in **(12)** and the interactions are similar as well (see Table 4-12), although there are small deviations in the angles observed. In particular, the O–C–O angle from the carboxylate, and the linearity observed across N–Cu–N, O–Cu–O and S–Cu–S bonds which are seen in **(12)**, are not as clearly defined in **WIGGOI**.

Complexes **(10)** $[Cu^{(II)}(pic)_2]Na_2(NCS)_2.2H_2O$, **(11)** $Na_2[Cu^{(II)}(pic)_2(NCS)_2](H_2O)_2$ and **(12)** $[Cu^{(II)}(pic)_2]\cdot Na_2[Cu^{(II)}(pic)_2(NCS)_2]$ are all structurally quite similar; however their global packing is quite different. All three complexes are able to form ionic networks through sodium cation interactions. Complexes **(10)** and **(11)** have additional species in the crystal structure, be it water or benzoic acid, but this was not observed in complex **(12)**. In all three complexes the sodium cation clusters form dimeric units, for example, in **(12)** the $Na^+\cdots Na^+$ non-bonding distance is 3.703 Å and the O···O non-bonding distance is 3.011 Å (The corresponding distances observed in **(10)** and **(12)** for the $Na^+\cdots Na^+$ non-bonding distances are 3.641 and 3.502 Å, respectively and the O···O non-bonding distances are 2.963 and 3.081 Å, respectively).

In complex **(12)** the sodium cation connects the copper ions in two ways. The first is by interacting with the oxygen atoms on the *pic* ligand (from the square planar copper) and nitrogen atoms on thiocyanate (from the octahedral copper), thus forming a polymer chain of alternating copper species in the sequence, *octahedral copper-sodium-square planar copper-sodium*, and this unit is repeated along the chain. The second is by connecting the chains together to form a sheet, and this occurs through sodium interactions between neighbouring oxygen atoms on the *pic* ligand from the octahedral copper. The distances between the square planar copper centres, between

the linking chains, is 10.042 Å, which is identical to the corresponding distance between the octahedral copper centres, as illustrated in Figure 4-39.

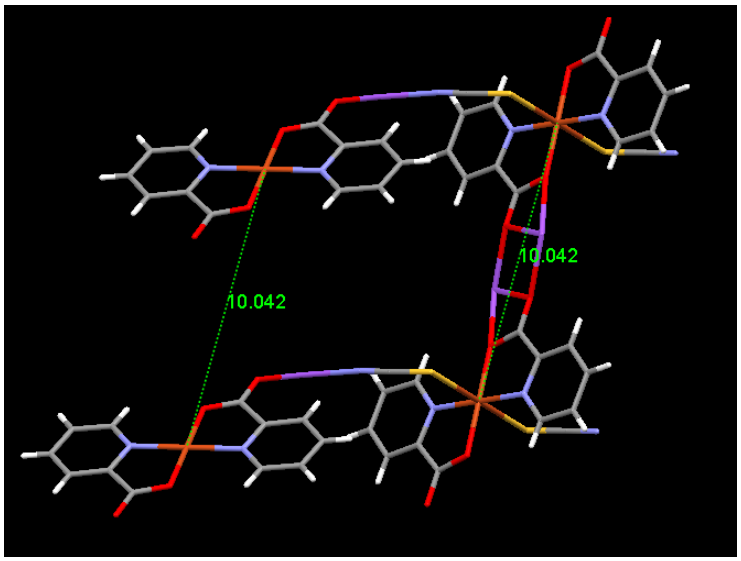

Figure 4-39 Distances between chains in complex **(12)** $[Cu^{(II)}(pic)_2]\cdot Na_2\ [Cu^{(II)}(pic)_2(NCS)_2]$

4.3.6.5. Chemical and Mechanistic Considerations

The formation of the 2-picolinate anion (*pic)* from *dpk* has not been reported previously, although, *pic* has been synthesised through the degradation of bis(2-pyridylketone) (*bpk*) (Figure 4-40) via a C–C bond scission.[25, 29, 173, 175] The structure of *bpk* contains two pyridyl rings, which is similar to *dpk*, but where *dpk* has one keto-carbonyl, *bpk* has two, presenting an additional site for coordination. When coordinated to a metal centre *bpk* can also undergo metal-promoted hydration, which has been suggested as the initial step in the formation of the *pic* ligand. In each reported case, the reaction mixture which gave rise to the *pic* ligand included a redox-active M(II) cation (where M = Cu, or Mn) and *bpk* in methanolic solution.[29, 173]

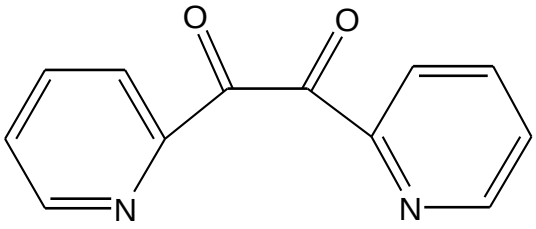

Figure 4-40 Structure of bis(2-pyridylketone) (*bpk*)

In order for *pic* to form, from *dpk*, the ligand must undergo oxidative cleavage of a C–C single bond. This type of bond scission normally requires high temperatures, but in this instance it has occurred at room temperature, albeit over a long period of time; 5 weeks for complexes **(10)** $[Cu^{(II)}(pic)_2]Na_2(NCS)_2.2H_2O$ and **(11)** $Na_2[Cu^{(II)}(pic)_2(NCS)_2](H_2O)_2$, and 3 months for complex **(12)** $[Cu^{(II)}(pic)_2]\cdot Na_2\,[Cu^{(II)}(pic)_2(NCS)_2]$.

The oxidative cleavage of the OC-pyridyl bond in unbound *dpk* can be summarised by the redox half-reactions (using O_2 as an oxidant) shown in Scheme 4-5.

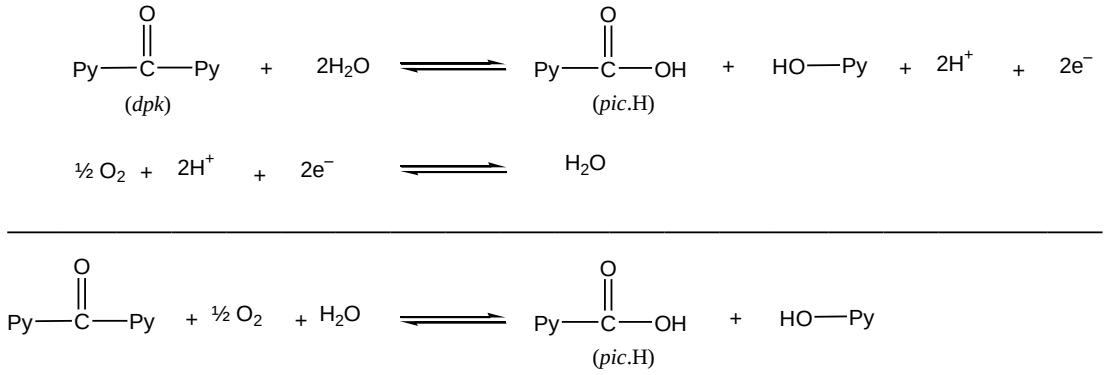

Scheme 4-5 Suggested formation of *pic* from *dpk* through oxidative cleavage.

It is not uncommon for copper to assist in redox reactions involving oxygen, and this is what may have occurred in this instance, although at this time it is not possible to specify which oxidation states of copper are involved, or which oxygen species (oxygen O_2, superoxide O_2^-, or peroxide H_2O_2) activate the reaction.[176-177] One possible reaction sequence is summarised in Scheme 4-6.

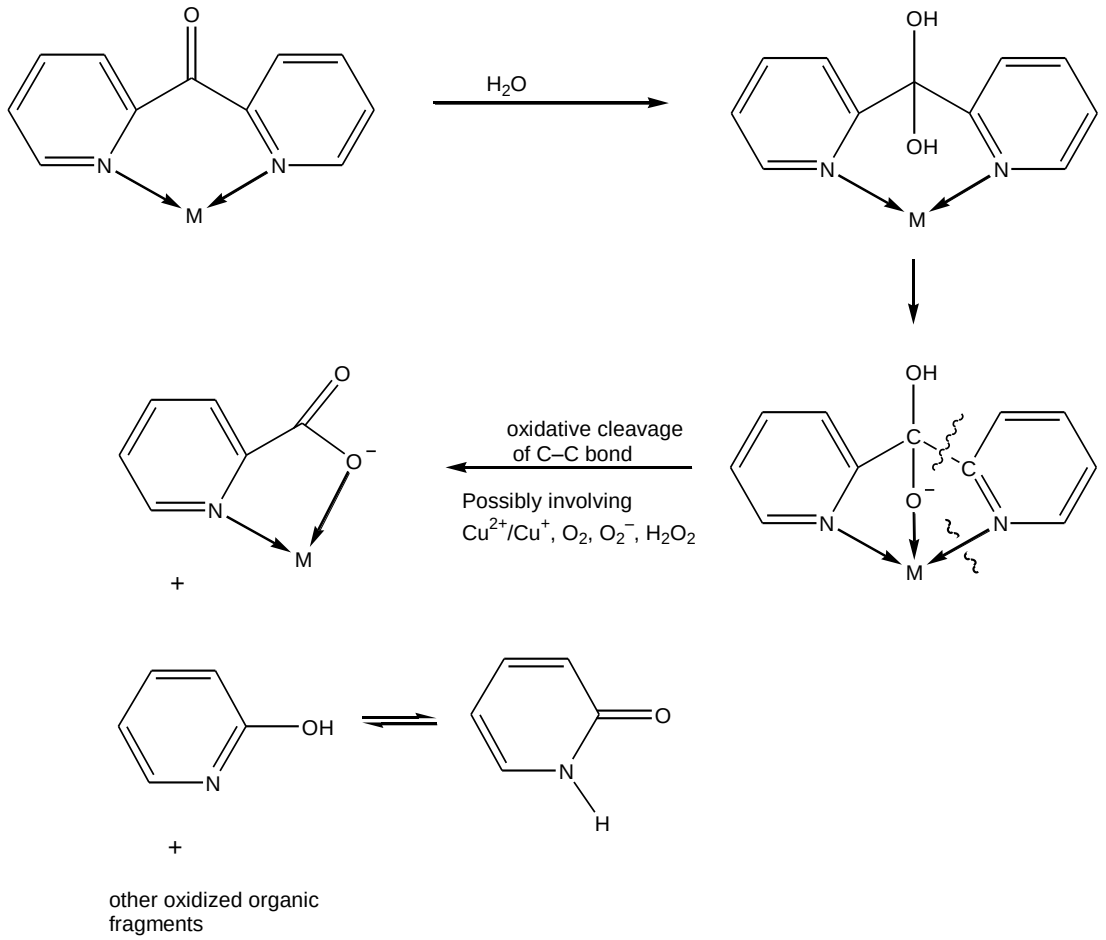

Scheme 4-6 Possible sequence for the formation of **(10)** $[Cu^{(II)}(pic)_2]Na_2(NCS)_2.2H_2O$, **(11)** $Na_2[Cu^{(II)}(pic)_2(NCS)_2](H_2O)_2$ and **(12)** $[Cu^{(II)}(pic)_2]\cdot Na_2\,[Cu^{(II)}(pic)_2(NCS)_2]$.

The sequence proposed above represents one possible route to the formation of **(10)**, **(11)** and **(12)**, but it should be noted that the reaction effectively involves the conversion of a ketone to a carboxylic acid (Scheme 4-7). This suggests that the Baeyer-Villiger (BV) rearrangement may also provide a plausible mechanism for the process occurring in the present reaction:

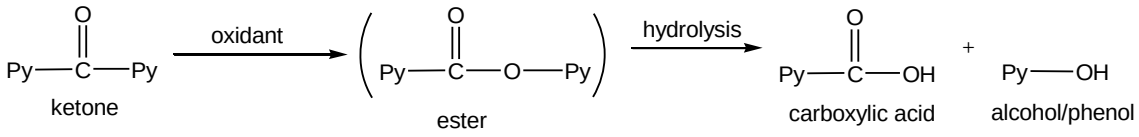

Scheme 4-7 Baeyer-Villiger rearrangement.

The BV rearrangement (oxidation) is a standard reaction used in organic synthesis for the conversion of ketones to esters. In 1899 Adolf von Baeyer and Victor Villiger discovered that a ketone could be transformed into an ester, or a cyclic ketone into a lactone,[178-180] by treatment with a peracid.

The usual oxidant is H_2O_2 or a peroxyacid RCO_2OH as shown below:

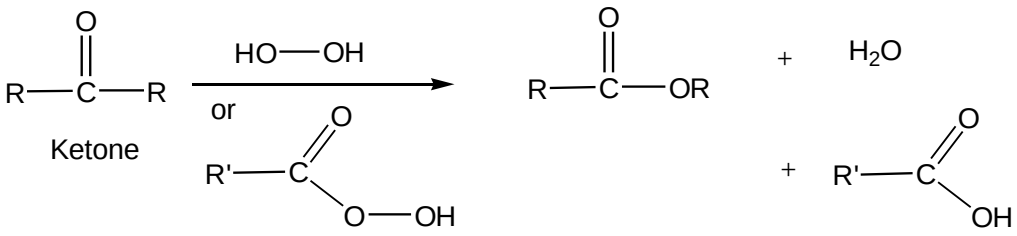

Such a reaction can take 1-2 weeks, or more to proceed.[178] For example:

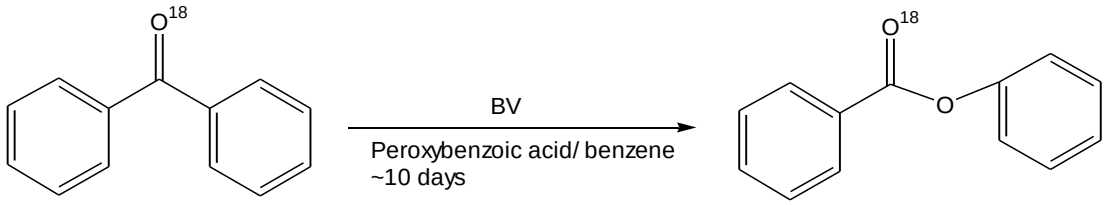

In the present case the most plausible oxygen species is hydrogen peroxide, formed via:

$$2\,Cu^{+} + O_2 + 2H^{+} \longrightarrow H_2O_2 + 2Cu^{2+}$$

These types of oxygen species are becoming more common as a 'greener' oxidant route to activate BV reactions, rather than peracids.[176] In addition to this, transition metals and transition metal complexes have been used as catalysts in BV reactions,[181] therefore it may be possible that the presence of copper may influence this reaction.

The accepted "Criegee Mechanism" for the BV reaction is presented in Scheme 4-8. Initially, the ketone can be protonated to form a carbocation intermediate which can then undergo a nucleophilic attack by the deprotonated peracid, forming what is known as the "*Criegee intermediate*".[182-183] This tetrahedral intermediate species is

unstable, with migration of the carbon fragment attached to the carbonyl group yielding an ester. The ester may then undergo hydrolysis to form a carboxylic acid and alcohol (Schemes 4-6 and 4-8).

Coordination of *dpk* is known to activate the keto-carbonyl, as observed in complexes **(6)** $[Cu^{(II)}_2(dpk.acetone)_2(NCS)_2]$ and **(9)** $[Cu^{(II)}(dpk.H_2O](NCS)_2$, which were mentioned earlier in this chapter, where *dpk* underwent either a mixed-aldol condensation or hydration. In both these instances it is clear that the nucleophilic nature of the carbonyl has been enhanced due to metal coordination. Thus, the keto-group could readily react according to Scheme 4-8, in which an anionic peroxo-species is the attacking agent, as suggested by the BV mechanism.

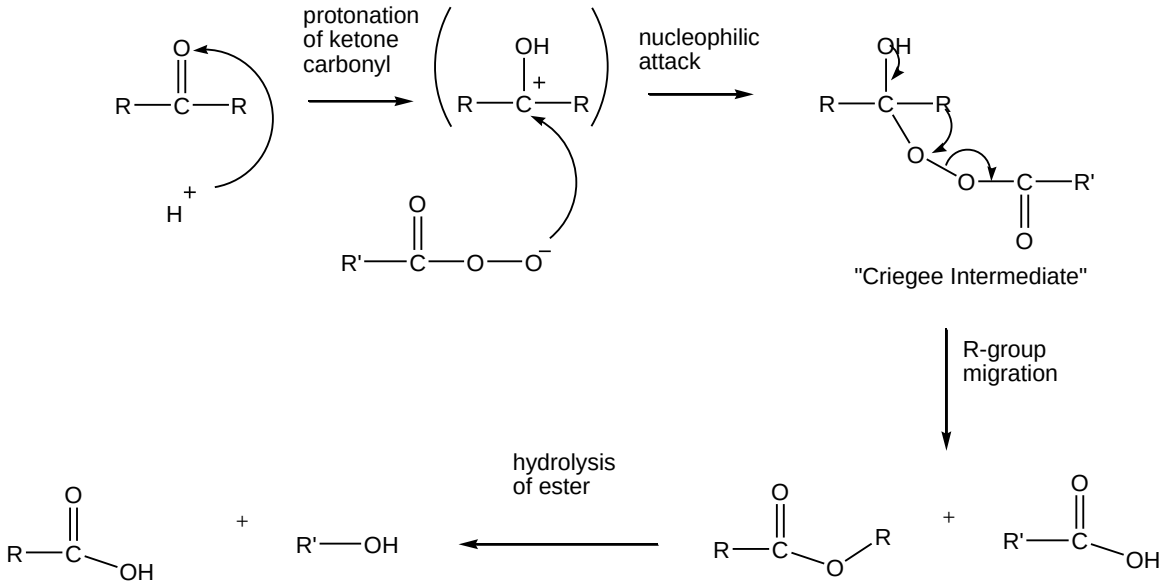

Scheme 4-8 BV rearrangement and Criegee intermediate

In the case of *dpk*, 2-picolinic acid (*pic*-H) and the 2-pyridinol form (Schemes 4-5, 4-6 and 4-9); the deprotonated *pic* is coordinated to the copper, whilst the 2-pyridinol remains in solution.

Since the BV rearrangement appears to have occurred with the *dpk*, other ketones within the reaction mixture may also be able to react in a similar way. Therefore, in the reaction mixture containing acetophenone the BV rearrangement could form either benzoic acid and ethanol, or phenol and acetic acid, or a combination of both.

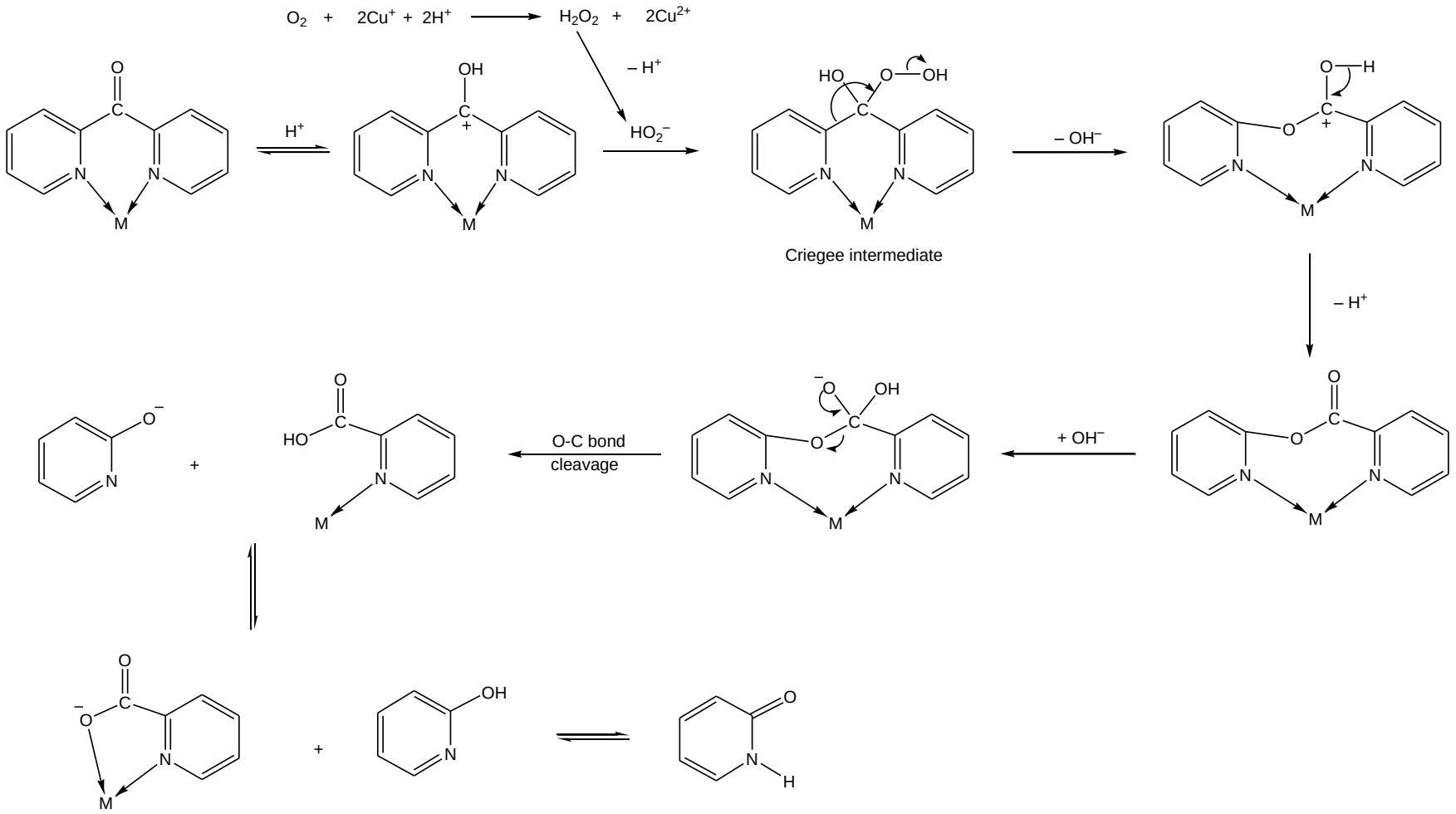

Scheme 4-9 Possible reaction sequence for Baeyer-Villiger rearrangement of *dpk* to *pic*

The presence of phenol was confirmed by the addition of ferric chloride to the mother liquor, thus verifying the usual BV reactions expected for an aromatic ketone. The phenol gave a characteristic red colour which was not observed on addition of aqueous ferric chloride to acetophenone or *dpk*. Therefore, the benzoic acid has arisen from a parallel, but far less kinetically favourable BV reaction. This fact is supported by the very low yield of product isolated, where the formation of benzoic acid from acetophenone was observed as a disordered intercalate within the crystal structure of complex **(11)** $Na_2[Cu^{(II)}(pic)_2(NCS)_2](H_2O)_2$ (Figures 4-32 and 4-33).

4.4. Conclusion

Reaction of the Cu(I) species Cu_2X_2 (where X= NCS^- and I^-), in the presence of excess X^-, with *dpk* in aqueous acetone, produced three new copper(I) compounds and a novel copper(II) complex. These included two Cu(I) polymeric complexes **(4)** and **(5)** $[Cu^{(I)}(dpk)(NCS)]_n$, a dinuclear homoleptic Cu(II) compound **(6)** $[Cu^{(II)}_2(dpk.acetone)_2(NCS)_2]$, and a neutral Cu(I) dimeric complex **(7)** $[Cu^{(I)}_2(dpk)_2I_2]$. Complexes **(4)** and **(5)** are polymorphs, forming polymeric structures in a *syndiotactic* and *isotactic* configuration, respectively, and are intermediates in the formation of **(6)**. Complex **(6)** formed as a result of dissolution and oxidation of **(4)/(5)** followed by a transition metal-promoted mixed aldol condensation reaction between the solvent and the keto-carbonyl of (*dpk*) to form a covalent bond between the *dpk* and acetone. This produced the novel ligand, *dpk.acetone*, which has been observed for *dpk* once before but not fully described.[25] The magnetic behaviour observed in **(6)** is consistent with *ferromagnetic* coupling between the Cu(II) centres.

Following the formation of **(6)** in the presence of acetone, the reaction of $Cu_2(SCN)_2$ with excess SCN^- and stoichiometric amounts of *dpk*, in various other aqueous ketone and aldehyde solvents was investigated. Products were isolated from two of the solvent systems. In the *methyl ethyl ketone system*, complexes **(8)** $[Cu^{(II)}(dpk)_2(NCS)_2]$ and **(9)** $[Cu^{(II)}(dpk.H_2O)_2]^{2+}(NCS)_2$ were isolated. Compound **(8)** is a neutral mononuclear Cu(II) compound, which preserves the *dpk* carbonyl group, whereas **(9)** is a mononuclear Cu(II) compound where *dpk* has been hydrated. Complexes **(10)** $[Cu^{(II)}(pic)_2]Na_2(NCS)_2.2H_2O$ and **(11)** $Na_2[Cu^{(II)}(pic)_2(NCS)_2](H_2O)_2$ were isolated

from an *acetophenone solvent system*. Complex **(12)**, $[Cu^{(II)}(pic)_2]\cdot Na_2[Cu^{(II)}(pic)_2(NCS)_2]$, was isolated from another *acetophenone solvent system* as a mixed coordination Cu(II) compound. All three complexes contain coordinated picolinate, with thiocyanate and sodium ions in the crystal lattice. The formation of the picolinate arose from the cleavage of a C–C bond in *dpk* and can be rationalized on the basis of a Baeyer-Villiger rearrangement.

The focus of the investigation into copper(I) complexes formed with *dpk* was to explore the luminescent behaviour of such complexes, and the possibility that they may be suitable as "dyes" in solar electro-chemical cells. In this respect, UV-Vis spectroscopy of all the copper(I) *dpk* complexes prepared here revealed promising results, as strong absorbance was observed across the entire visible spectrum. Fluorescence spectroscopy revealed that only the iodo-analogue **(7)** $[Cu^{(I)}_2(dpk)_2I_2]$ exhibited weak MLCT, and the luminescence of the thiocyanate bridged polymeric copper(I) complex was quenched.

The complexes also contained unbound carbonyl groups on the *dpk* with potential for binding to metal oxide semiconducting surfaces in DSSC. However, the insolubility of the complexes precluded their fabrication into solar cells, and therefore the potential binding mode could not be tested. Therefore, complexes **(4)**, **(5)** and **(7)** were not considered appropriate candidates in terms of solar energy capture, despite their strong absorbance and binding potential.

The other six complexes, **(6)**, **(8)**, **(9)**, **(10)**, **(11)** and **(12)** all contain copper(II) metal centres and therefore do not have the desired luminescent behaviour; hence they are not suitable for this energy capture process.

Thus, the next phase of the work described in this thesis concentrated on developing new binding moieties for the attachment of polypyridyl metal complexes to semiconductor substrates for use in DSSCs with particular emphasis on Ru(II)/Ru(III) compounds.

CHAPTER 5

Ruthenium bipyridine-type complexes incorporated into dye-sensitized solar cells.

5.1. Summary

In dye-sensitized solar cells (DSSC's) a strong chemical interaction "chemisorption" between the "dye" species and the semiconducting metal oxide surface (such as TiO_2 or WO_3), is crucial for rapid and efficient electron transfer, and subsequently the generation of an electrical current.

Initial studies, based on work previously reported in the literature, [1-24] and described in the introduction of this thesis, explored the synthesis and properties of ruthenium complexes which contained the highly polar carboxylate or phosphonate ionic linker groups. Although these ionically bound linkers have been studied extensively, and while they have been extremely successful, the surface binding of the carboxylate and phosphonate to metal is not stable over the full pH range, or to all solvents. To overcome this deficiency, a covalent linker was deemed necessary. This led to the adoption of a novel silyl ester linkage. The synthesis of two ruthenium complexes which contain a silatrane-propyl amide link on the (4,4'-dicarboxylic acid)-2,2'bipyridine ligand are reported.

In addition to this, an extensive study, which concentrated on synthesising pyridine-type ligands with short distances between the silatrane linker and the pyridine ring, was undertaken.

5.2. Introduction

Bidentate N-heterocycles such as bipyridine (*bipy*) and 'bipyridine-type' ligands are important building blocks for coordination complexes. In particular, those coordinated to ruthenium(II) have been explored extensively for their photochemical and photophysical behaviour.[1-2] The bipyridine-type ligands tend to have substituents in the 4,4'-positions, which are usually anchoring groups that allow electron transfer between the metal species and the semiconductor to occur, for electricity generation.

Currently, carboxylate and phosphonate linkages are the most commonly used anchoring groups for adhesion to semiconducting surfaces, and both have been explored extensively.[2, 4-8, 16-18, 28, 35, 43, 45, 53-54, 113, 184] A linkage group which has not been explored to its full potential is the silyl linkage. Silanes have several advantages over the current carboxylate and phosphonate linkages as they are more stable over a wider range of pH's and solvents.[16, 57] The silyl interaction with the hydroxyl groups on the semiconducting TiO_2 surface is quite strong, forming a Ti–O–Si–C bond. The two possible modes of a silane linkage to TiO_2, containing either one, two or three covalent bonds, are illustrated in Figure 5-1.[185]

One of the many reasons why silyl coupling has not been explored is the rather tedious synthetic procedure required to prepare appropriate precursor ligands.[186] An *in-situ* synthetic method has been reported,[185] whereby the first step involved modification of titania with organoalkoxysilane materials (3-chloropropylmethoxysilane), followed by reaction with a 2-aminothiazole ligand, and finally coordination to a Pd(II) ion. This particular investigation focused on photocatalytic activity for the degradation of phenols, but it is still representative of a silyl linkage to a metal oxide. A silyl linkage has also been prepared by *in-situ* pyrazole silylation on the ruthenium complex, $[Ru(py\text{-}pzH)_3]^{2+}$ (where *py-pzH*=3-(2'-pyridyl)pyrazole), Figure 5-1.[47]

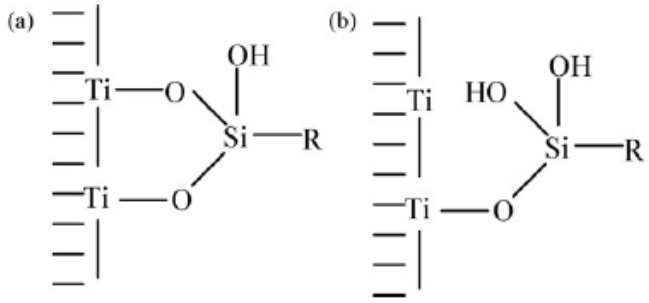

where R = a palladium 2-aminothiazole complex

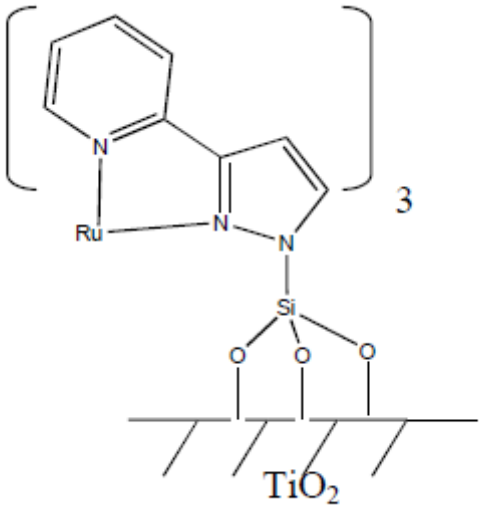

Figure 5-1 Possible linkage of silyl to TiO_2 [47, 185]

Although these linkers have not been exploited to any degree in DSSC's, Brennan *et al.*[48] have investigated silicon-oxygen based linkages with SnO_2 semiconducting surfaces and found the silyl-ester bond a promising alternative linker to carboxylates and phosphonates. To this end, the potential for anchoring of 'dyes' to metal oxides using silyl groups are explored within this chapter.

5.3. Results and Discussion

5.3.1. Preparation and Characterization of Complexes

A series of ruthenium coordination complexes containing either *bis*- or *tris*- *bipy* ligands were investigated in this study and are listed in Table 5-1.

The *bis*-*bipy* ruthenium dye complexes were synthesised by refluxing ruthenium (III) chloride with various 2,2'-bipyridine derivatives in DMF, under N_2, to initially form the ruthenium(II) *cis*-dichloro species.[53] These were then refluxed with excess NaNCS to form the *cis*-dithiocyanato species (see Scheme 5-1 for the overall reaction sequence). The N-coordinated thiocyanato group enables fine tuning of the physico-chemical properties of such ruthenium species to optimise their function in a DSSC.

The *tris*-*bipy* ruthenium complexes, whereby one of the *bipy* ligands contained a linker and the others were unsubstituted, were synthesised by refluxing Ru(*bipy*)$_2$Cl$_2$ with various 2,2'-bipyridine derivatives in DMF under N_2. Each complex was precipitated from solution by addition of excess NH_4PF_6 (See Scheme 5-2 for overall reaction).

Table 5-1 Observed wavelength maxima and molar extinction coefficient data for ruthenium complexes **(13)-(19)**.

Dye	Number	λ_{max} (*nm*)	ε ($L\ mol^{-1}cm^{-1}$)
[Ru(*bipy*)$_2$(*dcbipy*)](PF$_6$)$_2$	**(13)**	460	14350
[Ru(*bipy*)$_2$(*dpbipy*)](PF$_6$)$_2$	**(14)**	450	17600
[Ru(*bipy*)$_2$(*bipy-sil*)](PF$_6$)$_2$	**(15)**	457	10520
[Ru(*dcbipy*)$_2$Cl$_2$]	**(16)**	467	20790
[Ru(*dcbipy*)$_2$(NCS)$_2$] **N3**	**(17)**	492	29630
[Ru(*bipy-sil*)$_2$Cl$_2$]	**(18)**	485	11070
[Ru(*bipy-sil*)$_2$(NCS)$_2$]	**(19)**	500	20750

* The *dcbipy*, *dpbipy* and *bipy-sil* ligands in complexes **(13)-(19)** are shown in Scheme 5-1.

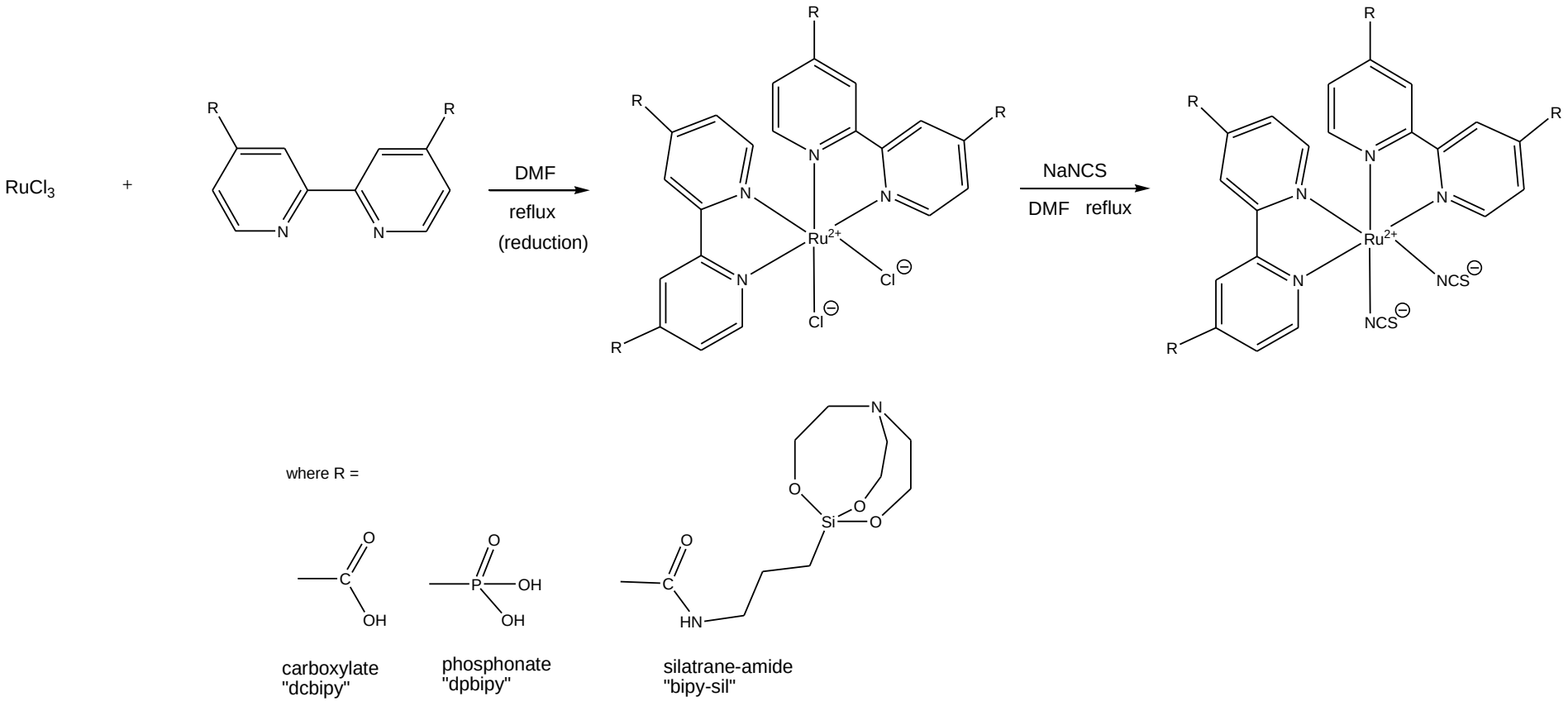

Scheme 5-1 Overall reaction sequence for the formation of *bis*-chelated Ru(II) complexes

While the *tris*-chelated ruthenium complexes are known to be less efficient in terms of solar energy capture, not all of the ligands with anchoring groups could be incorporated into *bis*-chelated ruthenium complexes. For example, the *dpbipy* analogue could not be successfully prepared in a *bis*-form. Therefore, the *tris* complexes were used to compare the efficiency of various anchoring ligands and to make a reasonable comparison between existing ruthenium dyes and the dyes prepared here.

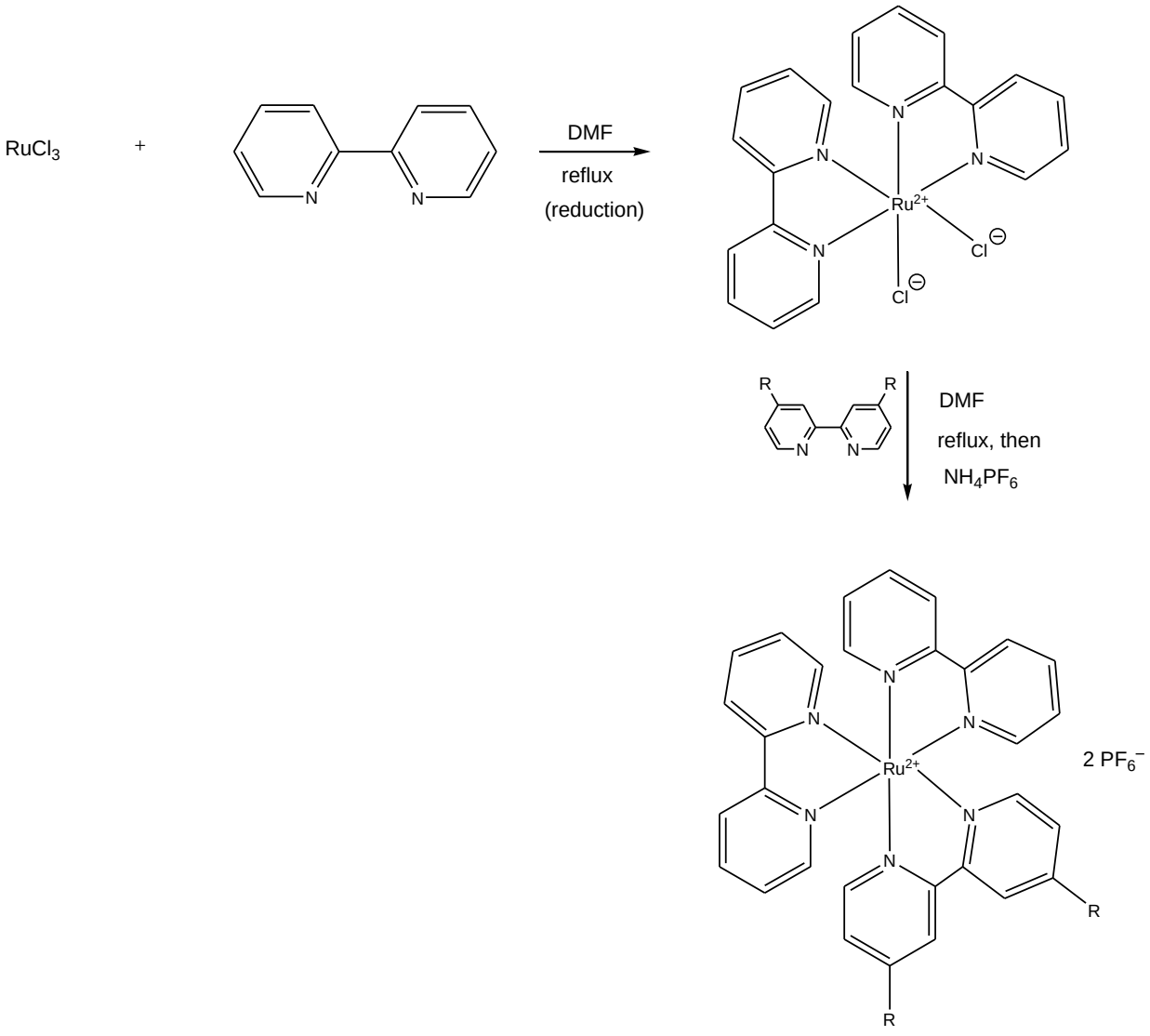

Scheme 5-2 Overall reaction sequence for the formation of *tris*-chelated Ru(II) complexes.

Bipy ligands possessing carboxylate and phosphonate linkers were incorporated into Ru(II) complexes, and various analogues of the ruthenium dye containing the *tris-bipy*, *cis*-dichloro and *cis*-dithiocyanto type were prepared and examined using FT-IR,

^{1}H, ^{13}C and, where possible, ^{31}P NMR, UV-Visible, and fluorescence spectroscopic analysis.

The current commercial dyes, **N3** and **N719** (Figure 5-2), contain carboxylate anchoring groups. There are very few commercial options for other linkers such as the phosphonate analogue, and none for the silyl. A silatrane ligand has been synthesised by Brennan *et al.*[48] and successfully anchored to SnO_2 but, adhesion of silyl groups to TiO_2, or any other semiconducting surface, have not been exploited to their full potential. Also, the ligand used by Brennan *et al.* [48] contains a saturated propyl-chain which does not assist with electron transfer, as electron conduction is poor through the three carbon, non-conjugated chain.[49] Electron transfer would be improved if a conjugated system was incorporated in the linker, rather than the propyl-chain, or if this chain was removed completely.

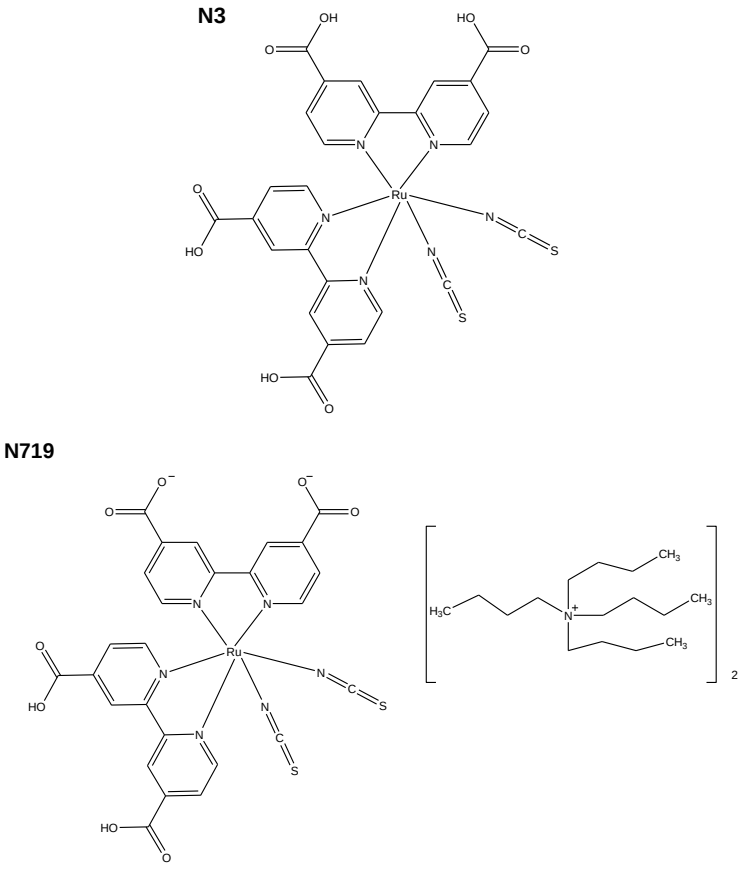

Figure 5-2 N3 and **N719** Commercial Dyes[38]

The carboxylate functionalised *dcbipy* ligand was purchased from Dyesol and used without further purification. However, the phosphonate[12] and silatrane[48] analogues were synthesised in this work (refer to the "Materials and Methods" section of this thesis for a more detailed description of the preparation and characterization of these materials).

Clearly, the most efficient dye complexes will be those that: (a) absorb the most light, (b) are able to transfer the excited electron to the semi-conductor substrate and (c) are readily reduced to the starting complex, to continue the photoexcitation redox cycle (See Figure 5-3). All seven complexes **(13)-(19)** satisfy condition (a), which was observed in their absorption data (refer to Table 5-1). But they require testing in a simulated solar cell to rate their efficiency in conditions (b) and (c).

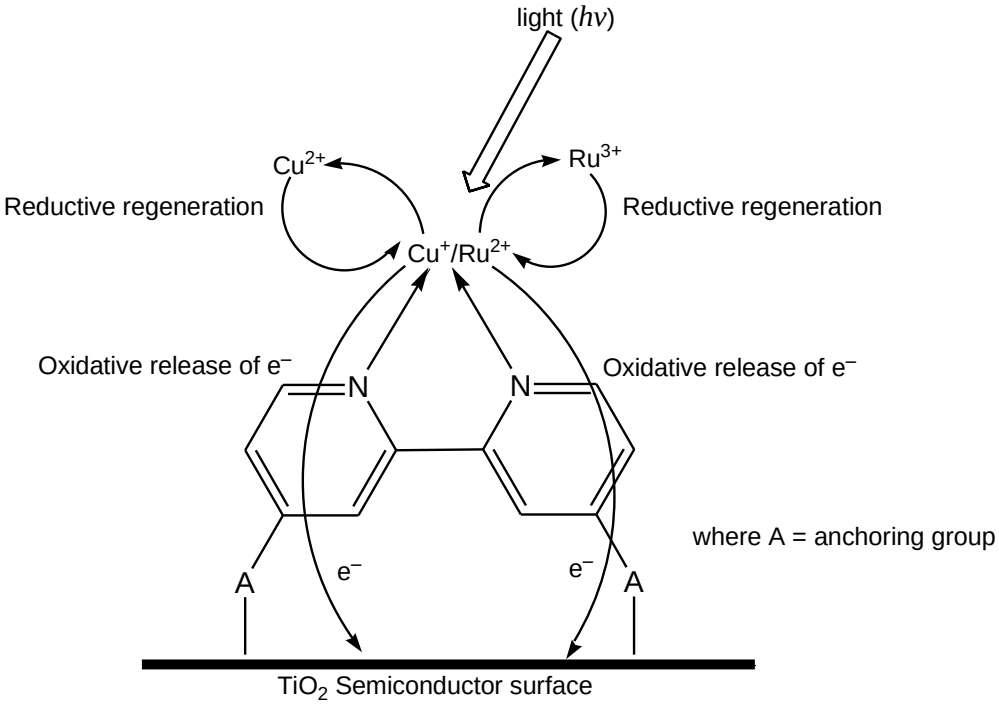

Figure 5-3 Schematic of dye complex absorbing light and transfering the excited electron to the semiconductor substrate.

As mentioned earlier, (refer to the introduction chapter of this thesis), the surface binding of the carboxylic acid and phosphonic acid analogues is not stable across a wide pH range, however the silyl ester bond is, and this is one of its advantages. [47] The *tris*-bipyridine based ruthenium complexes were found to desorb from TiO_2 in

aqueous solution at pH ~4 for the carboxylate, and pH~7 for the phosphonate.[47-48, 184] The stability of the silyl linkage allows it to function over a wider pH range and in the presence of significant amounts of organic solvents.[47]

In the past, the synthesis of silane materials was not reliable, but recently Brennan *et al.*[48] introduced a method whereby the silane was protected by a silatrane group. The latter is resistant to hydrolysis, and thus the synthesis of silyl-functionalised ligands became a viable option. The reaction scheme for the preparation of *bipy-sil* is illustrated in Scheme 5-3, and details of the synthesis and characterisation are given in section 2.2.1.2.

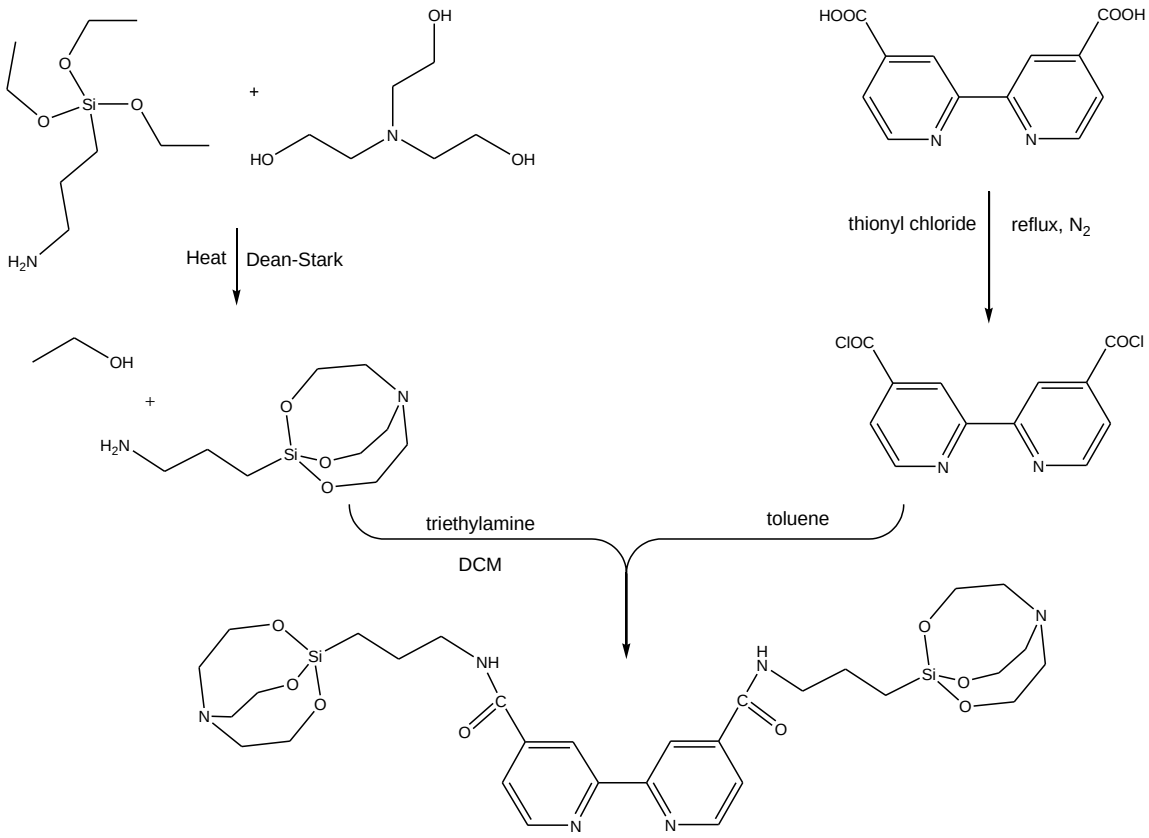

Scheme 5-3 Reaction scheme for synthesis of *bipy-sil* [48]

The silatrane is able to bind to the metal oxide surface after mild heating, upon which the triethanolamine group is lost and a silyl ester bond is formed at the surface, according to the reaction shown in Figure 5-4.

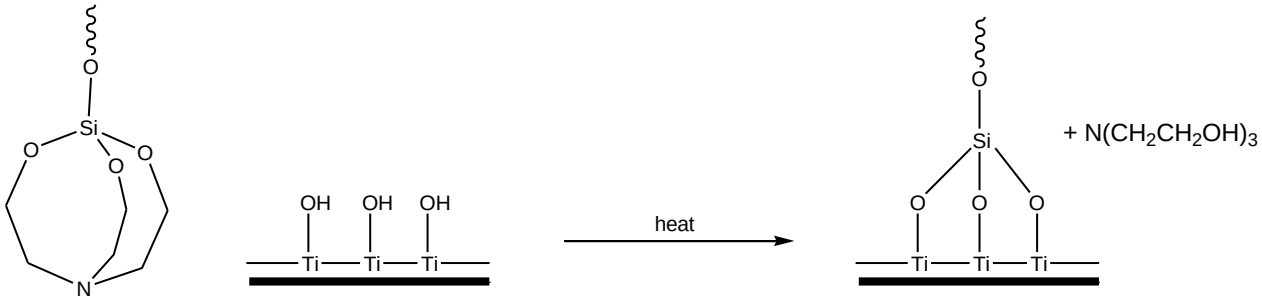

Figure 5-4 Silyl linkage: "chemisorption" to TiO_2.

The ruthenium complex prepared by Brennan *et al.* [48] was *bis*(2,2'-bipyridine)-4,4-dicarboxyl-(3-silatranylpropylamide)ruthenium(II) dihexafluorophosphate, and was anchored successfully to a SnO_2 semiconducting surface (See Scheme 5-3). The same complex **(15)** [Ru(*bipy*)$_2$(*bipy-sil*)](PF$_6$)$_2$ has also been prepared here. Two new ruthenium complexes **(18)** [Ru(*bipy-sil*)$_2$Cl$_2$] and **(19)** [Ru(*bipy-sil*)$_2$(NCS)$_2$] were also prepared and investigated for their performance in DSSC's. These complexes are similar in structure to existing *bis-bipy* type dyes in that they contain ruthenium coordinated to two anchoring ligands and either two chloro- **(18)** or two thiocyanato- **(19)** anions, hence they do not require the non-bonding counter anions (PF_6^-) as reported in Brennan's complex **(15)**, see Scheme 5-1.

[Ru(*bipy*)$_2$(*bipy-sil*)](PF$_6$)$_2$ **(15)** was prepared according to the method detailed by Brennan *et al.*,[48] by coordination of *bipy-sil* to [Ru(*bipy*)$_2$Cl$_2$] (See Section 2.2.5.4) . [Ru(*bipy-sil*)$_2$Cl$_2$] **(18)** was prepared by coordination of the *bipy-sil* ligand to ruthenium trichloride, utilising methods previously published, but replacing *dcbipy* with *bipy-sil* (See Section 2.2.5.7). [Ru(*bipy-sil*)$_2$(NCS)$_2$] **(19)** was prepared by reacting [Ru(*bipy-sil*)$_2$Cl$_2$] **(18)** with excess sodium thiocyanate (See Section 1.1.1.1) . In all cases the identity of the complexes was confirmed by FT-IR and ^{1}H NMR spectroscopy (Refer to the "Materials and Methods" section of this thesis for a more detailed description of the preparation and spectral interpretation).

5.3.2. UV-Vis data

UV-visible absorption studies of complexes **(13)** [Ru(*bipy*)$_2$(*dcbipy*)](PF$_6$)$_2$, **(14)** [Ru(*bipy*)$_2$(*dpbipy*)](PF$_6$)$_2$ and **(15)** [Ru(*bipy*)$_2$(*bipy-sil*)](PF$_6$)$_2$ (See Figures 5-5 and 5-6) were carried out in DMF solution at concentrations of 2mM, 3mM and 4mM. The molar extinction coefficients are averages of the three concentrations, and the spectra shown below are from the 3mM solutions. In the solid-state, all three complexes were orange-red in colour and this colour persisted when they were dissolved in solution.

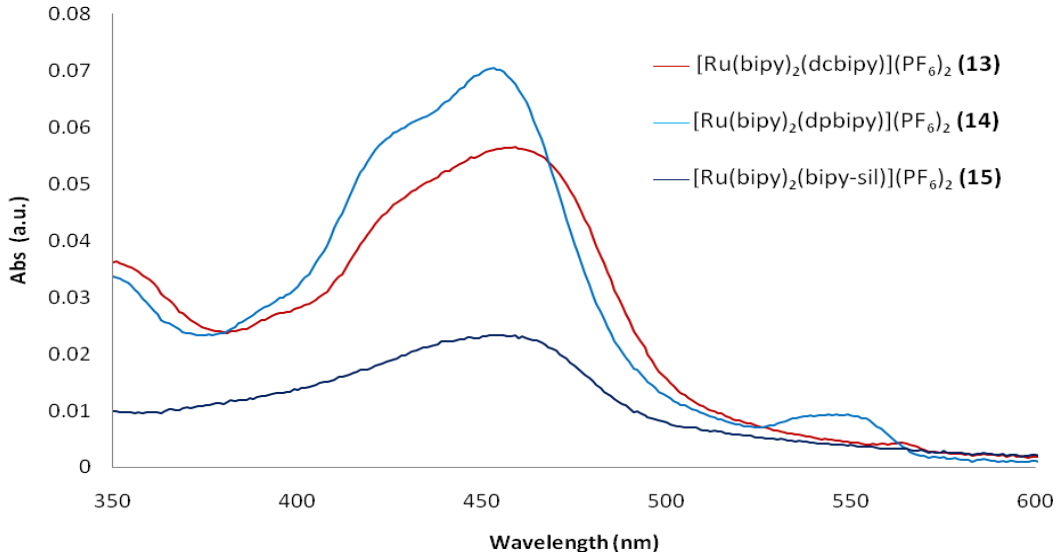

Figure 5-5 UV-Vis spectra of complexes **(13)**, **(14)** and **(15)** (3mM, 350-600nm)

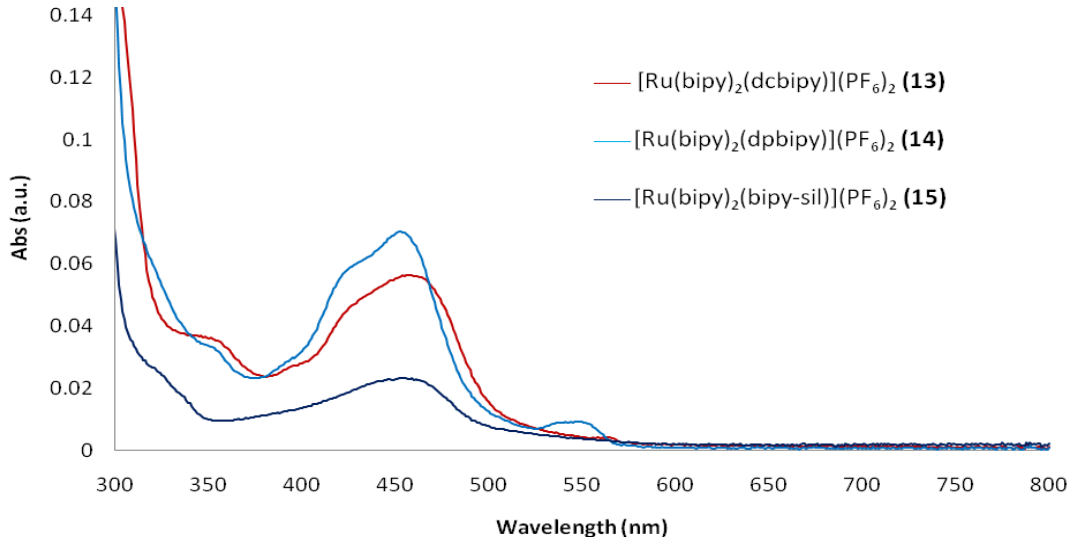

Figure 5-6 UV-Vis spectra of complexes **(13)**, **(14)** and **(15)** (3mM, 300-800nm)

In the spectrum of **(13)** [Ru(*bipy*)$_2$(*dcbipy*)](PF$_6$)$_2$ one distinct band in the visible region between 400-600nm was observed with a λ_{max} at 460nm. The mean molar extinction coefficient of **(13)** was calculated to be 14350 ± 320 L mol^{-1} cm^{-1} using the Beer-Lambert relationship, as expressed by Equation 2-2. See Table 5-1 for a summary of λ_{max} and ε data.

The UV-visible spectrum of the *dpbipy* complex **(14)** [Ru(*bipy*)$_2$(*dpbipy*)](PF$_6$)$_2$ is similar to that of the *dcbipy* complex **(13)**, with a broad band observed between 400-500nm having a λ_{max} at 450nm and a shoulder at about 425nm, with a second small band at 545nm. The structure of the absorption at 450nm, with one band having a shoulder within the visible region is characteristic of tris-*bipy* ruthenium complexes and arises from metal-to-ligand charge transfer (MLCT), from the metal t_2 orbital to the excited t_1 orbital, see Figures 1-3 and 1-11.[11, 39] The mean molar extinction coefficient of **(14)** was calculated to be 17600 ± 640 L mol^{-1} cm^{-1}.

The UV-visible spectrum of the *bipy-sil* complex **(15)** [Ru(*bipy*)$_2$(*bipy-sil*)](PF$_6$)$_2$ is similar to both **(13)** and **(14)**, with a λ_{max} at 457nm, but with a lower absorbance. The mean molar extinction coefficient of **(15)** was calculated to be 10520 ± 440 L mol^{-1} cm^{-1}.

As stated previously, *tris-bipy* ruthenium complexes have limited absorbance in the visible region, which has been observed here in the UV-visible spectra of complexes **(13)**, **(14)** and **(15)**. In all three complexes the bands are believed to arise from metal-to-ligand charge transfer (MLCT) transitions.

The UV-visible absorption studies of complexes **(16)** [Ru(*dcbipy*)$_2$Cl$_2$] and **(17)** [Ru(*dcbipy*)$_2$(NCS)$_2$] were carried out in acetonitrile solution. In the solid state, both **(16)** and **(17)** are dark red in colour, and this dark colour persisted in solution for complex **(17)**, although complex **(16)** formed a red-pink solution. The UV-visible spectrum of complex **(16)** exhibited one broad absorption band from 410-510nm, with a pronounced shoulder from 420-440nm as can be seen in Figure 5-7 not unlike the absorbance profiles seen for **(13)** and **(14)**. The absorption band of **(16)** had a λ_{max} at 467nm, with a corresponding mean molar extinction coefficient of 20790 ± 510 L mol^{-1} cm^{-1}.

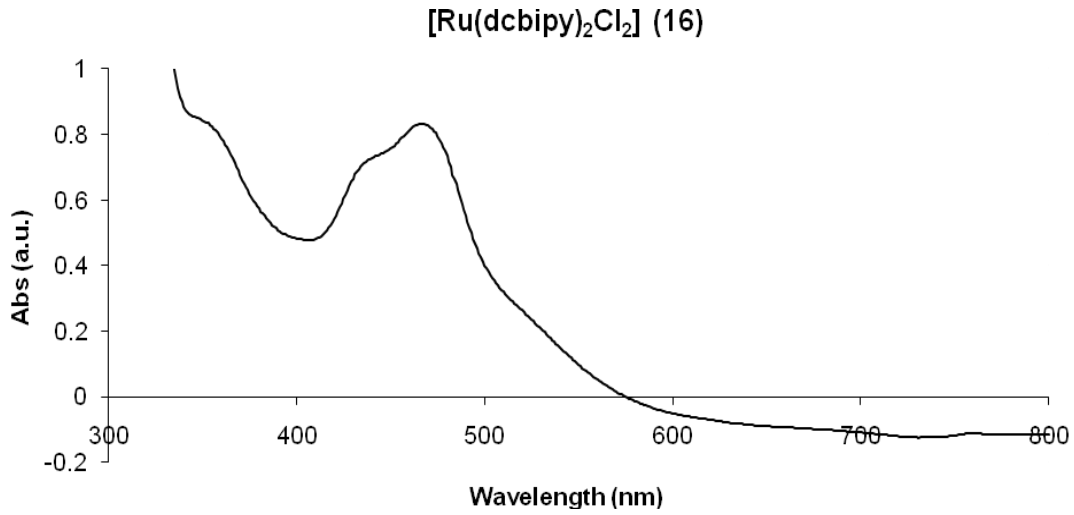

Figure 5-7 UV-Vis spectrum of complex **(16)** (3mM, 300-800nm)

The UV-visible spectrum of complex **(17)**, the commercial '**N3**' dye, displayed two intense broad absorption bands in the visible region; band (1) from 425-550nm with $\lambda_{max(1)}$ = 492nm and band (2) from 610-750nm with $\lambda_{max(2)}$ = 685nm, as seen in Figure 5-8, which is characteristic of *bis-bipy* ruthenium complexes and has been observed with the **N3** dye.[17] For band (1) the molar extinction coefficient is 29630 ± 870 L mol^{-1} cm^{-1}and for band (2) 23380 ± 690 L mol^{-1} cm^{-1}

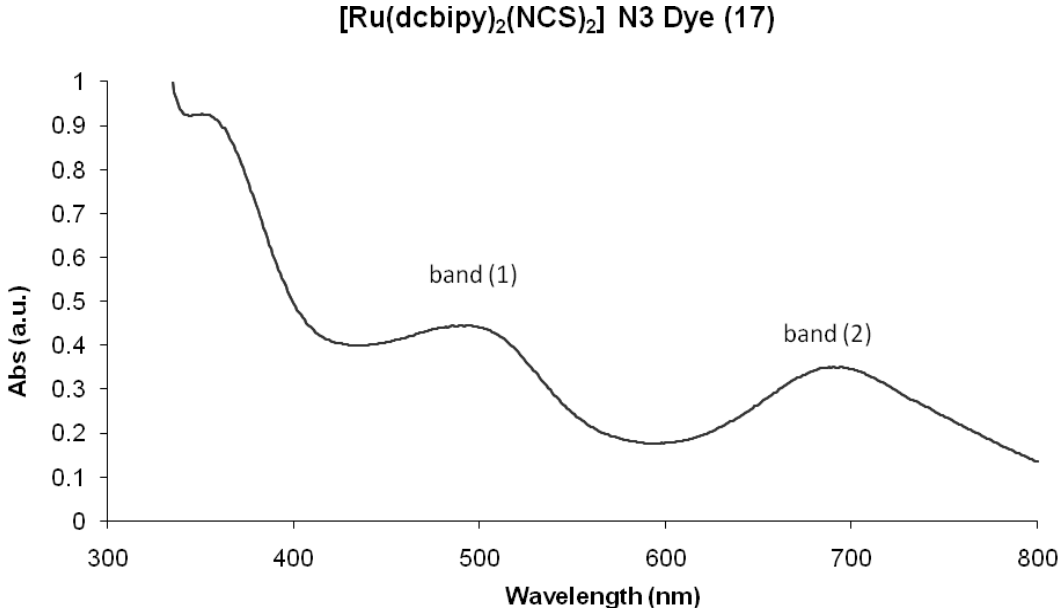

Figure 5-8 UV-Vis spectrum of complex **(17)** '**N3** dye' (3mM, 300-800nm)

UV-visible absorption studies of the *bipy-sil* complexes **(18)** and **(19)** were carried out in DMF *solution*. In the *solid state* both **(18)** and **(19)** are dark red in colour and this colour persisted in solution. Like the commercial **N3** dye, two broad bands were observed in the spectrum of **(18) [**Ru(*bipy-sil*)$_2$Cl$_2$], one in the UV region, band (1) from 340-370nm λ_{max} at 365nm and a molar extinction coefficient of 12716 ± 180 L mol^{-1} cm^{-1}, the second, band (2) from 440-540nm, with a λ_{max} at 485nm, and a molar extinction coefficient of 11070 ± 150 L mol^{-1} cm^{-1}, as seen in Figure 5-9.

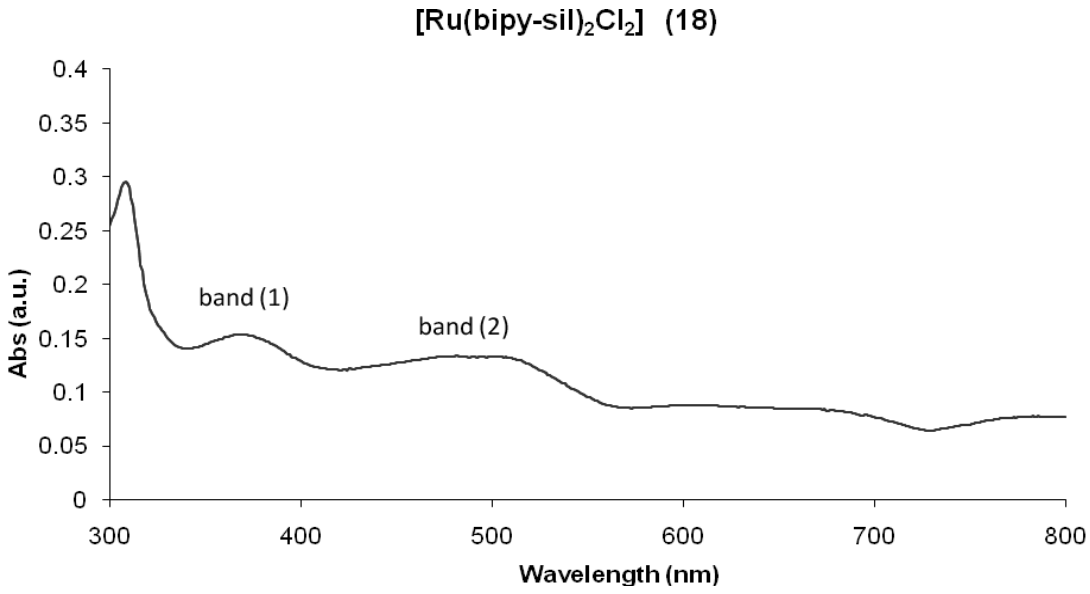

Figure 5-9 UV-Vis spectrum of complex **(18)** (3mM, 300-800nm)

The UV-visible spectrum of complex **(19)** [Ru(*bipy-sil*)$_2$(NCS)$_2$] is similar to that observed in complex **(18)**. But the bands in **(19)** are better defined and contain a band in the UV-region ranging from 340-400nm (band (1)) with λ_{max} at 371nm and molar extinction coefficient of 20690 ± 485 L mol^{-1} cm^{-1}, and the second visible band range from 460-530nm (band (2)) with a λ_{max} at 500nm and molar extinction coefficient of 20750 ± 487 L mol^{-1} cm^{-1}.

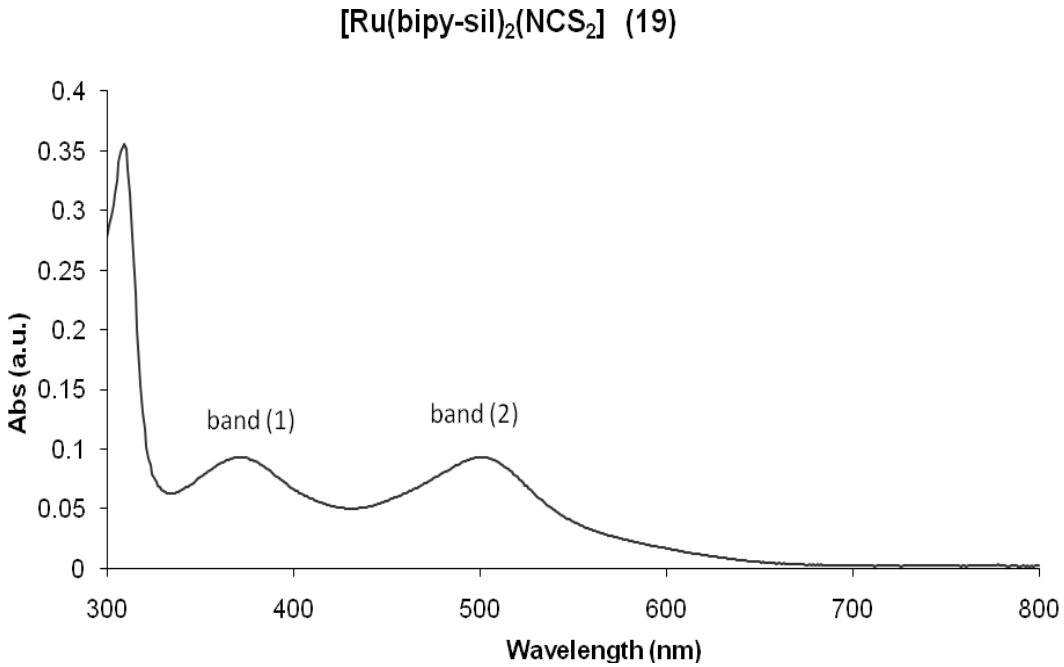

Figure 5-10 UV-Vis Spectrum of complex **(19)** (3mM, 300-800nm)

As expected, the *bis-bipy* ruthenium complexes absorbed more visible light than the *tris-bipy* ruthenium complexes, as indicated by the presence of two absorption bands and the higher ε values. The absorption bands have been assigned to metal-to-ligand charge transfer (MLCT) transitions, while the narrow intense bands at ~300nm observed in the UV region are attributed to ligand π-π* transitions. Complex **(16)** was slightly different, but does have a distinct shoulder, compared to the other three complexes in that only one band was observed, whereas in the others, two bands could be seen.

5.3.3. Solar Cells

All seven complexes were deposited successfully onto TiO_2 and/or WO_3 films supported on an FTO-glass (Fluorine doped Tin Oxide) wafer. This was achieved by immersing a TiO_2 or WO_3 annealed FTO-glass substrate into a 0.3mM solution of the dye species. The TiO_2 substrates were purchased from Dyesol, and were annealed at 450°C for one hour in a tube furnace before use. The WO_3 substrates were prepared by the School of Electrical and Computer Engineering at RMIT University, and annealed in a similar way to the TiO_2 substrates. Complexes **(13)**

[Ru(*bipy*)$_2$(*dcbipy*)](PF$_6$)$_2$, **(14)** [Ru(*bipy*)$_2$(*dpbipy*)](PF$_6$)$_2$, **(16)** [Ru(*dcbipy*)$_2$Cl$_2$] and **(17)** [Ru(*dcbipy*)$_2$(NCS)$_2$] were dissolved in acetonitrile or ethanol, and the substrate immersed in the solution for 24 hours. Complexes **(15)** [Ru(*bipy*)$_2$(*bipy-sil*)](PF$_6$)$_2$, **(18)** [Ru(*bipy-sil*)$_2$Cl$_2$] and **(19)** [Ru(*bipy-sil*)$_2$(NCS)$_2$] were dissolved in DMF and then heated gently at approximately 70°C for one hour, under subdued light, in a glass container fitted with a condenser. The coated-substrates were then washed with ethanol, to remove excess dye, and air dried.

A thin film of the dye solution coated the substrate, as evidenced by a colour change. Attempts to quantify the degree of binding of the dye to the coated substrates by FT-IR or Raman spectroscopy were not successful, as there were no observable differences in the spectra of the pure semiconductor layer and that of the dye deposited on the semiconductor, despite an obvious change in the colour of the substrate. This is most likely due to the very thin film of the dye i.e. too low a concentration of the dye to be detected. As a result, the most effective way to determine whether the dye had adhered to the semiconductor was by visual comparison. Photos of the DSSCs produced using complexes **(13)** to **(19)** are shown in Figure 5-11.

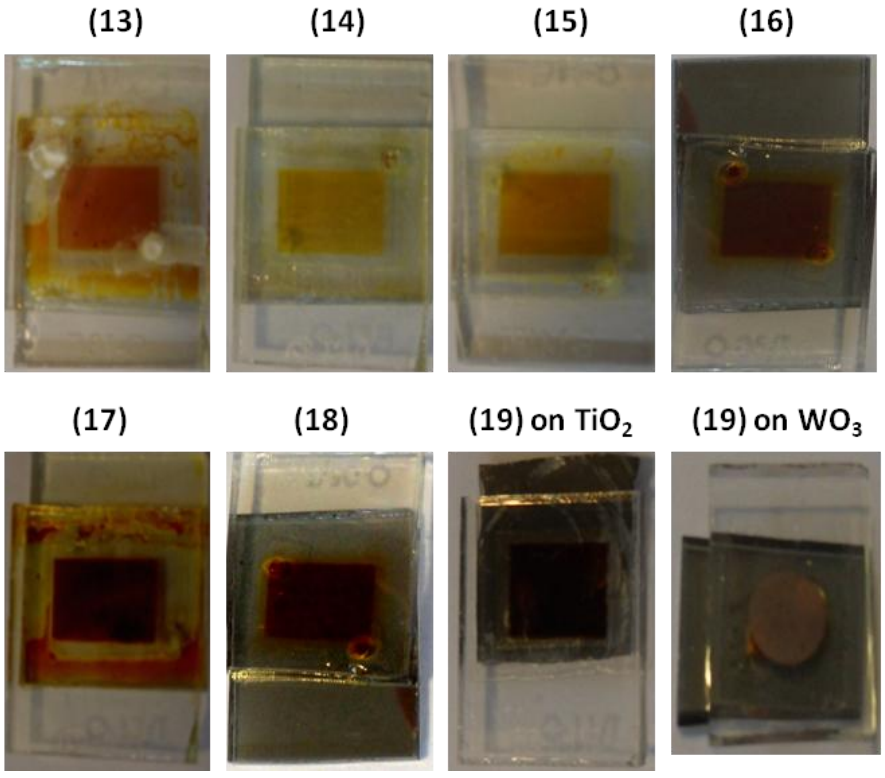

Figure 5-11 Photos of DSSCs produced using complexes **(13)** – **(19)**

The dye coated semiconductor was then assembled into a DSSC. This was done by first placing a heat-activated gasket, with a film thickness of 30µm around the dye-coated surface. The gasket has the centre removed so that it forms a border around the dye coated area, and is used to bind the two FTO-glass plates together. The second FTO-glass plate has two holes drilled into it; this allows the electrolyte to be injected. However, before the electrolyte is injected, the two FTO-glass plates with the gasket sandwiched between them, is heated to ~60°C, thus essentially gluing the plates together. The liquid electrolyte is then injected through the two holes, followed by the addition of a heat activated gasket, to seal the cell. A schematic of the DSSC is shown in Figure 5-12 and the solar cell preparation is illustrated in Figure 5-13. The same method was used to prepare all of the samples for testing in a DSSC.

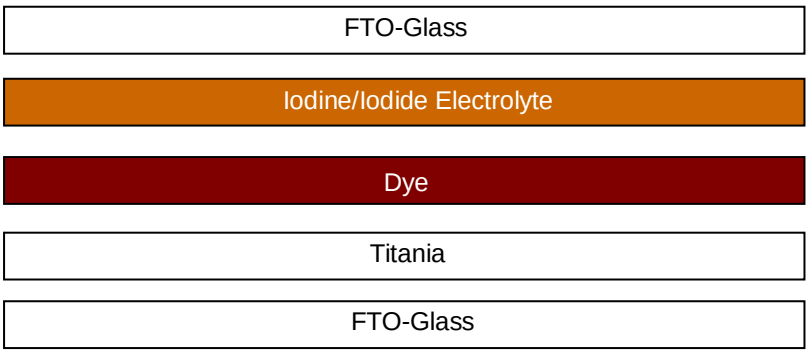

Figure 5-12 Schematic of a DSSC, showing the composition of the layers

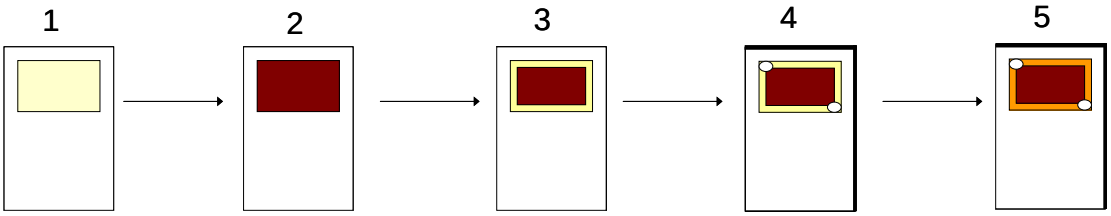

Figure 5-13 TiO_2 solar cell preparation – (1) Annealed TiO_2, (2) Dye coated TiO_2, (3) Dye coated TiO_2 with gasket, (4) Second FTO-glass plate added and (5) Liquid electrolyte (I_3^-/I^-) injected.

The performance of the DSSC's was tested at the School of Electrical and Computer Engineering, RMIT University, using a custom-made solar cell testing station, with a simulated solar light source. The incident-photon-to-electron conversion efficiency

(IPCE) was measured using a 1000W Xe lamp fitted with monochromators. The recorded current and voltage for each of the solar cells is listed in Table 5-2.

Table 5-2 Current, voltage and efficiency of prepared solar cells on TiO_2/FTO (complexes **(13) – (19)**) and WO_3/FTO (complex **(19)**).

Dye	Number	Current (μA)	Voltage (mV)	Fill factor (ff)[#]	Efficiency (%)[^]	Power μwatt*
[Ru(*bipy*)$_2$(*dcbipy*)](PF$_6$)$_2$	**(13)**	180	394	0.5	0.04	70.92
[Ru(*bipy*)$_2$(*dpbipy*)](PF$_6$)$_2$	**(14)**	2.2	80	0.5	0.0001	0.18
[Ru(*bipy*)$_2$(*bipy-sil*)](PF$_6$)$_2$	**(15)**	50	100	0.5	0.003	5.0
[Ru(*dcbipy*)$_2$Cl$_2$]	**(16)**	1000	590	0.5	0.3	590
[Ru(*dcbipy*)$_2$(NCS)$_2$] **N3**	**(17)**	1500	651	0.5	0.5	977
[Ru(*bipy-sil*)$_2$Cl$_2$]	**(18)**	100	350	0.5	0.02	35
[Ru(*bipy-sil*)$_2$(NCS)$_2$]	**(19) TiO_2**	400	410	0.5	0.09	164
[Ru(*bipy-sil*)$_2$(NCS)$_2$]	**(19) WO_3**	1000	140	0.5	0.07	140

[#] The fill factor was calculated using the following equation:[2]

Equation 5-1

$$ff = \frac{I\,mpp \times Vmpp}{Isc \times Voc}$$

$I\,mpp$ = Current measured at the power point (maximum), the power point is the maximum product obtained from the cell voltage and current

$V\,mpp$ = Voltage measured at the power point (maximum)

Isc = Short-circuit current

$V\,oc$ = Open-circuit voltage

[^] The efficiency was calculated using the 'Power conversion efficiency' equation (refer to Chapter 1- Equation 1-3)

* The power in μwatt units was calculated using the following equation:

Equation 5-2

$$Power_{(\mu watt)} = V_{(volt)} \times I_{(\mu amp)}$$

The voltage is the energy carried by the charge and in DSSCs this corresponds to the difference between the Fermi level (which is the energy of the electrons in a semiconductor under illumination), compared to the Nernst potential of the electrolyte redox couple.[2] The macroscopic voltage and current are the sum total of all the individual molecular photo-excitation events. It is found that the array generates a voltage which can be modelled as a series of cells linked in parallel. Hence, the numerical value of the voltage is determined by the characteristics of the dye/semiconductor combination, and its capacity (total Joule/Coulomb) by the number of such molecular units in the array.[2, 13-14, 34]

The current is directly linked to the efficiency of electron transfer between the semiconductor and the dye, and the reductive regeneration of the metal centre. The current can be modelled as a series sum of the number of electrons collected from each molecular event; it is this factor which is critical in the efficiency of photon-to-electrical conversion, and will be dependent on the extent of coating, the tightness of dye binding, and the facilitation of e^- transfer from the dye to the semiconductor. [2, 7, 13-14, 34]

The *tris-bipy* complexes **(13)** to **(15)** formed light yellow-orange layers on the semiconducting surface, the light colour of the dye on the surface implies that only a limited amount of dye has been adsorbed on the oxide. This in turn limits the amount of light which can be absorbed, and therefore a high current or voltage was not expected. The main purpose of investigating the *tris-bipy* ruthenium complexes was to compare them with the *bis-bipy* complexes and note any effects of the anchoring ligands.

Of this group, the anchoring ligand which gave the best current, voltage and overall efficiency was *dcbipy*, while *dpbipy* gave surprisingly low results. However, the molar extinction coefficient of complex **(14),** [Ru(*bipy*)(*dpbipy*)]$(PF_6)_2$, was the highest of the three *tris-bipy* complexes at 17603 L mol^{-1} cm^{-1}, indicating strong light absorption. The *bipy-sil* compound **(15)** gave about 25% of the current and voltage observed for the *dcbipy* complex **(13)**. The efficiency of this cell is therefore quite low; approximately one tenth (1/10) that of the *dcbipy* complex cell. This may be due to the *bipy-sil* ligand being incorporated into a *tris-bipy* ruthenium system, but may also be due to inefficient electron-transfer through the long saturated propyl chain of the linkers.

More promising results were observed for the *bis-bipy* systems. Complex **(16)** [Ru(*dcbipy*)$_2Cl_2$], formed a dark orange-red layer on the semiconductor surface. The voltage and current of the cell was good, with 1mA being recorded for the current and 590mV for the voltage. These results improved for the dithiocyanato analogue, **(17)** [Ru(*dcbipy*)$_2(NCS)_2$] (the commercial **N3** dye), which gave a dark orange-red layer on the semiconductor surface, and a measured current and voltage of 1.5 mA and 651 mV, respectively. It must be noted that these values are rather low, when compared to the current and voltage of that observed by a number of authors, with the commercial dye measured using similar systems (see Table 5-3).[19] There are however, slight variations in each of the reported systems: in the semiconductor surface, the electrolyte, the concentration of the dye, or the amount of time the cell was immersed in the dye solution. In the present work, the voltage recorded for **(17)** does not differ significantly from other systems; however the current is about 3-4 times lower. Therefore, the method of assembly may require perfecting to achieve currents observed in the literature.

Table 5-3 Comparison of voltage, current, fill factor and overall efficiency of complex **(17) N3** dye.[19]

V_{oc} (V)	I_{sc} (mA cm^{-2})	Fill factor	η_{cell} (%)	Power μwatt	Ref
0.651	1.5	0.5	0.5	975	This work
0.698	17.9	0.56	7.4	12530	[187]
0.662	14.5	0.55	6.8	9570	[23]
0.55	10.4	0.52	2.99	5720	[188]
0.70	15.0	0.74	7.8	1050	[189]
0.61	6.4	0.42	6.1	3904	[190]
0.640	5.0	0.76	10.4	3200	[113]
0.660	7.9	0.76	10.4	5214	[113]
0.670	11.5	0.74	10.3	7705	[113]
0.720	18.2	0.73	10.0	13104	[113]

Complex **(18)**, [Ru(*bipy-sil*)$_2$Cl$_2$], formed a dark red layer on the semiconductor surface, but despite the appearance, the current (100 µA) and voltage (350 mV) were quite low, and if the fill-factor is assumed to be 50%, then the overall efficiency of the dye is 0.02%, which is incredibly low when compared to values of 6-10% observed by other authors for **N3** (calculated using the power conversion efficiency equation, Equation 1-1, in the Introduction).

Complex **(19)**, [Ru(*bipy-sil*)$_2$(NCS)$_2$], gave a significant improvement in the current, voltage and overall efficiency when compared to **(18)**. Like **(18)**, **(19)** also formed a dark-red film over the TiO_2, but while the same silyl ligand is contained in both complex **(18)** and **(19)**, complex **(19)** also contains the thiocyanate anion which is known to improve efficiency and extend wavelength absorption. This was also apparent in the UV-visible spectrum of **(19)**, see Figure 5-10. The measured current and voltage were 400 µA and 410 mV respectively, once again the fill factor was assumed to be 50%, therefore the overall efficiency of the dye is calculated to be 0.09%. Thus, for **(19)**, the voltage has increased by 60 mV, and the current has quadrupled, so that the overall efficiency has increased four-fold compared to that of

(18). Therefore, by changing the counter-anion the efficiency of the cell can be improved considerably.

Amongst the solar energy community, there is also interest in using the intrinsic semiconductor, WO_3, as a substrate in DSSC's, as WO_3 can absorb light directly. When complex **(19)** was adsorbed onto a WO_3 semiconductor substrate, the current measured (1000μA) was significantly higher than that observed with the same complex adsorbed on TiO_2 (400μA), but, the voltage measurement was significantly lower at 140mV. The latter observation is attributed to a combination of low dye coverage, which may be due to poor adhesion of the dye to the substrate and the difference between the Fermi level of WO_3, when compared to the Nerst potential.

In summary, the measured current and voltage of the two new *bis*-ligand complexes **(18)** and **(19)** which contain silyl linkages, are both quite low, compared to that of *dcbipy* analogues **(16)** and **(17)**. However, significant improvements to the overall efficiency were achieved by replacing the chloride counter ion with thiocyanate, and further improvements may be achieved through the modification of the silyl linker. It is known that the presence of saturated bonds in the bridge between the anchoring group and the dye lowers the efficiency of electronic coupling between the dye and semiconductor substrate.[44] Thus, the non-conjugated propyl chain between the amide group and the silatrane in **(18)** and **(19)** is likely to reduce electron transfer significantly (Figure 5-14).

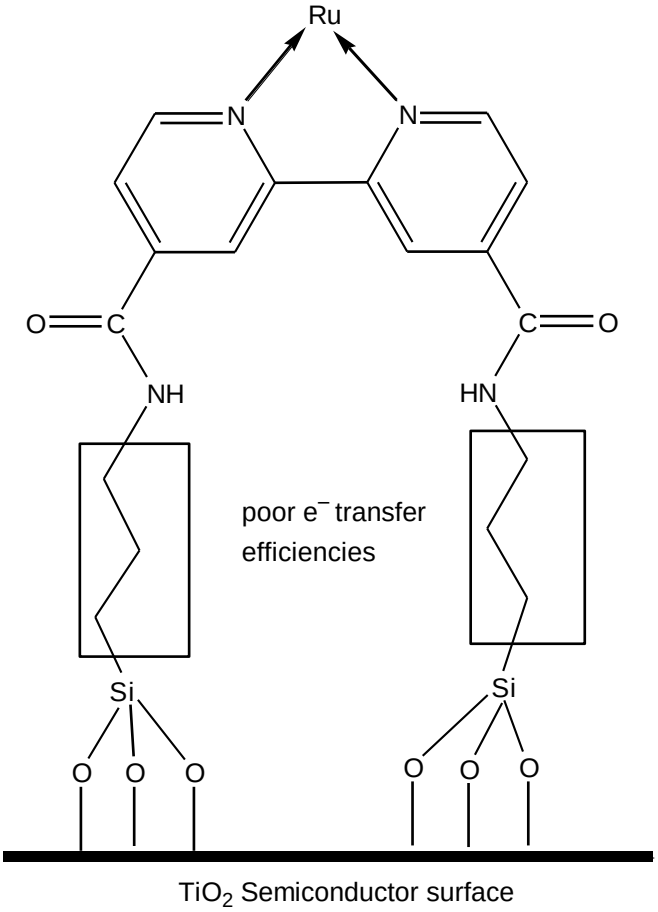

Figure 5-14 The long, non-conjugated propyl chain linker of *bipy-sil* to TiO_2

5.3.4. Synthesis of modified silyl linkers

In a system where electron transfer between the dye and the semiconductor surface is crucial, the connection/linker either needs to incorporate conjugation, e.g. replace the propyl chain with a phenyl group, or the distance between the dye and substrate needs to be considerably shorter e.g. by removal of the amide-propyl group (Figure 5-15). The former option was considered, but the cost of the starting material proved prohibitive, and thus was not considered a viable option. More favourable options were: (a) direct addition of a silatrane group to the bipyridine ligand, (b) alternative binding through an amide linkage, or (c) an ester linkage (using a carboxylate group), as indicated in Figure 5-15.

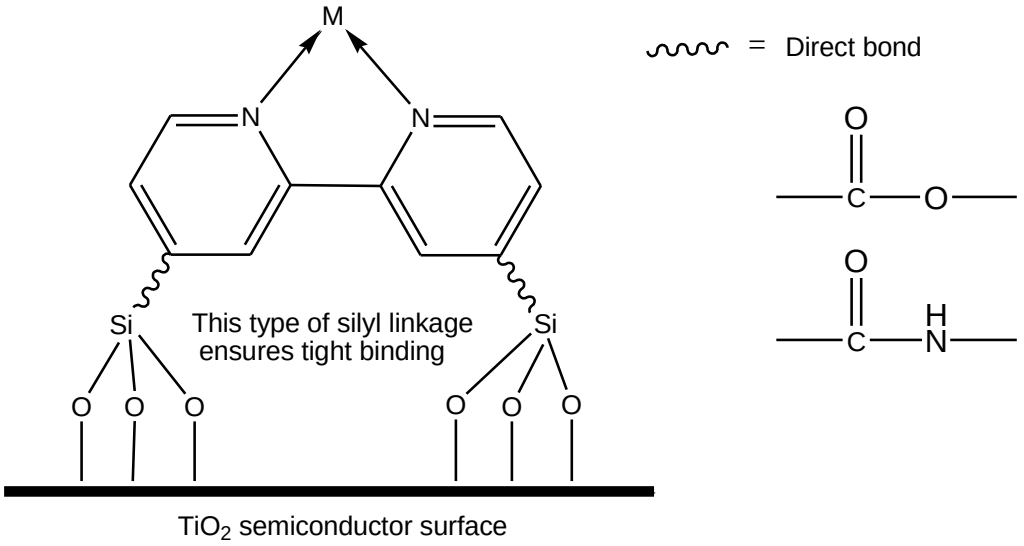

Figure 5-15 Short silyl linkage options

Ligands of this description were not available commercially, and therefore needed to be synthesised. The "direct linkage" (a) was investigated initially, by replacing 1-(3-aminopropyl) triethoxysilane with tetraethylorthosilicate (TEOS), to produce the target ligand 4,4'-disilatrane-2,2'-bipyridine. Three different organic schemes, using a silatrane form of TEOS were trialled, to determine whether the formation of a direct C–Si bond was possible in a bipyridine ligand. These methods included (i) the use of a Grignard reagent (ii) a Pd-catalysed reaction, and (iii) a Butyl-lithium route.

5.3.4.1. (a) Direct Linkage: (i) Grignard Reagent

The first method was based on the utilization of a Grignard reagent, which is an excellent leaving group. The predicted reaction sequence, using 4,4'-dibromo-2,2'-bipyridine (*bipy-Br_2*) as the starting material, is illustrated in Figure 5-16.

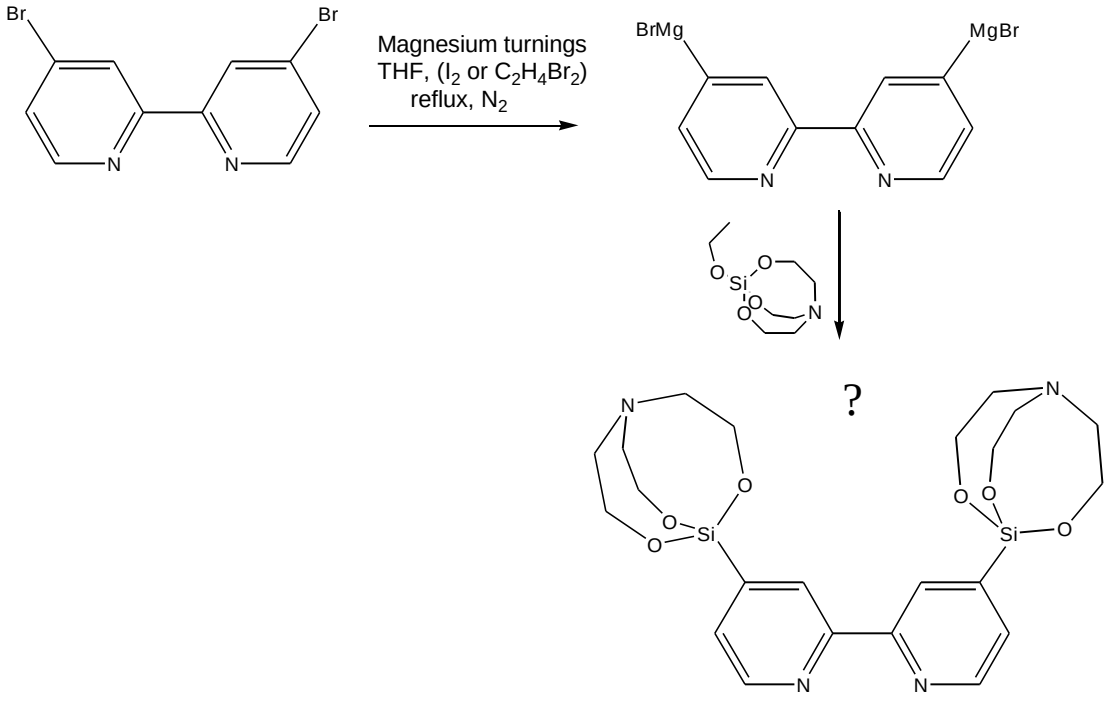

Figure 5-16 Grignard reaction sequence – Target ligand 4,4'-disilatrane-2,2'-bipyridine.

Two methods were investigated to activate the magnesium turnings, dibromoethane and iodide. The first method used dibromoethane with the magnesium turnings in a slight excess, but dibromoethane was found to be an ineffective activating agent for the bipyridine. A similar method, whereby 2-bromopyridine was reacted with magnesium powder and dibromoethane under sonication, has been reported in the literature,[191] and was also found to be unsuccessful, therefore this result was not surprising, and iodine, a more aggressive activator, was employed in further syntheses. Iodine appeared to be more effective in activating the magnesium as oxidation at the magnesium surface was observed. However, reaction of the subsequent 'Grignard reagent' with 1-ethoxysilatrane was ultimately unsuccessful, and NMR and mass spectroscopy confirmed that only the starting materials *bipy-Br*$_2$ and 1-ethoxysilatrane, were isolated.

It is possible that the Grignard reagent never formed. While Grignard reagents are able to form with phenyl rings quite readily, pyridine rings generally prove to be more troublesome. Nitrogen is more electronegative than carbon, and therefore the carbon π-orbitals may be more attracted to the nitrogen atom thus deforming the orbitals, and

consequently producing π-deficient pyridine rings.[180] In addition to this, the lone pair of electrons on the nitrogen are basic and not delocalised over the ring.

It must also be noted that it is difficult to ascertain whether a Grignard reagent has been formed successfully, as isolation of the reagent is often not possible owing to its instability, and thus immediate use is preferential.

Subsequently, a Pd-catalysed reaction was investigated as an alternative.

5.3.4.2. (a) Direct Linkage: (ii) Palladium Catalysed

The second route employed a Palladium-catalyst, $Pd(PPh_3)_4$. See Figure 5-17 for the predicted reaction sequence. The use of Pd-catalysts in organic synthesis has been studied extensively, in particular for the formation of C–C bonds. Indeed, in this thesis a Pd-catalyst was used successfully to form a C–P bond, in the synthesis of 4,4-diphosphonic acid-2,2'-biypridine, (see Sections 2.2.2.9 and 2.2.5.3).[12] However, the use of a Pd-catalyst with *bipy* may lead to deactivation of the Pd-catalyst as *bipy* can compete with the triphenylphosphine ligand for coordination to the metal centre. To limit this from occurring, a large excess of triphenylphosphine was added to the reaction mixture.[192-193]

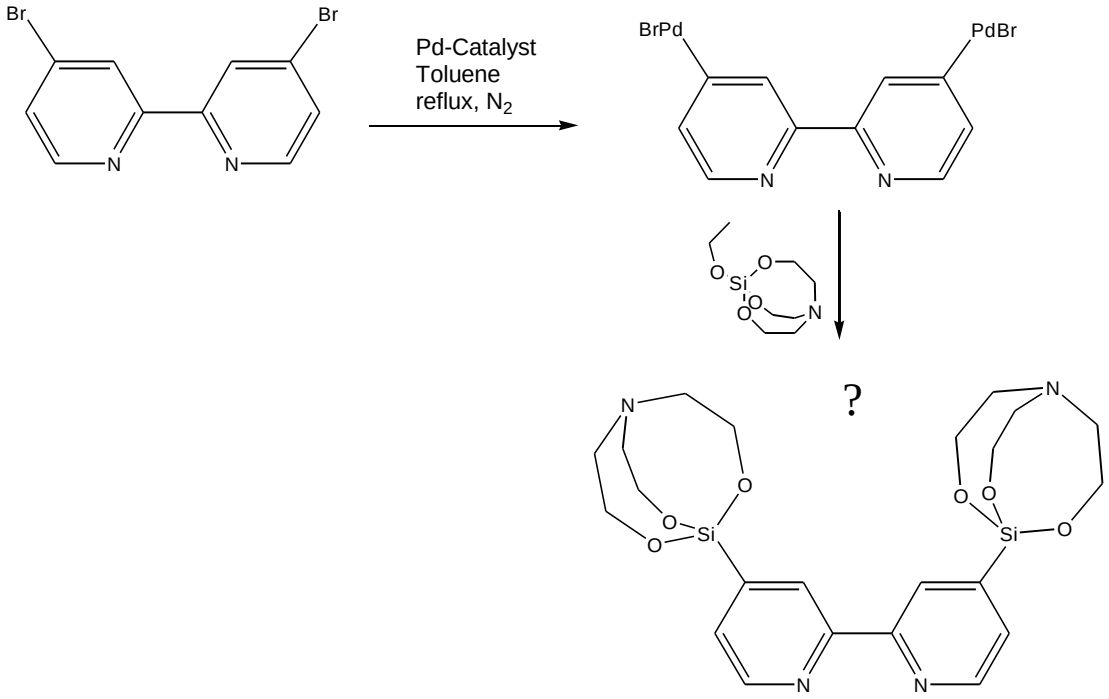

Figure 5-17 Pd- reaction sequence – Target ligand 4,4'-disilatrane-2,2'-bipyridine.

The initial oxidative-addition of the Pd-catalyst is analogous to the formation of the Grignard reagent, where the carbon-halogen covalent bond is cleaved to form a new complex. The product was purified by distillation. The NMR data however indicated that only the bipyridine starting material was isolated.

5.3.4.3. (a) Direct Linkage: (iii) Butyl-Lithium

The third synthetic method involved the use of butyl-lithium, which out of all the methods attempted in forming a direct silicon-carbon bond, was the most successful. Riedmiller *et al.* have reported the successful reaction of *n*-butyllithium and tetraethoxysilane at -78°C under N_2 to form 3-triethoxysilylpyridine.[102] In general, this method was found to be successful for the formation of *ortho*- and *meta*-substituted bromo-pyridine systems, but *para*-substituted bromo-pyridine systems were not investigated. The Riedmiller *et al.* [102] method was adapted here using 4,4'-dibromo-2,2'-bipyridine and 1-ethoxysilatrane instead of 3-bromopyridine and tetraethoxysilane.

NMR data of the product indicated that peaks corresponding to the silatrane group and aromatic groups were present, although not in the expected ratios. The compound decomposed quite rapidly, hence further analysis could not be undertaken, and for this reason was not chosen as a viable option, as the compound was not stable under atmospheric conditions.

In summary, the formation of a direct Si–C bond from a Br–C bond in a *para*-substituted bromo pyridine ring was not found to be possible by any of the three organic routes, using TEOS. This may be due to the nitrogen inhibiting the formation of a direct bond, the insufficient reactivity of the ethoxy group to enable this formation, and/or the bulky nature of TEOS. Therefore, synthetic methods which incorporate a more reactive and a less-bulky group were investigated.

5.3.4.4. (a) Direct Linkage: (iv) TMS-Cl and 1-chlorosilatrane

The reaction of TMS-Cl with 4,4'-dibromo-2,2'-bipyridine successfully produced 4,4'-di(trimethylsilyl)-2,2'-bipyridine (confirmed by ^{1}H NMR, see Section 2.2.2.7), forming a direct-silicon bond. Unfortunately, the material was found to be extremely unstable and decomposed quickly in the presence of air. Attempts to react *bipy-Br*$_2$ with 1-chlorosilatrane were unsuccessful.

5.3.4.5. (b) Amide Linkage: (i) TMS-Cl and 1-chlorosilatrane

To determine whether a silicon-amide bond (Si–NH–C(O)) or a direct silicon bond (Si–C) to the pyridine ring would be possible, reaction of trimethylsilyl chloride (TMS-Cl) with an amide-pyridine or bromo-pyridine, followed by reaction with 1-chlorosilatrane (a more reactive group than ethoxy), was investigated.

N-(trimethylsilyl)pyridine-3-carboxamide has been prepared previously by Gilg *et al.* [104-105] The reaction of TMS-Cl with the model compound, nicotinamide in boiling hexamethyldisilizane was successful, forming an amide-silicon bond (confirmed by ^{1}H NMR, see Section 2.2.2.5). However, reaction of nicotinamide with 1-chlorosilatrane proved to be more difficult, with no reaction taking place.

A possible reason for this lack of reaction may be due to the bulkier nature of the silatrane group when compared to that of trimethylsilyl. There is also the possibility that the hexamethyldisilizane may compete with the chlorosilatrane for bonding to the ring, as it is may be possible that both hexamethyldisilizane and TMS-Cl contribute to the formation of an amide-silicon bond. Synthetic methods which did not incorporate hexamethyldisilizane were therefore investigated, but unfortunately, they were also unsuccessful.

5.3.4.6. (c) Ester Linkage: (i) Carboxy-sil

As methods (a) and (b) were unsuccessful, a carboxy-sil bond (Si–O–C(O)) was considered. This type of bonding has been observed previously with ferrocenyl carboxylic acid and 1-ethoxysilatrane,[194] where, a carboxylic acid and a silatrane were reacted together in an azeotropic solvent to form 1-ferrocenecarboxysilatrane. This method was successful for Chen and co-workers, [194] with isolation of 1-ferrocenecarboxysilatrane in good yields and crystals of suitable quality for single-crystal XRD analysis. Ferrocene is able to undergo similar reactions to those observed with aromatic compounds.

Owing to the success of Chen *et al.* [194] a similar method using the reaction scheme illustrated in Figure 5-18 was explored. However, as observed with the other routes, a mixture of starting materials was isolated. The NMR spectrum indicated the presence of aromatic and methylene protons, however mass spectroscopy suggested that no new oxygen-silicon bond had formed. This result is not surprising, as this bond is known to be quite unstable, decomposing rapidly.[195] This point is further emphasized by the limited amount of research in this field.[196]

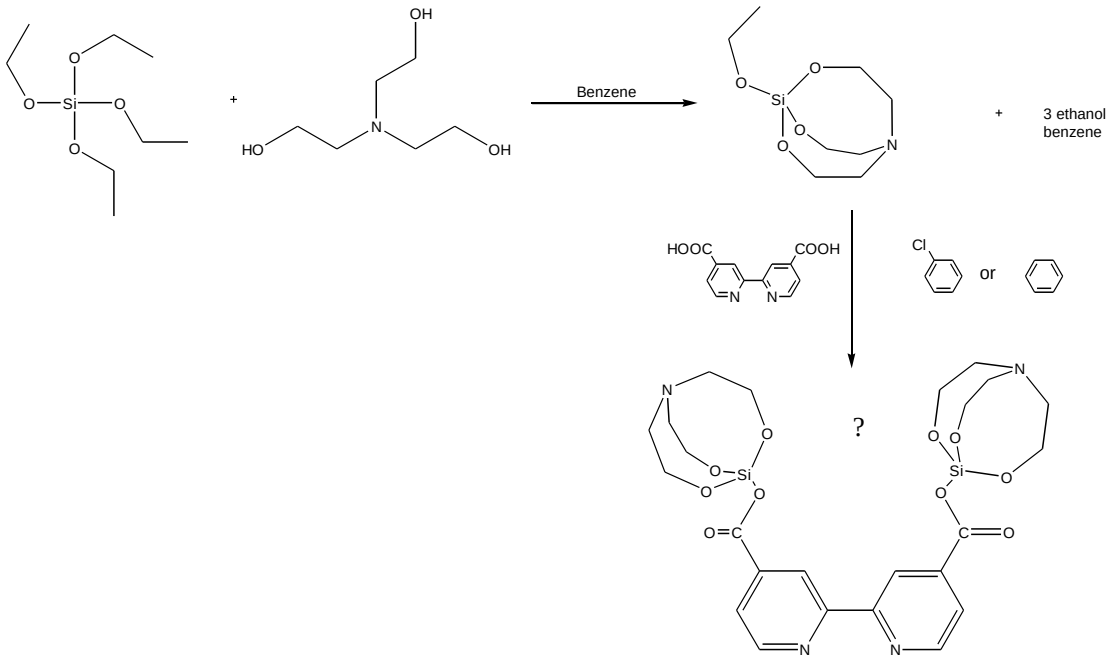

Figure 5-18 Carboxy-sil reaction sequence – target ligand 4,4'-dicarboxysilatrane-2,2'-bipyridine.[194]

5.4. Conclusion

A series of ruthenium(II) complexes with bipyridine-type coordination were synthesised and incorporated into DSSCs and their respective current and voltage characteristics measured. Three of these were *tris-bipy* complexes containing carboxylate, phosphonate or silyl linkers, complexes **(13)** [Ru(*bipy*)$_2$(*dcbipy*)](PF$_6$)$_2$, **(14)** [Ru(*bipy*)$_2$(*dpbipy*)](PF$_6$)$_2$ and **(15)** [Ru(*bipy*)$_2$(*bipy-sil*)](PF$_6$)$_2$. The remaining four were *bis-bipy* based complexes with *cis*-dichloro or *cis*-dithiocyanato ligands. Two of the bis-bipy based complexes were new complexes that contained silyl linkers, complexes **(18)** [Ru(*bipy-sil*)$_2$Cl$_2$] and **(19)** [Ru(*bipy-sil*)$_2$(NCS)$_2$], the other two contained carboxylate linkers, complexes **(16)** [Ru(*dcbipy*)$_2$Cl$_2$] and **(17)** [Ru(*dcbipy*)$_2$(NCS)$_2$]. All of the complexes were characterised using FT-IR and/or NMR spectroscopic techniques, as well as UV-visible spectroscopy.

All seven complexes were found to have the desired properties for solar energy capture and therefore were incorporated into solar cells, all with a TiO_2 semiconducting substrate, and one complex, **(19)**, also with a WO_3 semiconducting

surface. The current observed with the WO_3 surface was significantly higher than with the TiO_2 surface, however the voltage was lower.

The performance and efficiency of all of the dyes, established by measurement of the current and voltage of their respective DSSC's, were calculated and compared to one another. The commercial carboxylate linker, *dcbipy*, was found to outperform the phosphonate linker, *dpbipy*, and the silyl linker, *bipy-sil*, with both the *tris-bipy* and the *bis-bipy* based complexes. The commercial **N3** dye, complex **(17)** [Ru(*dcbipy*)$_2$(NCS)$_2$], performed significantly better than any of the new dyes prepared in this work. However, the silyl linker proved to be more efficient than the phosphonate linker in the *tris-bipy* based complexes.

One of the reasons for such a large difference in efficiency is that the *bipy-sil* ligand contained a non-conjugated propyl chain which does not provide effective electron transfer, hence leading to a reduction in the current. Therefore, alternative shorter linkers were investigated. As the appropriate *bipy-sil* ligands were not available commercially, attempts were made to synthesise these ligands. Unfortunately, in this work, despite significant effort, the bipyridyl compounds with a direct Si–C bond, amide Si–NH–C(O) link, or ester Si–O–C(O) bond to silatrane, could not be obtained or were insufficiently stable under ambient conditions to allow their incorporation into Ru(II) complexes, and subsequent DSSC fabrication. It is however, believed that the silyl linkage will be an important component of more robust dyes used to sensitize metal oxide surfaces (TiO_2, WO_3, SnO_2, etc) and it is therefore recommended that further studies be pursued in this challenging synthetic area.

CHAPTER 6

Further Conclusions and Recommendations for Future Work

The work described in this thesis concerned the synthesis of materials with light harvesting properties, which could be used for specific applications in particular dye sensitizing solar cell technology. The work involved exploring existing dye materials, mainly ruthenium coordination complexes, and also investigated some copper compounds.

As copper had not been explored to the same extent as ruthenium in light harvesting complexes, stable copper(I) compounds with bipyridine-type coordination were investigated initially.

Chapter Three described copper *Ophen* complexes, which were synthesised hydrothermally. Three complexes were isolated and characterised through single crystal XRD, the desired Cu(I) dimer, $[Cu_2(Ophen)_2]$, and two complexes which were possible intermediate products in the formation of 'covalent hydrates'.[161] The Cu(I) dimer $[Cu_2(Ophen)_2]$ exhibited a broad absorption peak in the visible region, although its luminescence behaviour was quenched in solution. However, whilst the Cu(I) dimer did possess some of the desirable properties for solar energy capture, the unpredictable nature of the hydrothermal preparation could not guarantee that Cu(I) species were isolated exclusively.

Nevertheless, copper(I) complexes provide an economical and environmentally-friendly alternative to ruthenium (II) complexes in DSSC, and therefore it is recommended that copper(I) complexes be explored more extensively. In particular, copper(I) complexes which are stable, soluble in a range of solvents, and contain ligands with anchoring potential should be prepared. For example, a more concerted effort could be undertaken to prepare *Ophen* homologues containing solubilising functionalities, such as sulphonate ($-SO_3H$). In addition, further work with phosphane ligand complexes should be undertaken to improve visible light absorption and solubility.

Chapter Four also focused on copper complexes. In this section nine complexes were isolated and characterised through single crystal XRD, three of which were copper(I) *dpk* complexes, all of which exhibited strong absorbance across the entire electromagnetic spectrum. The fact that these Cu(I) *dpk* complexes were air stable makes them a desirable target, even though they were poorly soluble. As an extension of this work, modification of the *dpk* ligand should be explored to improve its solubility and adsorption properties.

The remaining six complexes contained copper in the +2 oxidation state: one incorporating the novel *dpk*.acetone ligand, which formed through a novel transition metal-promoted mixed aldol condensation reaction between *acetone* and *dpk*;[197] and three containing picolinate which arose from cleavage of an ArC–CO bond in *dpk* as a result of a Baeyer-Villiger type reaction, which has not been observed previously. [198]

Chapter Five concentrated on ruthenium(II) complexes with bipyridine-type ligands. In this section seven complexes were prepared, isolated and characterised through FT-IR and NMR. All of the complexes were incorporated into solar cells and their current, voltage and efficiencies determined. Three types of surface linkers were investigated (carboxylate, phosphonate and silane) with the most efficient complexes being those which contained carboxyl linkers.

Two new ruthenium complexes containing a silyl linker were examined, but only showed low efficiencies possibly due to the saturated propyl chain with this link. However, despite the limited success with silyl linkages in this work, it is still

believed that there is considerable potential for silyl linkers in DSSC's and therefore it is recommended that synthetic methods to incorporate this linker into appropriate ligands be explored further. Of the synthetic methods outlined in Chapter 5, the formation of C–Si and N–Si bonds was successful using TMS-Cl, but owing to the considerable reactivity difference between methyl and ethoxy groups, these methods could not be extended to synthesise the target compounds containing ethoxy linkers. Therefore, one possible synthetic route may be to form a stable C–Si or N–Si bond initially, and then introduce the ethoxy groups followed by the silatrane.

As a final note, the alternative semiconducting metal oxide, WO_3, which gave a large photo-current, has substantial scope for improvement, and slight modifications to the oxide surface should be investigated to improve dye binding. Also, further investigation into the physical conditions, such as temperature and immersion-time, for binding of the silyl linkers to WO_3, could be carried out.

Reference List

[1] S. Campagna, F. Puntoriero, F. Natasi, G. Bergamini, V. Balzani, *Top. Curr. Chem* **2007**, *280*, 117-214.

[2] M. K. Nazeeruddin, M. Grätzel, in *Comprehensive Coordination Chemistry II, Vol. 9* (Eds.: J. A. McCleverty, T. J. Meyer), Elsevier Pergamon, **2004**.

[3] N. Alonso-Vante, J.-F. Nierengarten, J.-P. Sauvage, *J. Chem. Soc., Dalton Trans.* **1994**, 1649-1654.

[4] E. Bae, W. Choi, *J. Phys. Chem. B* **2006**, *110*, 14792-14799.

[5] M. Grätzel, *Prog. Photovolt. Res. Appl.* **2000**, *8*, 171-185.

[6] M. Grätzel, *Nature* **2001**, *414*, 338-344.

[7] M. Grätzel, *J. Photochem. Photobiol., A* **2004**, *164*, 3-14.

[8] A. Hagfeldtt, M. Grätzel, *Chem. Rev.* **1995**, *95*, 49-68.

[9] A. F. Haught, *J. Sol. Ener. Engin* **1984**, *106*, 3-15.

[10] P. M. Jayaweera, S. S. Palayangoda, K. Tennakone, *J. Photochem. Photobiol., A* **2001**, *140*, 173-177.

[11] K. Kalyanasundaram, *Coord. Chem. Rev.* **1982**, *46*, 159-244.

[12] K. Kanaizuka, S. Kato, H. Moriyama, C. Pac, *Res. Chem. Intermed,* **2007**, *33*, 91-100.

[13] F.-T. Kong, S.-Y. Dai, K.-J. Wang, *Advances in Optoelectronics* **2007**, *75384*, 1-13.

[14] F. O. Lenzmann, J. M. Kroon, *Advances in Optoelectronics* **2007**, *65073*, 1-10.

[15] G. J. Meyer, *Inorg. Chem.* **2005**, *44*, 6852-6864.

[16] M. K. Nazeeruddin, P. Pechy, M. Grätzel, *Chem. Commun.* **1997**, 1705-1706.

[17] M. K. Nazeeruddin, S. M. Zakeeruddin, R. Humphry-Baker, M. Jirousek, P. Liska, N. Vlachopoulos, V. Shklover, C.-H. Fischer, M. Grätzel, *Inorg. Chem.* **1999**, *38*, 6298-6305.

[18] B. O'Regan, M. Grätzel, *Nature* **1991**, *353*, 737-740.

[19] A. S. Polo, M. K. Itokazu, N. Y. m. Iha, *Coord. Chem. Rev.* **2004**, *248*, 1343-1361.

[20] A. H. Redondo, E. C. Constable, C. E. Housecroft, *Chimia* **2008**, *63*, 205-207.

[21] T. Renouard, R.-A. Fallahpour, M. K. Nazeeruddin, R. Humphry-Baker, S. I. Gorelsky, A. B. P. Lever, M. Grätzel, *Inorg. Chem.* **2002**, *41*, 367-378.

[22] N. Robertson, *ChemSusChem* **2008**, *1*, 977-979.

[23] Z.-S. Wang, C.-H. Huang, Y.-Y. Huang, B.-W. Zhang, P.-H. Xie, Y.-J. Hou, K. Ibrahim, H.-J. Qian, F.-Q. Liu, *Sol. Energy Mater. Sol. Cells* **2002**, *71*, 261-271.

[24] P. Balraju, M. Kumar, M. S. Roy, G. D. Sharma, *Synthetic Met.* **2009**, *159*, 1325-1331.

[25] T. C. Stamatatos, C. G. Efthymiou, C. C. Stoumpos, S. P. Perlepes, *Eur. J. Inorg. Chem.* **2009**, 3361-3391.

[26] J.-H. Yu, Z.-L. Lu, J.-Q. Xu, H.-Y. Bie, J. Lu, X. Zhang, *New. J. Chem.* **2004**, *28*, 940-945.

[27] N. Armaroli, G. Accorsi, F. Cardinali, A. Listorti, *Top. Curr. Chem* **2007**, *280*, 69-115.

[28] K. Kalyanasundaram, M. Grätzel, *Coord. Chem. Rev.* **1998**, *77*, 347-414.

[29] M. G. Barandika, Z. Serna, M. K. Urtiaga, J. I. R. de Larramendi, M. I. Arriortua, R. Cortés, *Polyhedron* **1999**, *18*, 1311-1316.

[30] B. Graham, M. T. W. Hearn, P. C. Junk, C. M. Kepert, F. E. Mabbs, B. Mourbaraki, K. S. Murray, L. Spiccia, *Inorg. Chem.* **2001**, *40*, 1536-1543.

[31] M. Fondo, N. Ocampo, A. M. Garcia-Deibe, M. Corbella, M. R. Bermejo, J. Sanmartin, *Dalton Trans.* **2005**, 3785-3784.

[32] S. S. Tandon, L. K. Thompson, M. E. Manuel, J. N. Bridson, *Inorg. Chem.* **1994**, *33*, 5555-5570.

[33] K. Latham, K. F. White, K. B. Szpakolski, C. J. Rix, J. M. White, *Inorg. Chim. Acta* **2009**, *362*, 1872-1886.

[34] Q. Wang, S. Ito, M. Grätzel, F. Fabregat-Santiago, I. Mora-Ser, J. Bisquert, T. Bessho, H. Imai, *J. Phys. Chem. B* **2006**, *110*, 25210-25221.

[35] M. Grätzel, *J. Photochem. Photobiol., C* **2003**, *4*, 145-153.

[36] W. E. Ford, M. A. J. Rodgers, *J. Phys. Chem.* **1994**, *98*, 3822-3831.

[37] M. Fujihira, N. Ohishi, T. Osa, *Nature* **1977**, *268*, 226-228.

[38] S. Ardo, G. J. Meyer, *Chem. Soc. Rev.* **2009**, *38*, 115-164.

[39] A. Juris, V. Balzani, F. Barigelletti, S. Campagna, P. Belser, A. v. Zelewsky, *Coord. Chem. Rev.* **1988**, *84*, 85-277.

[40] N. Armaroli, *Chem. Soc. Rev.* **2001**, *30*, 113-124.

[41] F. A. Cotton, G. Wilkson, C. A. Murillo, M. Bochmann, *Advanced Inorganic Chemistry*, 6th ed., John Wiley & Sons Inc., Toronto, **1999**.

[42] V. Balzani, G. Bergamini, S. Campagna, F. Puntoriero, *Top. Curr. Chem* **2007**, *280*, 1-36.

[43] R. Argazzi, C. A. Bignozzi, T. A. Heimer, F. N. Castellano, G. J. Meyer, *Inorg. Chem.* **1994**, *33*, 5741-5749.

[44] E. Galoppini, *Coord. Chem. Rev.* **2004**, *248*, 1283-1297.

[45] P. Wang, C. Klein, J.-E. Moser, R. Humphry-Baker, N.-L. Cevey-Ha, R. Charvet, Pascal Comte, S. M. Zakeeruddin, M. Grätzel, *J. Phys. Chem. B* **2004**, *108*, 17553-17559.

[46] K. Kilså, E. I. Mayo, B. S. Brunschwig, H. B. Gray, N. S. Lewis, J. R. Winkler, *J. Phys. Chem. B* **2004**, *108*, 15640-15651.

[47] A. K. M. Fung, B. K. W. Chiu, M. H. W. Lam, *Water Research* **2003**, *37*, 1939-1947.

[48] B. J. Brennan, A. E. Keirstead, P. A. Liddell, S. A. Vail, T. A. Moore, A. L. Moore, *Nanotechnology* **2009**, *20*, 505203.

[49] P. Atkins, J. d. Paula, *Physical Chemistry*, 7th ed., Oxford University Press, New York, **2002**.

[50] R. A. Marcus, *J. Chem. Phys.* **1965**, *43*, 679-701.

[51] Z.-S. Wang, H. Kawauchi, T. Kashima, H. Arakawa, *Coord. Chem. Rev.* **2004**, *248*, 1381-1889.

[52] E. C. Constable, *Metal and Ligand Reactivity - An Introduction to the Organic Chemistry of Metal Complexes*, Wiley-VCH, Weinheim, **1996**.

[53] P. Liska, N. Vlachopoulos, M. K. Nazeeruddin, P. Comte, M. Grätzel, *J. Am. Chem. Soc.* **1988**, *110*, 3686-3687.

[54] M. K. Nazeeruddin, P. Pechy, T. Renouard, S. M. Zakeeruddin, R. Humphry-Baker, P. Comte, P. Liska, L. Cevey, E. Costa, V. Shklover, L. Spiccia, G. B. Deacon, C. A. Bignozzi, M. Grätzel, *J. Am. Chem. Soc.* **2001**, *123*, 1613-1624.

[55] T. Bessho, E. Yoneda, J.-H. Yum, M. Guglielmi, I. Tavernelli, H. Imai, U. Rothlisberger, M. K. Nazeeruddin, M. Grätzel, *J. Am. Chem. Soc.* **2009**, *131*, 5930-5934.

[56] B. J. Walter, C. M. Elliott, *Inorg. Chem.* **2001**, *40*, 5924-5927.

[57] P. A. Anderson, G. F. Strouse, J. A. Treadway, F. R. Keene, T. J. Meyer, *Inorg. Chem.* **1994**, *33*, 3863-3864.

[58] D. Kumaresan, K. Shankar, S. Vaidya, R. H. Schmehl, *Top. Curr. Chem* **2007**, *281*, 101-142.

[59] K. Szaciłowski, W. Macyk, G. Stochel, Z. Stasicka, S. Sostero, O. Traverso, *Coord. Chem. Rev.* **2000**, *208*, 277-297.

[60] C. Creutz, M. Chou, T. L. Netzel, M. Okumura, N. Sutin, *J. Am. Chem. Soc.* **1980**, *102*, 1309-1319.

[61] J. E. Fergusson, G. M. Harris, *J. Chem. Soc.* **1966**, 1293-1296.

[62] J. N. Demas, B. A. DeGraff, *Anal. Chem.* **1991**, *63*, 829-837.

[63] M. Alebbi, C. A. Bignozzi, T. A. Heimer, G. M. Hasselmann, G. J. Meyer, *J. Phys. Chem. B* **1998**, *102*, 7577-7581.

[64] Chemicool Periodic Table. 29/06/2011 <http://www.chemicool.com/>.

[65] T. Bessho, E. C. Constable, M. Grätzel, A. H. Redondo, C. E. Housecroft, W. Kylberg, M. K. Nazeeruddin, M. Neuburgerb, S. Schaffner, *Chem. Commun.* **2008**, 3717-3719.

[66] S. Sakiki, T. Kuriki, T. Hamada, *J. Chem. Soc., Dalton Trans.* **2002**, 840-842.

[67] D. V. Scaltrito, D. W. Thompson, J. A. O'Callaghan, G. J. Meyer, *Coord. Chem. Rev.* **2000**, *208*, 243-266.

[68] A. Barbieri, G. Accorsi, N. Armaroli, *Chem. Commun.* **2008**, 2185-2193.

[69] M. Ruthkosky, C. A. Kelly, F. N. Castellano, G. J. Meyer, *Coord. Chem. Rev.* **1998**, *171*, 309-322.

[70] D. R. McMillin, M. T. Buckner, B. T. Ahn, *Inorg. Chem.* **1977**, *16*, 943-945.

[71] D. R. McMillin, *Chem. Rev.* **1998**, *98*, 1201-1219.

[72] M. W. Blaskie, D. R. McMillin, *Inorg. Chem.* **1980**, *19*, 3519-3522.

[73] W.-F. Fu, X. Gan, J. Jiao, Y. Chen, M. Yuan, S.-M. Chi, M.-M. Yu, S.-X. Xiong, *Inorg. Chim. Acta* **2007**, *360*, 2758-2766.

[74] M. T. Miller, P. K. Gantzel, T. B. Karpishin, *J. Am. Chem. Soc.* **1999**, *121*, 4292-4293.

[75] M. K. Eggleston, D. R. McMillin, K. S. Koenig, A. J. Pallenberg, *Inorg. Chem.* **1997**, *36*, 172-176.

[76] R. A. Rader, D. R. McMillin, M. T. Buckner, T. G. Matthews, D. J. Casadonte, R. K. Lengel, S. B. Whittaker, L. M. Darmon, F. E. Lytke, *J. Am. Chem. Soc.* **1981**, *103*, 5906-5912.

[77] A. J. M. Miller, J. L. Dempsey, J. C. Peters, *Inorg. Chem.* **2007**, *46*, 7244-7246.

[78] K. Saito, T. Arai, N. Takahashi, T. Tsukuda, T. Tsubomura, *Dalton Trans.* **2006**, 4444-4448.

[79] Y. Chen, J.-S. Chen, X. Gan, W.-F. Fu, *Inorg. Chim. Acta* **2009**, *362*, 2492-2498.

[80] A. E. Mauro, C. C. Porta, S. R. Ananias, V. Sargentelli, R. H. D. A. Santos, M. T. Do, P. Gambardella, *J. Coord. Chem* **1999**, *49*, 9-15.

[81] X. Gan, W.-F. Fu, Y.-Y. Lin, M. Yuan, S.-M. Che, S.-M. Chi, H.-F. J. Li, J.-H. Chen, Z.-Y. Zhou, *Polyhedron* **2008**, *27*, 2202-2208.

[82] Z. Mao, H.-Y. Chao, Z. Hui, C.-M. Che, W.-F. Fu, K.-K. Cheung, N. Zhu, *Chem. Eur. J.* **2003**, *9*, 2885-2897.

[83] V. W.-W. Yam, K. K.-W. Lo, *Chem. Soc. Rev.* **1999**, *28*, 323-334.

[84] S. Z. Vatsadze, A. V. Dolganov, A. V. Yakimanskii, M. Y. Goikhman, I. V. Podeshvo, K. A. Lyssenko, A. L. Maksimov, T. V. Magdesievaa, *Russ. Chem. Bull. Int. Ed.* **2010**, *59*, 724-732.

[85] H.-K. Fun, S. Shanmuga Sundara Raj, R.-G. Xiong, J.-L. Zuo, Z. Yu, X.-L. Zhu, X.-Z. You, *J. Chem. Soc., Dalton Trans.* **1999**, 1711-1712.

[86] M. Henary, J. L. Wootton, S. I. Khan, J. I. Zink, *Inorg. Chem.* **1997**, *36*, 796-801.

[87] P. C. Ford, E. Cariata, J. Bourassa, *Chem. Rev.* **1999**, *99*, 3625-3647.

[88] E. C. Constable, A. H. Redondo, C. E. Housecroft, M. Neuburgerb, S. Schaffner, *Dalton Trans.* **2009**, 6634-6644.

[89] C. L. Linfoot, P. Richardson, T. E. Hewat, O. Moudam, M. M. Forde, A. Collins, F. White, N. Robertson, *Dalton Trans.* **2010**, 8945-8946.

[90] T. Kern, U. Monkowius, M. Zabel, G. Knör, *Eur. J. Inorg. Chem.* **2010**, 4148-4156.

[91] B. Bozic-Weber, E. C. Constable, C. E. Housecroft, M. Neuburgerb, J. R. Price, *Dalton Trans.* **2010**,*39*, 3585-3594.

[92] C. A. Bignozzi, R. Argazzi, C. J. Kleverlaan, *Chem. Soc. Rev.* **2000**, *29*, 87-96.

[93] J. B. Asbury, E. Hao, Y. Wang, H. N. Ghosh, T. Lian, *J. Phys. Chem. B* **2001**, *105*, 4545-4557.

[94] T. Osa, M. Fujihira, *Nature* **1976**, *25*, 349-350.

[95] R. W. Fessenden, P. V. Kamat, *J. Phys. Chem.* **1995**, *99*, 12902-12906.

[96] R. Memming, *Prog. Surf. Sci.* **1984**, *17*, 7-74.

[97] T. Gerfin, M. Grätzel, L. Walder, *Prog. Inorg. Chem.* **1997**, *44*, 345-393.

[98] H. Zheng, Y. Tachibana, K. Kalantar-zadeh, *Langmuir* **2010**, *26*, 19148-19152.

[99] J. Kallioinen, G. Benkö, V. Sundström, J. E. I. Korppi-Tommola, A. P. Yartsev, *J. Phys. Chem. B* **2002**, *106*, 4396-4404.

[100] V. V. Semenov, N. F. Cherepennikova, S. Y. Khorshev, T. G. Mushtina, M. A. Lopatin, G. A. Domrachev, *Russ. J. Coord. Chem.* **2002**, *28*, 856-863.

[101] V. V. Kazakova, O. B. Gorbatsevich, S. A. Skvortsova, N. V. Demchenko, A. M. Muzafarov, *Russ. Chem. Bull. Int. Ed.* **2005**, *54*, 1350-1351.

[102] F. Reidmiller, A. Jockisch, H. Schmidbaur, *Organomet.* **1998**, *17*, 4444-4453.

[103] D. G. Anderson, M. A. M. Bradney, D. E. Webster, *J. Chem. Soc. (B)* **1968**, 450-452.

[104] K. Gilg, P. Klüfers, *Acta Cryst.* **2007**, *E63*, o4764.

[105] P. Franchetti, M. Pasqualini, R. Petrelli, M. Ricciutelli, P. Vita, L. Cappellacci, *Bioorg. Med. Chem. Lett.* **2004**, *14*, 4655-4658.

[106] L. Chen, Q. Xie, L. Sun, H. Wang, *J. Org. Chem.* **2003**, *678*, 90-94.

[107] X.-M. Zhang, M.-L. Tong, M.-L. Gong, H.-K. Lee, L. Luo, K.-F. Li, Y.-X. Tong, X.-M. Chen, *Chem. Eur. J.* **2002**, *8*, 3178-3194.

[108] G. Sprintschnik, H. W. Sprintschnik, P. P. Kirsch, D. G. Whitten, *J. Am. Chem. Soc.* **1977**, *99*, 4947-4954.

[109] W. R. Browne, P. Passaniti, M. T. Gandolfi, R. Ballardini, W. Henry, A. Guckian, N. O'Boyle, J. J. McGarvey, J. G. Vos, *Inorg. Chim. Acta* **2007**, *360*, 1183-1190.

[110] E. Terpetschnig, H. Szmacinski, H. Malak, J. R. Lakowicz, *Biophys. J.* **1995**, *68*, 342-350.

[111] B. Smith, *Infrared Spectral Interpreatation: A Systematic Approach*, CRC, New York, **1999**.

[112] O. Kühl, *Phosphorus-31 NMR Spectroscopy : A Concise Introduction for the Synthetic Organic and Organometallic Chemist*, Springer-Verlag, Berlin, **2008**.

[113] M. K. Nazeeruddin, A. Kay, I. Rodicio, R. Humphry-Baker, E. Müller, P. Liska, N. Vlachopoulos, M. Grätzel, *J. Am. Chem. Soc.* **1993**, *115*, 6382-6390.

[114] P. W. Selwood, *Magnetochemistry*, Interscience Publishers, Inc., New York, **1943**.

[115] A. F. Orchard, *Magnetochemistry*, Oxford University Press, Oxford, **2003**.

[116] D. W. Bennett, *Understanding Single-Crystal X-Ray Crystallography*, Wiley-VCH, Weinheim, **2010**.

[117] G. M. Sheldrick, *SHELXS-97 and SHELXL-97*, University of Göttingen, Germany, **1997**.

[118] P. v. d. Sluis, A. L. Spek, *Acta Crystallogr.* **1990**, *A46*, 194-201.

[119] L. Zsolani, *ZORTEP* **1994**, University of Heidelberg, Germany.

[120] Bruker SHELXTL Wisconsin, USA. Verson 6.12, **2001**, Brujer AXS Inc., Madison, USA.

[121] I. J. Bruno, J. C. Cole, P. R. Edgington, M. K. Kessler, C. F. Macrae, P. McCabe, J. Pearson, R. Taylor, *Acta Crystallogr.* **2002**, *B58*, 389-397.

[122] J.-P. Sauvage, *Acc. Chem. Res.* **1990**, *23*, 319-327.

[123] M. Fujita, *Acc. Chem. Res.* **1999**, *32*, 53-61.

[124] M. Fujita, M. Tominaga, A. Hori, B. Therrien, *Acc. Chem. Res.* **2005**, *38*, 371-380.

[125] E. C. Constable, *Tetrahedron* **1992**, *48*, 10013-10059.

[126] S. Leninger, B. Olenyuk, P. J. Stang, *Chem. Rev.* **2000**, *100*, 853-908.

[127] J.-P. Zhang, Y.-Y. Lin, X.-M. Weng, X.-M. Chen, *Inorg. Chim. Acta* **2006**, *359*, 3666-3670.

[128] S.-L. Zheng, J.-P. Zhang, X.-M. Chen, Z.-L. Huang, Z.-Y. Lin, W.-T. Wong, *Chem. Eur. J.* **2003**, *9*, 3888-3896.

[129] J.-P. Zhang, Y.-Y. Lin, X.-C. Huang, X.-M. Chen, *Eur. J. Inorg. Chem.* **2006**, 3407-3412.

[130] S.-L. Zheng, J.-P. Zhang, W.-T. Wong, X.-M. chen, *J. Am. Chem. Soc.* **2003**, *125*, 6882-6883.

[131] J. McMurray, *Organic Chemistry*, 6th ed., Thomson - Brooks/Cole, Belmont, **2004**.

[132] R. D. Gillard, *Coord. Chem. Rev.* **1975**, *16*, 67-94.

[133] N. Serpone, G. Ponterini, M. A. Jamieson, *Coord. Chem. Rev.* **1983**, *50*, 209-302.

[134] K. Ueno, T. Imamura, K. L. Cheng, *CRC Handbook of Organic Analytical Reagents*, 2nd ed., CRC, Boca Raton, **1992**.

[135] H. Nakai, Y. Deguchi, *Bull. Chem. Soc. Japan* **1975**, *48*, 2557-2560.

[136] K. J. Catalan, S. Jackson, J. D. Zubkowski, D. L. Perry, E. J. Valente, L. A. Feliu, A. Polanco, *Polyhedron* **1995**, *14*, 2165-2171.

[137] V. Russell, M. Scudder, I. Dance, *J. Chem. Soc., Dalton Trans.* **2001**, 789-799.

[138] G. Murphy, C. Murphy, B. Murphy, B. Hathaway, *J. Chem. Soc., Dalton Trans.* **1997**, 2653-2660.

[139] C. M. Julien, A. Ait-Salah, A. Mauger, F. Gendron, *Ionics* **2006**, *12*, 21-32.

[140] B. Bleaney, K. D. Bowers, *Proc. Roy. Soc. (London) Ser. A* **1952**, *214*, 451-465.

[141] A. P. Gingsberg, *Inorg. Chim. Acta Rev.* **1971**, *5*, 45-68.

[142] O. Kahn, *Molecular Magnetism*, Wiley-VCH, New York, **1993**.

[143] N. A. Spaldin, *Magnetic Materials: Fundamentals and Applications*, 2nd ed., Cambridge University Press, New York, **2011**.

[144] L. Duò, M. Finazzi, F. Ciccacci, *Magnetic Properties of Antiferromagnetic Oxide Materials: Surfaces, Interfaces and Thin Films*, Wiley-VCH, Weinhelm, **2010**.

[145] X.-M. Zhang, M.-L. Tong, X.-M. Chen, *Angew. Chem. Int. Ed.* **2002**, *41*, 1029-1031.

[146] Z. Serna, G. Barandika, R. Cortés, M. K. Urtiaga, M. I. Arriortua, *Polyhedron* **1999**, *18*, 249-255.

[147] P. M. Graham, R. D. Pike, M. Sabat, R. D. Bailey, W. T. Pennington, *Inorg. Chem.* **2000**, *39*, 5121-5132.

[148] Z. E. Serna, R. Cortés, M. K. Urtiaga, G. Barandika, L. Lezama, M. I. Arriotua, *Eur. J. Inorg. Chem.* **2001**, 865-872.

[149] M.-L. Tong, M. Monfort, J. M. C. Juan, X.-M. Chen, X.-H. Bu, M. Ohba, S. Kitagawa, *Chem. Commun.* **2005**, 233-235.

[150] B. F. Abrahams, T. A. Hudson, R. Robson, *Chem. Eur. J.* **2006**, *12*, 7095-7102.

[151] B. Hussain, D. Savard, T. J. Burchell, W. Wernsdorfer, M. Murugesu, *Chem. Commun.* **2009**, 1100-1102.

[152] Y. Li, S. Xiang, T. Sheng, J. Zhang, S. Hu, R. Fu, X. Huang, X. Wu, *Inorg. Chem.* **2006**, *45*, 6577-6579.

[153] Z.-N. Lou, Z.-B. Han, P. Zhang, *Struct. Chem.* **2007**, *18*, 549-554.

[154] P. Kulkarni, S. Padhye, E. Sinn, C. E. Anson, A. K. Powell, *Inorg. Chim. Acta* **2002**, *332*, 167-175.

[155] D. Czakis-Sulikowska, J. Kaluzna, J. Radwanska-Doczekalska, *J. Therm. Anal.* **1998**, *54*, 103-113.

[156] G. O. Morpugo, G. Dessy, V. Fares, *J. Chem. Soc., Dalton Trans.* **1984**, *5*, 785-791.

[157] M. A. S. Goher, N. A. Al-Salem, T. C. W. Mak, *Polyhedron* **2000**, *19*, 1465-1470.

[158] W. B. Jennings, B. M. Farrell, J. F. Malone, *Acc. Chem. Res.* **2001**, *34*, 885-894.

[159] V. Tangoulis, C. P. Raptopoulou, S. Paschalidou, A. E. Tsohos, E. G. Bakalbassis, A. Terzis, S. P. Perlepes, *Inorg. Chem.* **1997**, *36*, 5270-5277.

[160] C.-M. Liu, D.-Q. Zhang, D. B. Zhu, *Inorg. Chim. Acta* **2009**, *362*, 1383-1386.

[161] K. B. Szpakolski, K. Latham, C. J. Rix, J. M. White, B. Mourbaraki, K. S. Murray, *Chem. Eur. J.* **2010**, *16*, 1691-1696.

[162] M. Fondo, A. M. Garcia-Deibe, J. Sanmartin, M. R. Bermejo, L. Lezama, T. Rojo, *Eur. J. Inorg. Chem.* **2003**, 3703-3706.

[163] N. P. Rath, E. M. Holt, K. Tanimura, *J. Chem. Soc., Dalton Trans.* **1986**, 2303-2310.

[164] N. P. Rath, J. L. Maxwell, E. M. Holt, *J. Chem. Soc., Dalton Trans.* **1986**, 2449-2453.

[165] B. W. Skelton, A. F. Waters, A. H. White, *Aust. J. Chem.* **1991**, *44*, 1207-1215.

[166] B. L. Westcott, K. M. Kopp-Vaughn, L. M. Daniels, M. Zeller, *Acta Crystallogr.* **2008**, *E64*, m1122-m1123.

[167] M. A. S. Goher, F. A. Mautner, *Polyhedron* **1999**, *18*, 3425-3431.

[168] M. C. Feller, R. Robson, *Aust. J. Chem.* **1968**, *21*, 2919-2927.

[169] R. R. Osborne, W. R. McWhinnie, *J. Chem. Soc. (A)* **1967**, *12*, 2075-2078.

[170] S. Bhaduri, N. Y. Sapre, P. G. Jones, *J. Chem. Soc., Dalton Trans.* **1991**, 2539-2543.

[171] R. A. Bailey, S. L. Kozak, T. W. Michelsen, W. N. Mills, *Coord. Chem. Rev.* **1971**, *6*, 407-445.

[172] M. A. S. Goher, F. A. Mautner, *Polyhedron* **1994**, *13*, 2149-2155.

[173] M. Du, X.-H. Bu, M. Shionoya, M. Shiro, *J. Mol. Struct.* **2002**, *607*, 155-161.

[174] M. Mikuriya, A. Azuma, R. Nukada, Y. Sayama, K. Tanaka, J.-W. Lim, M. Handa, *Bull. Chem. Soc. Japan* **2000**, *73*, 2493-2498.

[175] G. S. Papaefstathiou, C. P. Raptopoulou, A. E. Tsohos, A. Terzis, E. G. Bakalbassis, S. P. Perlepes, *Inorg. Chem.* **2000**, *39*, 4658-4662.

[176] G.-J. ten Brink, I. W. C. E. Arends, R. A. Sheldon, *Chem. Rev.* **2004**, *104*, 4105-4123.

[177] G. R. Krow, *Org. Reactions* **2004**, 251–798.

[178] M. Renz, B. Meunier, *Eur. J. Org. Chem.* **1999**, 737-750.

[179] A. Baeyer, V. Villiger, *Ber. Dtsch. Chem. Ges.* **1899**, *32*, 3625.

[180] P. Sykes, *A Guide to Mechanisms in Organic Chemistry*, 6th ed., Longman Scientific & Technical, Singapore, **1986**.

[181] R. A. Michelin, P. Sgarbossa, A. Scarso, G. Strukul, *Coord. Chem. Rev.* **2010**, *254*, 646-660.

[182] R. Crigee, *Justus Liebigs Ann. Chem.* **1948**, *560*, 127.

[183] L. Reyes, J. R. Alvarez-Idaboy, N. Mora-Diez, *J. Phys. Org. Chem.* **2009**, *22*, 643-649.

[184] E. Bae, W. Choi, J. Park, H. S. Shin, S. B. Kim, J. S. Lee, *J. Phys. Chem. B* **2004**, *108*, 14093-14101.

[185] V. M. Cristante, A. G. S. Prado, S. M. A. Jorge, J. P. S. Valente, A. O. Florentino, P. M. Padilha, *J. Photochem. Photobiol., A* **2008**, *195*, 23-29.

[186] P. K. Ghosh, T. G. Spiro, *J. Am. Chem. Soc.* **1980**, *102*, 5543-5549.

[187] Q.-H. Yao, Y.-Y. Huang, L.-Q. Song, B.-W. Zhang, C.-H. Huang, Z.-S. Wang, F.-Y. Li, X.-S. Zhao, *Sol. Energy Mater. Sol. Cells* **2003**, *77*, 319-330.

[188] R. Mosurkal, S. Roy, J. K. Lynne, L. A. Samuelson, S. K. Tripathy, *J. Macromol. Sci. Pure* **2002**, *39*, 1195-1206.

[189] M. Yanagida, L. P. Singh, K. Sayama, K. Hara, R. Katoh, A. Islam, H. Sugihara, H. Arakawa, M. K. Nazeeruddin, M. Grätzel, *J. Chem. Soc., Dalton Trans.* **2000**, 2817-2822.

[190] O. Schwarz, D. v. Loyen, S. Jockusch, N. J. Turro, H. Dürr, *J. Photochem. Photobiol., A* **2000**, *132*, 91-98.

[191] A. S.-Y. Lee, Y.-T. Chang, S.-F. Chu, K.-W. Tsao, *Tetrahedron Lett.* **2006**, *47*, 7085-7087.

[192] V. Penicaud, F. Odobel, B. Bujoli, *Tetrahedron Lett.* **1998**, *39*, 3689-3692.

[193] A. S. Manoso, P. DeShong, *J. Org. Chem.* **2001**, *66*, 7449-7455.

[194] L. Chen, Q. Xie, L. Sun, H. Wang, *J. Organomet. Chem.* **2003**, *678*, 90-94.

[195] H. Hügel, *Personal Communication* **2011**.

[196] M. G. Voronkov, G. Zelcans, Institute of Organic Synthesis, Academy of Sciences, Latvian S. S. R., U.S.S.R, **1968**.

[197] K. B. Szpakolski, K. Latham, C. J. Rix, J. M. White, *Eur. J. Inorg. Chem.* **2010**, 5660-5667.

[198] K. B. Szpakolski, K. Latham, C. J. Rix, J. M. White, *Inorg. Chim. Acta* **2011**, *376*, 628-633.